frontiers | Research Topics

Brain connectivity in neurological disorders

Edited by
Alessandro Salvalaggio, Maurizio Corbetta, Alessandra Griffa and Lorenzo Pini

Published in
Frontiers in Neurology
Frontiers in Systems Neuroscience

ISSN 1664-8714
ISBN 978-2-8325-3699-5
DOI 10.3389/978-2-8325-3699-5

About Frontiers

Frontiers is more than just an open access publisher of scholarly articles: it is a pioneering approach to the world of academia, radically improving the way scholarly research is managed. The grand vision of Frontiers is a world where all people have an equal opportunity to seek, share and generate knowledge. Frontiers provides immediate and permanent online open access to all its publications, but this alone is not enough to realize our grand goals.

Frontiers journal series

The Frontiers journal series is a multi-tier and interdisciplinary set of open-access, online journals, promising a paradigm shift from the current review, selection and dissemination processes in academic publishing. All Frontiers journals are driven by researchers for researchers; therefore, they constitute a service to the scholarly community. At the same time, the *Frontiers journal series* operates on a revolutionary invention, the tiered publishing system, initially addressing specific communities of scholars, and gradually climbing up to broader public understanding, thus serving the interests of the lay society, too.

Dedication to quality

Each Frontiers article is a landmark of the highest quality, thanks to genuinely collaborative interactions between authors and review editors, who include some of the world's best academicians. Research must be certified by peers before entering a stream of knowledge that may eventually reach the public - and shape society; therefore, Frontiers only applies the most rigorous and unbiased reviews. Frontiers revolutionizes research publishing by freely delivering the most outstanding research, evaluated with no bias from both the academic and social point of view. By applying the most advanced information technologies, Frontiers is catapulting scholarly publishing into a new generation.

What are Frontiers Research Topics?

Frontiers Research Topics are very popular trademarks of the *Frontiers journals series*: they are collections of at least ten articles, all centered on a particular subject. With their unique mix of varied contributions from Original Research to Review Articles, Frontiers Research Topics unify the most influential researchers, the latest key findings and historical advances in a hot research area.

Find out more on how to host your own Frontiers Research Topic or contribute to one as an author by contacting the Frontiers editorial office: frontiersin.org/about/contact

Brain connectivity in neurological disorders

Topic editors

Alessandro Salvalaggio — University Hospital of Padua, Italy
Maurizio Corbetta — Washington University in St. Louis, United States
Alessandra Griffa — Université de Genève, Switzerland
Lorenzo Pini — University of Padua, Italy

Citation

Salvalaggio, A., Corbetta, M., Griffa, A., Pini, L., eds. (2023). *Brain connectivity in neurological disorders*. Lausanne: Frontiers Media SA.
doi: 10.3389/978-2-8325-3699-5

Table of contents

frontiers | Frontiers in Systems Neuroscience

TYPE Editorial
PUBLISHED 26 September 2023
DOI 10.3389/fnsys.2023.1274801

OPEN ACCESS

EDITED AND REVIEWED BY
Federico Bermudez-Rattoni,
National Autonomous University of Mexico, Mexico

*CORRESPONDENCE
Alessandro Salvalaggio
✉ alessandro.salvalaggio@unipd.it

RECEIVED 08 August 2023
ACCEPTED 24 August 2023
PUBLISHED 26 September 2023

CITATION
Salvalaggio A, Pini L, Griffa A and Corbetta M (2023) Editorial: Brain connectivity in neurological disorders.
Front. Syst. Neurosci. 17:1274801.
doi: 10.3389/fnsys.2023.1274801

Editorial: Brain connectivity in neurological disorders

Alessandro Salvalaggio[1,2]*, Lorenzo Pini[1], Alessandra Griffa[3] and Maurizio Corbetta[1,2,4]

[1]Padova Neuroscience Center, University of Padua, Padua, Italy, [2]Department of Neuroscience, University of Padua, Padua, Italy, [3]Leenaards Memory Center, Department of Clinical Neurosciences, Lausanne University Hospital, Lausanne, Switzerland, [4]Veneto Institute of Molecular Medicine (VIMM), Padua, Italy

KEYWORDS

brain connectivity, disconnection, clinical, diseases, structural connectome, functional connectome

Editorial on the Research Topic
Brain connectivity in neurological disorders

The exploration of brain network connectivity has allowed us to unravel the complex functional and structural architecture of the human brain, uncovering its intricate composition of interconnected modules and networks. These groundbreaking studies have shed light on how various neurological and psychiatric disorders can be considered as "disconnectivity syndromes," paving the way for the identification of new biomarkers to aid in the diagnosis and treatment of these diseases. However, the clinical application and impact of these findings have fallen short of expectations. Currently, connectivity measures are not integrated into the clinical assessment of neurological and psychiatric patients, nor are they employed as surrogate markers in clinical trials. Nonetheless, with the substantial body of evidence available, it is crucial to seize this opportunity and translate these findings into practical applications in the clinical field. The aim of this Research Topic consists in collecting studies applying connectivity methods in different clinical populations alongside the hypothesis that neurological disorders are (at least partially) mediated by connectivity alterations.

Among the studies herein collected, case reports focusing on uncommon clinical presentation, offer valuable insights into the value of connectivity approach at the individual patient level. In a study by Monai et al., a patient with subclinical cognitive deficits across multiple domains, recurrent delirium, and a focal frontal lesion was examined using a multi-modal approach. By integrating various types of disconnections—including electroencephalography (EEG), functional and structural disconnectivity, and metabolism—the researchers found how brain dysfunction extended beyond the focal lesion, matching with cortical glucose hypometabolism and therefore justifying the broad clinical presentation. In another case report, Indovina et al. described a patient who developed

agoraphobia after the surgical removal of a glioma located in the right parietal cortex. The researchers reported extensive post-surgery reorganization within the vestibular network, as evidenced by changes in both structural and functional connectivity measures, thus helping in understanding the pathophysiology underlying the occurrence of agoraphobic symptoms. Overall, these case reports demonstrate the feasibility of applying connectivity analyses to individual subjects in a clinical setting thus providing an additional tool for the diagnosis and treatment. Brain connectivity approach may also provide biomarkers of cognitive impairment in multiple sclerosis, which is the most debilitating neurological disease among young adults. Several studies have already demonstrated a correlation between alterations in brain connectivity and the clinical severity of MS. Building upon these findings, Grothe et al. provided further evidence about the close relationship between processing speed performance and the structural connectivity of frontoparietal regions. Interestingly, connectivity changes may also appear (and be measured) when the damage is outside the central nervous system. Quettier et al. successfully employed an EEG-based approach to identify connectivity modulations in individuals with seventh cranial nerve damage. Specifically, their study revealed a reduced strength of connectivity between sensorimotor and visual regions in participants affected by facial palsy when compared to the matched controls.

Recent advancements have been made in the analysis of connectivity data, offering promising results and expanding our understanding of clinical information derived from connectivity. Spadone et al. conducted a dynamic functional connectivity study on stroke patients, introducing a novel functional dynamic approach. This analysis method examines the signal in terms of transient conditions of neural network reconfigurations. The findings from this study revealed that strokes leading to spatial attention deficits impact the temporal configuration of functional connections. The altered connectivity patterns were found to be associated with the severity of spatial neglect.

However, while these studies are intriguing, their practical application in clinical settings is limited due to various challenges. These include the complexity of performing comprehensive connectivity examinations, the patient's limited compliance for long acquisition time, the requirement for advanced processing and analysis skills, and the lack of access to clinical facilities. These limitations have hindered the widespread translation of these findings into clinical practice. In recent years, researchers have developed alternative approaches to assess brain disconnection. These approaches aim to overcome the need for extensive data acquisition and processing by utilizing a publicly available normative dataset. These methods have primarily been developed within the context of brain focal lesions, where the volume of the lesion is integrated into a normative functional or structural connectome allowing to estimate which regions or tracts have been likely disconnected by the pathology (Boes et al., 2015; Foulon et al., 2018). Implementing these approaches in the clinical assessment of brain lesions holds great potential. Nabizadeh and Aarabi conducted a comprehensive review of the recent literature in this field, highlighting the growing body of research. Their review revealed that more than fifty papers have been published recently, further substantiating the interest and progress in this area of study. Within this evolving context Klingbeil et al. conducted a comprehensive analysis of 270 stroke patients to assess the impact of post-stroke depressive symptoms in relation to structural and functional indirect disconnections. They identified a significant association between higher depression scores and both lesions topology and white-matter structural disconnection in the right temporal lobe. No significant associations were observed with functional disconnections. These findings indicate that in the context of stroke, structural disconnection may exert a more preeminent predictive role compared to functional disconnections, which aligns with recent findings (Salvalaggio et al., 2020). Finally, Sansone et al. investigated the pattern of network involvement of glioblastoma (GBM), reporting a preferential overlap between GBM and specific networks suggesting that tumor growth and spreading might not be independent of brain activity, although, network-topology information is overall scarcely informative about overall survival in these patients.

In conclusion, this Research Topic suggests that connectivity approaches might have the potential to be widely implemented in the clinical framework, despite several limitations which should be addressed by future research.

Author contributions

AS: Writing—original draft, Writing—review and editing. LP: Writing—original draft, Writing—review and editing. AG: Writing—review and editing. MC: Writing—review and editing.

Conflict of interest

The authors declare that the research was conducted in the absence of any commercial or financial relationships that could be construed as a potential conflict of interest.

Publisher's note

References

Boes, A. D., Prasad, S., Liu, H., Liu, Q., Pascual-Leone, A., Caviness, V. S. et al. (2015). Network localization of neurological symptoms from focal brain lesions. *Brain*. 138, 3061–3075. doi: 10.1093/brain/awv228

Foulon, C., Cerliani, L., Kinkingnéhun, S., Levy, R., Rosso, C., Urbanski, M., et al. (2018). Advanced lesion symptom mapping analyses and implementation as BCBtoolkit. *Gigascience*. 7, 1–17. doi: 10.1093/gigascience/giy004

Salvalaggio, A., De Filippo De Grazia, M., Zorzi, M., Thiebaut de Schotten, M., and Corbetta, M. (2020). Post-stroke deficit prediction from lesion and indirect structural and functional disconnection. *Brain*. 143, 2173–2188. doi: 10.1093/brain/awaa156

frontiers | Frontiers in Neurology

TYPE Original Research
PUBLISHED 04 November 2022
DOI 10.3389/fneur.2022.982964

OPEN ACCESS

EDITED BY
Lorenzo Pini,
University of Padua, Italy

REVIEWED BY
Ilaria Boscolo Galazzo,
University of Verona, Italy
Sindhuja T. Govindarajan,
University of Pennsylvania,
United States

*CORRESPONDENCE
Matthias Grothe
matthias.grothe@med.uni-greifswald.de

†These authors have contributed equally to this work

SPECIALTY SECTION
This article was submitted to Applied Neuroimaging, a section of the journal Frontiers in Neurology

RECEIVED 30 June 2022
ACCEPTED 20 September 2022
PUBLISHED 04 November 2022

CITATION
Grothe M, Jochem K, Strauss S, Langner S, Kirsch M, Hoffeld K, Penner IK, Nagels G, Klepzig K, Domin M and Lotze M (2022) Performance in information processing speed is associated with parietal white matter tract integrity in multiple sclerosis. *Front. Neurol.* 13:982964. doi: 10.3389/fneur.2022.982964

Performance in information processing speed is associated with parietal white matter tract integrity in multiple sclerosis

Matthias Grothe[1]*, Katharina Jochem[1], Sebastian Strauss[1], Sönke Langner[2], Michael Kirsch[2], Kai Hoffeld[1], Iris Katharina Penner[3,4,5], Guy Nagels[6,7], Kai Klepzig[8], Martin Domin[8†] and Martin Lotze[8†]

[1]Department of Neurology, University Medicine Greifswald, Greifswald, Germany, [2]Institute for Diagnostic Radiology and Neuroradiology, University Medicine of Greifswald, Greifswald, Germany, [3]Department of Neurology, Medical Faculty, Heinrich Heine University Düsseldorf, Düsseldorf, Germany, [4]COGITO Center for Applied Neurocognition and Neuropsychological Research Düsseldorf, Düsseldorf, Germany, [5]Department of Neurology, Inselspital, Bern University Hospital, University of Bern, Bern, Switzerland, [6]Center for Neurosciences, Vrije Universiteit Brussel, Brussels, Belgium, [7]National MS Center Melsbroek, Steenokkerzeel, Belgium, [8]Functional Imaging, Institute for Diagnostic Radiology and Neuroradiology, University Medicine of Greifswald, Greifswald, Germany

Background: The Symbol Digit Modalities Test (SDMT) is most frequently used to test processing speed in patients with multiple sclerosis (MS). Functional imaging studies emphasize the importance of frontal and parietal areas for task performance, but the influence of frontoparietal tracts has not been thoroughly studied. We were interested in tract-specific characteristics and their association with processing speed in MS patients.

Methods: Diffusion tensor imaging was obtained in 100 MS patients and 24 healthy matched controls to compare seed-based tract characteristics descending from the superior parietal lobule [Brodman area 7A (BA7A)], atlas-based tract characteristics from the superior longitudinal fasciculus (SLF), and control tract characteristics from the corticospinal tract (CST) and their respective association with ability on the SDMT.

Results: Patients had decreased performance on the SDMT and decreased white matter volume (each $p < 0.05$). The mean fractional anisotropy (FA) for the BA7A tract and CST ($p < 0.05$), but not the SLF, differed between MS patients and controls. Furthermore, only the FA of the SLF was positively associated with SDMT performance even after exclusion of the lesions within the tract ($r = 0.25$, $p < 0.05$). However, only disease disability and total white matter volume were associated with information processing speed in a linear regression model.

Conclusions: Processing speed in MS is associated with the structural integrity of frontoparietal white matter tracts.

KEYWORDS

multiple sclerosis, cognition, SDMT, diffusion tensor imaging, brain mapping

Introduction

Cognitive impairment is common in up to 40%−50% of patients with multiple sclerosis (MS) (1) and has been associated with both gray (2, 3) and white matter (4, 5) pathologies. Previous studies related to white matter abnormalities associated with cognitive impairment in MS have focused on lesion load (4), lesion location (5), or whole-brain white matter tract integrity (6). With these approaches, several fiber tracts, such as the fornix, corpus callosum, thalamic radiation, and superior longitudinal fasciculus (SLF), have been related to cognitive disturbances (7, 8).

The Symbol Digit Modalities Test (SDMT) assesses information processing speed and working memory, discriminating patients from healthy controls with high sensitivity (1, 9, 10). When applying functional magnetic resonance imaging (fMRI) to investigate the underlying neural resources, a network consisting of frontal (Brodman area [BA] 6 and 9), parietal (BA7), occipital (BA17), and medial posterior cerebellar (declive) regions have been identified (11–13). Based on the involvement of a widespread functional network in processing speed, the SLF, and especially its subdivisions SLF1 and SLF2, is presumably important because this tract bundle connects the super parietal lobule with the superior and middle frontal areas (14–16).

A recent fMRI approach of the oral version of the SDMT also emphasized the role of the superior parietal lobe (SPL), especially BA7A, for SDMT performance (17). This area is particularly involved in spatial attention and visual working memory (18, 19), which represent key components of the SDMT (20). Anatomically, BA7A is structurally interconnected with frontal, temporal, and brainstem areas, at least in part *via* the SLF (15), again highlighting the importance of this white matter tract bundle for cognition in MS.

Here, we investigated structural white matter alterations in MS patients to better understand the role of specific parietal white matter tracts, especially the SLF, and their associations with ability on the SDMT. We focused on tract integrity as quantified by fractional anisotropy (FA) using diffusion tractography (DTI) on diffusion weighted imaging (DWI), as FA is a highly sensitive, early, diffusion tensor-derived metric for demyelination (21). In the literature, different DTI methods are used – either in a whole brain approach, called tract based spatial statistics (6), or with a more hypothesis driven, regional approach. Based on the literature that highlights the importance of the SLF and BA7A, we chose a regional-based approach to associate the clinical impairment in the SDMT with white matter tract pathology, using a predefined probabilistic region-of-interest of the SLF and by performing probabilistic tractography originating in BA7A. As a reference tract we selected the corticospinal tract (CST), the integrity of which has been associated with motor, but not cognitive, performance (22). Whole-brain and tract-specific metrics were compared between MS patients and healthy controls.

We further analyzed the tract metrics for the whole tract and after exclusion of the lesions within the tract because we were especially interested in an association with the so-called normal appearing white matter (NAWM) tract alterations, which are also accompanied by a reduction in FA in MS (23, 24). In a final step, we performed correlation and linear regression analyses to investigate clinical and imaging variables and their association with SDMT.

Methods

Participants

A total of 100 MS patients were enrolled in this study [70 females, mean age 44.3 years, median Expanded Disability Status Scale (EDSS) 2.0]. All MS patients fulfilled the criteria for multiple sclerosis according to the 2017 McDonald criteria (25). Exclusion criteria were an acute relapse or steroid treatment within the previous 3 months and another central neurological disease. Twenty-four healthy controls (HCs) were added as a control group without any neurological or psychiatric disorder. The study was approved by the Ethics Committee of the Medical Faculty of the University of Greifswald (BB028/13) and all participants provided informed consent. Demographics are summarized in Table 1.

Neurological and neuropsychological examination

Each patient was investigated clinically and neuropsychologically with respect to clinical disability (EDSS) (26), depression [Beck Depression Inventory-II (BDI-II)] (27), fatigue [Fatigue Scale for Motor and Cognitive Functions (FSMC)] (28), and information processing speed (SDMT).

The control group was investigated with only the SDMT. Figure 1A demonstrates an example of the SDMT. All clinical assessments and MRI measurements were performed within 2 weeks.

MRI data acquisition

MRI was performed on a 3-T scanner (Magnetom Verio, SIEMENS, Erlangen) using a 32-channel head coil. The standard imaging protocol in all patients included a sagittal T1-weighted 3D-Magnetization Prepared Rapid Acquisition with Gradient Echoes (MPRAGE) sequence (TR: 1,690 ms; TE: 2.52 ms; TI: 900 ms; flip angle: 9°; matrix: 256 × 256; 176 slices; voxel size 0.98 × 0.98 × 1 mm), a 3D-T2-FLAIR sequence [TR:

TABLE 1 Group characteristics.

	Patient group	Control group	Test statistics
N	100	24	
Age (years)	44.1 ± 12.5	41.1 ± 11.56	$t = 1.1$; $p = 0.28$
Sex (male/female)	30/70	10/14	$\chi^2 = 2.8$; $p = 0.12$
Education (years)	14.5 ± 1.8	14.2 ± 2.8	$t = 0.59$; $p = 0.55$
Disease duration (years)	8.9 ± 7.0		
Disease course (RRMS/SPMS)	93/7		
EDSS	2.0 (0–7)		
zSDMT	−0.47 ± 1.3	0.12 ± 1.2	$t = 2.04$; $p = 0.04$
Gray matter volume (cm^3)	615.1 ± 72.8	644.4 ± 72.1	$t = -1.77$; $p = 0.08$
White matter volume (cm^3)	498.5 ± 65.8	546.3 ± 63.2	$t = -3.22$; $p = 0.002$
Lesion volume (cm^3)	8.5 ± 8.0	2.0 ± 1.2	$t = 7.8$; $p < 0.001$
FA, SLF	0.436 ± 0.02	0.439 ± 0.02	$t = 0.4$; $p = 0.69$
FA, BA7A tract	0.429 ± 0.04	0.447 ± 0.03	$t = 2.2$; $p = 0.03$
FA, CST	0.455 ± 0.02	0.465 ± 0.02	$t = 2.3$; $p = 0.02$
Lesion overlap (%): SLF	1.019 ± 1.344	n/a	
Lesion overlap (%): BA7A tract	1.951 ± 1.509	n/a	
Lesion overlap (%): CST	1.683 ± 1.281	n/a	

Values are given as mean ± standard deviation or median (range) unless otherwise noted.

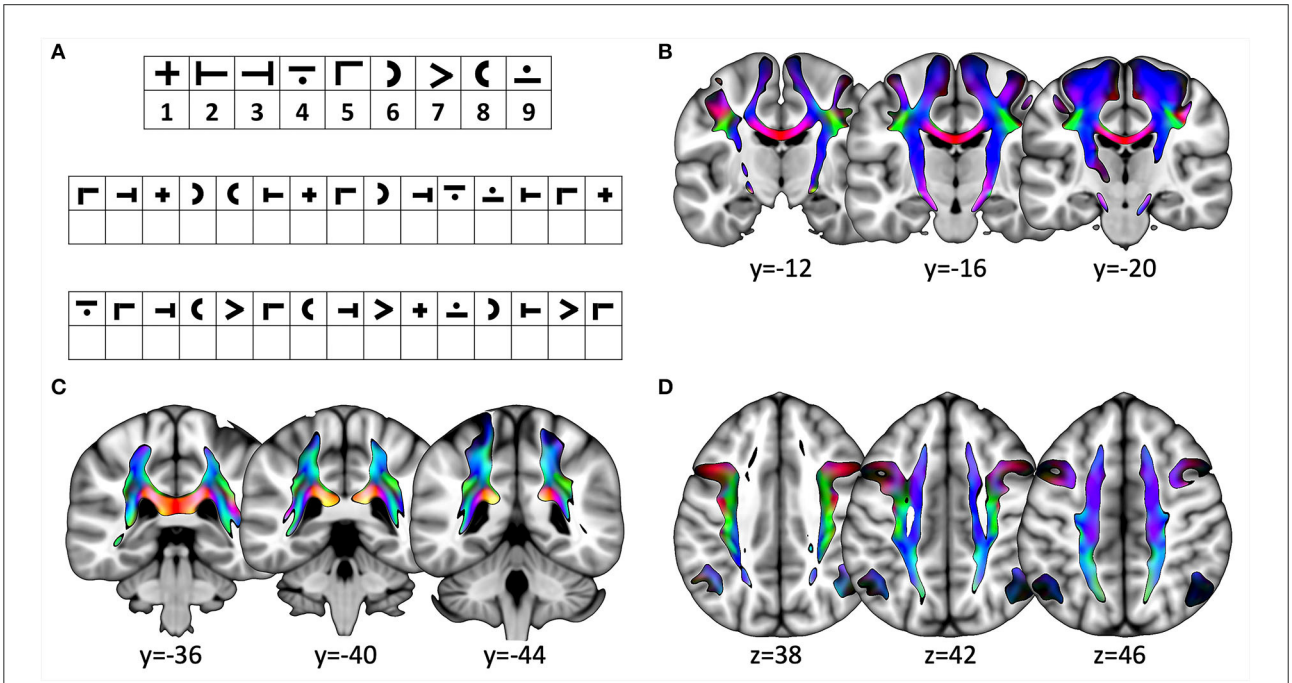

FIGURE 1
(A) Example for the Symbol Digit Modalities Test (SDMT). **(B–D)** Slices showing the three tracts from the diffusion-weighted imaging data for all participants. The direction of tractography is encoded in standardized colors: *z*, blue; *y*, green; *x*, red. **(B)** coronal slices depicting the tract originating in M1; **(C)** coronal slices showing the tract originating in BA7A; and **(D)** axial slices showing SLF. Slice position is indicated in the respective direction below slice.

5,000 ms; TE: 388 ms; TI: 1,800 ms; matrix: 512 × 512 (k-space interpolation); 160 slices; voxel size 0.49 × 0.49 × 1 mm], and a Siemens- Multi- Directional Diffusion Weighted (MDDW) sequence [TR: 10,900 ms; TE: 107 ms; flip angle: 90°; matrix: 128 × 128; voxel size: 1.8 × 1.8 × 2 mm; 70 slices; 1× unweighted volume ($b = 0$); 64× diffusion-weighted volumes ($b = 1{,}000$)].

MS lesion segmentation

Lesions were segmented by the lesion prediction algorithm (LPA) as implemented in LST toolbox version 3.0.0 (www.statistical-modeling.de/lst.html) for statistical parametric mapping (SPM; Wellcome Center, London, UK) (29). The LPA classifier was trained using a logistic regression model as described in detail elsewhere, providing an estimate for the lesion probability of each voxel (29). The 3D-T2- fluid-attenuated inversion recovery (FLAIR) sequence is sufficient as an exclusive source for lesion segmentation when using this prediction algorithm. The resulting lesion maps were visually inspected for gross deviations by an expert (MG), and no further correction was needed. The final maps were subsequently used as exclusion masks for later extraction of FA and to calculate a possible overlap for a quantification of lesion load of certain white matter tracts.

Image processing

The diffusion-weighted data were corrected for eddy current and motion-related artifacts [FSL eddy_correct (v6.0.1)], followed by appropriate correction of the diffusion gradient vector table. Afterwards, the diffusion tensor was calculated by least-square fitting (FSL dtifit) and the usual DWI metrics, such as FA. A spatial transformation was calculated from the diffusion image space into the MNI template space by generating a group template (antsMultivariateTemplateConstruction2, Advanced Normalization Tools v3.0.0.0.dev21-g1d890) based on the FA images of all patients and healthy subjects. This group template was then registered to the MNI 152 ICBM 6th gen. template brain using ANTs SyN (30).

The inverse of the merged registration (MNI template : group template : single subject) was used to transform regions-of-interest (ROIs) of the Juelich histological atlas (SPL, BA7A, left and right hemisphere) (31), the Brainnetome Atlas (primary motor cortex, M1, left and right hemisphere) (32), and the human XTRACT atlas (SLF parts 1 and 2, left and right hemisphere) (33) from the MNI template space into individual subject space.

Next, separately for each ROI and hemisphere, unconstrained structural connectivity was generated using probabilistic tractography FSL's probtrackx (34). For that purpose, FSL's bedpost (35) was applied to calculate the fiber orientation density function (FODf) from the diffusion MRI for each voxel. The FODf can then be randomly sampled to extract principal diffusion directions in each voxel. Starting at a seed voxel of a ROI these directions can be followed and put together to a streamline. As the FODf can contain multiple principal diffusion directions, a seed voxel will "spawn" many thousand different streamlines depending on the selected direction in each voxel. This process results in a frequency map in which each voxel encodes the number of valid streamlines running through that voxel. In addition, as the XTRACT atlas already contains these frequency maps, therefore tractography was not needed and the extracted ROIs were used as a generic tractogram.

Finally, the intensity values of each resulting tractogram were numerically normalized to 1 by dividing each voxel value by the highest voxel value of the respective tractogram and then used to calculate a weighted mean FA value for each tractogram in a way that each voxel's FA value was scaled (weighted) by the corresponding tractogram's normalized frequency.

For visualization purposes (see Figures 1B–D), each calculated tractogram was transformed into the MNI space and all tractograms belonging to the same ROI were averaged. This procedure was also applied to the individual lesion maps, resulting in an average lesion map in the MNI space.

In order to quantify the gray and white matter volumes, the CAT12 Toolbox (Christian Gaser, https://neuro-jena.github.io/cat/) for SPM (SPM12; Wellcome Department of Cognitive Neurosciences, London, UK) was used. As the CAT12 Toolbox is capable of identifying white matter hyperintensities, the lesions were removed from the calculation of white matter volume.

Statistical analysis processing

All statistical testing was performed using SPSS version 25. Descriptive statistics were performed according to the data using means with standard deviations or medians with ranges. Basic assumptions of normal distribution were assessed as recommended both visually and by the Shapiro-Wilk test. The raw score for the SDMT was corrected for age and education level based on the German validation study, resulting in SDMT z-scores (zSDMT) (36). Group differences between patients and HCs were assessed using the Student's *t*-test or Mann–Whitney *U*-test. Differences between each tract (SLF, BA7A tract, CST) with or without lesion masking were determined using paired *t*-tests.

To investigate the associations between zSDMT and imaging data, Pearson or Spearman correlations were computed depending on their normal distribution. A stepwise multiple linear regression model was finally calculated with zSDMT as the dependent variable and clinical (disease duration, EDSS, FSMC, BDI) and imaging (gray matter volume, white matter volume, lesion volume, FA SLF, FA BA7A-tract, FA CST) variables as independent variables.

A significance level of 0.05 was used and *p*-values adjusted by Benjamini–Hochberg's procedure in order to correct for multiple comparisons.

Results

Clinical characteristics

In the MS patient group, the mean disease duration was 7.1 years, median EDSS 2.0, mean zSDMT −0.47, mean FSMC 54.8, and mean BDI 9.7. In this group, 11.8% of patients were not treated, 62.3% were treated with first-line disease-modifying drugs (DMDs), and 25.7% were treated with second-line DMDs. The patient group performed worse than the control group on the SDMT ($t = 2.04$; $p = 0.04$). Group comparisons for MS patients and healthy controls are summarized in Table 1.

Imaging characteristics

Structural data revealed reduced white matter volume and higher lesion volume for MS patients compared to HCs (see Table 1, Figure 2). Comparison of the tracts without lesion exclusion revealed that FA for the SLF did not differ between patients and controls ($t = 0.4$, $p_{FDR} = 0.7$), whereas BA7A tract and CST showed lower FA in patients than in controls (BA7A tract: $t = 2.2$, $p_{FDR} = 0.045$; CST: $t = 2.3$, $p_{FDR} = 0.036$). Lesion exclusion did not have an impact on the main findings (SLF: $t = 0.4$, $p_{FDR} = 0.7$; BA7A $t = 2.8$, $p_{FDR} = 0.024$, CST: $t = 2.4$, $p_{FDR} = 0.036$).

For MS patients, FA of the SLF and BA7A tract, but not for the CST, differed significantly between the analysis with and without lesion exclusion (SLF: $t = 2.9$, $p_{FDR} = 0.0225$; BA7A tract: $t = 4.2$, $p_{FDR} = 0.009$; CST: $t = 0.8$, $p_{FDR} = 0.5$).

Correlation between clinical and imaging data

Visual inspection and the Shapiro-Wilk test revealed a normal distribution for zSDMT and FA for each tract. For MS patients, Pearson correlations between zSDMT and FA revealed a significant association of the SLF ($r = 0.246$, $p_{FDR} = 0.042$), but not the BA7A tract ($r = 0.113$, $p_{FDR} = 0.4$) or the CST ($r = 0.033$, $p_{FDR} = 0.75$). Plots and tract visualization are provided in Figure 3. The association of FA SLF and zSDMT remained significant after lesion exclusion ($r = 0.25$, $p_{FDR} = 0.04$). zSDMT and FA of tracts from the HCs (each $p > 0.2$) showed no relevant association.

Linear regression analysis

The stepwise linear regression model with zSDMT as a dependent variable revealed EDSS ($\beta = -0.365$, $p < 0.001$) and white matter volume ($\beta = 0.223$, $p = 0.02$) as significant independent variables ($R^2 = 0.221$, $p < 0.001$) for the MS patients.

Discussion

With our hypothesis-driven approach, we demonstrated a positive association between processing speed performance and white matter tract integrity for the SLF, which emphasizes the importance of intact frontoparietal structural connectivity for information processing speed performance. The significance remaining after lesion exclusion also indicates that the tract integrity depends not only on white matter lesions, but also on the NAWM.

For MS, several studies have investigated the relationship between white matter integrity and cognition, especially for processing speed (37–39). Cognitively impaired MS patients have been shown to have decreased FA values compared to unimpaired patients and controls at both the whole-brain level (37) and within several anatomically defined white matter regions, especially the corpus callosum, SLF, and internal capsule (7, 8).

Here, we focused on white matter tracts based on existing imaging studies on information processing speed performance in MS patients (11, 17). Based on the literature, BA7A is a crucial area for spatial attention and visuomotor control (15, 19) and of high importance for performance on the SDMT (17). Using probabilistic tractography in our cohort of 100 MS patients, we demonstrated that the integrity of this tract differs between MS patients and HCs but in contrast to our assumptions, no significant association was demonstrated between tract integrity and SDMT performance in the MS patients. We defined the tract bundle based on the anatomical maps of BA7A, resulting in a structural network merging with the posterior corona radiate, splenium and body of the corpus callosum, SLF, and the posterior and retrolenticular part of the internal capsule. This widespread structural network connecting frontal, temporal, and cerebellar regions (15) may be only partially involved in processing speed, resulting in low specificity of this predefined tract for the SDMT.

The tract originating in BA7A largely merges into the SLF. The SLF, and especially its subdivisions SLF I and SLF II, are mainly interconnecting frontal and parietal regions (16). The mean FA value of the SLF in our cohort did not differ between the groups, but the association between the mean FA and the individual SDMT score revealed a significant, albeit not strong correlation. Interestingly, this significance remained even after exclusion of the lesions within the tract. A few studies have suggested a role of the SLF in cognition in MS (8, 40), but these approaches did not test for specific tracts and did not control for lesions within the tract. Our data in this way confirm the importance of parietal white matter tract bundles for cognition in MS, and highlight the contribution of the NAWM tract

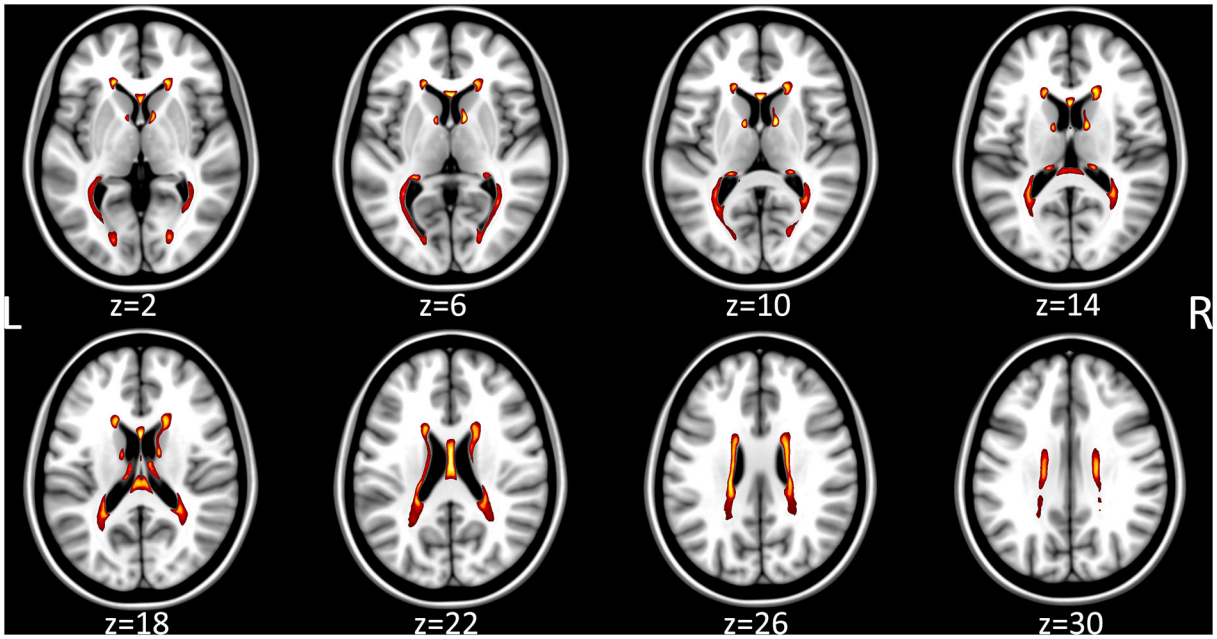

FIGURE 2
Heatmap of the individual multiple sclerosis lesion maps, which were transformed into MNI template space, averaged voxel-wise, thresholded to 25% and color-coded (white 100% overlap, red 25% overlap). Axial slice position is indicated below the MRI respectively.

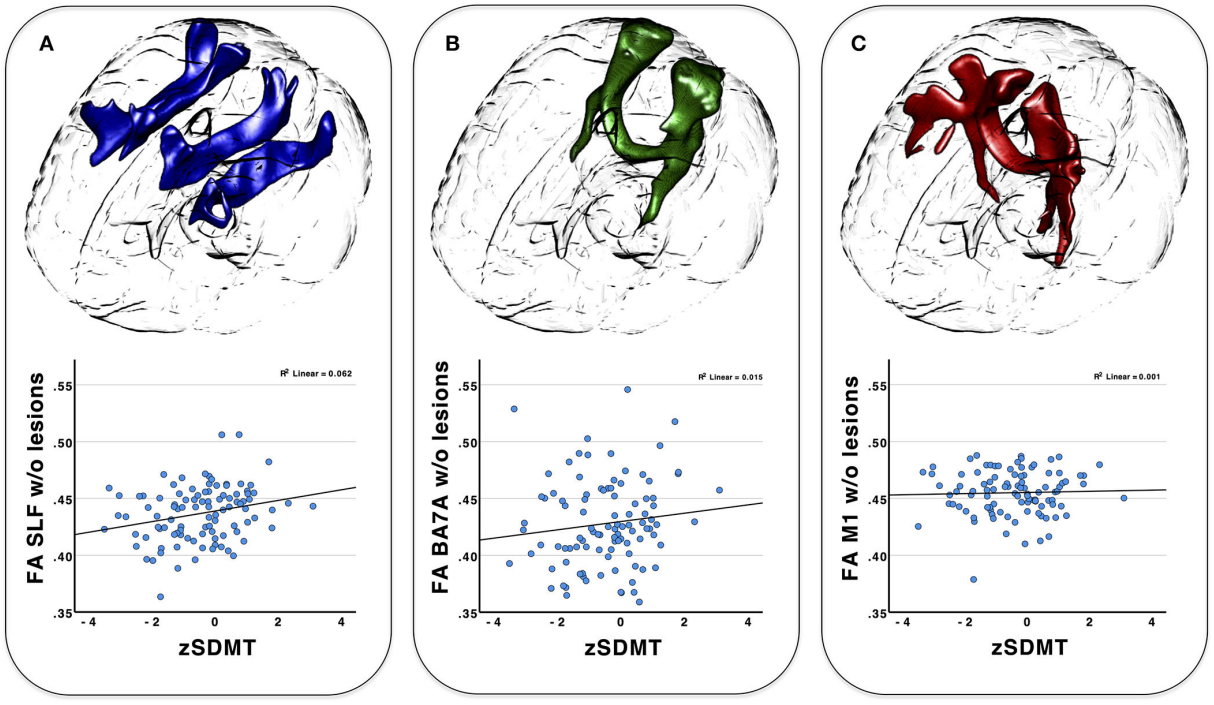

FIGURE 3
3D-tractogram of all three tracts investigated (top) and the plotted correlation of behavioral data (SDMT) with the weighted mean FA of the tracts after lesion exclusion (bottom). **(A)** superior longitudinal fasciculus (SLF); **(B)** BA7A tract; **(C)** corticospinal tract (CST).

integrity on clinical impairment (41, 42). We are aware that several other studies did not find any associations between SDMT and frontoparietal tracts (43, 44), but especially as we used a hypothesis driven approach, we highlight the importance of these tract bundles for cognition in MS.

In MS patients, myelin content and axon count within the NAWM correlate with FA (45, 46). Our data suggest that these alterations may lead to clinical impairment even if FA of the tract does not differ between the patients and controls, and that the alterations within the SLF are important for the clinical impairments.

Using a linear regression model, we demonstrated that disability and total white matter volume, not the integrity of presumed tracts, are the most important variables for processing speed. These findings were unexpected, especially as it is somewhat different from other studies (47). The disability and white matter volume as significant predictors for processing speed in our mildly disabled cohort highlight the importance of an intact structural network that extends beyond the tracts investigated in our study. Therefore, the contribution of parietal white matter tracts like the SLF should be considered in a larger structural network. Another possible explanation is that the structural alteration of the parietal tact was not so severe, especially for the SLF, as the FA was not significant different between the patients and the controls. The relationship with disease disability conceptualized with the EDSS, though known in principle (1, 38), was also somewhat surprising because our cohort was generally only mildly impaired with a median EDSS of 2.0. Both clinical and structural variables are contributing differentially on cognitive impairments in MS depending on increasing disability (48, 49), and future research should also focus especially on the NAWM pathology and their role in cognitive impairment in MS. In addition, as we focused on white matter alterations and their importance in processing speed, we only added the total gray matter volume as an independent variable, but we are aware of the importance of gray matter, especially deep gray matter volume, on cognition (8, 38). Other clinical variables in our cohort of moderately fatigued and minimally depressed patients could not explain the additional variance in our model.

Our study has several limitations. The main limitation is the selection of only a limited number of tracts. Keeping in mind that cognitive speed is dependent on a network of interacting neural resources and not limited to one or two structures, our hypothesis-driven approach showed the expected contribution of the SLF, but not the BA7A tract, in task ability. In addition, the level of disability in our cohort was rather low, which might affect the generalizability of our results. Furthermore, the used lesion segmentation algorithm only detects white matter hyperintensities, that cannot definitely be declared as MS related or of other origin like vascular. Future research has to combine functional and structural connectivity measurements to confirm our results in independent samples. Finally, the acquired diffusion data lacks technical merits, as at the time of acquisition only older protocols and sequences were available with a rather long echo time, only one b0-image and no inverse phase-encoded b0-image (or whole dataset) for distortion or noise correction.

In conclusion, we demonstrated that the structural integrity of the NAWM parts of the SLF is associated with processing speed in mildly impaired MS patients. The structural alterations also in NAWM should be kept in mind for future research into the underlying processes of information processing speed in MS as well as for therapeutic approaches such as noninvasive brain stimulation.

Data availability statement

The raw data supporting the conclusions of this article will be made available by the authors, without undue reservation.

Ethics statement

The studies involving human participants were reviewed and approved by Ethics Committee of the Medical Faculty of the University of Greifswald. The patients/participants provided their written informed consent to participate in this study.

Author contributions

MG and ML contributed to the study conception and design. MG and MD performed material preparation, data collection, and analysis. MG written the first draft of the manuscript. KK and KH measured and tested healthy controls. SL and MK helped with MRI of MS patients. All authors commented on previous versions of the manuscript, read, and approved the final manuscript.

Conflict of interest

MG received honoraria or speaking fees from Biogen, Celgene, Merck Serono, Novartis, Roche, Sanofi Genzyme, and Teva. IP has received honoraria for speaking at scientific meetings, serving on scientific advisory boards, and consulting activities from Adamas Pharma, Almirall, Bayer Pharma, Biogen, BMS, Celgene, Desitin, Sanofi-Genzyme, Janssen, Merck, Novartis, Roche, and Teva. She has also received research support from the German MS Society, Celgene, Novartis, Roche, and Teva. ML is a paid editor for the Thieme Verlag.

The remaining authors declare that the research was conducted in the absence of any commercial or financial relationships that could be construed as a potential conflict of interest.

Publisher's note

References

1. Chiaravalloti ND, DeLuca J. Cognitive impairment in multiple sclerosis. *Lancet Neurol.* (2008) 7:1139–51. doi: 10.1016/S1474-4422(08)70259-X

2. Amato MP, Bartolozzi ML, Zipoli V, Portaccio E, Mortilla M, Guidi L, et al. Neocortical volume decrease in relapsing-remitting MS patients with mild cognitive impairment. *Neurology.* (2004) 63:89–93. doi: 10.1212/01.WNL.0000129544.79539.D5

3. Benedict RH, Bruce JM, Dwyer MG, Abdelrahman N, Hussein S, Weinstock-Guttman B, et al. Neocortical atrophy, third ventricular width, and cognitive dysfunction in multiple sclerosis. *Arch Neurol.* (2006) 63:1301–6. doi: 10.1001/archneur.63.9.1301

4. Patti F, Amato MP, Trojano M, Bastianello S, Tola MR, Goretti B, et al. Cognitive impairment and its relation with disease measures in mildly disabled patients with relapsing-remitting multiple sclerosis: baseline results from the Cognitive Impairment in Multiple Sclerosis (COGIMUS) study. *Mult Scler.* (2009) 15:779–88. doi: 10.1177/1352458509105544

5. Reuter F, Zaaraoui W, Crespy L, Faivre A, Rico A, Malikova I, et al. Cognitive impairment at the onset of multiple sclerosis: relationship to lesion location. *Mult Scler.* (2011) 17:755–8. doi: 10.1177/1352458511398265

6. Smith SM, Jenkinson M, Johansen-Berg H, Rueckert D, Nichols TE, Mackay CE, et al. Tract-based spatial statistics: voxelwise analysis of multi-subject diffusion data. *Neuroimage.* (2006) 31:1487–505. doi: 10.1016/j.neuroimage.2006.02.024

7. Yu HJ, Christodoulou C, Bhise V, Greenblatt D, Patel Y, Serafin D, et al. Multiple white matter tract abnormalities underlie cognitive impairment in RRMS. *Neuroimage.* (2012) 59:3713–22. doi: 10.1016/j.neuroimage.2011.10.053

8. Riccitelli GC, Pagani E, Rodegher M, Colombo B, Preziosa P, Falini A, et al. Imaging patterns of gray and white matter abnormalities associated with PASAT and SDMT performance in relapsing-remitting multiple sclerosis. *Mult Scler.* (2019) 25:204–16. doi: 10.1177/1352458517743091

9. Benedict RH, DeLuca J, Phillips G, LaRocca N, Hudson LD, Rudick R, et al. Validity of the Symbol Digit Modalities Test as a cognition performance outcome measure for multiple sclerosis. *Mult Scler.* (2017) 23:721–33. doi: 10.1177/1352458517690821

10. Smith A. *Symbol Digit Modalities Test: Manual.* Los Angeles, CA: Western Psychological Services (1982).

11. Silva PHR, Spedo CT, Barreira AA, Leoni RF. Symbol digit modalities test adaptation for magnetic resonance imaging environment: a systematic review and meta-analysis. *Mult Scler Relat Disord.* (2018) 20:136–43. doi: 10.1016/j.msard.2018.01.014

12. Forn C, Belenguer A, Belloch V, Sanjuan A, Parcet MA, Avila C. Anatomical and functional differences between the paced auditory serial addition test and the symbol digit modalities test. *J Clin Exp Neuropsychol.* (2011) 33:42–50. doi: 10.1080/13803395.2010.481620

13. Forn C, Belloch V, Bustamante JC, Garbin G, Parcet-Ibars MA, Sanjuan A, et al. A symbol digit modalities test version suitable for functional MRI studies. *Neurosci Lett.* (2009) 456:11–4. doi: 10.1016/j.neulet.2009.03.081

14. Thiebaut de. Schotten M, Dell'Acqua F, Valabregue R, Catani M. Monkey to human comparative anatomy of the frontal lobe association tracts. *Cortex.* (2012) 48:82–96. doi: 10.1016/j.cortex.2011.10.001

15. Wang J, Yang Y, Fan L, Xu J, Li C, Liu Y, et al. Convergent functional architecture of the superior parietal lobule unraveled with multimodal neuroimaging approaches. *Hum Brain Mapp.* (2015) 36:238–57. doi: 10.1002/hbm.22626

16. Wang X, Pathak S, Stefaneanu L, Yeh FC Li S, Fernandez-Miranda JC. Subcomponents and connectivity of the superior longitudinal fasciculus in the human brain. *Brain Struct Funct.* (2016) 221:2075–92. doi: 10.07/s00429-015-1028-5

17. Grothe M, Domin M, Hoffeld K, Nagels G, Lotze M. Functional representation of the symbol digit modalities test in relapsing remitting multiple sclerosis. *Mult Scler Relat Disord.* (2020) 43:102159. doi: 10.1016/j.msard.2020.102159

18. Scheperjans F, Eickhoff SB, Homke L, Mohlberg H, Hermann K, Amunts K, et al. Probabilistic maps, morphometry, and variability of cytoarchitectonic areas in the human superior parietal cortex. *Cereb Cortex.* (2008) 18:2141–57. doi: 10.93/cercor/bhm241

19. Culham JC, Valyear KF. Human parietal cortex in action. *Curr Opin Neurobiol.* (2006) 16:205–12. doi: 10.1016/j.conb.2006.03.005

20. Costa SL, Genova HM, DeLuca J, Chiaravalloti ND. Information processing speed in multiple sclerosis: past, present, and future. *Mult Scler.* (2017) 23:772–89. doi: 10.1177/1352458516645869

21. Ding S, Guo Y, Chen X, Du S, Han Y, Yan Z, et al. Demyelination and remyelination detected in an alternative cuprizone mouse model of multiple sclerosis with 70 T multiparameter magnetic resonance imaging. *Sci Rep.* (2021) 11:11060. doi: 10.1038/s41598-021-90597-6

22. Kern KC, Sarcona J, Montag M, Giesser BS, Sicotte NL. Corpus callosal diffusivity predicts motor impairment in relapsing-remitting multiple sclerosis: a TBSS and tractography study. *Neuroimage.* (2011) 55:1169–77. doi: 10.1016/j.neuroimage.2010.10.077

23. Ozturk A, Smith SA, Gordon-Lipkin EM, Harrison DM, Shiee N, Pham DL, et al. MRI of the corpus callosum in multiple sclerosis: association with disability. *Mult Scler.* (2010) 16:166–77. doi: 10.1177/1352458509353649

24. Werring DJ, Clark CA, Barker GJ, Thompson AJ, Miller DH. Diffusion tensor imaging of lesions and normal-appearing white matter in multiple sclerosis. *Neurology.* (1999) 52:1626–32. doi: 10.1212/wnl.52.8.1626

25. Thompson AJ, Banwell BL, Barkhof F, Carroll WM, Coetzee T, Comi G, et al. Diagnosis of multiple sclerosis 2017: revisions of the McDonald criteria. *Lancet Neurol.* (2018) 17:162–73. doi: 10.1016/S1474-4422(17)30470-2

26. Kurtzke JF. Rating neurologic impairment in multiple sclerosis: an expanded disability status scale (EDSS). *Neurology.* (1983) 33:1444–52. doi: 10.1212/wnl.33.11.1444

27. Beck AT, Steer RA, Brown GK. *Manual for the Beck Depression Inventory-II.* San Antonio, TX: The Psychological Cooperation Inc. (1996). doi: 10.1037/t00742-000

28. Penner IK, Raselli C, Stocklin M, Opwis K, Kappos L, Calabrese P. The Fatigue Scale for Motor and Cognitive Functions (FSMC): validation of a new instrument to assess multiple sclerosis-related fatigue. *Mult Scler.* (2009) 15:1509–17. doi: 10.1177/1352458509348519

29. Schmidt P. *Bayesian Inference for Structured Additive Regression Models for Large-scale Problems with Applications to Medical Imaging.* [Dissertation]. Munich: LMU München (2017).

30. Avants BB, Tustison NJ, Song G, Cook PA, Klein A, Gee JC, et al. reproducible evaluation of ANTs similarity metric performance in brain image registration. *Neuroimage.* (2011) 54:2033–44. doi: 10.1016/j.neuroimage.2010.09.025

31. Eickhoff SB, Paus T, Caspers S, Grosbras MH, Evans AC, Zilles K, et al. Assignment of functional activations to probabilistic cytoarchitectonic areas revisited. *Neuroimage.* (2007) 36:511–21. doi: 10.1016/j.neuroimage.2007.03.060

32. Fan L, Li H, Zhuo J, Zhang Y, Wang J, Chen L, et al. The human brainnetome atlas: a new brain atlas based on connectional architecture. *Cereb Cortex.* (2016) 26:3508–26. doi: 10.1093/cercor/bhw157

33. Warrington S, Bryant KL, Khrapitchev AA, Sallet J, Charquero-Ballester M, Douaud G, et al. XTRACT - standardised protocols for automated tractography in the human and macaque brain. *Neuroimage.* (2020) 217:116923. doi: 10.1016/j.neuroimage.2020.116923

34. Behrens TE, Woolrich MW, Jenkinson M, Johansen-Berg H, Nunes RG, Clare S, et al. Characterization and propagation of uncertainty in diffusion-weighted MR imaging. *Magn Reson Med.* (2003) 50:1077–88: doi: 10.1002/mrm.10609

35. Jbabdi S, Sotiropoulos SN, Savio AM, Grana M, Behrens TE. Model-based analysis of multishell diffusion MR data for tractography: how to get over fitting problems. *Magn Reson Med.* (2012) 68:1846–55. doi: 10.1002/mrm.24204

36. Scherer P, Baum K, Bauer H, Gohler H, Miltenburger C. [Normalization of the Brief Repeatable Battery of Neuropsychological tests (BRB-N) for German-speaking regions. Application in relapsing-remitting and secondary progressive multiple sclerosis patients]. *Nervenarzt.* (2004) 75:984–90. doi: 10.1007/s00115-004-1729-0

37. Meijer KA, van Geest Q, Eijlers AJC, Geurts JJG, Schoonheim MM, Hulst HE. Is impaired information processing speed a matter of structural or functional damage in MS? *Neuroimage Clin.* (2018) 20:844–50. doi: 10.1016/j.nicl.2018.09.021

38. Benedict RHB, Amato MP, DeLuca J, Geurts JJG. Cognitive impairment in multiple sclerosis: clinical management, MRI, and therapeutic avenues. *Lancet Neurol.* (2020) 19:860–71. doi: 10.1016/S1474-4422(20)30277-5

39. Has Silemek AC, Fischer L, Pottgen J, Penner IK, Engel AK, Heesen C, et al. Functional and structural connectivity substrates of cognitive performance in relapsing remitting multiple sclerosis with mild disability. *Neuroimage Clin.* (2020) 25:102177. doi: 10.1016/j.nicl.2020.102177

40. Manca R, Stabile MR, Bevilacqua F, Cadorin C, Piccione F, Sharrack B, et al. Cognitive speed and white matter integrity in secondary progressive multiple sclerosis. *Mult Scler Relat Disord.* (2019) 30:198–207. doi: 10.1016/j.msard.2019.02.021

41. de Kouchkovsky I, Fieremans E, Fleysher L, Herbert J, Grossman RI, Inglese M. Quantification of normal-appearing white matter tract integrity in multiple sclerosis: a diffusion kurtosis imaging study. *J Neurol.* (2016) 263:1146–55. doi: 10. 1007/s00415-016-8118-z

42. Schiavi S, Petracca M, Sun P, Fleysher L, Cocozza S, El Mendili MM, et al. Non-invasive quantification of inflammation, axonal and myelin injury in multiple sclerosis. *Brain.* (2021) 144:213–23. doi: 10.1093/brain/awaa381

43. Abel S, Vavasour I, Lee LE, Johnson P, Ackermans N, Chan J, et al. Myelin damage in normal appearing white matter contributes to impaired cognitive processing speed in multiple sclerosis. *J Neuroimaging.* (2020) 30:205–11. doi: 10.1111/jon.12679

44. Govindarajan ST, Liu Y, Parra Corral MA, Bangiyev L, Krupp L, Charvet L, et al. White matter correlates of slowed information processing speed in unimpaired multiple sclerosis patients with young age onset. *Brain Imaging Behav.* (2021) 15:1460–68. doi: 10.1007/s11682-020-00345-z

45. Schmierer K, Wheeler-Kingshott CA, Boulby PA, Scaravilli F, Altmann DR, Barker GJ, et al. Diffusion tensor imaging of post mortem multiple sclerosis brain. *Neuroimage.* (2007) 35:467–77. doi: 10.1016/j.neuroimage.2006.12.010

46. Filippi M, Rocca MA, Barkhof F, Bruck W, Chen JT, Comi G, et al. Association between pathological and MRI findings in multiple sclerosis. *Lancet Neurol.* (2012) 11:349–60. doi: 10.1016/S1474-4422(12)70003-0

47. Sbardella E, Petsas N, Tona F, Prosperini L, Raz E, Pace G, et al. Assessing the correlation between grey and white matter damage with motor and cognitive impairment in multiple sclerosis patients. *PLoS ONE.* (2013) 8:e63250. doi: 10.1371/journal.pone.0063250

48. Grzegorski T, Losy J. Cognitive impairment in multiple sclerosis - a review of current knowledge and recent research. *Rev Neurosci.* (2017). 28:845–60. doi: 10.1515/revneuro-2017-0011

49. Sumowski JF, Benedict R, Enzinger C, Filippi M, Geurts JJ, Hamalainen P, et al. Cognition in multiple sclerosis: state of the field and priorities for the future. *Neurology.* (2018) 90:278–88. doi: 10.1212/WNL.0000000000004977

frontiers | Frontiers in Neurology

TYPE Case Report
PUBLISHED 17 March 2023
DOI 10.3389/fneur.2023.1142734

OPEN ACCESS

EDITED BY
Alessia Sarica,
University of Magna Graecia,
Italy

REVIEWED BY
Lei Gao,
Wuhan University,
China
Paolo Bonanni,
Eugenio Medea (IRCCS),
Italy

*CORRESPONDENCE
Maurizio Corbetta
✉ maurizio.corbetta@unipd.it

SPECIALTY SECTION
This article was submitted to Applied Neuroimaging, a section of the journal Frontiers in Neurology

RECEIVED 12 January 2023
ACCEPTED 03 March 2023
PUBLISHED 17 March 2023

CITATION
Monai E, Silvestri E, Bisio M, Cagnin A, Aiello M, Cecchin D, Bertoldo A and Corbetta M (2023) Case report: Multiple disconnection patterns revealed by a multi-modal analysis explained behavior after a focal frontal damage. *Front. Neurol.* 14:1142734. doi: 10.3389/fneur.2023.1142734

Case report: Multiple disconnection patterns revealed by a multi-modal analysis explained behavior after a focal frontal damage

Elena Monai[1,2], Erica Silvestri[3,4], Marta Bisio[4,5], Annachiara Cagnin[1,2,4], Marco Aiello[6], Diego Cecchin[4,7], Alessandra Bertoldo[3,4] and Maurizio Corbetta[1,2,4,8]*

[1]Clinica Neurologica, University Hospital of Padova, Padua, Italy, [2]Department of Neuroscience, University of Padova, Padua, Italy, [3]Department of Information Engineering, University of Padova, Padua, Italy, [4]Padova Neuroscience Center (PNC), University of Padova, Padua, Italy, [5]Department of Biomedical Sciences, University of Padova, Padua, Italy, [6]IRCCS SDN, Naples, Italy, [7]Nuclear Medicine Unit, Department of Medicine, University Hospital of Padova, Padua, Italy, [8]Venetian Institute of Molecular Medicine (VIMM), Padua, Italy

Introduction: There is overwhelming evidence that focal lesions cause structural, metabolic, functional, and electrical disconnection of regions directly and indirectly connected with the site of injury. Unfortunately, methods to study disconnection (positron emission tomography, structural and functional magnetic resonance imaging, electroencephalography) have been applied primarily in isolation without capturing their interaction. Moreover, multi-modal imaging studies applied to focal lesions are rare.

Case report: We analyzed with a multi-modal approach the case of a patient presenting with borderline cognitive deficits across multiple domains and recurrent delirium. A post-surgical focal frontal lesion was evident based on the brain anatomical MRI. However, we were able to acquire also simultaneous MRI (structural and functional) and [18F]FDG using a hybrid PET/MRI scan along with EEG recordings. Despite the focality of the primary anatomical lesion, structural disconnection in the white matter bundles extended far beyond the lesion and showed a topographical match with the cortical glucose hypometabolism seen both locally and remotely, in posterior cortices. Similarly, a right frontal delta activity near/at the region of structural damage was associated with alterations of distant occipital alpha power. Moreover, functional MRI revealed even more widespread local and distant synchronization, involving also regions not affected by the structural/metabolic/electrical impairment.

Conclusion: Overall, this exemplary multi-modal case study illustrates how a focal brain lesion causes a multiplicity of disconnection and functional impairments that extend beyond the borders of the anatomical irrecoverable damage. These effects were relevant to explain patient's behavior and may be potential targets of neuro-modulation strategies.

KEYWORDS

disconnection, multi-modal mapping, networks, brain lesion, behavior

1. Introduction

There is overwhelming evidence that local structural damage induces structural and functional disconnection effects remotely from the site of injury (1–4) hence directly supporting Von Monakow's concept of diaschisis (5, 6).

The discovery of remote physiological alterations and their behavioral effects has been documented in neuroscience research over the last 40 years using several methods (7) that are available in the clinical setting. Among these, measures of glucose metabolism with positron emission tomography (PET) (8, 9); alterations of local activity and inter-regional correlation among brain regions or networks through resting-state fMRI (rs-fMRI) (2, 4, 10–12); structural disconnection (SDC) with diffusion imaging or structural connectome atlas (13–15); and finally, electrophysiological alterations with electroencephalography (EEG) (16–18). However, most investigations have been conducted using these methods in isolation or partial combination (19–21), with the result that a clear understanding of how different signals relate to each other is missing (22, 23).

An understanding of the relationship among multiple type of disconnection has wide relevance in clinical neuroscience (24–30).

Moreover, a detailed investigation at the level of single subjects represents an opportunity to improve our knowledge of structure–function relationships and an opportunity to differentiate between the irreversible anatomical damage and network-related functional impairment.

Relevantly, the latter may benefit of neuro-modulatory strategies in patients with focal lesions (31).

We report here a patient with a post-surgical focal lesion of the right medial frontal lobe and fornix after craniopharyngioma excision whose disconnection was studied with multiple brain imaging methodologies. His cognitive profile showed borderline performance across multiple cognitive domains. In addition, the patient presented recurrent delirium with VHs with worsening cognitive performance.

We acquired simultaneous structural and functional MRI and [^{18}F]FDG metabolic information using a hybrid PET/MRI scan along with multiple neuropsychological evaluations (NPEs) and EEGs (obtained both in and out of the delirium episodes). This allowed us to document local and remote disconnection and metabolic effects as well as the dynamic of electrophysiological abnormalities that explained patient's behavior.

2. Materials and methods

2.1. Case description

The patient, a 52-year-old man, underwent brain surgery *via* craniotomy for craniopharyngioma a year and a half before the study. Brain MRI after surgery showed post-surgical damage in the right frontal lobe (Supplementary Figure S1). Hormonal replacement therapy was started due to post-surgical hypopituitarism. At home, the family, and the patient himself noted problems with episodic memory. Nine months after surgery he underwent an EEG recording (EEG1). One year and a half after surgery he was admitted due to his first episode of delirium with visual hallucinations.

The patient presented with psychomotor slowing, drowsiness, spatiotemporal disorientation and the development of a psychotic state with agitation and disorganized thoughts. Two EEGs, a structural MRI and a NPE were performed during delirium, respectively at 3 (EEG2) and 12 (EEG3), 9, and 11 days after admission. There was bilateral slowing on the EEG during delirium (Supplementary Figure S2).

A systemic infection with a raise in serum inflammatory indices was detected. Cerebral spinal fluid was negative for infections and neuro-degenerative markers. He recovered from delirium after 15 days from admission, after treatment with a cycle of antibiotics and antipsychotics (risperidone). He was discharged after 28 days. At day 20 of admission, when delirium symptoms were resolved, he underwent an integrated [^{18}F]FDG PET/MRI scan and, 4 days and 1 month later, repeated NPEs. A total of 14 months after the first episode, another frank episode of delirium occurred with disorientation, agitation and disorganized thoughts, and the patient underwent another EEG (EEG4) the day after symptoms' acme (day 7 of admission). This second episode of delirium lasted for 8 days and resolved after treatment with haloperidol.

2.2. Neuropsychological assessment

Neuropsychological evaluations were obtained during delirium, out of delirium on day 24 after admission and at 1 month after discharge at his baseline. Patient performed a multiple domain battery consisting of memory, attention, executive functions, language, and visuo-spatial sections (Supplementary Table S1; Supplementary Figure S3).

2.3. Pet/MRI data details

A simultaneous hybrid [^{18}F]FDG PET/MRI scan was acquired on a Siemens Biograph mMR (Siemens Healthcare, Erlangen, Germany) equipped with a PET compatible 16-channels head–neck coil.

The MR imaging protocol included: (a) a T1-weighted image (TR/TE 2400/3.2 ms, voxel 1x1x1mm^3), (b) a T2-weighted image (TR/TE 3200/536 ms, voxel 1 mm × 1 mm × 1 mm), (c) a T2-weighted Fluid Attenuated Inversion Recovery (FLAIR, TR/TE 5000/395 ms, voxel 1 mm × 1 mm × 1 mm), and (d) 10 min of eyes-open resting state fMRI (rs-fMRI: TR/TE 1100/30 ms, voxel 3 mm × 3 mm × 3 mm, 40 slices).

PET imaging started 45 min after the [^{18}F]FDG intravenous bolus injection and lasted 20 min. The PET static image (voxel size 2.8×2.8×2.0 mm^3) was reconstructed off-line by means of the Siemens e7-tool software according to (31).

Two different datasets were used as healthy control groups. For the rs-fMRI data, we used 308 subjects (125 females; mean age 36.96 ± 18.40 years) of the publicly available MPI-Leipzig Mind-Brain–Body (LEMON) dataset (32, 33).

For the PET data set, the healthy control group (henceforth PET HC dataset) consisted of 26 subjects (16 females, age range 40–78 years) from a previous study by Aiello and colleagues (34). PET measurements started 30 min post injection and acquired for 15 min with reconstruction voxel size of 1.12 × 1.12 × 2.03 mm.

2.4. MRI data: Methods and analyses

The patient's lesion was manually segmented on structural MRI scan (T1-weighted, considering also FLAIR and T2-weighted sequences) using the itk-SNAP software.[1]

The lesion mask was non-linearly mapped into the MNI152 standard space and the SDC map was calculated with BCB toolkit (14) using the default set of healthy controls. We identified the most affected white matter (WM) tracts by computing the percentage overlap between the SDC map and each anatomical tract provided by the toolbox (a full list of tracts is reported in the Supplementary Table S2) and normalizing for the volume of the tract. A tract with a volume involvement of more than 10% was considered to be severely impaired.

Functional scans underwent a state-of-the-art preprocessing as in (35). In addition, a high pass filtering (cutoff frequency 0.008 Hz) and an independent component analysis (ICA)-based denoising (36) were performed to remove further sources of noise.

The functional data were used to extract three main measures: 1) the spatial pattern and strength of the main resting state networks (RSNs); 2) their inter-network connectivity; and 3) the local activity synchronization.

To address the first two, we followed the same procedure as in Silvestri et al. (37). Overall, 45 independent components (IC) were identified as representative of intrinsic connectivity networks (or RSNs) and grouped into 10 different networks: visual (VIS), sensorimotor (SMN), auditory (AUD), cingulo-opercular (CON), dorsal-attention (DAN), frontoparietal (FPN), default mode (DMN), cognitive control (CCN), frontal (FRN) and language (LANG) network. Components were estimated at the single subject level through the group guided ICA (38). Then, modification of RSNs spatial pattern and strength were quantified using the cosine similarity (CSM) between patient's and group's independent component maps. Statistically significant alterations were assessed comparing the patient's CSM value with the empirical statistical distribution of the CSM obtained in the control dataset within a permutation test framework (50,000 permutations, threshold of-2 standard deviations from the HC average CSM, significance level 0.05).

In both the patient and each HC subject, the inter-network connectivity was quantified computing the Person's correlation between each pair of independent components (RSN) time courses. For statistical purposes, the correlation values were z-Fisher transformed. As for intrinsic connectivity: significantly hyper-or hypo-connected couple of RSNs were detected by comparing the strength of each inter-network connection with the empirical statistical distribution of this connection in the control group (50,000 permutations, threshold of ±2 standard deviations from the HC average, significance level 0.05).

Finally, we computed the regional homogeneity (ReHo) of the resting state functional signal, a measure of local activity synchronization, as introduced in (39). The ReHo measures were computed in regions of interest (ROI) of the Hammersmith anatomical atlas (40) averaging voxel-wise ReHo values within each region. With a permutation test framework, hyper-or hypo-integrated ROIs were detected as regions with ReHo values outside of the normal range of average ReHo ±2 standard deviations (50,000 permutations, significance level 0.05).

1 http://www.itksnap.org/

2.5. Pet data: Quantification and statistical analysis

Since the patient and control PET data were acquired using the same scanner but with slightly different protocols, we designed an analysis strategy less sensitive to acquisition protocols. The [^{18}F]FDG standard uptake value ratio (SUVR) was computed on both dataset using the pons [as defined in the Hammersmith atlas (40)] as reference region. Next, regional changes of brain metabolism were estimated at the ROI-wise level though the metabolic laterality index (LI). As for ReHo, ROIs were defined according to the Hammersmith atlas for the gray matter. The SUVR values at the voxel level were averaged within each ROI (i), and a LI was computed as the difference between each left hemisphere ROI and its homologous regions in the right hemisphere normalized by the sum of the SUVR of the two regions:

$$LI_i = \frac{SUVR_{i,L} - SUVR_{i,R}}{SUVR_{i,L} + SUVR_{i,R}}.$$

Hence, since the lesion was in the right hemisphere, a positive LI indicates a relative hypometabolism in the damaged (right) hemisphere, as compared to the undamaged (left) hemisphere. Regions with significant hypo/hyper metabolism were identified by comparing each patient's ROI LI with an empirical distribution of the same ROI LI in the PET HC dataset. Using a permutation test framework (50,000 permutations, threshold of ±2 standard deviations from the PET HC average, significance level 0.05).

2.6. Electroencephalography data: Detailed description and analyses

EEG were recorded using 21 electrodes placed according to the standard 10–20 international system.

All the sessions consisted of about 20 min of resting state activity during which the patient was asked to rest and keep his eyes closed. Raw EEG data underwent the following pre-processing in EEGLAB toolbox (41): high-pass filtering with a cut-off frequency of 0.5 Hz; low-pass filtering with a cut-off frequency of 45 Hz; re-referencing using the average signal as reference (42); ICA computation (43).

In addition, a visual inspection was carried out to mark and delete additional bad temporal epochs (44). The rest of the analysis was then carried out on post-processed clean data.

We ran a power spectral density analysis in four consecutive frequency bands: delta (1÷4 Hz), theta (4÷8 Hz), alpha (8÷13 Hz), and beta (13÷20 Hz) (45).

3. Results

3.1. Neuropsychology

At his baseline, the patient was oriented to space/person, and partially to time. The NPE highlighted borderline performance in multiple cognitive domains including memory, executive, and visuo-spatial functions (Supplementary Figure S3).

During delirium he showed severe attentive, executive, memory, and visuo-spatial deficits (Supplementary Figure S3), and visual hallucinations.

At day 25 post-admission he underwent a multi-domain NPE that showed a substantial return to baseline condition (Supplementary Table S1). A total of 14 months later, he suffered a second episode of delirium. At that time no neuropsychology was obtained.

3.2. Lesion, structural disconnection, and hypometabolism

The structural lesion was limited to anterior mesial region located along a track between the right posterior dorsolateral part of the superior frontal gyrus (SFG) and the hypothalamus, passing through the anterior cingulate, the anterior portion of the corpus callosum (CC), and the fornix (Figure 1A).

This lesion was associated with widespread WM tract disconnection in both anterior and posterior regions of the brain. The disconnection was predominant in the ipsilesional hemisphere with a partial contralateral extension due to the involvement of the CC, fornix and anterior commissure (Figure 1A). Among the significantly disconnected tracts there were FST (fronto-striatal tract), ATP (anterior thalamic projection), OR (optic radiation), FAT (fronto-aslant tract), SFG (see Supplementary Table S2 for all significantly disconnected tracts).

Overall, the lesioned hemisphere showed a relative hypometabolism (Supplementary Figure S4) as compared to the contralateral. The regions with a statistically significant relative hypometabolism were adjacent to the lesion like the SFG or along the medial wall like the posterior cingulate cortex (PCC). Homolateral subcortical regions like thalamus, putamen, and caudate were also affected. Finally, remote regions in the occipital cortex (lingual gyrus and cuneus) were hypometabolic (Figure 1B). When we examined the pattern of SDC vis-à-vis the map of significantly hypometabolic regions, we found a good topographic match between the WM disconnections and the relative reduced metabolism of the cortical and subcortical areas linked by the impaired bundles (Figure 1B). This match was even more evident when looking at unthresholded maps of structural disconnection (Supplementary Figure S5). Of note, regions that were bilaterally disconnected, as medial prefrontal cortices (mPFC), showed on the [^{18}F]FDG PET SUVR map an hypometabolism not captured by the LI (Figure 1B; Supplementary Figure S6).

3.3. Alterations of functional connectivity and local synchronization

Figure 2 (top) shows representative altered components for the most five affected RSNs (VIS, DMN, DAN, FPN and CCN; Supplementary Figures S7, S8 shows all altered components).

We also analyzed the FC within-between components divided by RSN. Figure 2 (bottom) shows the FC matrix of the group of healthy controls vs. that of the patient, and the statistically significant altered connections based on a permutation test. The VIS network was the most affected in terms of number of altered connections ($n = 13$), even though visual regions were farther away from the primary lesion. Within DAN, FPN, CCN, FRN alterations also occurred. The VIS network lost connectivity with many non-sensory networks as DAN, DMN, CON, CCN and FPN. Links between DMN and DAN and DMN and FPN were additionally impaired. Of relevance, the altered connections also involved

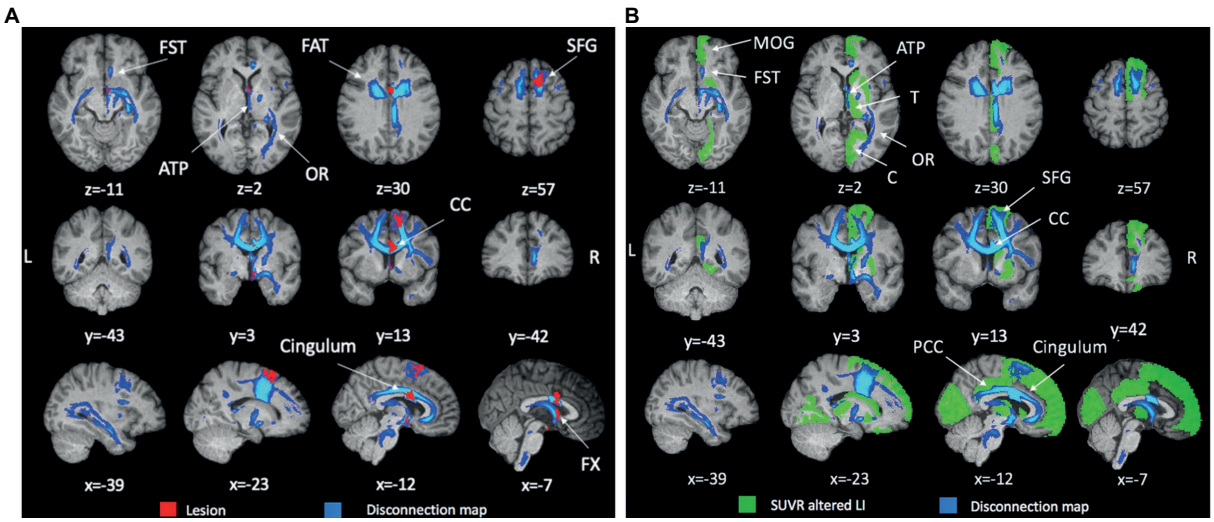

FIGURE 1
Anatomical lesion, structural disconnection map and metabolic asymmetry. **(A)** Anatomical lesion and associated structural disconnection map. T1-weighted structural MRI scan showing the anatomical lesion (red) in the midline frontal structures and the associated structural disconnection (blue) extending posteriorly and contralaterally (FST, fronto-striatal tract; ATP, anterior thalamic projection; OR, optic radiation; FAT, fronto-aslant tract; SFG, superior frontal gyrus; CC, corpus callosum). **(B)** *Structural disconnection and metabolic asymmetry*. T1-weighted structural MRI scan showing the structural disconnection (blue, threshold 20%) and regions with significative metabolic asymmetry (>2SD; green; SFG, medial orbital gyrus (MOG), caudate, putamen, thalamus (T), posterior cingulate cortex (PCC), cuneus, lingual gyrus).

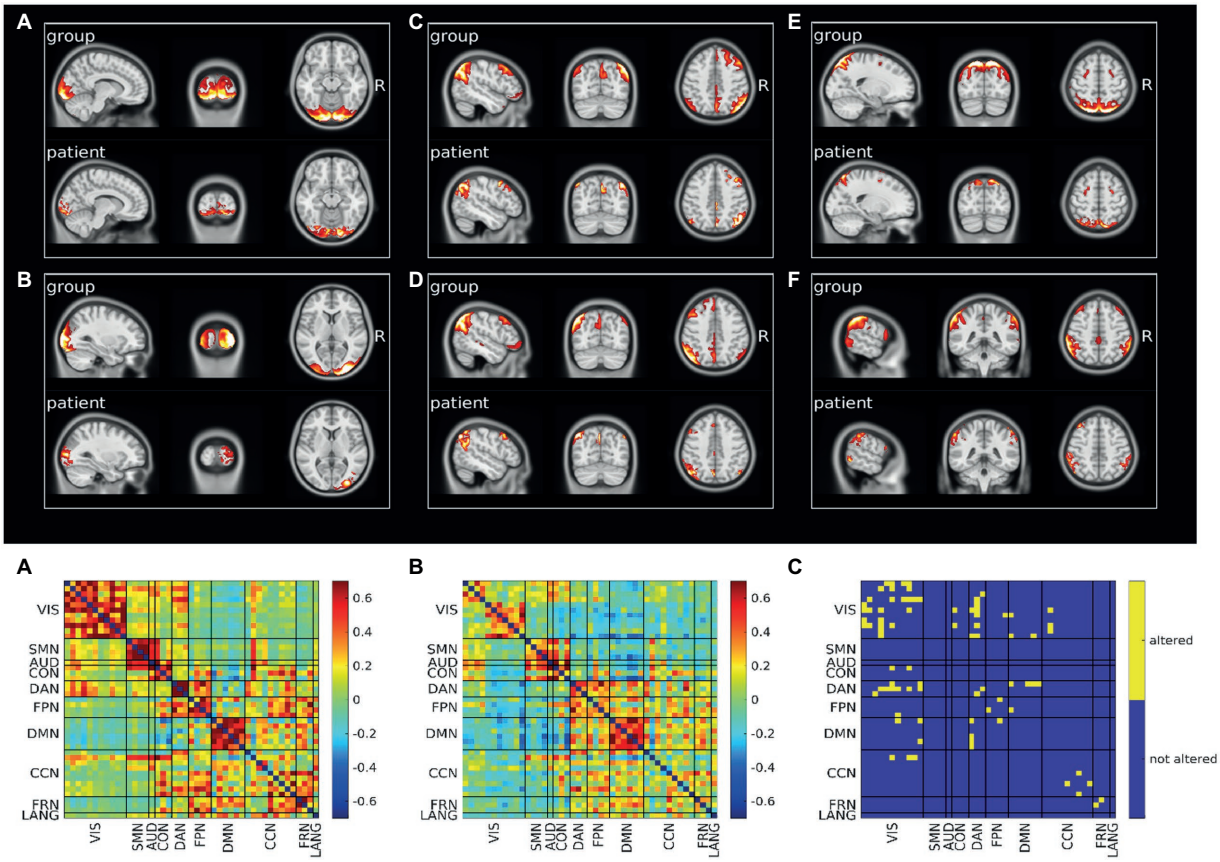

FIGURE 2
Resting state networks functional connectivity analysis. Top: Spatial pattern of representative altered resting state networks. VIS **(A,B)**, DMN **(C,D)**, DAN **(E)**, and FPN **(F)**. In each panel resting state network spatial pattern is reported for the group of healthy subjects and for the patient, respectively in the upper and lower part of the panel. Bottom: Functional connectivity between resting state networks. Average across the healthy group is shown in panel **A**, patient's connectivity in panel **B**, and patient's altered connections in panel **C**.

networks that were not affected in their spatial extent (Supplementary Table S3). When we compared the spatial maps of SDC, glucose metabolism and voxels showing altered FC, FC alterations showed a pattern more widespread than alterations of SDC or metabolism (Supplementary Figure S9).

The final analysis concerned the level of local activity synchronization (ReHo). In details, the following ROIs showed a decreased ReHo: SFG (bilateral), middle frontal gyrus (bilateral), precentral gyrus (bilateral), posterior temporal lobe (right), lateral part of anterior temporal lobe and middle and inferior temporal gyrus (left), inferior-lateral remainder of parietal lobe (left), superior parietal gyrus (bilateral), lateral reminder of occipital lobe (bilateral), fusiform gyrus (right), cuneus (bilateral).

Figure 3 shows a voxel wise overlap map comparing ReHo abnormalities with relative hypometabolism and SDC. Note that the cortical regions showing both metabolic asymmetry (i.e., a LI different from normality) and decreased ReHo are relatively few and mainly near the lesion in prefrontal cortices. The regions showing a decrease of local synchronization are widespread and bilateral, and match those showing abnormal FC (compare Figure 3 with Supplementary Figure S9).

3.4. Global and local electroencephalography abnormalities

Baseline EEG showed a lower alpha peak frequency (APF) value (7.2632 Hz) compared to the standard reference (8–13 Hz) with a slight left–right alpha asymmetry in occipital regions (left>right). Delta activity was present on right frontal regions. A predominance of beta power over the right frontal regions was also observed. This pattern is consistent with the right frontal lesion causing increase delta/beta power in the right hemisphere, and a relative loss of alpha power in the right occipital lobe, with an overall lower APF.

During the episodes of delirium (EEG2-4), at the global level, there was a general slowing of the background activity with an increase in delta activity and a reduction in the value and power of the alpha peak (Figure 4).

At the spatial level, the delta activity increased in power over right frontal region and extended contralaterally and posteriorly to centra-parietal regions. Furthermore, in correspondence of the posterior regions, there was an increase in theta and a reduction in alpha activity. Alpha activity showed a left>right asymmetry

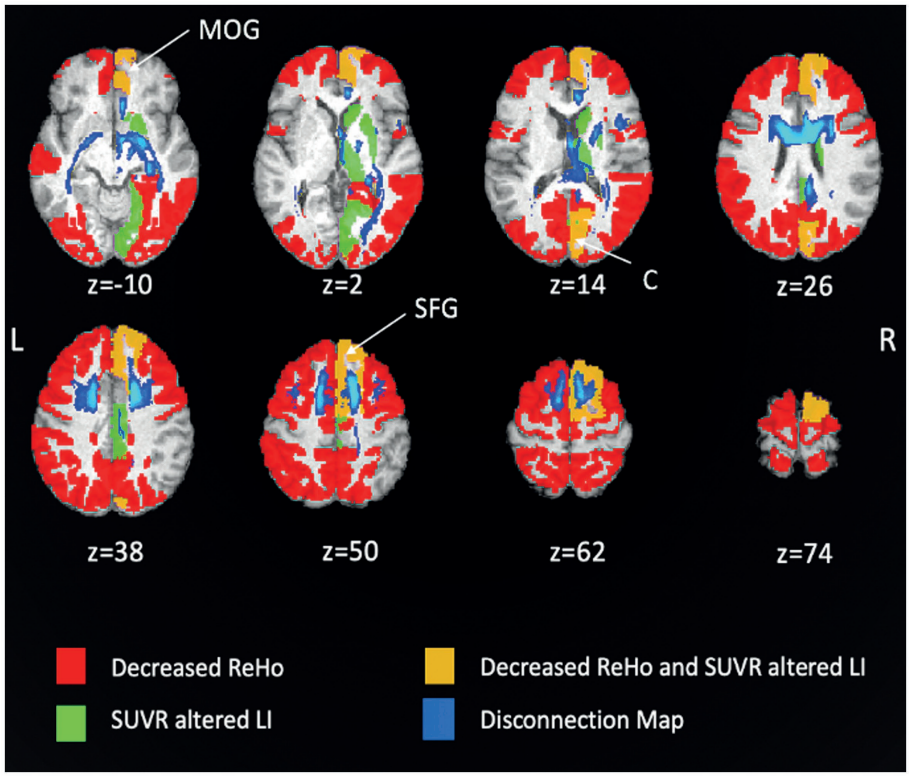

FIGURE 3
Overlap maps of decreased ReHo, [^{18}F]FDG SUVR altered laterality index (LI) and disconnection map. Patient's regions with decreased ReHo are shown in red, SUVR altered LI in light green. The overlap between decreased ReHo and SUVR altered LI is depicted in orange and corresponds to right medial prefrontal and right medial occipital cortices. The structural disconnection map is shown in blue (MOG, medial orbital gyrus; C, cuneus; SFG, superior frontal gyrus).

that was more evident during delirium with also a slight posterior-to-anterior shift in EEG3-4 (left>right).

4. Discussion

In the present case study, we had the unique opportunity to integrate different types of disconnections emerged from different techniques that were performed on the same patient presenting with a post-surgical frontal lesion.

This integrated picture, derived *via* the adoption of a multi-modal analysis, explained patient's behavior.

For instance, patient's visuo-spatial impairment and constructional apraxia (46, 47) were not directly explained based on the focal lesion, while the multi-modal analysis revealed SDC/FDC and metabolic disconnection of occipital-parietal regions and the VIS/DAN alterations that well matched with these deficits (Figures 1–3).

Executive and memory impairment can be linked to lesion of SFG and fornix, though, the multi-modal approach captured a more widespread dysfunction of prefrontal-temporo-parietal (FPN/DAN) and meso-limbic structures (DMN) (48–50).

Indeed, even though the degree of the neuropsychological impairment appeared rather modest vis-à-vis the widespread functional alteration, the multi-modal approach revealed a fragile structure/functional scaffold (involving distributed networks) that was more subjected to transitory pathological modulation, as evident in the EEGs during delirium, with a spreading of delta activity associated with worsening in cognitive performance (Figure 4).

Therefore, this case study highlights the complexity and the clinical relevance of diaschisis in focal lesions at single-subject level.

Focal lesions produce remote physiological effects that are related to the disconnection of incoming/outgoing/passing WM fibers to/from the lesion. This SDC, in turn, causes remote metabolic and functional effects that have been documented using different techniques (PET, fMRI) (4). The mapping between anatomical disconnection, metabolic/functional disconnection, and dynamic changes of synchronization/activity remains to-date largely unknown due to the dearth of multimodal studies that have addressed these issues using multiple imaging modalities on the same subject (51).

Here we had the chance to study concurrently anatomical-metabolic-functional organization along with EEG measures in a patient with a frontal lesion. There were three main findings detected in the multi-modal mapping.

A first notable result was the presence of a widespread intra-hemispheric and inter-hemispheric SDC. The SDC involved tracts near the structural lesion, but it also extended to commissural fibers, long-range association pathways and cortico-subcortical pathways.

Secondly, this disconnection nicely matched the spatial pattern of glucose hypometabolism measured through the LI or qualitatively observed on the [^{18}F]FDG SUVR map (e.g., bilateral mPFC).

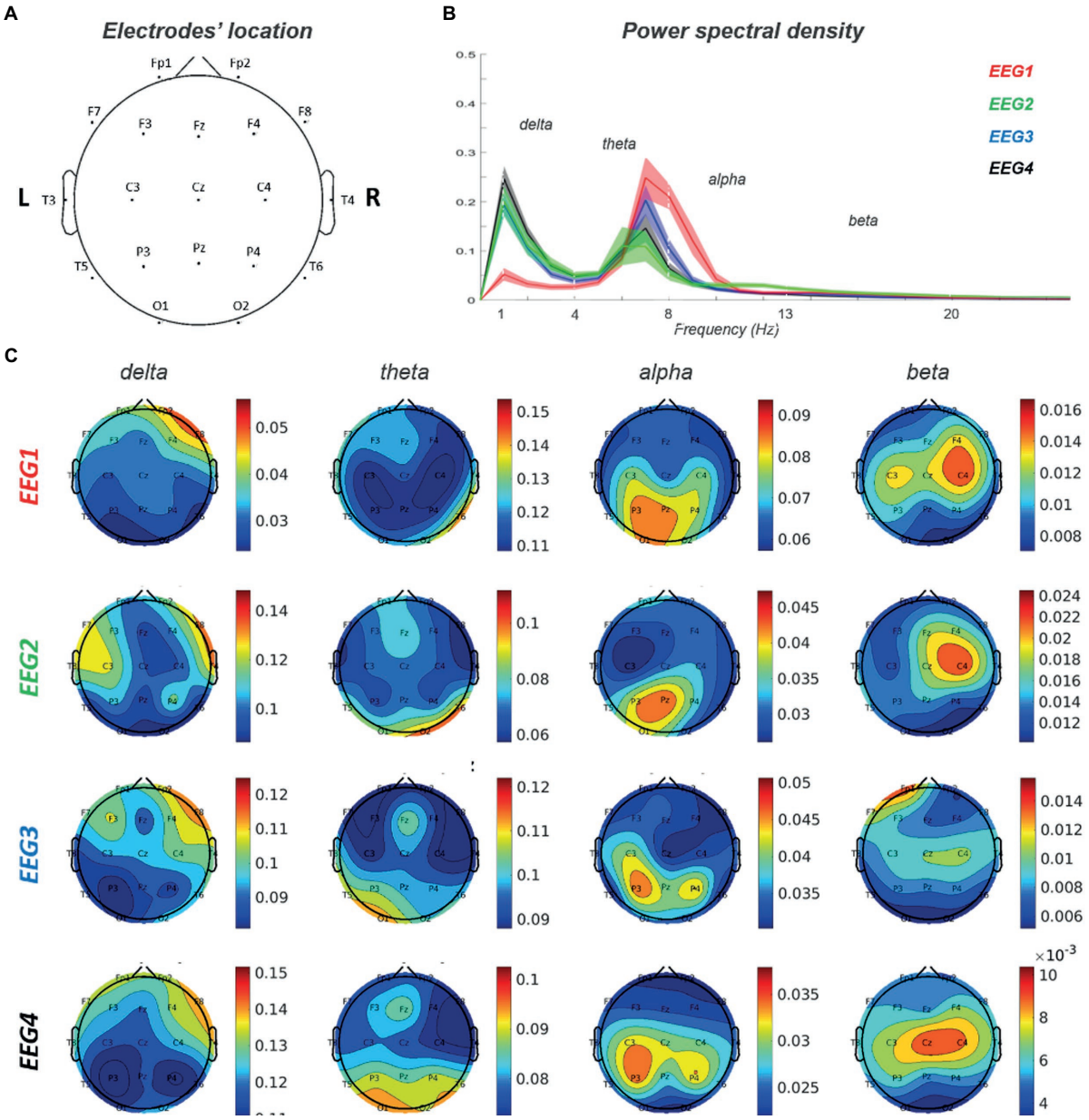

FIGURE 4
EEG 1–4 power spectra analysis. **(A)** Electrodes' location on the scalp. **(B)** Power spectral density for each of the four EEG records. **(C)** Topoplots for each frequency band (delta, theta, alpha and beta) in EEG 1–4. EEG1 is out of delirium while EEG 2–4 are during delirium.

This SDC-[^{18}F]FDG PET result supports the hypothesis that metabolic changes reflect diaschisis (52) (e.g., neural disconnection due to reduction of direct connections/synaptic inputs). In contrast, alterations of local (ReHo) and remote synchronization (RSN independent components and FC within/between networks) were more widespread involving multiple networks. Hence different mechanisms may underly the broader FC-fMRI and ReHo dysfunction, such as the propagation of the effect through BOLD oscillations or through large-scale networks dynamics (53, 54).

Thirdly, the baseline EEG was abnormal both anteriorly near the lesion (delta activity) as well as posteriorly in the occipital lobe and was then subjected to similar changes (e.g., spreading of delta activity) during the episodes of delirium, likely reflecting the dynamic effects of delirium on a baseline altered structural-functional scaffold (29, 30).

5. Conclusion

This case study illustrates the presence and the complexity of remote effects induced by a brain lesion. An integrated multi-modal approach can capture multiple disconnection patterns induced by a focal lesion. These are relevant to explain patient's behavior and to develop novel biomarkers of individualized treatment targeting networks' dysfunction.

Data availability statement

The original contributions presented in the study are included in the article/Supplementary material, further inquiries can be directed to the corresponding author.

Ethics statement

The studies involving human participants were reviewed and approved by Local Ethical Committee University of Padova. The patients/participants provided their written informed consent to participate in this study. Written informed consent was obtained from the individual(s) for the publication of any potentially identifiable images or data included in this article.

Author contributions

EM, ES, MB, AC, DC, AB, and MC: conception and design. EM, AC, and DC: acquisition of data. EM, ES, MB, AC, MA, DC, AB, and MC: analysis, interpretation of data, writing, review, and/or revision of the manuscript. All authors contributed to the article and approved the submitted version.

Funding

MC was supported by FLAG-ERA JTC 2017 (grant ANR-17-HBPR-0001), MIUR–Departments of Excellence Italian Ministry of Research (MART_ECCELLENZA18_01), Fondazione Cassa di Risparmio di Padova e Rovigo (CARIPARO)–Ricerca Scientifica di Eccellenza 2018–(Grant Agreement number 55403), Ministry of Health Italy Brain connectivity measured with high-density electroencephalography: a novel neurodiagnostic tool for stroke-NEUROCONN (RF-2008-12366899), Celeghin Foundation Padova (CUP C94I20000420007), BIAL Foundation grant (No. 361/18), H2020 European School of Network Neuroscience-euSNN, H2020-SC5-2019-2 (Grant Agreement number 869505), H2020 Visionary Nature Based Actions For Heath, Wellbeing & Resilience in Cities (VARCITIES), H2020-SC5-2019-2 (Grant Agreement number 869505), and Ministry of Health Italy: Eye-movement dynamics during free viewing as biomarker for assessment of visuospatial functions and for closed-loop rehabilitation in stroke–EYEMOVINSTROKE (RF-2019-12369300).

Conflict of interest

The authors declare that the research was conducted in the absence of any commercial or financial relationships that could be construed as a potential conflict of interest.

Publisher's note

All claims expressed in this article are solely those of the authors and do not necessarily represent those of their affiliated organizations, or those of the publisher, the editors and the reviewers. Any product that may be evaluated in this article, or claim that may be made by its manufacturer, is not guaranteed or endorsed by the publisher.

Supplementary material

The Supplementary material for this article can be found online at: https://www.frontiersin.org/articles/10.3389/fneur.2023.1142734/full#supplementary-material

References

1. Carrera E, Tononi G. Diaschisis: past, present, future. *Brain*. (2014) 137:2408–22. doi: 10.1093/brain/awu101

2. He BJ, Snyder AZ, Vincent JL, Epstein A, Shulman GL, Corbetta M. Breakdown of functional connectivity in frontoparietal networks underlies behavioral deficits in spatial neglect. *Neuron*. (2007) 53:905–18. doi: 10.1016/j.neuron.2007.02.013

3. Honey CJ, Sporns O, Cammoun L, Gigandet X, Thiran JP, Meuli R, et al. Predicting human resting-state functional connectivity from structural connectivity. *Proc Natl Acad Sci U S A*. (2009) 106:2035–40. doi: 10.1073/pnas.0811168106

4. Baldassarre A, Ramsey LE, Siegel JS, Shulman GL, Corbetta M. Brain connectivity and neurological disorders after stroke. *Curr Opin Neurol*. (2016) 29:706–13. doi: 10.1097/WCO.0000000000000396

5. Monakow CV. Die Lokalisation im Grosshirn und der Abbau der Funktion durch Kortikale Herde. *J Am Med Assoc*. (1914) LXIII:797

6. Feeney DM, Baron JC. Diaschisis. *Stroke*. (1986) 17:817–30. doi: 10.1161/01.STR.17.5.817

7. Siegel JS, Ramsey LE, Snyder AZ, Metcalf NV, Chacko RV, Weinberger K, et al. Disruptions of network connectivity predict impairment in multiple behavioral domains after stroke. *Proc Natl Acad Sci U S A*. (2016) 113:E4367–76. doi: 10.1073/pnas.1521083113

8. Pantano P, Baron JC, Samson Y, Bousser MG, Derouesne C, Comar D. Crossed cerebellar diaschisis: further studies. *Brain*. (1986) 109:677–94. doi: 10.1093/brain/109.4.677

9. Baron JC, Bousser MG, Comar D, Castaigne P. "Crossed cerebellar diaschisis" in human supratentorial brain infarction. *Trans Am Neurol Assoc*. (1981) 105:459–61. PMID: 19645126

10. Baldassarre A, Ramsey L, Hacker CL, Callejas A, Astafiev SV, Metcalf NV, et al. Large-scale changes in network interactions as a physiological signature of spatial neglect. *Brain*. (2014) 137:3267–83. doi: 10.1093/brain/awu297

11. Biswal B, Zerrin Yetkin F, Haughton VM, Hyde JS. Functional connectivity in the motor cortex of resting human brain using echo-planar MRI. *Magn Reson Med*. (1995) 34:537–41. doi: 10.1002/mrm.1910340409

12. Fox MD, Raichle ME. Spontaneous fluctuations in brain activity observed with functional magnetic resonance imaging. *Nat Rev Neurosci*. (2007) 8:700–11. doi: 10.1038/nrn2201

13. Thiebaut De Schotten M, Tomaiuolo F, Aiello M, Merola S, Silvetti M, Lecce F, et al. Damage to white matter pathways in subacute and chronic spatial neglect: a group study and 2 single-case studies with complete virtual "in vivo" tractography dissection. *Cereb Cortex*. (2014) 24:691–706. doi: 10.1093/cercor/bhs351

14. Foulon C, Cerliani L, Kinkingnéhun S, Levy R, Rosso C, Urbanski M, et al. Advanced lesion symptom mapping analyses and implementation as BCB toolkit. *Gigascience*. (2018) 7:1–17. doi: 10.1093/gigascience/giy004

15. Thiebaut de Schotten M, Foulon C, Nachev P. Brain disconnections link structural connectivity with function and behavior. *Nat Commun*. (2020) 11:8920. doi: 10.1038/s41467-020-18920-9

16. Poryazova R, Huber R, Khatami R, Werth E, Brugger P, Barath K, et al. Topographic sleep EEG changes in the acute and chronic stage of hemispheric stroke. *J Sleep Res*. (2015) 24:54–65. doi: 10.1111/jsr.12208

17. Assenza G, Zappasodi F, Pasqualetti P, Vernieri F, Tecchio F. A contralesional EEG power increase mediated by interhemispheric disconnection provides negative prognosis in acute stroke. *Restor Neurol Neurosci*. (2013) 31:177–88. doi: 10.3233/RNN-120244

18. Wu J, Srinivasan R, Quinlan EB, Solodkin A, Small SL, Cramer SC. Utility of EEG measures of brain function in patients with acute stroke. *J Neurophysiol*. (2016) 115:2399–405. doi: 10.1152/jn.00978.2015

19. Griffis J, Metcalf N, Corbetta M, Shulman G. Structural disconnections explain brain network dysfunction after stroke. *bioRxiv*. (2019) 28:2527–2540.e9.

20. Gerloff C, Bushara K, Sailer A, Wassermann EM, Chen R, Matsuoka T, et al. Multimodal imaging of brain reorganization in motor areas of the contralesional hemisphere of well recovered patients after capsular stroke. *Brain*. (2006) 129:791–808. doi: 10.1093/brain/awh713

21. Sebok M, Van Niftrik CHB, Piccirelli M, Bozinov O, Wegener S, Esposito G, et al. Bold cerebrovascular reactivity as a novel marker for crossed cerebellar diaschisis. *Neurology*. (2018) 91:e1328–37. doi: 10.1212/WNL.0000000000006287

22. Tomasi D, Wang GJ, Volkow ND. Energetic cost of brain functional connectivity. *Proc Natl Acad Sci U S A*. (2013) 110:13642–7. doi: 10.1073/pnas.1303346110

23. Cecchin D, Palombit A, Castellaro M, Silvestri E, Bui F, Barthel H, et al. Brain PET and functional MRI: why simultaneously using hybrid PET/MR systems? *Q J Nuc Med Mol Imag*. (2017) 61:345–59. doi: 10.23736/S1824-4785.17.03008-4

24. Coyle JT, Balu DT, Puhl MD, Konopaske GT. History of the concept of disconnectivity in schizophrenia. *Harv Rev Psychiatry*. (2016) 24:80–6. doi: 10.1097/HRP.0000000000000102

25. Brier MR, Thomas JB, Ances BM. Network dysfunction in Alzheimer's disease: refining the disconnection hypothesis. *Brain Connect*. (2014) 4:299–311. doi: 10.1089/brain.2014.0236

26. Cagnin A, Gnoato F, Jelcic N, Favaretto S, Zarantonello G, Ermani M, et al. Clinical and cognitive correlates of visual hallucinations in dementia with Lewy bodies. *J Neurol Neurosurg Psychiatry*. (2013) 84:505–10. doi: 10.1136/jnnp-2012-304095

27. Tsukada H, Fujii H, Aihara K, Tsuda I. Computational model of visual hallucination in dementia with Lewy bodies. *Neural Netw*. (2015) 62:73–82. doi: 10.1016/j.neunet.2014.09.001

28. Zorzi G, Thiebaut de Schotten M, Manara R, Bussè C, Corbetta M, Cagnin A. White matter abnormalities of right hemisphere attention networks contribute to visual hallucinations in dementia with Lewy bodies. *Cortex*. (2021) 139:86–98. doi: 10.1016/j.cortex.2021.03.007

29. Young JWS. The network model of delirium. *Med Hypotheses*. (2017) 104:80–5. doi: 10.1016/j.mehy.2017.05.027

30. van Montfort SJT, van Dellen E, Stam CJ, Ahmad AH, Mentink LJ, Kraan CW, et al. Brain network disintegration as a final common pathway for delirium: a systematic review and qualitative meta-analysis. *NeuroImage: Clinical*. (2019) 23:101809. doi: 10.1016/j.nicl.2019.101809

31. Izquierdo-Garcia D, Hansen AE, Förster S, Benoit D, Schachoff S, Fürst S, et al. An SPM8-based approach for attenuation correction combining segmentation and nonrigid template formation: application to simultaneous PET/MR brain imaging. *J Nucl Med*. (2014) 55:1825–30. doi: 10.2967/jnumed.113.136341

32. Mendes N, Oligschläger S, Lauckner ME, Golchert J, Huntenburg JM, Falkiewicz M, et al. A functional connectome phenotyping dataset including cognitive state and personality measures. *Sci Data*. (2019) 6:180307. doi: 10.1038/sdata.2018.307

33. Babayan A, Baczkowski B, Cozatl R, Dreyer M, Engen H, Erbey M, et al. MPI-Leipzig_mind-brain-body. *OpenNeuro*. (2020) [Dataset]. doi: 10.18112/openneuro.ds000221.v1.0.0

34. Aiello M, Salvatore E, Cachia A, Pappatà S, Cavaliere C, Prinster A, et al. Relationship between simultaneously acquired resting-state regional cerebral glucose metabolism and functional MRI: a PET/MR hybrid scanner study. *NeuroImage*. (2015) 113:111–21. doi: 10.1016/j.neuroimage.2015.03.017

35. Glasser MF, Sotiropoulos SN, Wilson JA, Coalson TS, Fischl B, Andersson JL, et al. The minimal preprocessing pipelines for the human connectome project. *NeuroImage*. (2013) 80:105–24. doi: 10.1016/j.neuroimage.2013.04.127

36. Salimi-Khorshidi G, Douaud G, Beckmann CF, Glasser MF, Griffanti L, Smith SM. Automatic denoising of functional MRI data: combining independent component analysis and hierarchical fusion of classifiers. *NeuroImage*. (2014) 90:449–68. doi: 10.1016/j.neuroimage.2013.11.046

37. Silvestri E, Moretto M, Facchini S, Castellaro M, Anglani M, Monai E, et al. Widespread cortical functional disconnection in gliomas: an individual network mapping approach. Brain. *Communications*. (2022) 4:fcac082. doi: 10.1093/braincomms/fcac082

38. Du Y, Fan Y. Group information guided ICA for fMRI data analysis. *NeuroImage*. (2013) 69:157–97. doi: 10.1016/j.neuroimage.2012.11.008

39. Zang Y, Jiang T, Lu Y, He Y, Tian L. Regional homogeneity approach to fMRI data analysis. *NeuroImage*. (2004) 22:394–400. doi: 10.1016/j.neuroimage.2003.12.030

40. Hammers A, Allom R, Koepp MJ, Free SL, Myers R, Lemieux L, et al. Three-dimensional maximum probability atlas of the human brain, with particular reference to the temporal lobe. *Hum Brain Mapp*. (2003) 19:224–47. doi: 10.1002/hbm.10123

41. Delorme A, Makeig S. EEGLAB: an open source toolbox for analysis of single-trial EEG dynamics including independent component analysis. *J Neurosci Methods*. (2004) 134:9–21. doi: 10.1016/j.jneumeth.2003.10.009

42. Nunez PL, Srinivasan R. *Electric fields of the brain the Neurophysics of EEG. 2nd Edn*. Oxford University Press (2006) doi: 10.1093/acprof:oso/9780195050387.001.0001.

43. Makeig S, Jung T-P, Bell AJ, Sejnowski TJ. "Independent component analysis of electroencephalographic data," in *Advances in Neural Information Processing systems*. eds. D Touretzky, M Mozer and M Hasselmo, *Vol.* 8, Cambridge MA: MIT Press (1996) 145–151.

44. Michel CM, Brunet D. EEG source imaging: a practical review of the analysis steps. *Front Neurol*. (2019) 10:325. doi: 10.3389/fneur.2019.00325

45. Dustman RE, Boswell RS, Porter PB. Beta brain waves as an index of alertness. *Science*. (1962) 80:533–534.

46. Corbetta M, Shulman GL. Spatial neglect and attention networks. *Annu Rev Neurosci*. (2011) 34:569–99. doi: 10.1146/annurev-neuro-061010-113731

47. Trés ES, Brucki SMD. Visuospatial processing: a review from basic to current concepts. *Dement Neuropsychol*. (2014) 8:175–81. doi: 10.1590/S1980-57642014DN82000014

48. Catani M, Dell'Acqua F, Thiebaut de Schotten M. A revised limbic system model for memory, emotion and behavior. *Neurosci Biobehav Rev*. (2013) 37:1724–37. doi: 10.1016/j.neubiorev.2013.07.001

49. Miller EK. The prefontral cortex and cognitive control. *Nat Rev Neurosci*. (2000) 1:59–65. doi: 10.1038/35036228

50. Raichle ME. The Brain's default mode network. *Annu Rev Neurosci*. (2015) 38:433–47. doi: 10.1146/annurev-neuro-071013-014030

51. Longarzo M, Cavaliere C, Orsini M, Tramontano L, Aiello M, Salvatore M, et al. A multimodal imaging study in a case of bilateral thalamic damage with multimodal cognitive impairment. *Front Neurol*. (2019) 10:1048. doi: 10.3389/fneur.2019.01048

52. Forkel SJ, de Schotten MT. Towards metabolic disconnection–symptom mapping. *Brain*. (2020) 143:718–21. doi: 10.1093/brain/awaa060

53. Adachi Y, Osada T, Sporns O, Watanabe T, Matsui T, Miyamoto K, et al. Functional connectivity between anatomically unconnected areas is shaped by collective network-level effects in the macaque cortex. *Cereb Cortex*. (2012) 22:1586–92. doi: 10.1093/cercor/bhr234

54. Deco G, Corbetta M. The dynamical balance of the brain at rest. *Neuroscientist*. (2011) 17:107–23. doi: 10.1177/1073858409354384

frontiers | Frontiers in Systems Neuroscience

TYPE Original Research
PUBLISHED 02 May 2023
DOI 10.3389/fnsys.2023.1163147

OPEN ACCESS

EDITED BY
Alessandro Salvalaggio,
University Hospital of Padua, Italy

REVIEWED BY
Michele Allegra,
Dipartimento di Fisica e Astronomia "G. Galilei", Italy
Anna Bonkhoff,
Massachusetts General Hospital and Harvard Medical School, United States

*CORRESPONDENCE
Antonello Baldassarre
✉ a.baldassarre@unich.it

RECEIVED 10 February 2023
ACCEPTED 11 April 2023
PUBLISHED 02 May 2023

CITATION
Spadone S, de Pasquale F, Digiovanni A, Grande E, Pavone L, Sensi SL, Committeri G and Baldassarre A (2023) Dynamic brain states in spatial neglect after stroke.
Front. Syst. Neurosci. 17:1163147.
doi: 10.3389/fnsys.2023.1163147

Dynamic brain states in spatial neglect after stroke

Sara Spadone[1], Francesco de Pasquale[2], Anna Digiovanni[1], Eleonora Grande[1], Luigi Pavone[3], Stefano L. Sensi[1], Giorgia Committeri[1] and Antonello Baldassarre[1]*

[1]Department of Neuroscience, Imaging and Clinical Sciences, University G. d'Annunzio of Chieti-Pescara, Chieti, Italy, [2]Faculty of Veterinary Medicine, University of Teramo, Teramo, Italy, [3]IRCCS NEUROMED, Pozzilli, Italy

Previous studies indicated that spatial neglect is characterized by widespread alteration of resting-state functional connectivity and changes in the functional topology of large-scale brain systems. However, whether such network modulations exhibit temporal fluctuations related to spatial neglect is still largely unknown. This study investigated the association between brain states and spatial neglect after the onset of focal brain lesions. A cohort of right-hemisphere stroke patients ($n = 20$) underwent neuropsychological assessment of neglect as well as structural and resting-state functional MRI sessions within 2 weeks from stroke onset. Brain states were identified using dynamic functional connectivity as estimated by the sliding window approach followed by clustering of seven resting state networks. The networks included visual, dorsal attention, sensorimotor, cingulo-opercular, language, fronto-parietal, and default mode networks. The analyses on the whole cohort of patients, i.e., with and without neglect, identified two distinct brain states characterized by different degrees of brain modularity and system segregation. Compared to non-neglect patients, neglect subjects spent more time in less modular and segregated state characterized by weak intra-network coupling and sparse inter-network interactions. By contrast, patients without neglect dwelt mainly in more modular and segregated states, which displayed robust intra-network connectivity and anti-correlations among task-positive and task-negative systems. Notably, correlational analyses indicated that patients exhibiting more severe neglect spent more time and dwelt more often in the state featuring low brain modularity and system segregation and vice versa. Furthermore, separate analyses on neglect vs. non-neglect patients yielded two distinct brain states for each sub-cohort. A state featuring widespread strong connections within and between networks and low modularity and system segregation was detected only in the neglect group. Such a connectivity profile blurred the distinction among functional systems. Finally, a state exhibiting a clear separation among modules with strong positive intra-network and negative inter-network connectivity was found only in the non-neglect group. Overall, our results indicate that stroke yielding spatial attention deficits affects the time-varying properties of functional interactions among large-scale networks. These findings provide further insights into the pathophysiology of spatial neglect and its treatment.

KEYWORDS

neglect, dynamic functional connectivity, brain states, modularity, cluster analysis

Introduction

Spatial neglect, a neuropsychological syndrome affecting around ∼20–30% of all stroke patients (Buxbaum et al., 2004; Ringman et al., 2004), is characterized by an impairment in attending, processing, and responding to targets which are presented in the side of the space and body opposed to the brain lesion, which is more frequently in the right hemisphere (Halligan et al., 1989; Verdon et al., 2010; Corbetta and Shulman, 2011). This contralesional spatial bias is also associated with non-spatial deficits of sustained attention, arousal, and vigilance (Husain and Rorden, 2003).

Albeit investigated for a long-time, the neurofunctional correlates of spatial neglect are still debated (Husain and Rorden, 2003; Corbetta and Shulman, 2011; Bartolomeo et al., 2012; Karnath and Rorden, 2012). Lesion-to-symptom mapping studies have identified several brain structures related to neglect, such as inferior frontal (Husain and Kennard, 1996; Committeri et al., 2007; Corbetta et al., 2015), insular (Karnath et al., 2009; Corbetta et al., 2015), temporo-parietal (Karnath et al., 2001, 2004; Committeri et al., 2007; Corbetta et al., 2015) and inferior parietal (Mort et al., 2003) cortex, basal ganglia (Karnath et al., 2005; Corbetta et al., 2015), thalamus (Corbetta et al., 2015) as well as underlying white matter (Doricchi and Tomaiuolo, 2003; Karnath et al., 2009; Thiebaut de Schotten et al., 2014; Corbetta et al., 2015).

In recent years, such a challenge has been attempted within the framework of the so-called "connectomal diaschisis", a novel type of diaschisis, which posits that a focal brain injury leads to widespread changes of large-scale networks among areas that are structurally spared and distant from the lesion site (Carrera and Tononi, 2014) (for reviews on stroke, see Varsou et al., 2014; Baldassarre et al., 2016; Siegel et al., 2022). Indeed, two pioneer studies showed that the extent of the rightward bias in neglect patients is associated with a breakdown of the inter-hemispheric resting-state functional connectivity (FC) MRI among intact fronto-parietal areas of the dorsal attention network that is involved in the control of visuo-spatial attention (He et al., 2007; Carter et al., 2010). Subsequently, in our previous work (Baldassarre et al., 2014), we detected two large-scale patterns of abnormal functional connectivity associated with the severity of spatial neglect in a large cohort of acute stroke patients: reduction of inter-hemispheric FC within dorsal attention/sensory motor networks as well as loss of negative FC (i.e., anti-correlation) between these networks and the default mode network. More recently, by adopting a graph-theoretic approach, in two companion studies, we have shown that spatial neglect is characterized by widespread changes in the brain topological organization at different scales of network analysis (de Pasquale et al., 2021a; Spadone et al., 2022). At the micro-scale level, we identified two sets of neglect-relevant hubs derived using the betweenness centrality metric [i.e., the number of the shortest paths passing through a given node (Rubinov and Sporns, 2010; de Pasquale et al., 2021a)]. Specifically, one group of neglect hubs was detected in higher-order associative systems, such as the dorsal and ventral attention, frontoparietal, and default mode networks. These hubs exhibited lower centrality as well as higher shortest paths length (i.e., less efficient) associated with severe neglect. Conversely, a reverse pattern was observed in a second cohort of neglect hubs dislocated in lower-level sensory-processing systems such as the visual and motor networks. At meso-scale level, neglect was associated with a loss of system segregation, i.e., the balance between the functional specialization and dynamic integration of distinct and segregated (sub)networks (Tononi et al., 1994; Wig, 2017), involving higher-order associative networks such as dorsal attention, fronto-parietal and default mode as well as the sensorimotor network (Spadone et al., 2022).

Overall, these lines of evidence indicate that neglect is characterized by widespread alteration of resting-state networks as well topological changes in the brain, suggesting a maladaptive shift from higher-order to low-level sensory-processing systems.

However, the brain is a dynamic system characterized by transient states with different degrees of integration and segregation among multiple large-scale networks (de Pasquale et al., 2021a,b). Notably, recent functional MRI studies adopting a dynamic functional connectivity approach have identified time-varying properties of functional connections among brain networks (Calhoun et al., 2014). Clinically, several reports indicated that such brain states are affected after stroke (Bonkhoff et al., 2020, 2021a,b; Wang et al., 2020; Favaretto et al., 2022). Hence, the dynamic connectivity method can capture transient conditions of network reconfigurations as they happen after a focal brain lesion. Therefore, the goal of the current study was to investigate whether the above-described network modulations exhibit temporal variations which can be potentially related to spatial neglect. To this aim, we estimated functional connectivity dynamics (Calhoun et al., 2014) on our previously collected dataset (de Pasquale et al., 2021a; Spadone et al., 2022) to characterize the temporal fluctuations of brain states associated with spatial neglect after right hemisphere strokes. Since neglect has been associated with changes of functional connectivity in multiple large-scale networks, we expect to identify brain states characterized by widespread alterations of their functional architecture.

Methods

Stroke patients and assessment of neglect

A cohort of twenty right-hemisphere damaged patients (mean age 65.1 y, SD = 12.3 y) was enrolled within 2 weeks since first-time stroke onset. The Inclusion criteria were as follows: (1) Clinical diagnosis of right hemisphere stroke (ischemic or hemorrhagic) at hospital discharge; (2) Persistent stroke symptom(s) at hospital discharge; (3) Awake, alert, and able to complete study tasks; (4) Age > 18. Exclusion criteria: (1) Severe psychiatric or neurological disorders/conditions; (2) Claustrophobia; (3) Body metal not allowing 3T MRI. Table 1 displays the demographic and clinical information of stroke patients. The Bells Cancellation Test and Letter Cancellation Test assessed the severity of visual neglect. Patients were classified as having neglect if their Center of Cancellation (CoC) (Binder et al., 1992) score was above the normative cut-off in at least one test, 0.081 and 0.083, respectively (Rorden and Karnath, 2010) (Table 1 displays demographic and clinical information of the cohort of patients).

TABLE 1 Demographic and clinical characteristics of the stroke patients.

ID	Age at stroke (y)	Sex	Education (y)	Time post-stroke (y)	Neglect	Lesion type	Lesion site
4	69	F	8	3	+	I	Cau; Pal; Pu; STG
8	92	F	5	2	+	I	Cau; Pal; Put; Ins; IntCap; ExtCap
9	67	M	13	7	+	I	Cau; Pal; Put;
11	65	F	8	14	+	H	Pal; Put; Ins; ExtCap; STG
14	60	M	13	2	+	I	Tha
21	73	F	5	5	+	I	Put; IntCap
22	53	M	8	10	+	H	Pal; Put
24	74	F	5	5	+	I	Put; Ins; Cau; CorRad; IntCap
31	56	M	13	4	+	I	Tha
32	73	F	5	11	+	I	IFG; Ins; Put; ExtCap
33	76	F	5	7	+	I	Put; Ins; STG; IFG; CorRad; IntCap
3	84	F	8	7	–	I	BS
6	73	M	13	5	–	H	PHG; LG
7	41	M	13	14	–	I	SPL; PreCun; AG; SLF
16	62	M	13	5	–	I	Tha
20	65	M	13	8	–	I	LOG; FFG; PHG
23	77	F	5	14	–	I	MFG; PrCG; SPL
26	73	M	5	12	–	I	CorRad
30	62	F	8	4	–	I	SLF
34	51	M	8	9	–	I	Put; Cau; CorRad; IntCap; SLF

Y, year; M, male; F, female; +, presence of neglect; –, absence of neglect; I, ischemic; H, hemorrhagic; PHG, Parahippocampal Gyrus; Put, Putamen; Cau, Caudate; Pal, Pallidum; BS, Brain Stem; STG, Superior Temporal Gyrus; Lingual Gyrus; SPL, Superior Parietal Lobule; PreCun, Precuneus; AG, Angular Gyrus; SLF, Superior Longitudinal Fasciculus; Ins, Insula; Tha, Thalamus; LOG, Lateral Occipital Gyrus; FFG, Fusiform Gyrus; IntCap, Internal capsule; ExtCap, External Capsule; MFG, Middle Frontal Gyrus; PrCG, Pre-Central Gyrus; CorRad, Corona Radiata; IFG, Inferior Frontal Gyrus.

Functional MRI acquisition

MRI scanning was performed with a GE Signa HDxt 3T at the IRCCS NEUROMED (Pozzilli, Italy) within 24 h of the neuropsychological assessment. Structural scans consisted of: (1) an axial T1-weighted 3D SPGR (TR = 1,644 ms, TE = 2.856 ms, flip angle = 13 deg, voxel size = 1.0 × 1.0 × 1.0 mm) and (2) an axial T2-weighted turbo spin-echo (TR = 2.856 ms, TE = 127.712 ms, slice thickness 3 mm, matrix size: 512 × 512). Resting-state functional scans were acquired with a gradient echo EPI sequence with TR = 1,714 ms, TE = 30 ms, 34 contiguous 3.6 mm slices, during which participants were instructed to keep open eyes in a low luminance environment. Three resting-state fMRI runs of 7.5 min were collected.

Lesion segmentation

The lesions were manually segmented using MRIcron software (www.mayo.edu) by examining T1-weighted and T2-weighted images simultaneously displayed in the atlas space. All segmentations were reviewed by a trained radiologist of NEUROMED (GG in de Pasquale et al., 2021a).

fMRI data pre-processing

Functional data were pre-processed in CONN toolbox (https://www.nitrc.org/projects/conn/; Whitfield-Gabrieli and Nieto-Castanon, 2012) by employing the default pre-processing pipeline (Nieto-Castanon, 2020) which included the steps of functional realignment and unwarping, slice-timing correction, potential outlier scans identification, direct segmentation and normalization in Montreal Neurological Institute (MNI) space and smoothing with a 6-mm kernel. Head-motion contaminated frames were identified through the global BOLD signal and the amount of patient-motion. Specifically, all the functional volumes in which the global BOLD signal changes was above 5 SD or the framewise displacement was above 0.9 mm were classified as outliers and then employed as confounding regressors of non-interest to remove their influence on the BOLD signal timeseries. Furthermore, pre-processed functional data underwent the CONN's default

denoising pipeline to estimate and regress out physiological and other noise sources. Specifically, an anatomical component-based noise correction procedure (aCompCor) (Behzadi et al., 2007) was employed to identify and remove physiological noise from white matter and cerebrospinal fluid, subject-motion parameters (Friston et al., 1995), and outlier scans (Power et al., 2014). Next, based on previous dynamic functional connectivity MRI studies (Leonardi and Van De Ville, 2015), a temporal band-pass filter of 0.029–0.15 Hz was applied to the time series. Overall, several denoising steps, including CompCor correction, outlier censoring, motion regression, and linear detrending, were computed simultaneously before the band-pass filtering. Finally, the residual BOLD time-series for each region of interest were employed for estimating the dynamic brain states.

Resting-state networks

In the current study, we employed a functional brain parcellation implemented in CONN toolbox that includes a set of 30 regions of interest (ROIs) defined from CONN's Independent Component Analyses of Human Connectome Project dataset (497 subjects) (Whitfield-Gabrieli and Nieto-Castanon, 2012; Nieto-Castanon, 2020). Specifically, the ROIs belonged to seven resting state networks comprising visual, dorsal attention, sensorimotor, cingulo-opercular, language, fronto-parietal, and default mode networks (Supplementary Table 1).

Brain state analysis in the whole cohort of patients

Brain states identification

To estimate the dynamic functional connectivity, the time course of the BOLD signal of the 260 volumes (in all participants) was segmented into 34-s (20 TRs) sliding windows (see recommendation by Leonardi and Van De Ville, 2015), moving the onset every 1.7 s (1 TR), for a total of 241 sliding windows. Next, for each sliding window, the functional connectivity was obtained through the Pearson correlation coefficient (r) among fMRI signals of all the possible pairs of the 30 parcellation nodes. To obtain normally distributed values, r scores were Fisher-transformed into z-scores. The output of this analysis is a temporal series of FC matrices. To identify a set of states representing the most recurrent connectivity patterns over time, we ran a K-means clustering. Specifically, the clustering algorithm was applied to the set of windowed FC matrices of all subjects concatenated along the time dimension resulting in 241*20 = 4,820 FC patterns. The clustering algorithm was implemented using the Manhattan (cityblock) as the distance among the 4,820 observations.

To estimate the optimal number of clusters, we ran the clustering algorithm for different values of classes. For each output, we computed a mixed performance criterion (MPFC, see Spadone et al., 2012; de Pasquale et al., 2021b) which is the product of different clustering performance criteria:

$$MPFC = \frac{CS^{*}AS^{*}DI}{DB},$$

where CS is the average cluster size, AS is the average silhouette, DI is the Dunn Index, and DB is the Davies Bouldin index. In this way, several aspects can be combined and considered in the cluster number estimation. A detailed discussion on these parameters can be found in Spadone et al. (2012). The optimal number of clusters corresponds to the peak of the MPFC. The centroid of each cluster putatively reflects a connectivity "state". These analyses were performed using in-house developed software in MATLAB (2022, Natick, Massachusetts: The MathWorks Inc.).

Brain states characterization

To characterize the identified brain states, we investigated their internal arrangement into modules or communities (Medaglia, 2017). To this aim, we computed on the centroid matrix of each state in each individual patient, the brain modularity, and the system segregation. These two indices are behaviorally relevant for spatial neglect (Siegel et al., 2018; Spadone et al., 2022). Specifically, brain modularity represents a measure of the goodness of network subdivision into well-defined modules or communities (Bullmore and Sporns, 2009). Such a score was estimated by employing the Louvain modularity algorithm implemented in the brain connectivity toolbox (Rubinov and Sporns, 2010). This procedure yielded for each patient a brain modularity value associated with each brain state. Moreover, we computed the system segregation, a measure that captures the balance between functional specialization and dynamic integration of distinct and segregated (sub)networks (Tononi et al., 1994; Wig, 2017). In detail, the system segregation was computed as described in Chan et al. (2014): for each patient and each of the seven resting state networks, the within-network FC (WNFC) and the between-network FC (BNFC) were computed for each of the seven resting state networks. Specifically, for each centroid matrix of each state, WNFC was derived as the mean correlation, among all possible pairs of regions within that network, whereas BNFC as the averaged correlation among regions of a given network and all other nodes of the rest of the brain connectome. This computation produced seven values (one for each network) that were then averaged to obtain the system segregation score. As for the estimation of the modularity, this analysis returned for each patient a system segregation value for each brain state.

Temporal dynamics of brain states

Furthermore, we computed two dynamic connectivity measures: the fraction time (the percentage of the total time a subject spent in a given connectivity state) and the dwell time (the time a subject spent in a state without switching to another one) for each of the states. Furthermore, we investigated the differences in time-varying properties of the identified brain states among neglect and non-neglect groups. To this aim, for each brain state, we carried out a two-sample (i.e., neglect vs. non-neglect) t-test on fraction times and dwell times. Finally, to examine the link between neglect severity and the temporal dynamics of brain states, we computed a set of Spearman rank correlations between the averaged CoC scores of Bells and Letter tests with the fraction times and dwell times of each brain state.

Brain state analysis in the sub-cohorts of patients with and without neglect

Finally, to study neglect-specific brain states, we separately extracted them from the sub-cohorts of patients with and without neglect by employing the above-described pipeline. Specifically, we computed the K-means clustering on the patient's dynamic functional connectivity matrices by grouping them in two distinct sub-groups (neglect, $n = 11$/non-neglect, $n = 9$). Of note, compared to the main analysis, this procedure yielded two sets of centroid matrices obtained with the unique contribution of the two sub-cohorts. Next, we computed the modularity and system segregation based on these centroid matrices. Finally, fraction times and dwell times were also extracted.

Results

Behavior and lesion topography

As reported in our previous studies (de Pasquale et al., 2021a; Spadone et al., 2022), 11 patients (55%) were classified as neglect since they scored above the CoC cut-off at least in one cancellation test (Rorden and Karnath, 2010). Moreover, within the neglect sub-group, some patients also exhibited deficits in general cognitive efficiency (60%), executive functions (57%), praxis abilities (37%), and verbal memory (66%). Finally, as previously described, the spatial topography of lesion distribution indicated that the highest incidence of strokes was present in the middle cerebral artery territory, with the thalamus and putamen as the most frequently damaged regions.

Static functional connectivity

Before estimating the dynamic functional connectivity, we computed the brain modularity and system segregation based on the average of the dynamic functional connectivity matrices. The analyses revealed that neglect patients exhibited lower static system segregation (mean = 0.5085, SD = 0.2071) as compared to non-neglect patients (mean = 0.6726, SD = 0.1020) [$t_{(18)} = -2.1646, p = 0.0441$]. Furthermore, no differences in terms of brain modularity were detected among two sub-groups [neglect, mean = 0.8211, SD = 0.4712; non-neglect, mean = 0.9869, SD = 0.4945; $t_{(18)} = -0.7656, p = 0.4538$].

Brain states in the whole cohort of patients

To perform the k-means analysis on the entire sample, i.e., patients with and without neglect, we first estimated the number of optimal classes through MPFC. We observed a clear MPFC peak corresponding to two clusters. Thus, we run K-means and we identified two distinct functional connectivity states, i.e., brain states, reoccurring during the functional MRI scans. Specifically, brain state 1 (43.8% of occurrence) was characterized by robust positive connectivity within each network (see structures around the diagonal of the reported matrix in Figure 1A). We observed a strong interaction, i.e., positive coupling, among two sets of systems comprising dorsal attention, sensorimotor, and cingulo-opercular networks as well as language, fronto-parietal, and default mode networks, respectively (Figure 1A). Finally, state 1 exhibited strong anti-coupling, i.e., negative inter-networks connectivity (i.e., anti-correlations), among two groups of networks: dorsal attention, sensorimotor, and cingulo-opercular on one side, vs. fronto-parietal and default mode (Figure 1A). By contrast, state 2 (56.2% of occurrence) featured weaker intra- and inter-network positive connections and a neglectable inter-network negative connectivity (Figure 1B). In state 2, apart from the visual, sensorimotor, and default mode network, the other networks lose their internal coupling and show sparse connections with the rest of the brain.

Next, to characterize the organization of brain networks of the two states, we computed the brain modularity and system segregation indices (see Section Methods). A two-tails paired t-test indicated that state 1 exhibited higher modularity (mean = 1.44; SD = 0.81) as compared to state 2 (mean = 0.65; SD = 0.33) ($t = 4.6$; $p < 0.0005$). Similarly, state 1 exhibited higher system segregation (mean = 0.6439; SD = 0.163) as compared to state 2 (mean = 0.5; SD = 0.2) ($t = 4.53$; $p = 0.0006$). Taken together, these results indicate that in state 1, as compared to state 2, network communities are more clearly differentiated (see Figures 1C, D for the spring-embedded representation of the centroid graph of state 1 and state 2, respectively). We note a strong interaction between default mode and fronto-parietal networks (see Figure 1C).

Successively, we investigated the differences in time-varying properties of two brain states among neglect and non-neglect groups. A set of two-sample t-tests on fraction times of state 1 and state 2 (high/low modularity and system segregation) indicated that neglect patients, as compared to non-neglect patients, exhibited lower and higher fraction times in state 1 ($t = -2.68$, $p = 0.036$, FDR-corrected) and in state 2 ($t = 2.68$, $p = 0.036$, FDR-corrected), respectively (Figure 2A). Moreover, two-sample t-tests on dwell times showed two marginally significant trends: in state 1 neglect group displayed lower dwell times as compared to non-neglect ($p = 0.08$, FDR-corrected); in state 2 it was observed a reverse pattern ($p = 0.09$, FDR-corrected) (Figure 2B). Taken together, these results indicate that neglect patients, compared to non-neglect ones, are generally less involved in state 1. In fact, they spend more continuous time and dwelt more in state 2 (vs. state 1).

Association between neglect severity and temporal dynamics of brain states

To investigate the association between neglect severity and the temporal dynamics of brain states, we employed the Spearman rank test to correlate the averaged CoC scores of Bells test and Letter test with the fraction times and dwell times of each brain state. The analyses revealed that neglect score was negatively correlated with fraction times of state 1 (high modularity and system segregation) ($r = -0.56$, $p = 0.009$, FDR-corrected) such that patients with severe neglect (high score) spent less amount of time in such state and vice versa (Figure 3A). By contrast, the neglect measure exhibited positive correlation with the fraction times of state 2 (low modularity and system segregation) ($r = 0.56$, $p = 0.009$,

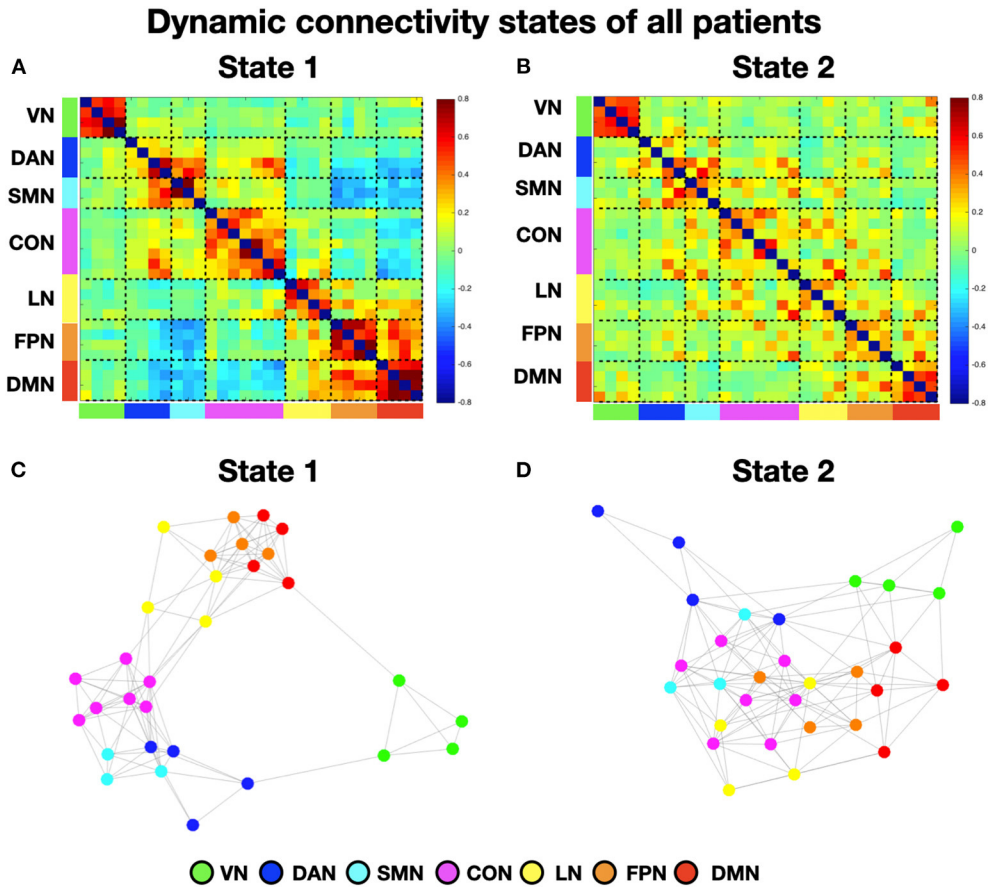

FIGURE 1
Dynamic connectivity states of all patients. **(A, B)** Display the centroid of the functional network connectivity states identified in the whole cohort (i.e., with and without neglect) of patients. The color bar indicates the Fisher-transformed *z*-scores of the Pearson correlation coefficient (*r*) among fMRI signals between all the possible pairs of nodes. **(C, D)** Show the spring-embedded representation of the centroid of the functional network connectivity states. VN, visual network; DAN, dorsal attention network; SMN, sensory-motor network; CON, cingulo-opercular network; LN, language network; FPN, fronto-parietal network; DMN, default mode network.

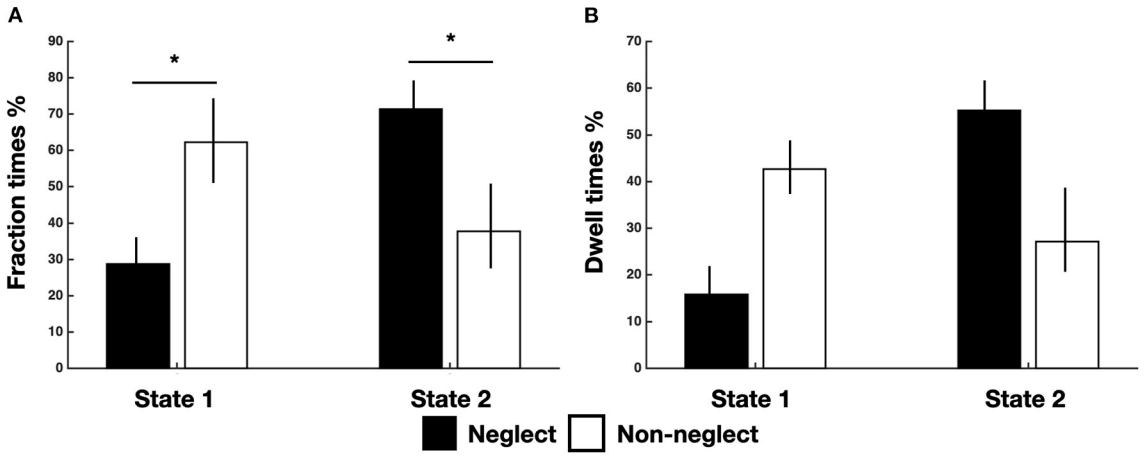

FIGURE 2
Temporal properties of brain states for neglect and non-neglect patients. Bar graphs indicate fraction **(A)** and dwell **(B)** times of each state for neglect (black) and non-neglect (white) patients, respectively. *$p < 0.05$, FDR-corrected.

FDR-corrected), indicating that patients with severe neglect (high score) spent more amount of time in that state and vice versa (Figure 3B). On the same line, it was detected that neglect score was negatively correlated with dwell times in state 1 ($r = -0.51$, $p = 0.022$) as well as positively correlated with dwell times in state 2 ($r = -0.52$, $p = 0.019$). These associations indicate that more impaired patients dwelt less and more often in state 1 and state 2, respectively (Figures 3C, D). Overall, these findings show that patients exhibiting stronger rightward bias (i.e., more severe neglect) spent more time and dwelt more often in the state featuring low brain modularity and system segregation and vice versa.

Brain states in the sub-cohorts of patients with and without neglect

To investigate neglect-specific aspects of the brain states, we extracted again them from each sub-cohort separately (see Section Methods). For the neglect cohort, we identified two brain states characterized by distinct connectivity profiles. Specifically, state 1 (28.5% of occurrence) featured widespread high positive functional connections both within and between networks (Figure 4A). Hence, such connectivity pattern blurred the distinction among functional systems. This state was not detected in the whole sample analysis. Furthermore, state 2 (71.5% of occurrence) was characterized by modest intra-network connections as well as exclusively positive values of inter-network connectivity (Figure 4B). Of note, the network connectivity configuration of this state resembled the one of state 2 detected in the whole cohort of patients (Figure 1B). The analyses in the non-neglect group also identified two brain states. In detail, state 1 (62.2% of occurrence) featured robust positive intra-network connectivity as well as interactions between networks (Figure 4C). Moreover, state 2 (37.8% of occurrence) (Figure 4D) exhibited a connectivity profile that strongly recapitulates that one of state 1 (i.e., positive intra-network and negative between-networks connectivity) identified in the whole sample (Figure 1A). Next, as in the whole sample analyses, we investigated the network configurations of the four states by computing and comparing the brain modularity and system segregation metrics (see Section Methods) with the caveat that the sample size of the sub-cohorts is relatively small (see Figure 5 for the spring-embedded representation of the centroid graph of state 1 and state 2 in the 2 sub-cohorts). A set of paired and two-sample *t*-tests on the modularity values indicated that state 1 of neglect group exhibited lower modularity as compared to state 2 of neglect group ($t = -5.83$; $p = 0.01$) as well as state 1 ($t = -2.66$; $p = 0.02$) and state 2 ($t = -10.2$; $p = 0.000005$) of non-neglect group. Furthermore, it was observed that state 2 of non-neglect group showed higher modularity as compared to state 1 of non-neglect group ($t = 7.28$; $p = 0.0003$) as well as state 1 ($t = 10.2$; $p = 0.000005$) and state 2 ($t = 4.66$; $p = 0.0003$) of neglect group. The same set of analyses on the system segregation indicated that state 2 of the non-neglect group exhibited a higher score than state 1 ($t = 6.05$; $p = 0.0001$) of the neglect group.

To summarize, the analyses on the sub-groups of patients with and without neglect indicated that: (i) a state featuring the lowest degree of modularity and system segregation, with blurred separation among networks, was detected solely in the sub-group of neglect patients (Figures 4A, 5A). Notably, this configuration was not highlighted by the analysis in the whole sample of patients; (ii) two states with comparable connectivity profiles were observed one in each sub-cohort (Figures 4B, 5B for neglect; Figures 4C, 5C for non-neglect); (iii) a highly modular and segregated state showing a clear distinction among sub-systems as well as robust negative connectivity between task-positive and task-negative systems was described only in the non-neglect group (Figures 4D, 5D).

Control analyses

We carried out a set of control analyses to assess whether the differences in terms of brain states among two sub-groups of patients were related to variables of interests. Specifically, we compared the overall NIHSS scores, the lesion size, and the number of outlier scans between neglect and non-neglect patients, by means of two-tail two-sample *t*-tests. Regarding the NIHSS, the overall symptom severity of neglect group (mean = 11.6, SD = 5.33, $n = 10$ since for one patient the score was not available) was not different as compared to the one of non-neglect group (mean = 8.5, SD = 5.95, $n = 8$ since for one patient the score was not available) ($t = 1.16$, $p = 0.26$). Furthermore, the lesion size of neglect group (mean = 9.98 cm^3; SD = 9.23 cm^3; $n = 11$) and non-neglect group (mean = 8.95 cm^3; SD = 16.51 cm^3; $n = 9$) did not differ ($t = 0.1762$, $p = 0.862$). Finally, no differences were observed between groups ($t = 1.49$, $p = 0.159$) in terms of outlier scans. Taken together, these analyses indicate that the overall symptom severity, the amount of structural damage as well as the head movements do not account for the association between spatial neglect and patterns of dynamic functional connectivity.

Discussion

In the current study, we investigated the brain states associated with the pathology of spatial neglect in a cohort of acute right-hemisphere damaged patients. To this aim, we estimated the dynamic functional connectivity MRI which allows us to assess brain network variations in a time-scale resolution of seconds (Allen et al., 2014; Calhoun et al., 2014). By employing the sliding window approach and clustering analysis we identified two brain states featuring distinct connectivity profiles characterized by the degree of brain modularity and system segregation. Specifically, we observed that neglect, compared to non-neglect patients, spent more time in a low modularity and segregation state, characterized by weak intra-module connections and widespread positive interactions among modules. By contrast, non-neglect patients occupy larger fractions of time in high modularity and segregation states comprising high within-network functional connections, sparse between-networks interactions, and anti-correlation between the so-called task-positive and task-negative systems. Finally, a state with robust intra- and inter-network connectivity, low modularity and system segregation was detected exclusively in the neglect sub-group.

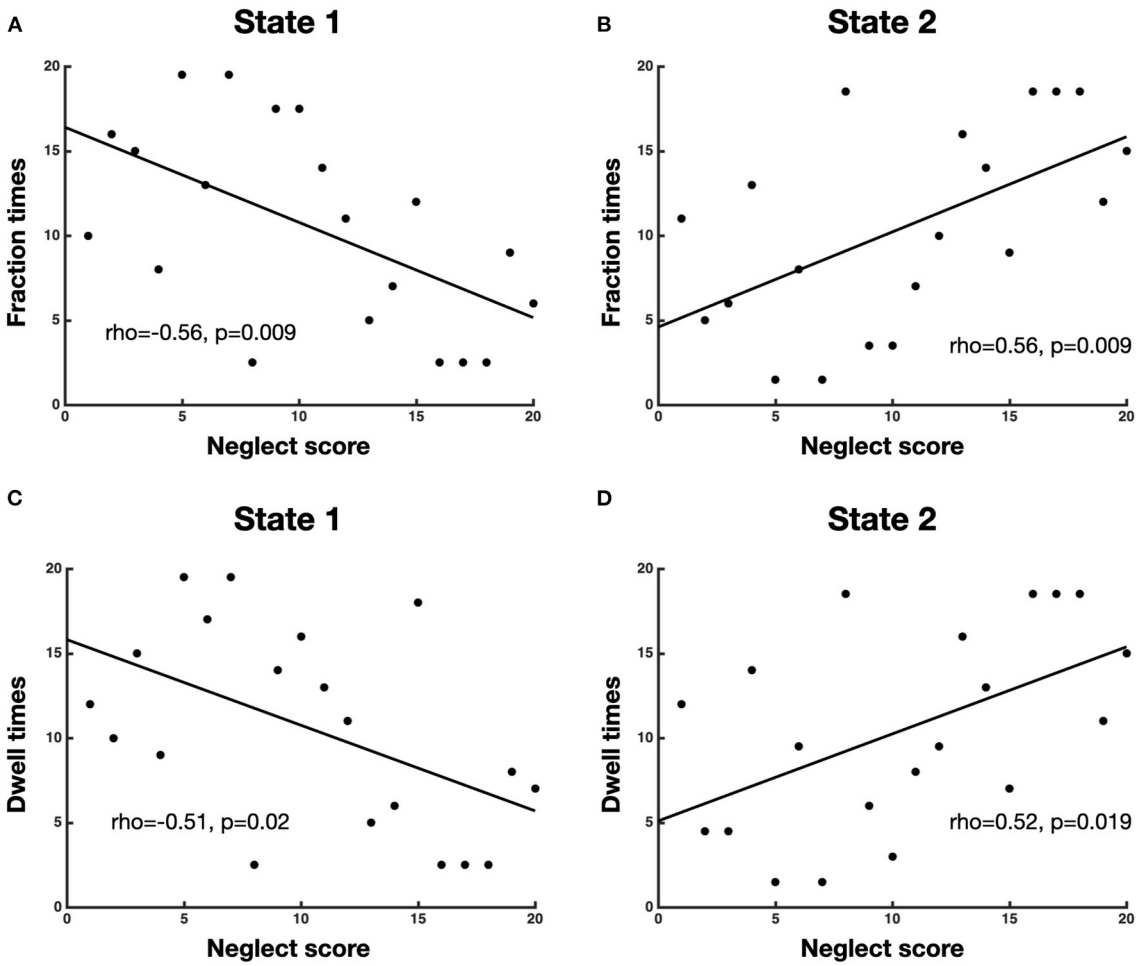

FIGURE 3
Association between neglect severity and temporal dynamics of brain states. The scatterplots display the Spearman rank correlation between neglect score and fraction times of state 1 **(A)** and state 2 **(B)** as well as dwell times of state 1 **(C)** and state 2 **(D)**. Each dot represents a patient ($n = 20$). To be noted, high value on x-axis (neglect score) means severe neglect and vice versa.

Brain modularity and system segregation represent key features of the mesoscale organization of the functional architecture of the brain, which orchestrate the processing of information among multiple networks (Bullmore and Sporns, 2009; Medaglia, 2017; Wig, 2017). The former indexes the extent to which a network can be subdivided into clearly distinct and non-overlapping communities or sub-systems. The latter quantifies the balance of intra-network integration and between-networks segregation. Our results clearly indicate that neglect patients exhibit a preference for brain states in which the distinctions among functional sub-systems are less defined or even blurred. Such brain configurations might represent a maladaptive response to a brain insult, i.e., focal lesion, such as a dedifferentiation-like mechanism (Fornito et al., 2015) characterized by the loss of the physiological balance between excitation and inhibition within neural systems. In this scenario, impaired behavior, e.g., visuo-spatial attention deficit, would be mediated by activations of task-irrelevant brain areas and by interactions among multiple functional systems that are not usually related to such behavior. Therefore, such pattern would result into the reduction of the network specialization (Li et al., 2001). This interpretation is consistent with several observations described in prior neuroimaging studies in neglect patients, both acutely and longitudinally. First, the rightward bias has been associated with the hyper- and hypo-activations of the left (contra-lesional) and right (ipsilesional) dorsal fronto-parietal attention regions, respectively (He et al., 2007). Such inter-hemispheric functional imbalance would result from affected excitatory and inhibitory mechanisms among the two hemispheres (Friedland and Weinstein, 1977; Kinsbourne, 1977). Notably, this pattern resolves over time as the recovery takes place. Second, the degree of spatial and non-spatial deficits in neglect has been linked, both acutely and longitudinally, to a loss of negative functional connectivity (i.e., segregation) between the dorsal attention and default mode networks in the right hemisphere (Baldassarre et al., 2014). Once again, a restoration of this pattern occurred in parallel with recovery (Ramsey et al., 2016). Finally, a neglect-relevant reduction of static system segregation of multiple large-scale networks at the acute stage (Spadone et al., 2022), as well as a restoration of brain modularity alongside the spontaneous recovery, has been reported (Siegel et al., 2018). Converging lines of evidence indicate that the

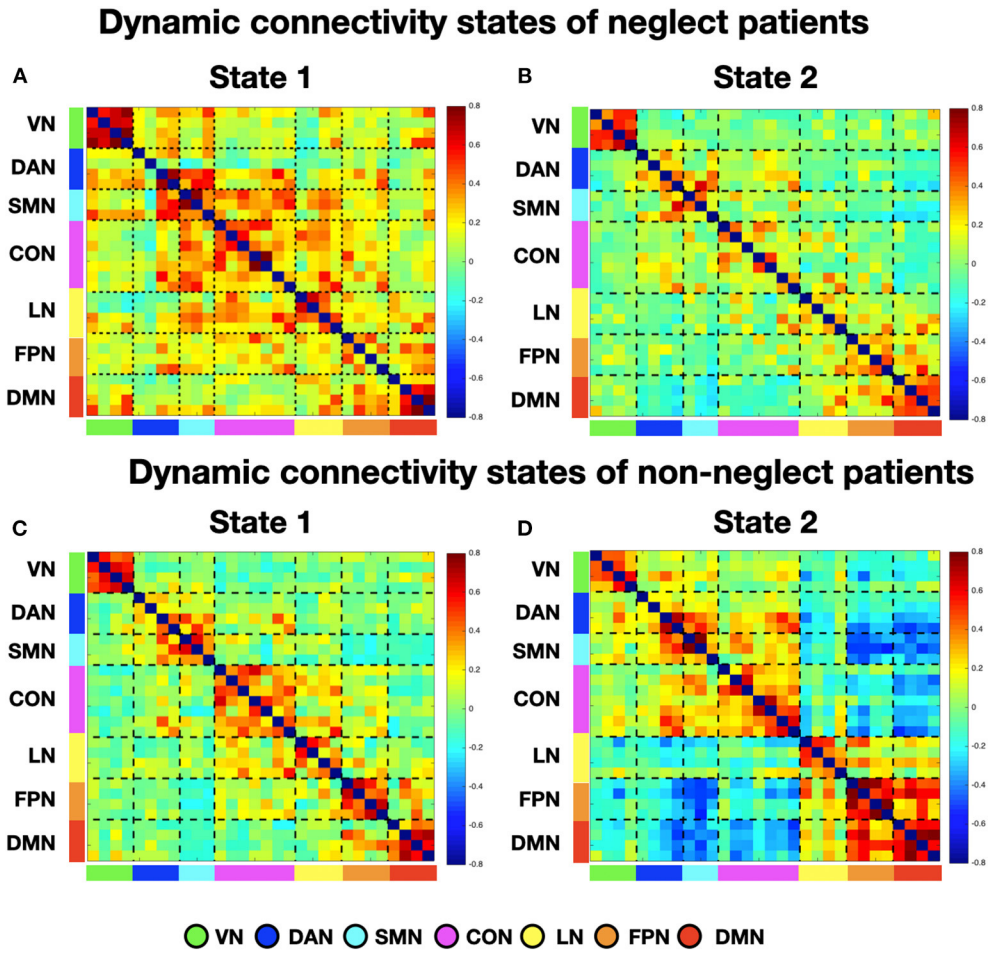

FIGURE 4
Dynamic connectivity states of neglect and non-neglect patients. **(A, B)** Display the centroid of the functional network connectivity states identified in the sub-cohort of neglect patients, whereas **(C, D)** indicate those of non-neglect patients. Color bar and abbreviations as in Figure 1.

degree of brain modularity and system segregation is relevant for the functional brain organization during lifespan in health and diseases (Chan et al., 2014; Marek et al., 2015; Ewers et al., 2021).

An important question is whether brain states featuring low modularity and system segregation might represent a key feature of the brain functional organization in other neurological conditions after focal lesions. Overall, current results generally agree with the findings obtained by recent studies that investigated brain states in stroke cohorts by employing a similar approach to that adopted in our work. Favaretto et al. (2022) identified five brain states characterized by different degrees of modularity as well as anti-correlation between dorsal attention and default mode networks in a large cohort of stroke patients. Crucially, the authors observed a preference of patients toward two states characterized by a high degree of integration among multiple networks and relatively high positive dorsal attention-default mode connectivity. This is in line with what we described here as state 2 of the whole cohort. Similarly, Wang et al. (2020) described four brain states and showed that patients with pontine stroke, compared to healthy controls, spent larger fraction times in a state featuring low segregation between networks as well as less fraction times in a state characterized by high segregation and anti-correlations among default mode network and task-positive systems. Notably, these two network configurations are very similar to the ones of our state 1 and state 2, respectively. In a longitudinal study, Bonkhoff et al. (2021b) identified three brain states: state 1 exhibited the highest segregation, with highly positive intra-domain connectivity, negative connectivity of visual network with somatomotor and cognitive networks; state 2 showed weak positive connectivity within network and near zero inter-networks connections; state 3 featured a network configuration in between state 1 and state 3. Critically, it was observed that more severely affected patients spent more time in state 1, i.e., a highly segregated state. In another recent fMRI study in the motor domain by Bonkhoff et al. (2020), the authors investigated in a cohort of acute stroke patients the association between upper limb deficit and brain states derived from the dynamic functional connectivity of three regional domains of the motor system, namely, cortical, subcortical, and cerebellar. Notably, they showed that severely affected patients exhibited a preference for a brain state characterized by high positive connections within each domain as well as anti-correlations among regions of different

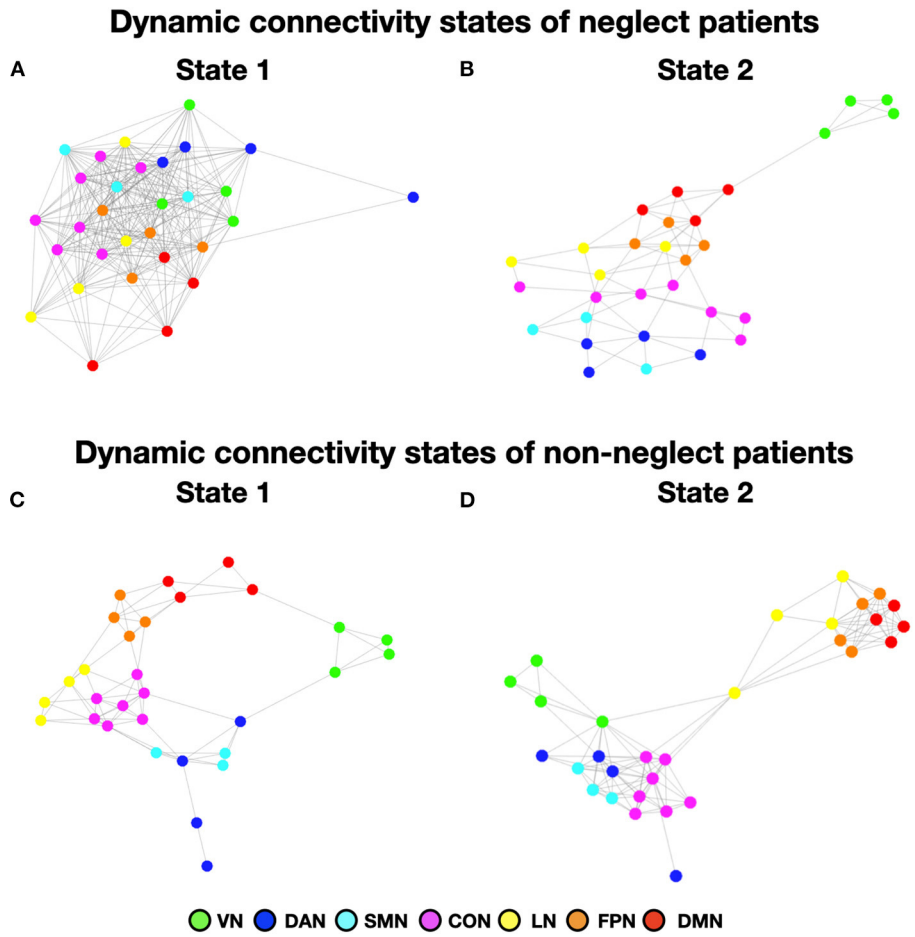

FIGURE 5
Dynamic connectivity states of neglect and non-neglect patients. **(A, B)** Show the spring-embedded representation of the centroid of the functional network connectivity states identified in the sub-cohort of neglect patients. In contrast, **(C, D)** refer to those of non-neglect patients. Abbreviations as in Figure 1.

modules, hence featuring high level of segregation. This set of results is in contrast with those described in our study as neglect patients spent more time in a state with low modularity and system segregation and without (or reduced) inter-networks anti-correlations. However, it has been proposed that both extremes of either low or high levels of modularity and system segregation, i.e., inverted U-shaped pattern, lead to maladaptive behavior (Wig, 2017). While increased connectivity among systems can generate a dedifferentiated state, a network configuration characterized by robust segregation would result in a loss of interactions among areas of different systems or even in a disconnected state. Hence, in such a scenario, other systems might not support isolated communities under attack. Moreover, while the latter study (Bonkhoff et al., 2020) focused on the sub-domains of the motor network, here we employed a whole-brain functional parcellation comprising seven large-scale networks. The difference in the granularity level makes the comparisons of the two results difficult. It also does not exclude the possibility that brain states derived from sub-components of neglect-relevant systems, e.g., parietal and frontal areas of the dorsal attention network, might feature in highly segregated configuration. Moreover, in their longitudinal study (Bonkhoff et al., 2021b), the authors estimated dynamic FC on independent components, which might not be directly comparable with time series of brain regions identified by an atlas. Finally, the parcellation used by Bonkhoff et al. emphasized visual and sensorimotor areas rather than association areas (i.e., yielded larger number of components).

Beside the above-described aspects, a key methodological point refers to the choice of the approach used for the identification of brain states. Many approaches have been developed to estimate dynamic functional connectivity, and among them the most popular one is the sliding window method which is based on the partitioning of the time-series into overlapped temporal segments and the calculation of the functional connectivity between two ROIs for each window (Hutchison et al., 2013a; Calhoun et al., 2014). The concept of functional connectivity is wide and includes any kind of statistical relationship between time series. A largely used approach to measure windowed correlation in resting-state fMRI research is Pearson correlation coefficient (Hutchison et al., 2013b; Zalesky et al., 2014; Kaiser et al., 2016; Spadone et al., 2021). Another approach employed for estimating dynamic correlation is the sparse inverse covariance matrix

(Allen et al., 2014; Damaraju et al., 2014). Among these methods, in the current study we estimated Pearson's correlation. As compared to other possible metrics, Pearson's correlation exhibits several advantages: (i) it requires less computational time; (ii) it is not dependent on the choice of the regularization parameter used to introduce spatial sparsity, which is currently discussed in the literature (see Zhang et al., 2021); (iii) it allows the comparison with our previous works on static functional connectivity in stroke patients (Baldassarre et al., 2014; de Pasquale et al., 2021a; Spadone et al., 2022). However, a common criticism of the Pearson correlation is its sensitivity to indirect functional relations between pairs of regions that are mediated by a third region. Notably, sparse representation approach is employed to overcome this issue, yielding a measure of direct interactions by removing the influence of other links among brain regions (Das et al., 2017). Therefore, it may be useful to combine our approach with other techniques for examining dynamic FC to gain a more complete view of the pathophysiology of neglect.

Overall, our results indicate that stroke leading to spatial neglect affects the temporal properties of functional interactions among large-scale networks, with a preferential configuration displaying low brain modularity and system segregation. In comparison to static functional connectivity studies, our findings offer two primary theoretical and clinical insights.

First, although in a small cohort of patients, the dynamic functional connectivity analyses identified a neglect-relevant brain state featuring widespread robust functional connections both within and between networks, with low modularity and system segregation. Notably, such brain configuration has not been described in previous studies employing static functional connectivity. Therefore, the dynamic interactions among brain systems might represent a key feature for higher functions such as spatial attention. Second, the temporal dynamics of neglect-relevant functional connectivity might guide protocol of non-invasive brain stimulation such as closed-loop, brain-state triggered TMS (Zrenner et al., 2016) for the treatment of spatial neglect.

Limitations

The current study has several limitations. First, the relatively small sample size ($n = 20$). Nonetheless, the proportion of patients classified as neglect is consistent with previous reports and is representative of a clinical population of patients who had suffered from a right-hemisphere lesion. However, future studies are needed to confirm the sub-group analyses given that the computation of connectivity states was carried out only on 11 and 9 patients with and without neglect, respectively. Second, in contrast with other recent studies, we did not include dynamic FC data from healthy controls in our analyses. However, comparing patients with vs. without the deficit of interest (i.e., spatial impairment) is a suitable approach to identify and characterize brain states selectively associated with neglect beside the mere effect of the underlying structural lesions. Third, we investigated extrapersonal, egocentric neglect, assessed by cancellation tests. Future studies are needed to link brain states to different components of neglect, like, for instance, personal neglect. Finally, we employed a fixed-length sliding window approach to identify brain states. Methods based on modeling brain states, such as the Hidden Markov models, should be applied to further dissect latent brain states.

Data availability statement

The raw data supporting the conclusions of this article will be made available by the authors, without undue reservation.

Ethics statement

The studies involving human participants were reviewed and approved by Institutional Review Board (IRB) of IRCCS NEUROMED. The patients/participants provided their written informed consent to participate in this study.

Author contributions

SS, FP, AD, and AB contributed to the study conception and design. LP and AB collected data. SS, AD, SLS, and AB analyzed data. SS and AB wrote the first draft of the manuscript. All authors commented on previous versions of the manuscript, read, and approved the final manuscript.

Funding

This work was supported by Ministry of Health, Italy.

Conflict of interest

The authors declare that the research was conducted in the absence of any commercial or financial relationships that could be construed as a potential conflict of interest.

Publisher's note

All claims expressed in this article are solely those of the authors and do not necessarily represent those of their affiliated organizations, or those of the publisher, the editors and the reviewers. Any product that may be evaluated in this article, or claim that may be made by its manufacturer, is not guaranteed or endorsed by the publisher.

Supplementary material

The Supplementary Material for this article can be found online at: https://www.frontiersin.org/articles/10.3389/fnsys.2023.1163147/full#supplementary-material

References

Allen, E. A., Damaraju, E., Plis, S. M., Erhardt, E. B., Eichele, T., Calhoun, V. D., et al. (2014). Tracking whole-brain connectivity dynamics in the resting state. *Cereb. Cortex* 24, 663–676. doi: 10.1093/cercor/bhs352

Baldassarre, A., Ramsey, L., Hacker, C. L., Callejas, A., Astafiev, S. V., Metcalf, N. V., et al. (2014). Large-scale changes in network interactions as a physiological signature of spatial neglect. *Brain* 137, 3267–3283. doi: 10.1093/brain/awu297

Baldassarre, A., Ramsey, L. E., Siegel, J. S., Shulman, G. L., and Corbetta, M. (2016). Brain connectivity and neurological disorders after stroke. *Curr. Opin. Neurol.* 29, 706–713. doi: 10.1097/WCO.0000000000000396

Bartolomeo, P., Thiebaut de Schotten, M., and Chica, A. B. (2012). Brain networks of visuospatial attention and their disruption in visual neglect. *Front. Hum. Neurosci.* 6, 110. doi: 10.3389/fnhum.2012.00110

Behzadi, Y., Restom, K., Liau, J., and Liu, T. T. (2007). A component based noise correction method (CompCor) for BOLD and perfusion based fMRI. *Neuroimage* 37, 90–101. doi: 10.1016/j.neuroimage.2007.04.042

Binder, J., Marshall, R., Lazar, R., Benjamin, J., and Mohr, J. P. (1992). Distinct syndromes of hemineglect. *Arch. Neurol.* 49, 1187–1194. doi: 10.1001/archneur.1992.00530350109026

Bonkhoff, A. K., Espinoza, F. A., Gazula, H., Vergara, V. M., Hensel, L., Michely, J., et al. (2020). Acute ischaemic stroke alters the brain's preference for distinct dynamic connectivity states. *Brain* 143, 1525–1540. doi: 10.1093/brain/awaa101

Bonkhoff, A. K., Rehme, A. K., Hensel, L., Tscherpel, C., Volz, L. J., Espinoza, F. A., et al. (2021a). Dynamic connectivity predicts acute motor impairment and recovery post-stroke. *Brain Commun.* 3, fcab227. doi: 10.1093/braincomms/fcab227

Bonkhoff, A. K., Schirmer, M. D., Bretzner, M., Etherton, M., Donahue, K., Tuozzo, C., et al. (2021b). Abnormal dynamic functional connectivity is linked to recovery after acute ischemic stroke. *Hum. Brain Mapp.* 42, 2278–2291. doi: 10.1002/hbm.25366

Bullmore, E., and Sporns, O. (2009). Complex brain networks: graph theoretical analysis of structural and functional systems. *Nat. Rev. Neurosci.* 10, 186–198. doi: 10.1038/nrn2575

Buxbaum, L. J., Ferraro, M. K., Veramonti, T., Farne, A., Whyte, J., Ladavas, E., et al. (2004). Hemispatial neglect: Subtypes, neuroanatomy, and disability. *Neurology* 62, 749–756. doi: 10.1212/01.WNL.0000113730.73031.F4

Calhoun, V. D., Miller, R., Pearlson, G., and Adali, T. (2014). The chronnectome: time-varying connectivity networks as the next frontier in fMRI data discovery. *Neuron* 84, 262–274. doi: 10.1016/j.neuron.2014.10.015

Carrera, E., and Tononi, G. (2014). Diaschisis: past, present, future. *Brain* 137, 2408–2422. doi: 10.1093/brain/awu101

Carter, A. R., Astafiev, S. V., Lang, C. E., Connor, L. T., Rengachary, J., Strube, M. J., et al. (2010). Resting interhemispheric functional magnetic resonance imaging connectivity predicts performance after stroke. *Ann. Neurol.* 67, 365–375. doi: 10.1002/ana.21905

Chan, M. Y., Park, D. C., Savalia, N. K., Petersen, S. E., and Wig, G. S. (2014). Decreased segregation of brain systems across the healthy adult lifespan. *Proc. Natl. Acad. Sci. U. S. A.* 111, E4997–5006. doi: 10.1073/pnas.1415122111

Committeri, G., Pitzalis, S., Galati, G., Patria, F., Pelle, G., Sabatini, U., et al. (2007). Neural bases of personal and extrapersonal neglect in humans. *Brain* 130, 431–441. doi: 10.1093/brain/awl265

Corbetta, M., Ramsey, L., Callejas, A., Baldassarre, A., Hacker, C. D., Siegel, J. S., et al. (2015). Common behavioral clusters and subcortical anatomy in stroke. *Neuron* 85, 927–941. doi: 10.1016/j.neuron.2015.02.027

Corbetta, M., and Shulman, G. L. (2011). Spatial neglect and attention networks. *Annu. Rev. Neurosci.* 34, 569–599. doi: 10.1146/annurev-neuro-061010-113731

Damaraju, E., Allen, E. A., Belger, A., Ford, J. M., McEwen, S., Mathalon, D. H., et al. (2014). Dynamic functional connectivity analysis reveals transient states of dysconnectivity in schizophrenia. *NeuroImage Clin.* 5, 298–308. doi: 10.1016/j.nicl.2014.07.003

Das, A., Sampson, A. L., Lainscsek, C., Muller, L., Lin, W., Doyle, J. C., et al. (2017). Interpretation of the precision matrix and its application in estimating sparse brain connectivity during sleep spindles from human electrocorticography recordings. *Neural Comput.* 29, 603–642. doi: 10.1162/NECO_a_00936

de Pasquale, F., Chiacchiaretta, P., Pavone, L., Sparano, A., Capotosto, P., Grillea, G., et al. (2021a). Brain topological reorganization associated with visual neglect after stroke. *Brain Connect*. doi: 10.1089/brain.2020.0969. [Epub ahead of print].

de Pasquale, F., Spadone, S., Betti, V., Corbetta, M., and Della Penna, S. (2021b). Temporal modes of hub synchronization at rest. *Neuroimage* 235, 118005. doi: 10.1016/j.neuroimage.2021.118005

Doricchi, F., and Tomaiuolo, F. (2003). The anatomy of neglect without hemianopia: a key role for parietal-frontal disconnection? *Neuroreport* 14, 2239–2243. doi: 10.1097/00001756-200312020-00021

Ewers, M., Luan, Y., Frontzkowski, L., Neitzel, J., Rubinski, A., Dichgans, M., et al. (2021). Segregation of functional networks is associated with cognitive resilience in Alzheimer's disease. *Brain* 144, 2176–2185. doi: 10.1093/brain/awab112

Favaretto, C., Allegra, M., Deco, G., Metcalf, N. V., Griffis, J. C., Shulman, G. L., et al. (2022). Subcortical-cortical dynamical states of the human brain and their breakdown in stroke. *Nat. Commun.* 13, 5069. doi: 10.1038/s41467-022-32304-1

Fornito, A., Zalesky, A., and Breakspear, M. (2015). The connectomics of brain disorders. *Nature Rev. Neurosci.* 16, 159–172. doi: 10.1038/nrn3901

Friedland, R. P., and Weinstein, E. A. (1977). Hemi-inattention and hemisphere specialization: introduction and historical review. *Adv. Neurol.* 18, 1–31.

Friston, K. J., Holmes, A. P., Poline, J. B., Grasby, P. J., Williams, S. C., Frackowiak, R. S., et al. (1995). Analysis of fMRI time-series revisited. *Neuroimage* 2, 45–53. doi: 10.1006/nimg.1995.1007

Halligan, P. W., Marshall, J. C., and Wade, D. T. (1989). Visuospatial neglect: underlying factors and test sensitivity. *Lancet* 2, 908–911. doi: 10.1016/S0140-6736(89)91561-4

He, B. J., Snyder, A. Z., Vincent, J. L., Epstein, A., Shulman, G. L., Corbetta, M., et al. (2007). Breakdown of functional connectivity in frontoparietal networks underlies behavioral deficits in spatial neglect. *Neuron* 53, 905–918. doi: 10.1016/j.neuron.2007.02.013

Husain, M., and Kennard, C. (1996). Visual neglect associated with frontal lobe infarction. *J. Neurol.* 243, 652–657. doi: 10.1007/BF00878662

Husain, M., and Rorden, C. (2003). Non-spatially lateralized mechanisms in hemispatial neglect. *Nat. Rev. Neurosci.* 4, 26–36. doi: 10.1038/nrn1005

Hutchison, R. M., Womelsdorf, T., Allen, E. A., Bandettini, P. A., Calhoun, V. D., Corbetta, M., et al. (2013a). Dynamic functional connectivity: promise, issues, and interpretations. *Neuroimage* 80, 360–378. doi: 10.1016/j.neuroimage.2013.05.079

Hutchison, R. M., Womelsdorf, T., Gati, J. S., Everling, S., and Menon, R. S. (2013b). Resting-state networks show dynamic functional connectivity in awake humans and anesthetized macaques. *Hum. Brain Mapp.* 34, 2154–2177. doi: 10.1002/hbm.22058

Kaiser, R. H., Whitfield-Gabrieli, S., Dillon, D. G., Goer, F., Beltzer, M., Minkel, J., et al. (2016). Dynamic resting-state functional connectivity in major depression. *Neuropsychopharmacology* 41, 1822–1830. doi: 10.1038/npp.2015.352

Karnath, H. O., Ferber, S., and Himmelbach, M. (2001). Spatial awareness is a function of the temporal not the posterior parietal lobe. *Nature* 411, 950–953. doi: 10.1038/35082075

Karnath, H. O., Fruhmann Berger, M., Kuker, W., and Rorden, C. (2004). The anatomy of spatial neglect based on voxelwise statistical analysis: a study of 140 patients. *Cereb. Cortex* 14, 1164–1172. doi: 10.1093/cercor/bhh076

Karnath, H. O., and Rorden, C. (2012). The anatomy of spatial neglect. *Neuropsychologia* 50, 1010–1017. doi: 10.1016/j.neuropsychologia.2011.06.027

Karnath, H. O., Rorden, C., and Ticini, L. F. (2009). Damage to white matter fiber tracts in acute spatial neglect. *Cereb. Cortex* 19, 2331–2337. doi: 10.1093/cercor/bhn250

Karnath, H. O., Zopf, R., Johannsen, L., Fruhmann Berger, M., Nagele, T., Klose, U., et al. (2005). Normalized perfusion MRI to identify common areas of dysfunction: patients with basal ganglia neglect. *Brain* 128, 2462–2469. doi: 10.1093/brain/awh629

Kinsbourne, M. (1977). Hemi-neglect and hemisphere rivalry. *Adv. Neurol.* 18, 41–49.

Leonardi, N., and Van De Ville, D. (2015). On spurious and real fluctuations of dynamic functional connectivity during rest. *Neuroimage* 104, 430–436. doi: 10.1016/j.neuroimage.2014.09.007

Li, S. C., Lindenberger, U., and Sikstrom, S. (2001). Aging cognition: from neuromodulation to representation. *Trends Cogn. Sci.* 5, 479–486. doi: 10.1016/S1364-6613(00)01769-1

Marek, S., Hwang, K., Foran, W., Hallquist, M. N., and Luna, B. (2015). The contribution of network organization and integration to the development of cognitive control. *PLoS Biol.* 13, e1002328. doi: 10.1371/journal.pbio.1002328

Medaglia, J. D. (2017). Graph theoretic analysis of resting state functional MR imaging. *Neuroimaging Clin. N. Am.* 27, 593–607. doi: 10.1016/j.nic.2017.06.008

Mort, D. J., Malhotra, P., Mannan, S. K., Rorden, C., Pambakian, A., Kennard, C., et al. (2003). The anatomy of visual neglect. *Brain* 126, 1986–1997. doi: 10.1093/brain/awg200

Nieto-Castanon, A. (2020). *Handbook of Functional Connectivity Magnetic Resonance Imaging methods in CONN*. Hilbert Press.

Power, J. D., Mitra, A., Laumann, T. O., Snyder, A. Z., Schlaggar, B. L., Petersen, S. E., et al. (2014). Methods to detect, characterize, and remove motion artifact in resting state fMRI. *Neuroimage* 84, 320–341. doi: 10.1016/j.neuroimage.2013.08.048

Ramsey, L. E., Siegel, J. S., Baldassarre, A., Metcalf, N. V., Zinn, K., Shulman, G. L., et al. (2016). Normalization of network connectivity in hemispatial neglect recovery. *Ann. Neurol.* 80, 127–141. doi: 10.1002/ana.24690

Ringman, J. M., Saver, J. L., Woolson, R. F., Clarke, W. R., and Adams, H. P. (2004). Frequency, risk factors, anatomy, and course of unilateral neglect in an acute stroke cohort. *Neurology* 63, 468–474. doi: 10.1212/01.WNL.0000133011.10689.CE

Rorden, C., and Karnath, H. O. (2010). A simple measure of neglect severity. *Neuropsychologia* 48, 2758–2763. doi: 10.1016/j.neuropsychologia.2010.04.018

Rubinov, M., and Sporns, O. (2010). Complex network measures of brain connectivity: uses and interpretations. *Neuroimage* 52, 1059–1069. doi: 10.1016/j.neuroimage.2009.10.003

Siegel, J. S., Seitzman, B. A., Ramsey, L. E., Ortega, M., Gordon, E. M., Dosenbach, N. U. F., et al. (2018). Re-emergence of modular brain networks in stroke recovery. *Cortex* 101, 44–59. doi: 10.1016/j.cortex.2017.12.019

Siegel, J. S., Shulman, G. L., and Corbetta, M. (2022). Mapping correlated neurological deficits after stroke to distributed brain networks. *Brain Struct. Funct.* 227, 3173–3187. doi: 10.1007/s00429-022-02525-7

Spadone, S., de Pasquale, F., Chiacchiaretta, P., Pavone, L., Capotosto, P., Delli Pizzi, S., et al. (2022). Reduced segregation of brain networks in spatial neglect after stroke. *Brain Connect*. doi: 10.1089/brain.2021.0184. [Epub ahead of print].

Spadone, S., de Pasquale, F., Mantini, D., and Della Penna, S. (2012). A K-means multivariate approach for clustering independent components from magnetoencephalographic data. *Neuroimage* 62, 1912–1923. doi: 10.1016/j.neuroimage.2012.05.051

Spadone, S., Perrucci, M. G., Di Cosmo, G., Costantini, M., Della Penna, S., Ferri, F., et al. (2021). Frontal and parietal background connectivity and their dynamic changes account for individual differences in the multisensory representation of peripersonal space. *Sci. Rep.* 11, 20533. doi: 10.1038/s41598-021-00048-5

Thiebaut de Schotten, M., Tomaiuolo, F., Aiello, M., Merola, S., Silvetti, M., and Lecce, F. (2014). Damage to white matter pathways in subacute and chronic spatial neglect: a group study and 2 single-case studies with complete virtual "in vivo" tractography dissection. *Cereb. Cortex* 24, 691–706. doi: 10.1093/cercor/bhs351

Tononi, G., Sporns, O., and Edelman, G. M. (1994). A measure for brain complexity: relating functional segregation and integration in the nervous system. *Proc. Natl. Acad. Sci. U. S. A.* 91, 5033–5037. doi: 10.1073/pnas.91.11.5033

Varsou, O., Macleod, M. J., and Schwarzbauer, C. (2014). Functional connectivity magnetic resonance imaging in stroke: an evidence-based clinical review. *Int. J. Stroke* 9, 191–198. doi: 10.1111/ijs.12033

Verdon, V., Schwartz, S., Lovblad, K. O., Hauert, C. A., and Vuilleumier, P. (2010). Neuroanatomy of hemispatial neglect and its functional components: a study using voxel-based lesion-symptom mapping. *Brain* 133, 880–894. doi: 10.1093/brain/awp305

Wang, Y., Wang, C., Miao, P., Liu, J., Wei, Y., Wu, L., et al. (2020). An imbalance between functional segregation and integration in patients with pontine stroke: a dynamic functional network connectivity study. *NeuroImage Clin.* 28, 102507. doi: 10.1016/j.nicl.2020.102507

Whitfield-Gabrieli, S., and Nieto-Castanon, A. (2012). Conn: a functional connectivity toolbox for correlated and anticorrelated brain networks. *Brain Connect.* 2, 125–141. doi: 10.1089/brain.2012.0073

Wig, G. S. (2017). Segregated systems of human brain networks. *Trends Cogn. Sci.* 21, 981–996. doi: 10.1016/j.tics.2017.09.006

Zalesky, A., Fornito, A., Cocchi, L., Gollo, L. L., and Breakspear, M. (2014). Time-resolved resting-state brain networks. *Proc. Natl. Acad. Sci. U. S. A.* 111, 10341–10346. doi: 10.1073/pnas.1400181111

Zhang, L., Fu, Z., Zhang, W., Huang, G., Liang, Z., Li, L., et al., (2021). Accessing dynamic functional connectivity using-regularized sparse-smooth inverse covariance estimation from fMRI. *Neurocomputing* 443, 147–161. doi: 10.1016/j.neucom.2021.02.081

Zrenner, C., Belardinelli, P., Muller-Dahlhaus, F., and Ziemann, U. (2016). Closed-loop neuroscience and non-invasive brain stimulation: a tale of two loops. *Front. Cell. Neurosci.* 10, 92. doi: 10.3389/fncel.2016.00092

frontiers | Frontiers in Systems Neuroscience

TYPE Original Research
PUBLISHED 05 May 2023
DOI 10.3389/fnsys.2023.1123221

OPEN ACCESS

EDITED BY
Alessandra Griffa,
Université de Genève, Switzerland

REVIEWED BY
Marianne Latinus,
INSERM U1253 Imagerie et Cerveau (iBrain), France
Marco Tamietto,
Tilburg University, Netherlands

*CORRESPONDENCE
Paola Sessa
✉ paola.sessa@unipd.it

†These authors have contributed equally to this work and share first authorship

RECEIVED 13 December 2022
ACCEPTED 17 April 2023
PUBLISHED 05 May 2023

CITATION
Quettier T, Maffei A, Gambarota F, Ferrari PF and Sessa P (2023) Testing EEG functional connectivity between sensorimotor and face processing visual regions in individuals with congenital facial palsy.
Front. Syst. Neurosci. 17:1123221.
doi: 10.3389/fnsys.2023.1123221

Testing EEG functional connectivity between sensorimotor and face processing visual regions in individuals with congenital facial palsy

Thomas Quettier[1,2†], Antonio Maffei[1,2†], Filippo Gambarota[1,2], Pier Francesco Ferrari[3] and Paola Sessa[1,2*]

[1]Department of Developmental and Social Psychology, University of Padua, Padua, Italy, [2]Padova Neuroscience Center (PNC), University of Padua, Padua, Italy, [3]Institut des Sciences Cognitives Marc Jeannerod, CNRS/Université Claude Bernard Lyon 1, Bron, France

Moebius syndrome (MBS) is characterized by the congenital absence or underdevelopment of cranial nerves VII and VI, leading to facial palsy and impaired lateral eye movements. As a result, MBS individuals cannot produce facial expressions and did not develop motor programs for facial expressions. In the latest model of sensorimotor simulation, an iterative communication between somatosensory, motor/premotor cortices, and visual regions has been proposed, which should allow more efficient discriminations among subtle facial expressions. Accordingly, individuals with congenital facial motor disability, specifically with MBS, should exhibit atypical communication within this network. Here, we aimed to test this facet of the sensorimotor simulation models. We estimated the functional connectivity between the visual cortices for face processing and the sensorimotor cortices in healthy and MBS individuals. To this aim, we studied the strength of beta band functional connectivity between these two systems using high-density EEG, combined with a change detection task with facial expressions (and a control condition involving non-face stimuli). The results supported our hypothesis such that when discriminating subtle facial expressions, participants affected by congenital facial palsy (compared to healthy controls) showed reduced connectivity strength between sensorimotor regions and visual regions for face processing. This effect was absent for the condition with non-face stimuli. These findings support sensorimotor simulation models and the communication between sensorimotor and visual areas during subtle facial expression processing.

KEYWORDS

Moebius syndrome, facial palsy, facial expressions, motor simulation, EEG functional connectivity, face processing

Introduction

Moebius Syndrome (MBS; Moebius, 1888) is a rare congenital neurological disorder characterized by the affection of cranial nerves VI and VII (Briegel, 2006), leading to impaired lateral eye movements and complete or nearly complete–usually bilateral–facial paralysis. In addition, other congenital conditions are sometimes present, such as limb anomalies (e.g., clubfoot and missing/underdeveloped fingers or hands; Richards, 1953; Verzijl et al., 2003). On the psychological side, individuals with MBS show difficulties in social interactions with different degrees of severity, mostly because they cannot express their emotions to others through their faces (Bogart and Matsumoto, 2010). Therefore, *per* the definition, MBS individuals are characterized by a deficit in the *production* of facial expressions.

A prominent theoretical model supports the existence of a close relationship between production (e.g., of gestures and facial expressions) and *perception* (e.g., of gestures and facial expressions) (Preston and de Waal, 2002; Rizzolatti and Sinigaglia, 2016). Several studies provided evidence in favor of shared neural representations of emotional facial expressions between production and perception in different brain regions. These include the inferior, middle, and superior frontal gyri, the amygdala, and the insula (Molenberghs et al., 2012), suggesting that these shared representations could hinge on mirror mechanisms (Van Overwalle and Baetens, 2009). Overall, this "shared representational system" is thought to subserve others' social understanding and emotion perception by *motor simulation* (Goldman and Sripada, 2005; Bastiaansen et al., 2009; Likowski et al., 2012). It has recently been hypothesized that the primary mechanism through which motor simulation supports emotion perception is that of an iterative communication between motor, premotor, somatosensory cortices (overall the sensorimotor system), and the visual cortices (Wood et al., 2016a,b). Specifically, iterative communication would increase the quality/precision of the visual percept, allowing for more efficient discriminations of facial expressions (Wood et al., 2016a,b). In this context, *facial mimicry*, the visible or invisible contraction of the facial muscles congruent with the observed expression, is conceived as a peripheral manifestation of the central sensorimotor simulation. Sensorimotor simulation models (Goldman and Sripada, 2005; Bastiaansen et al., 2009; Likowski et al., 2012; Wood et al., 2016a,b) assume that facial mimicry contributes to the motor simulation through the feedback provided to motor areas.

Within this theoretical framework, MBS individuals should be characterized by altered facial feedback to the central nervous system (especially to the motor cortex) because of facial palsy, and, as a consequence of the congenital condition, they should not have (at least complete) facial motor programs for facial expressions. In short, MBS individuals could not efficiently exert the hypothesized sensorimotor simulation mechanism in recognizing/discriminating facial expressions. Nevertheless, it is possible that by mechanisms of plasticity and compensation, individuals with MBS can achieve normotypical performances (Vannuscorps et al., 2020) and have developed alternative and efficient neural pathways for the recognition/discrimination of facial expressions (Sessa et al., 2022). Therefore investigations using neuroimaging techniques are necessary to explore the neural bases of the emotional expression processing in MBS individuals beyond their behavioral performance (in terms of accuracy and/or reaction times) that could be normotypical.

Due to the absence of a shared representational system/motor simulation, one might expect that the neurological population of MBS is characterized by: (a) impaired recognition/discrimination of emotional facial expressions (in the case of lack of compensation) and (b) lower degree of connectivity (compared to healthy individuals) between sensorimotor and visual systems during subtle discrimination of emotional facial expressions.

In a previous investigation, our findings corroborated the hypothesis of compensatory mechanisms, which, in terms of neural pathways, might hinge on the recruitment of different brain regions in MBS compared to healthy individuals during emotional expression discrimination tasks (Sessa et al., 2022). The specific aim of the present study, instead, is precisely to test the predicted reduced connectivity *between sensorimotor and visual systems in MBS, compared to healthy controls*.

To this aim, we administered our participants, healthy and MBS, an emotional expression discrimination task. Cortical activity was recorded with high-density electroencephalography (hd-EEG) to investigate functional connectivity, i.e., the strength to which activity between a pair of brain regions covaries or correlates over time (Lachaux et al., 1999). In the case of EEG signals, phase synchronization is one of the most widely used indexes to investigate functional connectivity under the assumption that the phase of two oscillations of different brain regions should be correlated if the two regions are functionally connected (Lachaux et al., 1999; López et al., 2014). We computed the phase locking value (corrected imaginary phase locking value; ciPLV; see section "Materials and methods") of the beta oscillatory activity according to the previous and convincing evidence that links the processing of stimuli with affective value to long-distance EEG connectivity in the beta band (Aftanas et al., 2002; Miskovic and Schmidt, 2010; Zhang et al., 2013; Wang et al., 2014; Kheirkhah et al., 2020; Kim et al., 2021).

Although not made explicit by the motor simulation models (Wood et al., 2016a,b), the visual cortices involved in the iterative communication must primarily entail regions delegated to the visual analysis of faces. The most accredited neural model of face processing, i.e., the distributed model of face processing by Haxby et al. (2000) and Haxby and Gobbini (2011), encompasses, indeed, a *core system* for faces' visual processing (comprising the fusiform face area, the occipital face area, and the posterior superior temporal sulcus; Haxby et al., 2000; Grill-Spector et al., 2004; Winston et al., 2004; Yovel and Kanwisher, 2004; Ishai et al., 2005; Rotshtein et al., 2005; Lee et al., 2010; Gobbini et al., 2011), and an *extended system* for additional non-visual processing steps, including the attribution of meaning to facial expressions in terms of emotion (comprising the sensorimotor cortices; Haxby and Gobbini, 2011).

Based on this knowledge, we expected *phase synchronization* (i.e., the connectivity index) *between the sensorimotor system and the core system* to be significantly greater in healthy participants than in MBS participants. As preliminary evidence to circumscribe and characterize this effect as face-sensitive, we included an identical task but involving non-face stimuli (i.e., animal shapes). We did not expect to observe any difference between healthy participants and MBS participants with regard to the strength of the connectivity index for non-face stimuli.

Materials and methods

Participants and task

In this research we enrolled 14 adults, seven MBS participants (MBS group: MBS 4 females and 3 males, mean age = 40, 43 years; s.d. = 11,03) and seven healthy control participants. Controls were matched for age, gender and level of education. Participants in the MBS group had a diagnosis of unilateral or bilateral facial paralysis (Terzis and Noah, 2003). See **Table 1** for demographic data and clinical information for MBS participants. All the participants did not report any psychiatric or physical illness.

Participants performed a simple change detection task in which they had to judge if a test image was different or not compared to a target image. This task has been successfully used to investigate changes in neural activity, as well as connectivity, during face processing (Wood et al., 2016a; Lomoriello et al., 2021; Maffei and Sessa, 2021a). In each trial the target image was presented on a screen for 750 ms, masked with noise for 350 ms and then followed by the test image which lasted on screen until response (**Figure 1**).

The stimuli were 11 digital images of faces and animals.

For each category, we created the morphing continuum as follows: for the face stimuli we had two continua, one ranging between the expression of anger and the expression of sadness, and one ranging between the expression of happiness and the expression of disgust (**Figure 2** shows stimuli of one of the morphing continuum); for the animal stimuli the continuum ranged between the image of a horse and the image of a cow, both presented in the same posture. Each continuum started with an expression/animal shape consisting in 100% of one expression/animal shape and 0% of the other (i.e., 100% anger–0% sadness or 100% happiness–0% disgust; 100% horse–0% cow), and then changed in 20% increments/decrements until reaching the opposite end (e.g., 0% sadness–100% anger, 0% horse–100% cow). The stimuli are available at the following link of the Open Science Framework repository: osf.io/krpfb.

On each trial, the *target* stimulus was randomly selected from one of the continua, then it was followed by the mask, and finally the *test* stimulus was presented. This latter test stimulus was selected from the same continuum of the target pseudorandomly, such that it was maximum 40% apart on the morph continuum, to control for discrimination difficulty across participants.

TABLE 1 Demographic data and clinical information for MBS participants.

Participant	Age	Gender	Cranial nerves involved	Disfunction
MBS1	54	Male	Abducens Nerve (VI)	No lateral eye movements
			Facial Nerve (VII)	Facial palsy
MBS2	57	Males	Abducens Nerve (VI)	No lateral eye movements
			Facial Nerve (VII)	Facial palsy
MBS3	38	Male	Abducens Nerve (VI)	No lateral eye movements
			Facial Nerve (VII)	Facial palsy
MBS4	25	Female	Abducens Nerve (VI)	No lateral eye movements
			Facial Nerve (VII)	Facial palsy
MBS5	65	Female	Facial Nerve (VII)	Facial palsy
MBS6	39	Female	Abducens Nerve (VI)	No lateral eye movements
			Facial Nerve (VII)	Facial palsy
MBS7	34	Female	Abducens Nerve (VI)	No lateral eye movements
			Facial Nerve (VII)	Facial palsy

EEG acquisition and pre-processing

Electroencephalography activity was recorded from 128 channels using an HydroCel Geodesic Sensor Net (HCGSN-128) connected to a Geodesic EEG System (EGI GES 300). Data were collected continuously with a sampling rate of 500 Hz using the vertex as online reference. Channel impedance was kept under 60 kΩ. For the purpose of the present research we analyzed the preprocessed data used in Sessa et al. (2022). Briefly, pre-processing consisted in downsampling the data to 250 Hz and band pass filtering (0.1–45 Hz), epoching between −500 to 1500 ms relative to target onset, rejection of artifactual components after ICA using the ICLabel algorithm (Pion-Tonachini et al., 2019), bad channel interpolation and referencing to the average of all channels. Further details regarding the pre-processing can be found in Sessa et al. (2022). The preprocessed data as well as the pre-processing script can be accessed at https://osf.io/krpfb/.

In order to estimate brain activity from the preprocessed scalp recordings, we first created a forward model using the three-layer boundary element method (BEM) from OpenMEEG, implemented in Brainstorm, and then estimated an inverse solution with the weighted Minimum Norm Estimation (wMNE) with default parameter. Finally, the estimated distributed source activity was downsampled to the 148 cortical parcels of the Destrieux et al. (2010), averaging the activity of all the vertices included in each parcel.

Functional connectivity analysis

Functional connectivity was estimated using the phase locking value, which is a widely used statistic able to quantify the degree of phase synchronization in a given frequency band (Lachaux et al., 1999; Maffei and Sessa, 2021a,b). Specifically, we employed an updated version of the original PLV statistics, recently introduced by Bruña et al. (2018): the corrected imaginary part of PLV (ciPLV). As with the original PLV, ciPLV analysis first requires a time-frequency decomposition of the signals, which can be obtained either through wavelets or applying the Hilbert transform on narrow-band filtered signals. Then, for each pair of signals, ciPLV is estimated as the imaginary part of the phase difference between the two signals. Contrary to the classic PLV, taking only the imaginary part of the phase difference allows to discard any zero-lag interactions, making ciPLV robust to volume conduction and/or

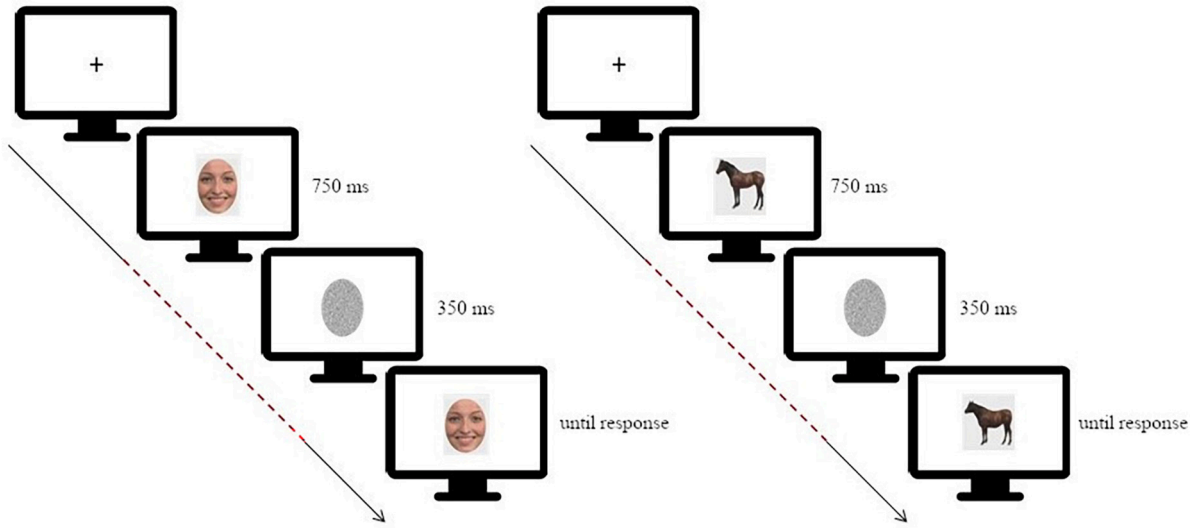

FIGURE 1
Schematic depiction of the experimental paradigm [on the **left**: for the facial expression discrimination task (morphing continua happiness-disgust); on the **right**: for the animal shape discrimination task]. The dashed line highlights the time window considered for the connectivity analysis, starting at target stimulus onset and ending before test stimulus onset. Adapted from Sessa et al. (2022).

source leakage which are known to inflate classic PLV (Bruña et al., 2018).

In this research, we first band-pass filtered the source estimated activity in the beta range (13–30 Hz), then applied the Hilbert transform to derive the analytical representation of the signals, and finally computed ciPLV for each pair of ROI of the Destrieux atlas in the time range between the onset of the target image and the onset of the test image (0–1100 ms). This workflow resulted in a 148 × 148 symmetric matrix M, where each entry represents the connectivity strength between each pair of regions. Then we subsampled this matrix, in order to extract a new rectangular matrix R, where the columns identify the regions belonging to the core system of the face processing network (Haxby and Gobbini, 2011; Maffei and Sessa, 2021a) and the rows identify the primary and secondary motor and somatosensory cortices (see **Supplementary material**). Each entry of this matrix thus represents the value of connectivity between a ROI belonging to the *core system* and a ROI belonging to the *sensorimotor system*. Finally, we computed the connectivity strength between the two systems as the sum of the matrix, $w = \sum_{i,j} R_{i,j}$ see **Figure 3**.

Statistical analysis

The main goal of this research was to test if participants with MBS are characterized by an impaired connectivity between visual and somatomotor regions during the processing of facial expressions. To test this hypothesis we performed an independent samples t-test on the connectivity strength estimated from trials in which participants were presented with facial expressions. The null hypothesis was that the two groups, MBS and controls, should not differ in the degree of functional connectivity between visual and sensorimotor regions. We also performed an additional analysis on the connectivity strength estimated from trials in which participants were presented with images of animals as a preliminary assessment to test the face-sensitivity of this effect. We present this analysis with caution as we are aware of the limitations of the statistical approach due to the extreme rarity of the MBS condition.

For the readers interested instead in analysis of the behavioral performance we refer to Sessa et al. (2022).

Results

Before running the statistical comparisons, we used the Shapiro-Wilk statistics to check for the normality of the data, and the test suggests that there is no violation of normality ($W_{face\_Moebius} = 0.92$, $p = 0.52$; $W_{face\_Controls} = 0.96$, $p = 0.83$;$W_{animal\_Moebius} = 0.93$, $p = 0.61$; $W_{animal\_Controls} = 0.97$, $p = 0.93$). The analysis performed for the *Face* condition revealed a significant difference [$t_{(12)} = -1.91$, $p < 0.05$, $d = -1.2$] between the two groups, showing that participants affected by facial palsy, compared to healthy controls, were characterized by a reduced connectivity strength between sensorimotor regions and visual regions comprised in the core system of the face processing network ($M_{MBS} = 0.7$, $M_{CTRL} = 1.2$; see **Figure 4**). Conversely, the analysis performed for the *Animal* condition did not reveal any significant difference between the two groups [$t_{(12)} = -1.36$, $p = 0.1$].

Discussion

Over the last 20 years, various models of (sensori)motor simulation (Goldman and Sripada, 2005; Bastiaansen et al., 2009; Likowski et al., 2012; Wood et al., 2016a,b) have been proposed, all sharing the central theoretical hypothesis that facial expressions' recognition and fine discrimination are supported by the recruitment–in the observer–of motor programs congruent

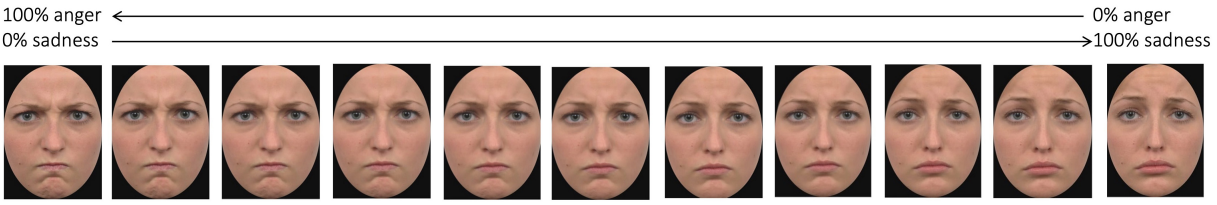

FIGURE 2
Example of stimuli of one of the morphing continua. Adapted from Sessa et al. (2022).

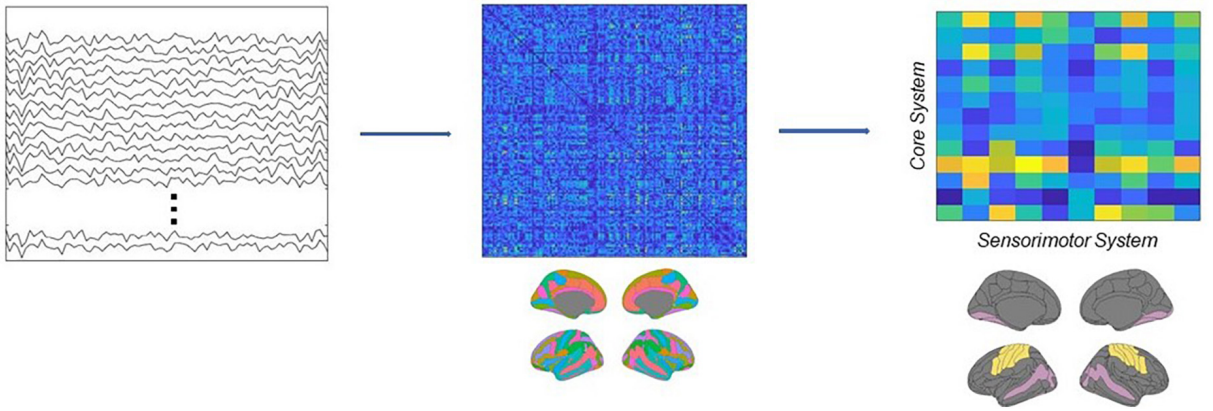

FIGURE 3
Schematic depiction of the analytical pipeline. Source activity was reconstructed from EEG recordings, then connectivity was estimated using the ciPLV in the beta band (13–30 Hz). Finally, the connectivity strength between the core and the sensorimotor systems was extracted from the full adjacency matrices.

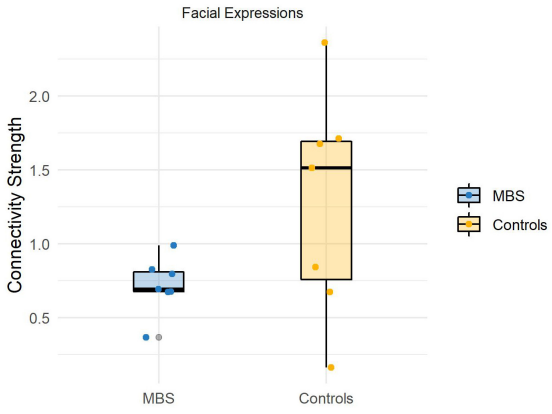

FIGURE 4
Individual connectivity strengths during facial expressions processing in the beta band (13–30 Hz) for each group.

with the facial expression observed, positing a relationship between production and recognition abilities. Therefore, it follows that individuals affected by clinical conditions limiting the production abilities, should also show recognition deficits. Although the congenital disorder in MBS subjects could trigger plastic cerebral modifications leading to alternative and efficient neural pathways to recognize emotional expressions, the deficiency of the simulation mechanism–if true–should necessarily translate into reduced functional connectivity between sensorimotor and visual systems, which is a central tenet of the most recent sensorimotor simulation models (see Wood et al., 2016b).

Here, we wanted to test this hypothesis by comparing the functional connectivity between the core system and the primary and secondary motor and somatosensory cortices in MBS and healthy individuals. We implemented a change detection task of facial expressions and animal shapes, and studied brain connectivity in terms of phase locking (corrected imaginary phase locking value; ciPLV; see section "Materials and method"). We restricted our analysis to beta oscillatory activity as the best approach to capture putative long-distance EEG connectivity involved in processing stimuli with affective value (Aftanas et al., 2002; Miskovic and Schmidt, 2010; Wang et al., 2014; Zhang et al., 2013; Kheirkhah et al., 2020; Kim et al., 2021).

The results supported our hypothesis. Indeed, as expected, for the facial expressions discrimination, reduced connectivity strength between sensorimotor regions and visual regions comprised in the core system of the face processing network was found in participants affected by facial palsy when compared to the matched healthy controls. Such a difference in the connectivity strength between the two groups was not observed for the animal shape condition. We are aware that the rarity of the syndrome and, consequently, the magnitude of the sample size cannot allow us to (statistically) conclude that the effect is selective for facial expressions.

Nevertheless, this reduction in the connectivity index for facial expressions was significant and, as such, it might indicate that the simulation mechanism is (at least) deficient in individuals with MBS. This result perfectly aligns with our hypothesis, since the alteration or absence of cranial nerves VI and VII as a consequence of the congenital condition restricts facial feedback to the central nervous system, and, more importantly, impairs the development (at least complete) of facial motor programs for facial expressions. Consequently, MBS individuals should not exhibit connectivity between the sensorimotor and the visual systems in the absence of a simulation mechanism (or, in the case of residual muscular functioning, they should exhibit reduced connectivity when compared to healthy individuals).

If the functional significance of this connectivity, as predicted in the model by Wood et al. (2016b), is to favor the fine processing of emotional facial expressions, one might expect that subjects with MBS should be less efficient in those tasks that require this type of processing. To note, however, studies that have investigated the ability to recognize emotional expressions in MBS individuals have produced conflicting results (e.g., De Stefani et al., 2019 for a review), although the most convincing evidence seems to indicate that the individuals with the syndrome may exhibit normotypical performance, at least in terms of correctness (i.e., accuracy) when recognizing/discriminating emotional faces (Rives Bogart and Matsumoto, 2010; Vannuscorps et al., 2020; Sessa et al., 2022). These last results, on the other hand, are in line with compensatory/plasticity mechanisms, plausibly starting from birth, as recently supported by a recent study by Sessa et al. (2022). This last study, indeed, provided evidence in favor of the recruitment of an alternative neural pathway in Moebius individuals (vs. healthy controls), which does not seem to involve the motor and somatosensory regions, but rather more ventral areas (from the occipital face area/fusiform face area to the anterior temporal lobe; compatible with the proposals by Duchaine and Yovel, 2015; Pitcher and Ungerleider, 2021) that in healthy individuals contribute to the processing of emotional expressions although preferentially involved in the processing of form information, for instance, for face identity processing (Vuilleumier et al., 2001; Ishai et al., 2004; Ganel et al., 2005; Xu and Biederman, 2010).

The present study has some limitations which should be mentioned.

First, the level and extension of the nerves alteration in MBS are different from one patient to another patient. From this point of view and due to the extreme rarity of the syndrome, it is not always possible recruiting a homogeneous group, so that one patient out of seven patients had a deficit of the facial/VII nerve alone in the absence of a concomitant impairment of the abducens/VI nerve (see **Table 1**).

Second, another potential limitation regards the smile surgery that allows MBS individuals to produce smile-like facial movements. Crucially, after smile surgery, MBS could develop smile-like motor programs and the associated motor representation, which could be also potentially dysfunctional for simulation. In the present study, the experimental procedure also envisaged the fine discrimination of facial expressions of happiness. However, the behavioral and connectivity analyses were not carried out on each category of emotional expression separately. As a consequence we cannot examine whether the processing (at the behavioral and neural level) of the expressions of happiness in patients who received smile surgery (all but one in our sample) differ from other emotional expressions.

Third, in the present study, we have used static facial expressions to investigate the impact of congenital facial palsy on the connectivity between the sensorimotor and visual systems. However, it is important to note that the dorsal pathway, which is involved in the processing of facial expressions, is more sensitive and more strongly recruited when dynamic rather than static facial expressions are processed (Duchaine and Yovel, 2015). This suggests that the sensorimotor simulation mechanism is more strongly triggered by dynamic facial expressions. Therefore, in the present study, we might have underestimated the impact of congenital facial palsy on the connectivity between the sensorimotor and visual systems. Future studies should consider using dynamic facial expressions to provide a more accurate understanding of the impact of congenital facial palsy on the sensorimotor and visual systems.

To conclude, our results support sensorimotor simulation models and the communication between sensorimotor and visual regions of the core system during subtle facial expression discrimination. Furthermore, they indicate that this communication is atypical in MBS individuals for facial expression processing.

Data availability statement

Publicly available datasets were analyzed in this study. This data can be found here: https://osf.io/krpfb/.

Ethics statement

The studies involving human participants were reviewed and approved by the Ethics Committee of the University of Padua (Protocol No. 2855). The patients/participants provided their written informed consent to participate in this study.

Author contributions

TQ: methodology and writing—original draft. AM: conceptualization, methodology, formal analysis, and writing—review and editing. FG: methodology and writing—review and editing. PF: conceptualization and writing—review and editing. PS: conceptualization, supervision, project administration, funding acquisition, and writing—review and editing. All authors contributed to the article and approved the submitted version.

Funding

This work was supported by funding assigned to PS (Fondazione Cariparo–"Ricerca Scientifica d'Eccellenza", call 2021).

Conflict of interest

The authors declare that the research was conducted in the absence of any commercial or financial relationships that could be construed as a potential conflict of interest.

Publisher's note

All claims expressed in this article are solely those of the authors and do not necessarily represent those of their affiliated organizations, or those of the publisher, the editors and the reviewers. Any product that may be evaluated in this article, or claim that may be made by its manufacturer, is not guaranteed or endorsed by the publisher.

Supplementary material

The Supplementary Material for this article can be found online at: https://www.frontiersin.org/articles/10.3389/fnsys.2023.1123221/full#supplementary-material

References

Aftanas, L. I., Varlamov, A. A., Pavlov, S. V., Makhnev, V. P., and Reva, N. V. (2002). Time-dependent cortical asymmetries induced by emotional arousal: EEG analysis of event-related synchronization and desynchronization in individually defined frequency bands. *Int. J. Psychophysiol.* 44, 67–82. doi: 10.1016/S0167-8760(01)00194-5

Bastiaansen, J. A. C. J., Thioux, M., and Keysers, C. (2009). Evidence for mirror systems in emotions. *Philos. Trans. R. Soc. London Series B Biol. Sci.* 364, 2391–2404. doi: 10.1098/rstb.2009.0058

Bogart, K. R., and Matsumoto, D. (2010). Living with Moebius syndrome: adjustment, social competence, and satisfaction with life. *Cleft Palate-Craniofacial J.* 47, 134–142. doi: 10.1597/08-257.1

Briegel, W. (2006). Neuropsychiatric findings of Möbius sequence – a review. *Clin. Genet.* 70, 91–97. doi: 10.1111/j.1399-0004.2006.00649.x

Bruña, R., Maestú, F., and Pereda, E. (2018). Phase locking value revisited: teaching new tricks to an old dog. *J. Neural Eng.* 15:056011. doi: 10.1088/1741-2552/aacfe4

De Stefani, E., Nicolini, Y., Belluardo, M., and Ferrari, P. F. (2019). Congenital facial palsy and emotion processing: the case of Moebius syndrome. *Genes Brain Behav.* 18:e12548. doi: 10.1111/gbb.12548

Destrieux, C., Fischl, B., Dale, A., and Halgren, E. (2010). Automatic parcellation of human cortical gyri and sulci using standard anatomical nomenclature. *NeuroImage* 53, 1–15. doi: 10.1016/j.neuroimage.2010.06.010

Duchaine, B., and Yovel, G. (2015). A revised neural framework for face processing. *Ann. Rev. Vis. Sci.* 1, 393–416. doi: 10.1146/annurev-vision-082114-035518

Ganel, T., Valyear, K. F., Goshen-Gottstein, Y., and Goodale, M. A. (2005). The involvement of the "fusiform face area" in processing facial expression. *Neuropsychologia* 43, 1645–1654. doi: 10.1016/j.neuropsychologia.2005.01.012

Gobbini, M. I., Gentili, C., Ricciardi, E., Bellucci, C., Salvini, P., Laschi, C., et al. (2011). Distinct neural systems involved in agency and animacy detection. *J. Cogn. Neurosci.* 23, 1911–1920. doi: 10.1162/jocn.2010.21574

Goldman, A. I., and Sripada, C. S. (2005). Simulationist models of face-based emotion recognition. *Cognition* 94, 193–213. doi: 10.1016/j.cognition.2004.01.005

Grill-Spector, K., Knouf, N., and Kanwisher, N. (2004). The fusiform face area subserves face perception, not generic within-category identification. *Nat. Neurosci.* 7, 555–562. doi: 10.1038/nn1224

Haxby, J., and Gobbini, M. I. (2011). "Distributed neural systems for face perception," in *Oxford Handbook of Face Perception*, eds G. Rhodes, A. Calder, M. Johnson, and J. Haxby (Oxford: OUP Oxford), 93–110. doi: 10.1093/oxfordhb/9780199559053.013.0006

Haxby, J. V., Hoffman, E. A., Gobbini, M. I., Haxby, J. V., Hoffman, E. A., and Gobbini, M. I. (2000). The distributed human neural system for face perception. *Trends Cogn. Sci.* 4, 223–233. doi: 10.1016/S1364-6613(00)01482-0

Ishai, A., Pessoa, L., Bikle, P. C., and Ungerleider, L. G. (2004). Repetition suppression of faces is modulated by emotion. *Proc. Natl. Acad. Sci. U S A.* 101, 9827–9832. doi: 10.1073/pnas.0403559101

Ishai, A., Schmidt, C. F., and Boesiger, P. (2005). Face perception is mediated by a distributed cortical network. *Brain Res. Bull.* 67, 87–93. doi: 10.1016/j.brainresbull.2005.05.027

Kheirkhah, M., Baumbach, P., Leistritz, L., Brodoehl, S., Götz, T., Huonker, R., et al. (2020). The temporal and spatial dynamics of cortical emotion processing in different brain frequencies as assessed using the cluster-based permutation test: an MEG study. *Brain Sci.* 10:352. doi: 10.3390/brainsci10060352

Kim, H., Seo, P., Choi, J. W., and Kim, K. H. (2021). Emotional arousal due to video stimuli reduces local and inter-regional synchronization of oscillatory cortical activities in alpha- and beta-bands. *PLoS One* 16:e0255032. doi: 10.1371/journal.pone.0255032

Lachaux, J. P., Rodriguez, E., Martinerie, J., and Varela, F. J. (1999). Measuring phase synchrony in brain signals. *Hum. Brain Mapp.* 8, 194–208. doi: 10.1002/(SICI)1097-0193(1999)8:4<194::AID-HBM4>3.0.CO;2-C

Lee, L. C., Andrews, T. J., Johnson, S. J., Woods, W., Gouws, A., Green, G. G. R., et al. (2010). Neural responses to rigidly moving faces displaying shifts in social attention investigated with fMRI and MEG. *Neuropsychologia* 48, 477–490. doi: 10.1016/j.neuropsychologia.2009.10.005

Likowski, K. U., Mühlberger, A., Gerdes, A. B. M., Wieser, M. J., Pauli, P., and Weyers, P. (2012). Facial mimicry and the mirror neuron system: simultaneous acquisition of facial electromyography and functional magnetic resonance imaging. *Front. Hum. Neurosci.* 6:214. doi: 10.3389/fnhum.2012.00214

Lomoriello, A. S., Maffei, A., Brigadoi, S., and Sessa, P. (2021). Altering sensorimotor simulation impacts early stages of facial expression processing depending on individual differences in alexithymic traits. *Brain Cogn.* 148:105678. doi: 10.1016/j.bandc.2020.105678

López, M. E., Bruña, R., Aurtenetxe, S., Pineda-Pardo, J. Á, Marcos, A., Arrazola, J., et al. (2014). Alpha-band hypersynchronization in progressive mild cognitive impairment: a magnetoencephalography study. *J. Neurosci.* 34, 14551–14559. doi: 10.1523/JNEUROSCI.0964-14.2014

Maffei, A., and Sessa, P. (2021a). Event-related network changes unfold the dynamics of cortical integration during face processing. *Psychophysiology* 58:e13786. doi: 10.1111/psyp.13786

Maffei, A., and Sessa, P. (2021b). Time-resolved connectivity reveals the "how" and "when" of brain networks reconfiguration during face processing. *Neuroimage: Rep.* 1:100022. doi: 10.1016/j.ynirp.2021.100022

Miskovic, V., and Schmidt, L. A. (2010). Cross-regional cortical synchronization during affective image viewing. *Brain Res.* 1362, 102–111. doi: 10.1016/j.brainres.2010.09.102

Moebius, P. J. (1888). Ueber angeborene doppelseitige Abducens-Facialis-Lahmung. *Munchener Medizinische Wochenschrift* 35, 91–94.

Molenberghs, P., Cunnington, R., and Mattingley, J. B. (2012). Brain regions with mirror properties: a meta-analysis of 125 human fMRI studies. *Neurosci. Biobehav. Rev.* 36, 341–349. doi: 10.1016/j.neubiorev.2011.07.004

Pion-Tonachini, L., Kreutz-Delgado, K., and Makeig, S. (2019). ICLabel: an automated electroencephalographic independent component classifier, dataset, and website. *NeuroImage* 198, 181–197. doi: 10.1016/j.neuroimage.2019.05.026

Pitcher, D., and Ungerleider, L. G. (2021). Evidence for a third visual pathway specialized for social perception. *Trends Cogn. Sci.* 25, 100–110. doi: 10.1016/j.tics.2020.11.006

Preston, S. D., and de Waal, F. B. M. (2002). Empathy: its ultimate and proximate bases. *Behav. Brain Sci.* 25, 1–20; discussion 20–71. doi: 10.1017/S0140525X02000018

Richards, R. N. (1953). The Möbius syndrome. *J. Bone Joint Surg.* 35, 437–444. doi: 10.2106/00004623-195335020-00017

Rives Bogart, K., and Matsumoto, D. (2010). Facial mimicry is not necessary to recognize emotion: facial expression recognition by people with Moebius syndrome. *Soc. Neurosci.* 5, 241–251. doi: 10.1080/17470910903395692

Rizzolatti, G., and Sinigaglia, C. (2016). The mirror mechanism: a basic principle of brain function. *Nat. Rev. Neurosci.* 17, 757–765. doi: 10.1038/nrn.2016.135

Rotshtein, P., Henson, R. N. A., Treves, A., Driver, J., and Dolan, R. J. (2005). Morphing marilyn into maggie dissociates physical and identity face representations in the brain. *Nat. Neurosci.* 8, 107–113. doi: 10.1038/nn1370

Sessa, P., Schiano Lomoriello, A., Duma, G. M., Mento, G., De Stefani, E., and Ferrari, P. F. (2022). Degenerate pathway for processing smile and other emotional expressions in congenital facial palsy: an hdEEG investigation. *Philos. Trans. R. Soc. London Series B Biol. Sci.* 377:20210190. doi: 10.1098/rstb.2021.0190

Terzis, J. K., and Noah, E. M. (2003). Dynamic restoration in Möbius and Möbius-like patients. *Plastic Reconstruct. Surg.* 111, 40–55. doi: 10.1097/00006534-200301000-00007

Van Overwalle, F., and Baetens, K. (2009). Understanding others' actions and goals by mirror and mentalizing systems: a meta-analysis. *NeuroImage* 48, 564–584. doi: 10.1016/j.neuroimage.2009.06.009

Vannuscorps, G., Andres, M., and Caramazza, A. (2020). Efficient recognition of facial expressions does not require motor simulation. *eLife* 9:e54687. doi: 10.7554/eLife.54687

Verzijl, H. T. F. M., van der Zwaag, B., Cruysberg, J. R. M., and Padberg, G. W. (2003). Möbius syndrome redefined: a syndrome of rhombencephalic maldevelopment. *Neurology* 61, 327–333. doi: 10.1212/01.WNL.0000076484.91275.CD

Vuilleumier, P., Armony, J. L., Driver, J., and Dolan, R. J. (2001). Effects of attention and emotion on face processing in the human brain: an event-related fMRI study. *Neuron* 30, 829–841. doi: 10.1016/S0896-6273(01)00328-2

Wang, X.-W., Nie, D., and Lu, B.-L. (2014). Emotional state classification from EEG data using machine learning approach. *Neurocomputing* 129, 94–106. doi: 10.1016/j.neucom.2013.06.046

Winston, J. S., Henson, R. N. A., Fine-Goulden, M. R., and Dolan, R. J. (2004). fMRI-Adaptation reveals dissociable neural representations of identity and expression in face perception. *J. Neurophysiol.* 92, 1830–1839. doi: 10.1152/jn.00155.2004

Wood, A., Lupyan, G., Sherrin, S., and Niedenthal, P. (2016a). Altering sensorimotor feedback disrupts visual discrimination of facial expressions. *Psychon. Bull. Rev.* 23, 1150–1156. doi: 10.3758/s13423-015-0974-5

Wood, A., Rychlowska, M., Korb, S., and Niedenthal, P. (2016b). Fashioning the face: sensorimotor simulation contributes to facial expression recognition. *Trends Cogn. Sci.* 20, 227–240. doi: 10.1016/j.tics.2015.12.010

Xu, X., and Biederman, I. (2010). Loci of the release from fMRI adaptation for changes in facial expression, identity, and viewpoint. *J. Vis.* 10:36. doi: 10.1167/10.14.36

Yovel, G., and Kanwisher, N. (2004). Face perception domain specific. not process specific. *Neuron* 44, 889–898. doi: 10.1016/S0896-6273(04)00728-7

Zhang, W., Lu, J., Liu, X., Fang, H., Li, H., Wang, D., et al. (2013). Event-related synchronization of delta and beta oscillations reflects developmental changes in the processing of affective pictures during adolescence. *Int. J. Psychophysiol.* 90, 334–340. doi: 10.1016/j.ijpsycho.2013.10.005

frontiers | Frontiers in Neurology

TYPE Case Report
PUBLISHED 12 May 2023
DOI 10.3389/fneur.2023.1163005

OPEN ACCESS

EDITED BY
Alessandro Salvalaggio,
University Hospital of Padua, Italy

REVIEWED BY
Elena Salillas,
University of Zaragoza, Spain
Florian Schöberl,
LMU Munich University Hospital, Germany

*CORRESPONDENCE
Iole Indovina
i.indovina@hsantalucia.it

†These authors share first authorship

RECEIVED 10 February 2023
ACCEPTED 14 April 2023
PUBLISHED 12 May 2023

CITATION
Indovina I, Cacciola A, Delle Monache S, Milardi D, Lacquaniti F, Toschi N, Cochereau J and Bosco G (2023) A case report of agoraphobia following right parietal lobe surgery: changes in functional and structural connectivities of the multimodal vestibular network. *Front. Neurol.* 14:1163005. doi: 10.3389/fneur.2023.1163005

A case report of agoraphobia following right parietal lobe surgery: changes in functional and structural connectivities of the multimodal vestibular network

Iole Indovina[1,2*†], Alberto Cacciola[1†], Sergio Delle Monache[2,3], Demetrio Milardi[1], Francesco Lacquaniti[2,4], Nicola Toschi[5,6], Jerome Cochereau[7,8,9] and Gianfranco Bosco[2,4]

[1]Brain Mapping Lab, Department of Biomedical and Dental Sciences and Morphofunctional Imaging, University of Messina, Messina, Italy, [2]Laboratory of Neuromotor Physiology, IRCCS Santa Lucia Foundation, Rome, Italy, [3]Departmental Faculty of Medicine and Surgery, Saint Camillus International University of Health and Medical Sciences, Rome, Italy, [4]Department of Systems Medicine and Centre of Space BioMedicine, University of Rome Tor Vergata, Rome, Italy, [5]Department of Biomedicine and Prevention, University of Rome "Tor Vergata", Rome, Italy, [6]Department of Radiology, Athinoula A. Martinos Center for Biomedical Imaging, Boston, MA, United States, [7]Department of Neurosurgery, Poitiers University Medical Center, La Miletrie Hospital, Poitiers, France, [8]Institute of Functional Genomics, INSERM 1191, University of Montpellier, Montpellier, France, [9]University of Montpellier, Montpellier, France

Agoraphobia is a visuo-vestibular-spatial disorder that may involve dysfunction of the vestibular network, which includes the insular and limbic cortex. We sought to study the neural correlates of this disorder in an individual who developed agoraphobia after surgical removal of a high-grade glioma located in the right parietal lobe, by assessing pre- and post-surgery connectivities in the vestibular network. The patient underwent surgical resection of the glioma located within the right supramarginal gyrus. The resection interested also portions of the superior and inferior parietal lobe. Structural and functional connectivities were assessed through magnetic resonance imaging before and 5 and 7 months after surgery. Connectivity analyses focused on a network comprising 142 spherical regions of interest (4 mm radius) associated with the vestibular cortex: 77 in the left and 65 in the right hemisphere (excluding lesioned regions). Tractography for diffusion-weighted structural data and correlation between time series for functional resting-state data were calculated for each pair of regions in order to build weighted connectivity matrices. Graph theory was applied to assess post-surgery changes in network measures, such as strength, clustering coefficient, and local efficiency. Structural connectomes after surgery showed a decrease of strength in the preserved ventral portion of the supramarginal gyrus (PFcm) and in a high order visual motion area in the right middle temporal gyrus (37dl), and decrease of the clustering coefficient and of the local efficiency in several areas of the limbic, insular cortex, parietal and frontal cortex, indicating general disconnection of the vestibular network. Functional connectivity analysis showed both a decrease in connectivity metrics, mainly in high-order visual areas and in the parietal cortex, and an increase in connectivity metrics, mainly in the precuneus, parietal and frontal opercula, limbic, and insular cortex. This post-surgery reorganization of

the vestibular network is compatible with altered processing of visuo-vestibular-spatial information, yielding agoraphobia symptoms. Specifically, post-surgical functional increases of clustering coefficient and local efficiency in the anterior insula and in the cingulate cortex might indicate a more predominant role of these areas within the vestibular network, which could be predictive of the fear and avoiding behavior characterizing agoraphobia.

KEYWORDS

agoraphobia, graph theory, case report, connectivity, parietal glioma

Introduction

Lesions in the posterior perisylvian cortex can be associated with several visuo-vestibular-spatial dysfunctions, such as spatial hemineglect syndrome (1, 2), pusher syndrome (3), and out-of-body experiences (4, 5). Another syndrome, potentially related to a visuo-vestibular-spatial disorder is agoraphobia (6), originally described as a condition of fear-related alterations in spatial orientation and locomotor control triggered by places or situations that might cause a patient to panic and feel trapped (7). Nowadays, this syndrome is considered largely of psychiatric interest and mostly related to panic attacks (8). Nonetheless, the visuospatial and vestibular components of agoraphobia should not be dismissed as increasing evidence indicates strong associations between vestibular and anxiety disorders (9–15). Indeed, the vestibular and anxiety systems do interact at multiple levels from the brainstem to the cortex (16). Moreover, functional MRI studies have highlighted that vestibular stimulation has profound effects on the activity and connectivity of both vestibular and anxiety-related brain regions, modulated by neuroticism and introversion (13–15). The basis for this extensive interaction may rest on the fact that vestibular information, unlike other sensory modalities, is not relayed directly to a classically defined "primary cortex," but it engages a widely distributed network of brain areas integrating vestibular, visual, and somatosensory stimuli for the processing of motion and space. The main nodes of the vestibular network are represented by several regions around the parietal opercula, posterior insula, and adjacent perisylvian regions of the posterior parietal and temporal cortex (17–19), which also contribute significantly to the perception of gravity effects (20). The vestibular network extends further to the medial superior temporal area (MST), posterior inferior temporal gyrus, ventral intraparietal area, superior parietal lobe, sensory-motor cortex, hippocampal formation, anterior insula, inferior frontal gyrus, and cingulate cortex (20–24). Remarkably, some of these areas (e.g., anterior insula and hippocampus) are critically involved in emotional processing (25, 26), accounting for the close associations between anxiety and vestibular disorders observed clinically, including agoraphobia.

Along these lines, a recent resting-state functional MRI study reported that networks integrating visual, vestibular, and emotional signals to guide movement in space may be altered in subclinical agoraphobia (27). Moreover, agoraphobic patients show increased fMRI activation of the ventral striatum and insula when they expect agoraphobia-specific visual stimuli (28).

This study further investigated the neural correlates of this disorder in a patient who developed agoraphobia after surgical resection of a parietal glioma. Direct involvement of the parietal lobe in panic/agoraphobic symptoms has previously been advocated (29, 30). The area removed by surgery encompassed the right superior parietal lobule (5l, lateral area 5; 7PC, 7ip, postcentral, and intraparietal area 7), the intraparietal sulcus (hIP1/2/3, human intraparietal 1/2/3), and the inferior parietal lobe PFt (area supramarginalis tenuicorticalis), reaching inferiorly the anterior ventral supramarginal gyrus [named PIC in Indovina et al. (19)]. These areas can be considered hubs of the vestibular network and show significant decreases in topological network measures (local efficiency and clustering coefficient) in individuals with subclinical agoraphobia (19, 27). Based on this, it might be hypothesized that agoraphobia symptoms developed by this patient might have resulted from the reorganization of the connectivity within the vestibular network following the removal of these vestibular areas in the right hemisphere. We tested this idea by performing structural and functional connectivity analyses on MRI images acquired prior to and after the surgery using 142 spherical regions of interest defining bilaterally the visuospatial-emotional network (19). Consistent with the hypothesis, we found significant differences in several metrics of structural and functional connectivities.

Methods

Patient

We report the case of a 41-year-old female patient, left-handed, working as a salesperson, with no particular medical or psychiatric history, who presented a partial comitial seizure, characterized by transient agraphia. The patient gave written informed consent to all the procedures, which was approved by the local Ethical Committee. Following MR scan at 3T MAGNETOM Skyra (Siemens Medical Systems, Erlangen, Germany) at La Miletrie Hospital (Poitiers University Medical Center, Poitiers, France), a FLAIR hypersignal localized in the superior portion of the right supramarginal gyrus was identified. Anti-comitial treatment with levetiracetam was initiated (1,000 mg twice a day) and, in view of the strong suspicion of diffuse glioma, the patient underwent surgery. The procedure was performed according to the local protocol, i.e., an asleep/awake/asleep surgery with positive cortical mapping without electrophysiology

10.3389/fneur.2023.1163005

recordings. Subcortical stimulations near the posterior insular cortex caused dizziness sensations. A post-operative MR scan confirmed the supra-total resection of the FLAIR anomaly. Post-operative follow-up was marked by rapidly resolving praxis difficulties and agraphia. However, as soon as she returned home, the patient reported symptoms suggestive of agoraphobia, leading to avoidance behavior.

The outcomes of psychiatric and cognitive tests performed prior to and after the surgery are reported in the Supplementary material.

MRI acquisitions

MRI images were acquired at three different times: pre-surgery (pre-op) and 5 months (post-op1) and 7 months after surgery (post-op2) on a 3T MAGNETOM Skyra (for details see Supplementary material).

Gray matter parcellation and location of the lesion

To identify the areas removed by surgery, we realigned the anatomical acquisitions to the MNI 152 T1 1 mm template with the ANTs toolbox (31).

We used a "Sphere atlas" described previously (19) to define nodes for the construction of functional (from resting-state data)- and structural (from DWIdata)-weighted connectivity matrices. This atlas consisted of spherical regions (4 mm radius) placed on the geometric centers of regions defined in the Eickhoff (32) and Fan (33) atlases [see (19) for details]. We limited our analysis to 77 regions belonging to the vestibular network (Table 1). To identify and exclude the areas lying within the surgical bed, we overlapped the anatomical image acquired after surgery with the Sphere atlas (Figure 1). Details on the functional imaging and graph analyses are reported in the Supplementary material.

Results

Structural connectivity

For each node of the network (see Table 1), we compared the nodal strength, clustering coefficient, and local efficiency measured before (pre-op session) and 7 months after surgery (post-op2 session). Although none of the network areas showed significant changes in connection strength, the network did show a general reorganization reflected by significant changes in the clustering coefficient and local efficiency. As Figure 2A shows, the majority of areas ($n = 54$, red) showed a decrease in the clustering coefficient. These 54 areas were located in the limbic cortex (hippocampal and parahippocampal cortex, cingulate gyri), bilateral insula, parietal opercula and inferior parietal cortex, left superior parietal cortex, right middle temporal gyrus, and right premotor cortex (see also Supplementary Figure). Only five areas (green in Figure 2A), mainly located in the parietal and limbic cortex, showed an increase in the local clustering coefficient.

TABLE 1 A total of 77 selected regions in the multimodal vestibular network.

Location	Label	Area
Inferior Frontal gyrus	44d	Dorsal area 44
	44op	Opercular area 44
	44v	Ventral area 44
	44	Caudal area 44
	45	Rostral area 45
	45c	Caudal area 45
Precentral gyrus	4tl	Area 4 (tongue and larynx region)
	6cdl	Caudal dorsolateral area 6
	6cvl	Caudal ventrolateral area 6
Postcentral gyrus	1/2/3/tonla	1/2/3 tongue, larynx
Middle and superior temporal gyrus	MT/MST	Visual motion complex
	37dl	Dorsolateral area37
	37vl	Ventrolateral area 37
	37mv	Medioventral area 37
	37lv	
	cpSTS	Caudal posterior superior temporal sulcus
	rpSTS	Rostral posterior superior temporal sulcus
Inferior temporal gyrus	20rv	Rostroventral area 20
Parahippocampal gyrus	Entorhinal Cortex	
	35/36c	Caudal area 35/36
	35/36r	Rostral area 35/36
	28/34	Area 28/34
	TL	Area TL (lateral posterior parahippocampal gyrus)
	TH	Area hippocampotemporalis
Hippocampus proper	Subiculum	
	cHipp	Caudal hippocampus
	rHipp	Rostral hippocampus
Insula	Id1	Dysgranular insula
	Ig1	Granular insula 1
	Ig2	Granular insula 2
	dIa	Dorsal agranular insula
	dId	Dorsal dysgranular insula
	dIg	Dorsal granular insula
	vIa	Ventral agranular insula
	vId/vIg	Ventral dysgranular and granular insula
	TI	Area TI (temporal agranular insular cortex)

(Continued)

TABLE 1 (Continued)

Location	Label	Area
Parietal operculum	OP1	Secondary somatosensory area (SII)
	OP2	Parieto insular vestibular cortex (PIVC)
	OP3	Ventral somatosensory area (VS)
	OP4	Parietal ventral area (PV)
Cingulate gyrus	23c	Caudal area 23
	23d	Dorsal area 23
	23v	Ventral area 23
	24cd	Caudodorsal area 24
	24rv	Rostroventral area 24
	32p	Pregenual area 32
	32sg	Subgenual area 32
Inferior parietal cortex	**PF**	Area supramarginalis
	PFcm	Area supramarginalis columnata magnocellularis (posterior)
	PFm	Area supramarginalis magnocellularis
	Pfop	Area supramarginalis opercularis
	PFt	Area supramarginalis tenuicorticalis
	PIC	Rostroventral area 40
	39rv	Rostroventral area 39
Intraparietal sulcus	**hIP1**	Human intraparietal 1
	hIP2	Human intraparietal 2
	hIP3	Human intraparietal 3
Superior parietal lobe	5Ci	
	5L	
	5l	Lateral area 5
	7A	Medial area 7
	7P	
	7c	Caudal area 7
	7ip	Intraparietal area 7
	7PC	Postcentral area 7
	7pc	
	7r	Rostral area 7
Precuneus	5M	Medial area 5
	7M	Medial area 7
	7m	Medial area 7
	dmPOS	Dorsomedial parieto-occipital sulcus
	31	Area 31
Thalamus	Thal Parietal	
	Thal Premotor	
	Thal Temporal	
Cerebellum	Fastigial Nuclei	

(Continued)

The 10 areas in bold are those within the lesion that are excluded from the analysis (5l, 7ip, 7PC, PIC, hIP1, hIP2, hIP3, PF, PFt, and PFm, only in the right hemisphere).

A subset of those areas ($n = 15$) showing a decrease in clustering coefficient (Figure 2A, brighter red areas) showed also a decrease in the local efficiency, indicating a lower degree of communication between the nodes' neighbors. These areas belonged to the insula, parietal opercula, and right BA 4tl and 45.

Overall, the results of the structural connectivity analysis indicated a general decrease in the local network connectivity in the limbic cortex (insula, hippocampal formation, and cingulate cortex), the parietal opercula, the area 44, and high-order visual areas.

Functional connectivity

For each node of the network, we compared the connectivity metrics before surgery with that observed 5 and 7 months after surgery (pre-op, post-op1, and post-op2 sessions, respectively).

Pre-op vs. post-op1

As illustrated in Figure 2B, two regions in the middle/superior temporal gyrus of the right hemisphere (dorsolateral BA 37, 37dl) and in the supramarginal gyrus (PFcm) showed a significant decrease in connectivity strength, clustering coefficient, and local efficiency.

Additional areas showed reduced clustering coefficient, such as other high-order visual areas and the superior parietal cortex in the left hemisphere. In a subset of these areas, clustering coefficient decreases were accompanied by decreases in local efficiency.

Conversely, the clustering coefficient increased significantly in the right entorhinal cortex, the right inferior temporal gyrus, the left postcentral gyrus, as well as bilaterally in the parietal opercula, the insula, the precuneus, and the cingulate cortex. Again, in a subset of these regions, local efficiency was also increased.

Pre-op vs. post-op2

With this comparison, we noted that the decrease in connectivity strength observed 5 months after the surgery in the right PFcm and in the right 37dl persisted. Similarly, in the inferior parietal cortex and opercula bilaterally, in bilateral high-order visual areas, and in the left superior parietal lobule (see Figure 2B, Supplementary Figure), the reduction in the clustering coefficient

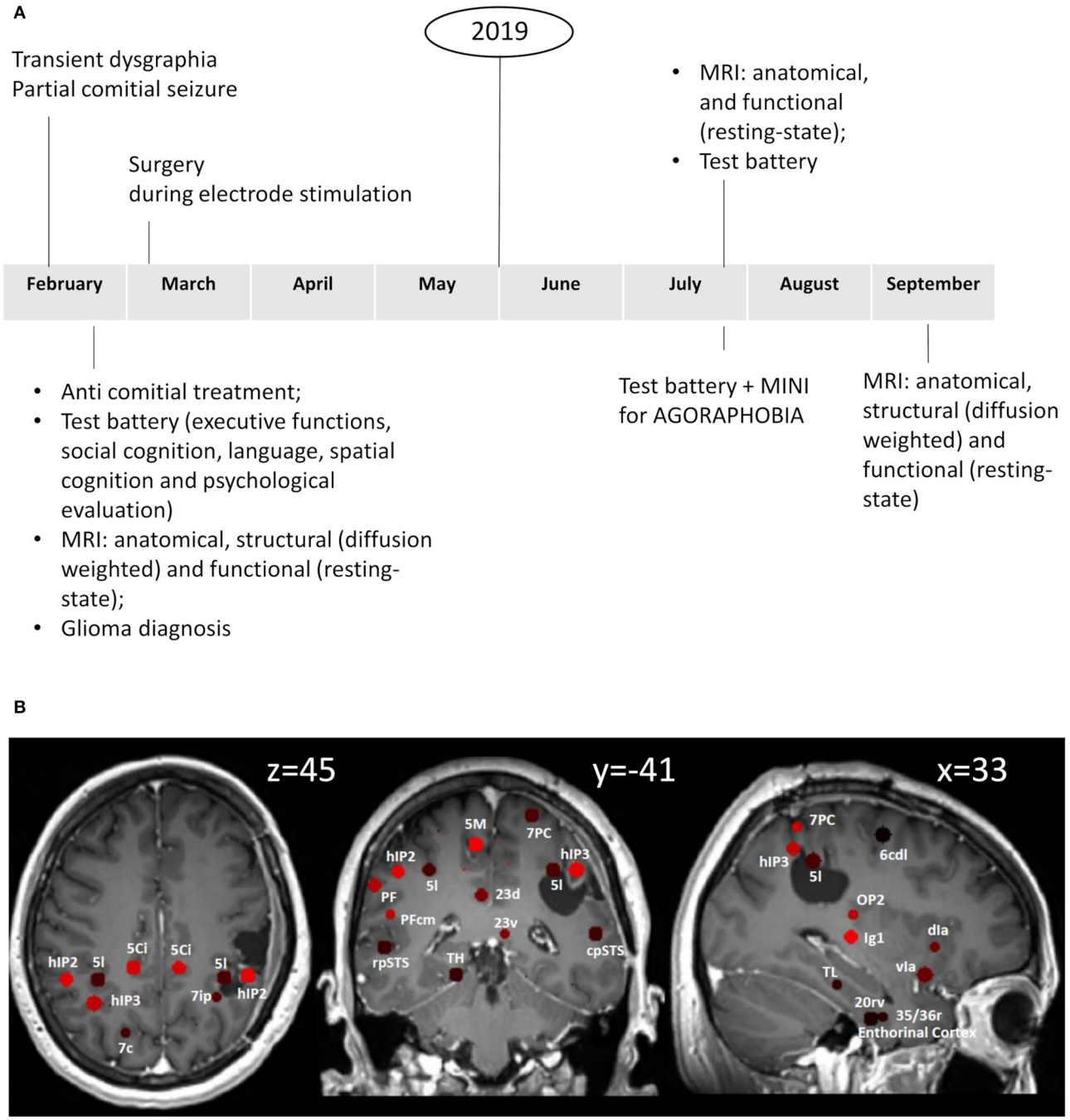

FIGURE 1
(A) Timeline with relevant episodes of care. **(B)** Sphere atlas superimposed on the first anatomical image taken after surgery. The anatomical image was realigned to the MNI 152 ICBM 2009a_nlin_hd_1mm template through ANTs.

was also evident at post-op2. Other cortical areas that did not show changes in post-op1, such as the premotor cortex and the anterior insula bilaterally, showed a reduction in the clustering coefficient in post-op2, mimicking the findings of the structural analysis performed on data drawn from the same sessions. Moreover, local efficiency was reduced in several of these regions.

Finally, a good degree of overlap with the pre-op vs. post-op1 comparison was also evident for the network nodes showing increased clustering coefficient and local efficiency.

In summary, unlike the structural connectivity analysis that showed a general decrease in the local network connectivity, functional analysis showed that the nodal clustering coefficient and local efficiency could decrease in some areas, notably high-order visual areas and parietal cortex, while increasing in some other areas, particularly the medial superior parietal cortex (precuneus) and opercula, hippocampal/parahippocampal cortex, and the insular cortex. Moreover, in some areas (right entorhinal cortex, left vId/vIg), significant changes were evident

in the first post-surgical session and partially reverted in the second session.

In other words, the results of the structural and functional analyses overlapped only partially. On the one hand, a good degree of overlap was evident, for example, in high-order visual 37dl, inferior parietal cortex (PFcm and rostral supramarginal gyrus PIC), and premotor areas, which showed a general decrease in both structural and functional connectivities. On the other hand, the two analyses showed divergent results in the limbic cortex where a general decrease in structural connectivity metrics was accompanied by a significant increase in functional connectivity metrics. Finally, other areas, such as the right anterior insula and frontal operculum, the subgenual cingulate, the bilateral precuneus, the left OP3, and the left 6cdl, showed an increase only in functional connectivity without significant changes in structural connectivity.

Discussion

Herein, we report the case of a patient who developed agoraphobic symptoms after surgical resection of a right parietal glioma. Glioma patients may experience impairments in motor and non-motor activities prior to treatment and are inherently at increased risk for further psychomotor, visuospatial, and emotional decline after surgery. While according to the localizationist theory, the anatomical location of tumors can predict specific symptoms, increasing evidence suggests that neuropsychiatric impairments may emerge from the disruption of more complex networks involving brain areas distributed both in close proximity to and far from the lesion (34–40).

This is of relevance, especially for gross total or supramaximal resections, in which the extent of resection exceeds any visible abnormalities. In this case report, the extent of surgery encompassed the right superior parietal lobule, the intraparietal sulcus, and the inferior parietal lobe, reaching inferiorly to the anterior ventral supramarginal gyrus. Considering the connectivity patterns of these areas and their involvement in the multimodal vestibular network, it may be reasonable to assume that the development of agoraphobic symptoms could derive from the disconnection caused by the resection and/or by adaptive compensatory mechanisms leading to abnormal network reorganization.

We previously hypothesized that agoraphobia is related to dysfunction of the multimodal vestibular network that relates visuospatial processing to the emotional system (27) based on the finding that subclinical agoraphobia was associated with decreases in the clustering coefficient and in the local efficiency in two specific networks highly overlapping with the vestibular network (Figure 3). The first network, considered visuospatial-emotional, comprised higher-order visual and visual motion areas, the inferior parietal cortex, the precuneus, premotor areas, the anterior thalamus, the basal ganglia, and the amygdala (Figure 3, red). The second network, defined as vestibular-navigational, comprised the hippocampus, posterior regions of the insula and parietal opercula, the superior parietal cortex, the primary somatosensory and motor cortex, and premotor regions (Figure 3, green). Together, these two networks integrate visual information, particularly visual motion stimuli generated during self-motion and processed by high-order temporal visual areas, with vestibular and somatosensory information from the posterior insula and parietal opercula to orient the body in space (parietal cortex) and to map the environment (hippocampus). Frontal regions within these networks (premotor and pre-frontal regions and cingulate cortex) elaborate this information to plan and either initiate or inhibit locomotion, which could be driven also by motivation and/or environmental threats processed by the amygdala, hippocampus, and associated subcortical structures. Thus, agoraphobia may not be related to the dysfunction of isolated brain regions, but it may involve the disruption of wider networks responsible for mapping the environment and driving the intention to interact with it (27).

Here, we provide further evidence that extensive post-surgery reorganization within the vestibular network, signified by the structural and functional connectivity metric changes shown by several network nodes, could account for the agoraphobic symptoms reported by this patient. Notably, the surgical lesion is prominently located within the visuospatial-emotional network (Figure 3, yellow contours), suggesting that, at least in part, the development of the agoraphobic symptoms could be accounted for by the surgical disruption of this network component *per se*. Moreover, both visuospatial-emotional and vestibular-navigational networks highly overlapped with regions that showed significant structural (Figure 3A, brown contours) and functional (Figure 3B, brown contours) connectivity changes. In particular, the high-order visual right 37dl (dorsolateral Brodmann area 37) and right PFcm in the inferior parietal lobe showed a generalized decrease in all connectivity metrics, including functional nodal strength (see Figure 2B). These areas are considered to be involved in navigation and orienting (22) and are also part of the visuospatial-emotional network that showed decreased connectivity in subclinical agoraphobia (Figure 3). Thus, plastic reorganization of the visuospatial-emotional network, consisting of a local disconnection of these areas, could have also contributed to the development of agoraphobia in this patient.

Conversely, regions that showed an increase in functional connectivity metrics and can be grouped in an attentional and action-reorienting network, such as the anterior insula, anterior cingulate cortex, and precuneus, do not show a great degree of overlap with the networks emerging in subclinical agoraphobia. Among these, the precuneus is involved in visual-spatial guided behavior, attentive tracking, and attentional shifting (43, 44), while the right anterior insula and the frontal operculum are associated with the exogenous ventral attention network, which is lateralized to the right hemisphere and can monitor environmental threats (45), initiating the sympathetic fight or flight response (26). In particular, the anterior insula integrates interoceptive information with emotional feelings, whereas the anterior cingulate cortex regulates the sympathetic response accompanying the avoidance or approaching behavior (26). It has also been proposed that these right hemisphere regions are involved in the appraisal of negative feelings and avoidance behavior, respectively, in contrast to the opposite role of the homolog contralateral areas in positive feelings appraisal and approaching behavior (26). In this respect, the post-surgical functional increase in clustering and efficiency of the anterior insula and cingulate cortex might be predictive of the fear of surrounding spaces and avoiding behavior, which is

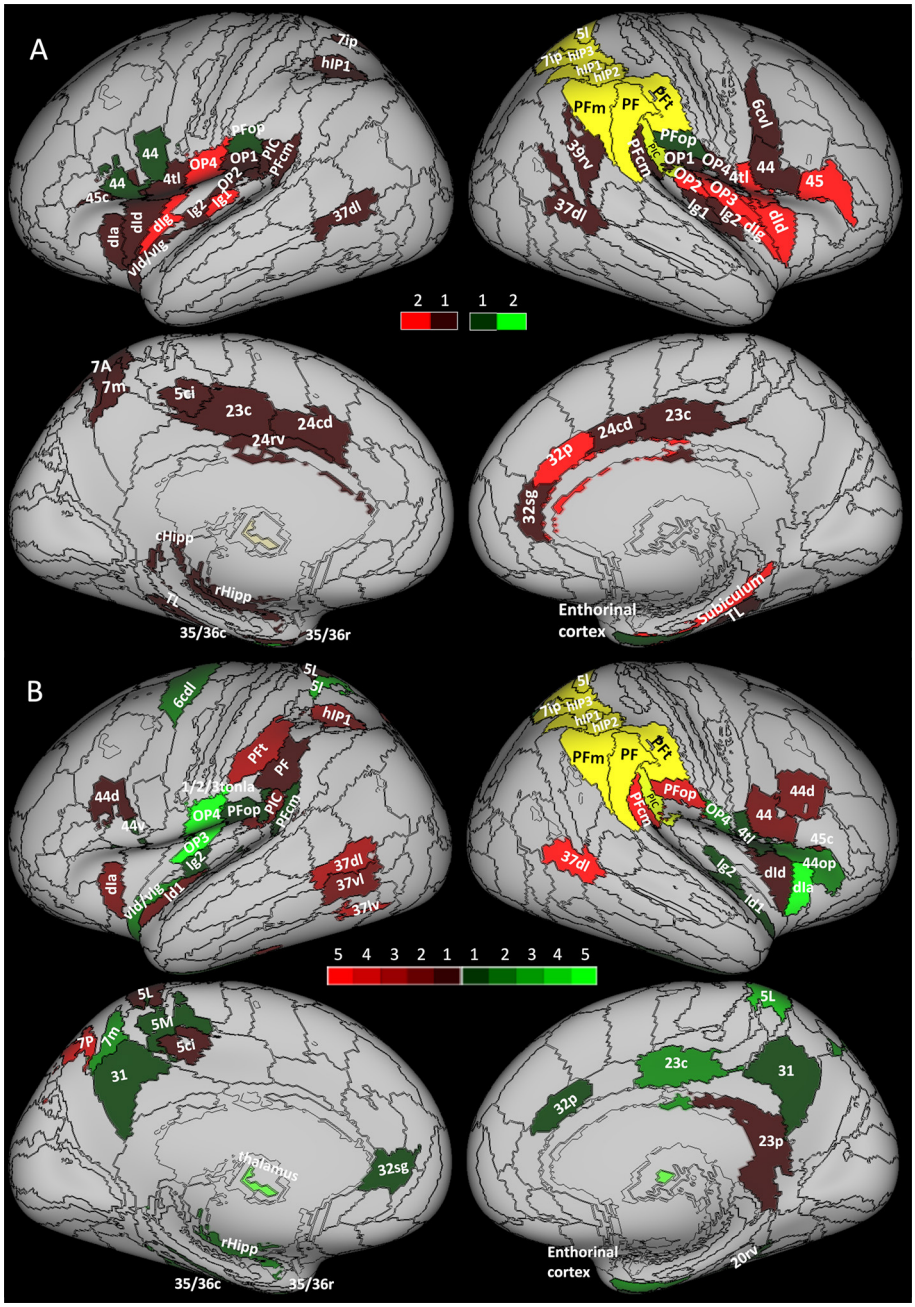

FIGURE 2
Increase (green) and decrease (red) of network measures between **(A)** structural sessions and **(B)** functional sessions. The yellow area represents the areas excluded from the analysis due to the surgical resection. **(A)** Brighter areas show changes in both clustering coefficient and local efficiency during pre-op session vs. post-op 2. The darkest areas show changes only in the clustering coefficient. **(B)** Brighter areas show changes in several comparisons in strength, cluster coefficient, and local efficiency (during pre-op vs. post-op 1 and pre-op vs. post-op2). The darkest areas show changes in only one comparison.

characteristic of agoraphobia. The involvement of these regions outlined by the current study might also account for the difference between subclinical and clinical agoraphobia.

On the other hand, no definite conclusions can be drawn from our results about a potential laterality bias since the cingulate cortex and the anterior insula showed mixed bilateral increases and decreases in the functional connectivity metrics. Moreover, the patient is left-handed, thus, possibly presenting a different pattern of lateralization, as left-handers, compared to right-handers, may show a more symmetrical organization of lateralized functions rather than opposite hemisphere lateralization (46). Indeed, recovery from a left-hemispheric stroke seems more rapid and complete in left-handers than in right-handers with right-hemispheric stroke, thus suggesting higher bilateral processing of vestibular stimuli in left-handers than right-handers (47, 48). Based on these considerations, we may

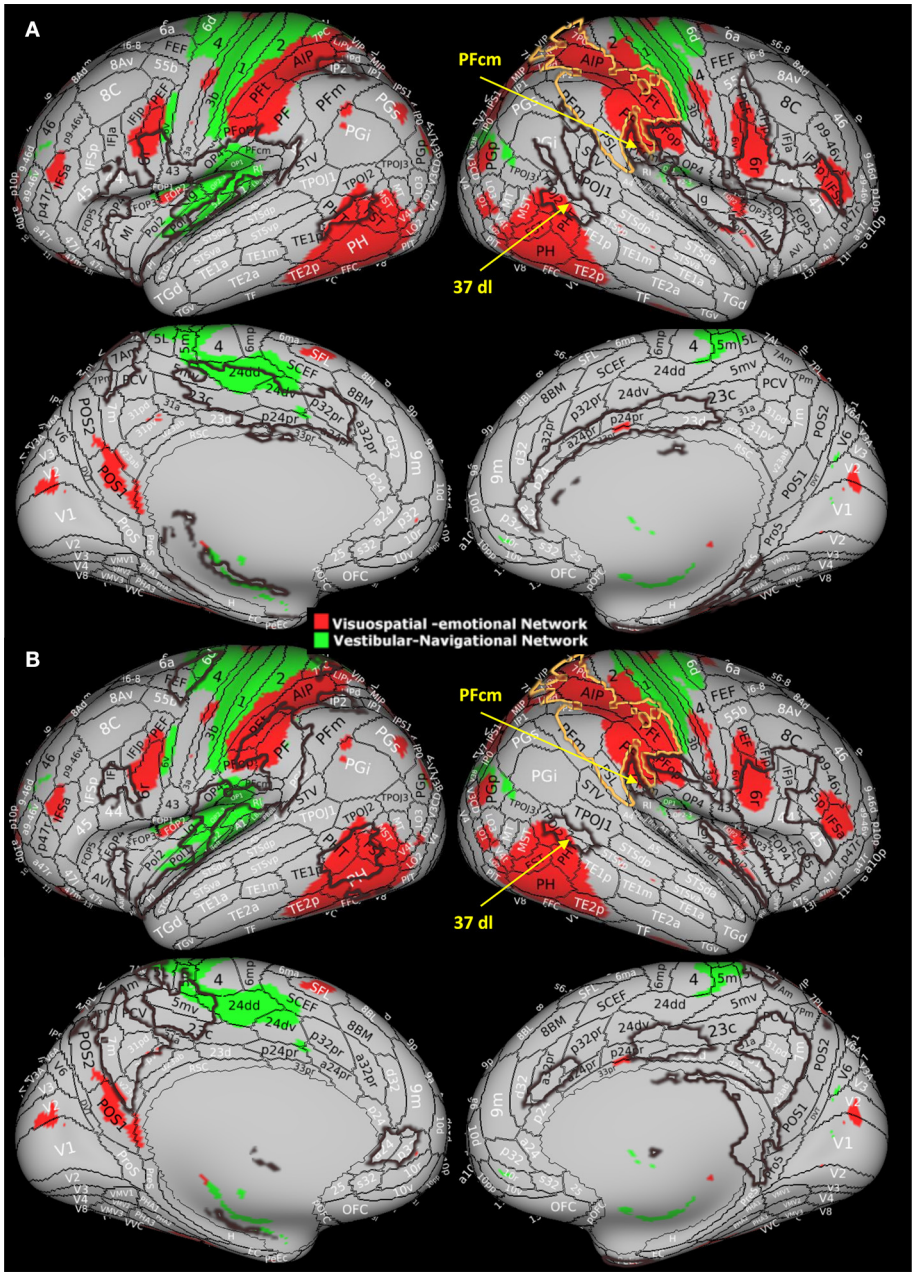

FIGURE 3
Visuospatial-emotional network (red) and vestibular-navigational network (green) from Indovina et al. (27) study. These networks showed reduced clustering coefficient and local efficiency in individuals with subclinical agoraphobia compared to controls. In this study, 37dl corresponds to PHT by von Economo and Koskinas (41, 42). Modified with permission from Indovina et al. (27) by superimposing current results, i.e., the area of surgical resection (yellow contour) and **(A)** areas presenting structural measures alterations and **(B)** areas presenting functional measures alterations (brown contours).

hypothesize that the patient's left-handedness had uncovered more subtle symptoms than the typical clinical picture of the visuospatial hemi-neglect manifested by patients with right parietal lesions.

Conclusion

We provided evidence that extensive reorganization of the multimodal vestibular network could account for the development of agoraphobic symptoms in a patient after the surgical removal of a right parietal glioma. Specifically, the decrease in the clustering coefficient and in the local efficiency observed with both structural and functional connectivity analyses in several areas of the limbic, insular, parietal, and frontal cortex was strongly indicative of a local disconnection of these regions belonging to the vestibular network. Conversely, the post-surgical functional increases in clustering coefficient and local efficiency in the anterior insula and in the cingulate cortex indicated a more predominant role of these areas within the vestibular network,

which could be predictive of the fear and avoiding behavior characterizing agoraphobia.

Data availability statement

The raw data supporting the conclusions of this article will be made available by the authors, without undue reservation.

Ethics statement

The studies involving human participants were reviewed and approved by Poitiers University Hospital. The patients/participants provided their written informed consent to participate in this study. Written informed consent was obtained from the individual(s) for the publication of any potentially identifiable images or data included in this article.

Author contributions

II and AC: conceptualization, data analysis, and wrote the manuscript. SD, DM, and FL: edited the manuscript. NT: data analysis. JC: data acquisition and wrote the manuscript. GB: conceptualization and wrote the manuscript. All authors contributed to the article and approved the submitted version.

Funding

The research was supported by the Italian Ministry of Health (RF-2019-12369194 and IRCCS Fondazione Santa Lucia Ricerca corrente), the U.S. Department of Defense Congressionally Directed Medical Research Program W81XWH1810760 PT170028, and the Italian Ministry of University and Research (PRIN2017: 2017KZNZLN_003).

Conflict of interest

The authors declare that the research was conducted in the absence of any commercial or financial relationships that could be construed as a potential conflict of interest.

Publisher's note

All claims expressed in this article are solely those of the authors and do not necessarily represent those of their affiliated organizations, or those of the publisher, the editors and the reviewers. Any product that may be evaluated in this article, or claim that may be made by its manufacturer, is not guaranteed or endorsed by the publisher.

Supplementary material

The Supplementary Material for this article can be found online at: https://www.frontiersin.org/articles/10.3389/fneur.2023.1163005/full#supplementary-material

References

1. Karnath H-O, Dieterich M. Spatial neglect–a vestibular disorder? *Brain.* (2006) 129:293–305. doi: 10.1093/brain/awh698

2. Karnath H-O, Rorden C. The anatomy of spatial neglect. *Neuropsychologia.* (2012) 50:1010–7. doi: 10.1016/j.neuropsychologia.2011.06.027

3. Abe H, Kondo T, Oouchida Y, Suzukamo Y, Fujiwara S, Izumi S-I. Prevalence length of recovery of pusher syndrome based on cerebral hemispheric lesion side in patients with acute stroke. *Stroke.* (2012) 43:1654–6. doi: 10.1161/STROKEAHA.111.638379

4. Blanke O. Out of body experiences and their neural basis. *BMJ.* (2004) 329:1414–5. doi: 10.1136/bmj.329.7480.1414

5. Blanke O, Landis T, Spinelli L, Seeck M. Out-of-body experience and autoscopy of neurological origin. *Brain.* (2004) 127:243–58. doi: 10.1093/brain/awh040

6. Staab JP. Chronic subjective dizziness. *Continuum (Minneap Minn).* (2012) 18:1118–41. doi: 10.1212/01.CON.0000421622.56525.58

7. Westphal C. Die Agoraphobie, eine neuropathische Erscheinung. *Zeitschrift für Psychiatrie, Berlin.* (1871) 3:138–61. doi: 10.1007/BF02156040

8. Sheehan DV, Lecrubier Y, Sheehan KH, Amorim P, Janavs J, Weiller E, et al. The Mini-International Neuropsychiatric Interview (M.I.N.I.): the development and validation of a structured diagnostic psychiatric interview for DSM-IV and ICD-10. *J Clin Psychiatry.* (1998) 59:22–33.

9. Jacob RG, Lilienfeld SO, Furman JMR, Durrant JD, Turner SM. Panic disorder with vestibular dysfunction: Further clinical observations and description of space and motion phobic stimuli. *J Anxiety Disord.* (1989) 3:117–30. doi: 10.1016/0887-6185(89)90006-6

10. Lilienfeld SO, Jacob RG, Furman JM. Vestibular dysfunction followed by panic disorder with agoraphobia. *J Nerv Ment Dis.* (1989) 177:700–1. doi: 10.1097/00005053-198911000-00009

11. Balaban CD, Jacob RG. Background and history of the interface between anxiety and vertigo. *J Anxiety Disord.* (2001) 15:27–51. doi: 10.1016/S0887-6185(00)00041-4

12. Balaban CD. Neural substrates linking balance control and anxiety. *Physiol Behav.* (2002) 77:469–75. doi: 10.1016/S0031-9384(02)00935-6

13. Indovina I, Riccelli R, Staab JP, Lacquaniti F, Passamonti L. Personality traits modulate subcortical and cortical vestibular and anxiety responses to sound-evoked otolithic receptor stimulation. *J Psychosom Res.* (2014) 77:391–400. doi: 10.1016/j.jpsychores.2014.09.005

14. Riccelli R, Indovina I, Staab JP, Nigro S, Augimeri A, Lacquaniti F, et al. Neuroticism modulates brain visuo-vestibular and anxiety systems during a virtual rollercoaster task. *Hum Brain Mapp.* (2017) 38:715–26. doi: 10.1002/hbm.23411

15. Passamonti L, Riccelli R, Lacquaniti F, Staab JP, and Indovina I. Brain responses to virtual reality visual motion stimulation are affected by neurotic personality traits in patients with persistent postural-perceptual dizziness. *J Vestib Res.* doi: 10.3233/VES-190653

16. Staab JP, Balaban CD, Furman JM. Threat assessment and locomotion: clinical applications of an integrated model of anxiety and postural control. *Semin Neurol.* (2013) 33:297–306. doi: 10.1055/s-0033-1356462

17. Lopez C, Blanke O, Mast FW. The human vestibular cortex revealed by coordinate-based activation likelihood estimation meta-analysis. *Neuroscience.* (2012) 212:159–79. doi: 10.1016/j.neuroscience.2012.03.028

18. zu Eulenburg P, Caspers S, Roski C, Eickhoff SB. Meta-analytical definition and functional connectivity of the human vestibular cortex. *Neuroimage*. (2012) 60:162–9. doi: 10.1016/j.neuroimage.2011.12.032

19. Indovina I, Bosco G, Riccelli R, Maffei V, Lacquaniti F, Passamonti L, et al. Structural connectome and connectivity lateralization of the multimodal vestibular cortical network. *Neuroimage*. (2020) 222:117247. doi: 10.1016/j.neuroimage.2020.117247

20. Indovina I, Maffei V, Bosco G, Zago M, Macaluso E, Lacquaniti F. Representation of visual gravitational motion in the human vestibular cortex. *Science*. (2005) 308:416–9. doi: 10.1126/science.1107961

21. Indovina I, Maffei V, Pauwels K, Macaluso E, Orban GA, Lacquaniti F. Simulated self-motion in a visual gravity field: sensitivity to vertical and horizontal heading in the human brain. *Neuroimage*. (2013) 71:114–24. doi: 10.1016/j.neuroimage.2013.01.005

22. Indovina I, Maffei V, Mazzarella E, Sulpizio V, Galati G, Lacquaniti F. Path integration in 3D from visual motion cues: a human fMRI study. *Neuroimage*. (2016) 142:512–21. doi: 10.1016/j.neuroimage.2016.07.008

23. Lacquaniti F, Bosco G, Gravano S, Indovina I, La Scaleia B, Maffei V, et al. Multisensory integration and internal models for sensing gravity effects in primates. *Biomed Res Int*. (2014) 2014:615854. doi: 10.1155/2014/615854

24. Maffei V, Indovina I, Macaluso E, Ivanenko YP A, Orban G, Lacquaniti F. Visual gravity cues in the interpretation of biological movements: neural correlates in humans. *Neuroimage*. (2015) 104:221–30. doi: 10.1016/j.neuroimage.2014.10.006

25. Strange BA, Witter MP, Lein ES, Moser EI. Functional organization of the hippocampal longitudinal axis. *Nat Rev Neurosci*. (2014) 15:655–69. doi: 10.1038/nrn3785

26. Strigo IA, Craig ADB. Interoception, homeostatic emotions and sympathovagal balance. *Philos Trans R Soc Lond B Biol Sci*. (2016) 371:20160010. doi: 10.1098/rstb.2016.0010

27. Indovina I, Conti A, Lacquaniti F, Staab JP, Passamonti L, Toschi N. Lower functional connectivity in vestibular-limbic networks in individuals with subclinical agoraphobia. *Front Neurol*. (2019) 10:874. doi: 10.3389/fneur.2019.00874

28. Wittmann A, Schlagenhauf F, Guhn A, Lueken U, Gaehlsdorf C, Stoy M, et al. Anticipating agoraphobic situations: the neural correlates of panic disorder with agoraphobia. *Psychol Med*. (2014) 44:2385–96. doi: 10.1017/S0033291713003085

29. Kelly CB, Cooper SJ. Panic and agoraphobia associated with a cerebral arteriovenous malformation. *Ir J Psychol Med*. (1993) 10:94–6. doi: 10.1017/S0790966700012957

30. Grambal A, Hluštík P, Praško J. What fMRI can tell as about panic disorder: bridging the gap between neurobiology and psychotherapy. *Neuro Endocrinol Lett*. (2015) 36:214—25.

31. Avants BB, Tustison NJ, Song G, Cook PA, Klein A, Gee JC. A reproducible evaluation of ANTs similarity metric performance in brain image registration. *Neuroimage*. (2011) 54:2033–44. doi: 10.1016/j.neuroimage.2010.09.025

32. Eickhoff SB, Stephan KE, Mohlberg H, Grefkes C, Fink GR, Amunts K, et al. A new SPM toolbox for combining probabilistic cytoarchitectonic maps and functional imaging data. *Neuroimage*. (2005) 25:1325–35. doi: 10.1016/j.neuroimage.2004.12.034

33. Fan L, Li H, Zhuo J, Zhang Y, Wang J, Chen L, et al. The human brainnetome atlas: a new brain atlas based on connectional architecture. *Cereb Cortex*. (2016) 26:3508–26. doi: 10.1093/cercor/bhw157

34. Park JE, Kim HS, Kim SJ, Kim JH, Shim WH. Alteration of long-distance functional connectivity and network topology in patients with supratentorial gliomas. *Neuroradiology*. (2016) 58:311–20. doi: 10.1007/s00234-015-1621-6

35. Yuan T, Zuo Z, Ying J, Jin L, Kang J, Gui S, et al. Structural and functional alterations in the contralesional medial temporal lobe in glioma patients. *Front Neurosci*. (2020) 14:10. doi: 10.3389/fnins.2020.00010

36. Derks J, Kulik SD, Numan T, de Witt Hamer PC, Noske DP, Klein M, et al. Understanding global brain network alterations in glioma patients. *Brain Connect*. (2021) 11:865–74. doi: 10.1089/brain.2020.0801

37. Fang S, Wang Y, Jiang T. Epilepsy enhance global efficiency of language networks in right temporal lobe gliomas. *CNS Neurosci Ther*. (2021) 27:363–71. doi: 10.1111/cns.13595

38. Fang S, Li L, Weng S, Guo Y, Zhong Z, Fan X, et al. Contralesional sensorimotor network participates in motor functional compensation in glioma patients. *Front Oncol*. (2022) 12:882313. doi: 10.3389/fonc.2022.882313

39. Ng S, Deverdun J, Lemaitre A-L, Giampiccolo D, Bars EL, Moritz-Gasser S, et al. Precuneal gliomas promote behaviorally relevant remodeling of the functional connectome. *J Neurosurg*. (2022) 1–11. doi: 10.3171/2022.9.JNS221723

40. Zhang X, Zhang G, Wang Y, Huang H, Li H, Li M, et al. Alteration of default mode network: association with executive dysfunction in frontal glioma patients. *J Neurosurg*. (2022) 1–10. doi: 10.3171/2022.8.JNS22591

41. Glasser MF, Coalson TS, Robinson EC, Hacker CD, Harwell J, Yacoub E, et al. A multi-modal parcellation of human cerebral cortex. *Nature*. (2016) 536:171–8. doi: 10.1038/nature18933

42. von Economo C, Koskinas GN. *Atlas of cytoarchitectonics of the Adult Human Cerebral Cortex (trans, rev, ed: Triarhou LC)*. Basel: Karger. (2008).

43. Astafiev SV, Shulman GL, Stanley CM, Snyder AZ, Essen DCV, Corbetta M. Functional Organization of Human Intraparietal and Frontal Cortex for Attending, Looking, and Pointing. *J Neurosci*. (2003) 23:4689–99. doi: 10.1523/JNEUROSCI.23-11-04689.2003

44. Wang J, Becker B, Wang L, Li H, Zhao X, Jiang T. Corresponding anatomical and coactivation architecture of the human precuneus showing similar connectivity patterns with macaques. *Neuroimage*. (2019) 200:562–74. doi: 10.1016/j.neuroimage.2019.07.001

45. Corbetta M, Shulman GL. Control of goal-directed and stimulus-driven attention in the brain. *Nat Rev Neurosci*. (2002) 3:201–15. doi: 10.1038/nrn755

46. Janzen J, Schlindwein P, Bense S, Bauermann T, Vucurevic G, Stoeter P, et al. Neural correlates of hemispheric dominance and ipsilaterality within the vestibular system. *Neuroimage*. (2008) 42:1508–18. doi: 10.1016/j.neuroimage.2008.06.026

47. Vanderploeg RD. Left-handedness and variant patterns of cerebral organization: A case study. *Arch Clinical Neuropsychol*. (1986) 1:357–69. doi: 10.1016/0887-6177(86)90140-X

48. Dronkers NF, Knight RT. Right-sided neglect in a left-hander: Evidence for reversed hemispheric specialization of attention capacity. *Neuropsychologia*. (1989) 27:729–35. doi: 10.1016/0028-3932(89)90118-8

frontiers | Frontiers in Neurology

TYPE Original Research
PUBLISHED 17 May 2023
DOI 10.3389/fneur.2023.1144228

OPEN ACCESS

EDITED BY
Lorenzo Pini,
University of Padua, Italy

REVIEWED BY
Anna Bonkhoff,
Massachusetts General Hospital and Harvard Medical School, United States
Nicholas Thomas Trapp,
The University of Iowa, United States

*CORRESPONDENCE
Julian Klingbeil
✉ julian.klingbeil@medizin.uni-leipzig.de

RECEIVED 14 January 2023
ACCEPTED 20 April 2023
PUBLISHED 17 May 2023

CITATION
Klingbeil J, Brandt M-L, Stockert A, Baum P, Hoffmann K-T, Saur D and Wawrzyniak M (2023) Associations of lesion location, structural disconnection, and functional diaschisis with depressive symptoms post stroke.
Front. Neurol. 14:1144228.
doi: 10.3389/fneur.2023.1144228

Associations of lesion location, structural disconnection, and functional diaschisis with depressive symptoms post stroke

Julian Klingbeil[1]*, Max-Lennart Brandt[1], Anika Stockert[1], Petra Baum[2], Karl-Titus Hoffmann[3], Dorothee Saur[1] and Max Wawrzyniak[1]

[1]Neuroimaging Laboratory, Department of Neurology, University of Leipzig Medical Center, Leipzig, Germany, [2]Department of Neurology, University of Leipzig Medical Center, Leipzig, Germany, [3]Department of Neuroradiology, University of Leipzig Medical Center, Leipzig, Germany

Introduction: Post-stroke depressive symptoms (PSDS) are common and relevant for patient outcome, but their complex pathophysiology is ill understood. It likely involves social, psychological and biological factors. Lesion location is a readily available information in stroke patients, but it is unclear if the neurobiological substrates of PSDS are spatially localized. Building on previous analyses, we sought to determine if PSDS are associated with specific lesion locations, structural disconnection and/or localized functional diaschisis.

Methods: In a prospective observational study, we examined 270 patients with first-ever stroke with the Hospital Anxiety and Depression Scale (HADS) around 6 months post-stroke. Based on individual lesion locations and the depression subscale of the HADS we performed support vector regression lesion-symptom mapping, structural-disconnection-symptom mapping and functional lesion network-symptom-mapping, in a reanalysis of this previously published cohort to infer structure–function relationships.

Results: We found that depressive symptoms were associated with (i) lesions in the right insula, right putamen, inferior frontal gyrus and right amygdala and (ii) structural disconnection in the right temporal lobe. In contrast, we found no association with localized functional diaschisis. In addition, we were unable to confirm a previously described association between depressive symptom load and a network damage score derived from functional disconnection maps.

Discussion: Based on our results, and other recent lesion studies, we see growing evidence for a prominent role of right frontostriatal brain circuits in PSDS.

KEYWORDS

stroke, depression, diaschisis, disconnection, lesion network mapping

1. Introduction

Post-stroke depressive symptoms (PSDS) impose a significant burden on stroke survivors and are independent predictors of worse functional outcome and increased mortality (1, 2). From a clinical perspective, it is important to identify patients at risk of post-stroke depression (PSD) early on to provide adequate treatment and ensure optimal rehabilitation despite the depressive symptoms. Risk prediction based on medical factors and psychiatric history could promote timely screening for and recognition of depressive symptoms (3). In addition, lesion location is a readily available information in stroke patients and might be useful to estimate the individual risk for PSD (4). The assumption that the biological effect of a stroke lesion may also contribute to PSD is

consistent with the biopsychosocial disease model of major depressive disorder (MDD) (5). Mounting evidence indicates that PSD is not just caused by psychosocial factors such as difficulties to adjust to the new physical disabilities or the suddenly altered living circumstances, but could also be a direct consequence of brain damage (6). Strong support for this conclusion comes from a recent, large study that identified a 50% higher risk to develop a depressive disorder up to 1.5 years after the event when comparing stroke to myocardial infarction (7). But unlike MDD, PSD offers the possibility to draw causal inferences on the neural substrates of depressive symptoms based on lesion locations (6). Structure–function inference with stroke lesions has contributed significantly to our understanding of the human brain in the past two centuries (8). Admittedly, studies on lesion location and mood have had mixed results: despite over 80 lesion studies, no consistent association has been identified (9). But recently, larger studies using modern methods of structure–function inference such as voxel-based lesion-symptom mapping (VLSM) showed promising results (10–12).

Yet, inference for PSDS based on direct lesion effects may also fail despite the methodological advances of lesion-symptom mapping (4, 6, 13), because complex brain functions such as language or mood arise from interactions between large-scale distributed networks rather than single or specific brain regions (8). Lesions that fall into such networks are thought to also cause symptoms due to functional diaschisis (14, 15) or structural disconnection (16–18). The identification of diaschisis and disconnection in distributed networks as a cause of PSDS requires different methodological approaches. Several new methods have become available in the last decade. Functional diaschisis and structural disconnection can for example be examined based on normative functional and structural connectome data (8, 16, 17, 19). Three recent studies on PSDS applied these methods. Weaver and colleagues used measures of structural disconnection and identified right frontal cortico-striatal-thalamic circuits to be associated with PSDS (11). With a similar method, Pan and colleagues identified an association of structural disconnection with PSD bilaterally in the temporal, prefrontal and parietal white matter and the posterior corpus callosum (12). Furthermore, the inclusion of such indirect measures of structural disconnection improved predictive models for PSD (12). Padmanabhan and colleagues, on the other hand, used indirect measures of functional diaschisis to predict depressive symptoms (4). They demonstrated that the overlap between lesions and a depression circuit derived from the functional connectivity of the left DLPFC correlated with PSDS (4).

Here, we provide a reanalysis of a recently published large sample of stroke patients evaluated for depressive symptoms 6 months after stroke. In our recent study, we demonstrated an association of the right basal ganglia with PSDS using VLSM in the sense of a mass-univariate approach (10). In extension to that study, we here used multivariate analyses in combination with methods based on lesion location, structural disconnection and functional diaschisis to identify regions where lesions, disconnection or functional diaschisis might cause the development of depressive symptoms.

2. Methods

2.1. Patient recruitment and behavioral testing

Institutional review boards approved all study protocols and informed consent for study participation was obtained from all participants (or their legally designated surrogates). First ever stroke patients were recruited from the stroke unit of the Department of Neurology, University of Leipzig Medical Center from 01/2012 to 12/2014 and 11/2017 to 11/2018 as previously described (10). We excluded patients not speaking German, with a history of depression, other psychiatric or neurologic disorders affecting the CNS or other severe diseases and patients aged < 18 or > 90 years. For 270 patients, behavioral scores from the Hospital Anxiety and Depression Scale (HADS) around 6 months after stroke (189.5 ± 10.3 days, range 159–284) were available (10). We used the depression subscale (HADS-D) as a continuous measure for the severity of depressive symptoms in the subsequent analyses. However, to make our results comparable to those of Padmanabhan et al., we also used a cut-off value of > 10 on the HADS-D for the lesion network-symptom-mapping analyses. Stroke-related disability was quantified with the National Institute of Health Stroke Scale (NIHSS) and the Barthel-Index in the first weeks after stroke as previously described (10).

2.2. Brain imaging and preprocessing

We used pseudonymized clinical imaging acquired during clinical routine examinations at the Department of Neuroradiology, University of Leipzig Medical Center with the imaging and preprocessing procedures previously described (10). In brief, lesions were first delineated by two reviewers blinded to the patients' outcome in native space on 202 MRIs and 68 CTs with the semi-automated Clusterize Toolbox (20), manually edited using MRIcron (21) and finally supervised by a neurologist experienced in neuroimaging (JK). These lesions were used for cost-function masking during normalization of the corresponding MRI and CT scans to MNI (Montreal Neurological Institute) space. For spatial normalization, we used the Clinical Toolbox (22) for SPM12 (Wellcome Trust Centre for Neuroimaging, London, UK, RRID:SCR_007037) running on MATLAB (R2019a, The MathWorks Inc., Natick, MA, RRID:SCR_001622) and resliced all images to 1 mm isotropic voxels. The resulting non-linear normalization parameters were also applied to the native space lesion maps, which were then used for further analyses in MNI space.

2.3. SVR-LSM

In contrast to the univariate approach used in our previous publication (10), we here used multivariate support vector regression lesion-symptom mapping (SVR-LSM) to infer direct lesion-symptom relationships. We resampled all lesion maps to 2 mm isotropic voxels to enable reasonable computing times. All SVR-LSM analyses were performed with version 2 the multivariate lesion symptom mapping toolbox of DeMarco and Turkeltaub (23). Only voxels damaged in ≥ 5 patients were included, which resulted in the exclusion of 13 out of 270 lesions because they had no voxels inside the minimum lesion cutoff mask implemented in the toolbox. Lesion volume was controlled for in all analyses by regressing it out from both the behavioral data (HADS-D) and the raw lesion data (23). We used default values for the hyperparameters (see Supplementary Table S3) (23, 24). Prediction performance was calculated in-sample by determining the mean Pearson correlation coefficient between the real and predicted depression scores and ranked relative to 5,000

permuted models (see Supplementary Table S3). Statistical inference was based on SVR β-maps thresholded using the null-distribution of cluster sizes obtained by 5,000 random permutations with a threshold of $p < 0.005$ (uncorrected, one-tailed) on the voxel-level and of p(FWE) < 0.05 on the cluster-level. The analyses were repeated with age, sex, stroke severity (NIHSS) and functional impairment (Barthel-Index) as additional covariates, in analogy to the analyses described by Weaver and colleagues (11). To this end, the covariates were regressed out of behavior of interest (HADS-D) prior to the SVR-LSM. Notably, our analysis with covariates differed in two important aspects from the analysis by Weaver and colleagues – the measures where only available from the acute phase after stroke (6.1 ± 3.5 d post-stroke) and no measure for cognitive deficits was collected.

2.4. SVR-SDSM

We used a combination of support vector regression and structural disconnection mapping (support vector regression structural disconnection-symptom mapping, SVR-SDSM) to infer relationships between structural disconnection and depressive symptoms. Structural disconnection mapping was performed with BCBtoolkit (16). Deterministic fiber tracking seeding from the individual lesion masks was performed in the 10 healthy participants provided with the toolkit and transformed to MNI space. The resulting maps were binarized and overlapped for each patient resulting in individual disconnectome maps with values between 0 and 100%. These disconnectome maps were again binarized with a cutoff of ≥ 60%, since this cutoff had been shown to be optimal in a systematic evaluation of the method (25). Relationships between the binary disconnectome maps and depressive symptoms were analyzed in analogy to SVR-LSM described above. Five disconnectome maps were excluded because they had no voxels inside the minimum lesion mask. In all five cases, the corresponding lesions were very small cortical lesions for which the fiber-tracking algorithm failed to generate a meaningful disconnectome map. For the multivariate analyses, again, the multivariate lesion symptom mapping toolbox was used as described above (23). Instead of lesion maps, the binarized structural disconnection maps were used. All structural disconnection maps were resampled to 2 mm isotropic voxels prior to SVR-SDSM.

2.5. LNSM

Lesion network-symptom mapping (LNSM) was used to infer relationships between functional diaschisis and symptoms. The concept behind this method is that regions functionally connected to the lesion site are vulnerable to diaschisis effects. These analyses were performed with SPM12 and in-house tools with MATLAB as previously described (26, 27). LNSM was performed using a mass-univariate approach to avoid binarizing the functional map using arbitrary thresholds (26, 28). Specifically, we used functional connectome data ($n = 100$, young unrelated healthy adults) from the human connectome project (29). The functional data sets included two 15 min resting-state sessions (right–left and left–right phase encoding) with gradient-echo EPI sequence (TR of 720 ms, 2 mm isotropic voxels) and were downloaded already 'minimally preprocessed' (gradient distortion correction, motion correction, distortion correction, normalization to MNI space, intensity normalization and bias field removal) (30). We convolved all functional images with an isotropic Gaussian smoothing kernel (FWHM = 5 mm). Signal variance over time explained by nuisance variables (motion parameters, mean white matter, CSF and global signal) was removed using multiple regression. Residual BOLD time series were band-pass filtered (0.01–0.08 Hz). All images with a frame-wise displacement > 0.5 mm were discarded (31). Additionally, two data sets with heavy in-scanner motion were excluded entirely. Individual lesion masks were the regions of interest (ROIs) from which representative BOLD time series were extracted as the first eigenvariate of the time series of all voxels within that ROI. These ROIs were defined exclusively as the gray matter portion of the individual lesion masks, as meaningful BOLD signal is restricted to the gray matter (32, 33). This was achieved by masking the lesions with the gray matter probability mask provided with the functional data thresholded at 10% and resulted in the exclusion of 14 patients with pure white matter lesions. Finally, lesion networks were calculated based on functional connectivity (i.e., Fisher-transformed Pearson correlation coefficients) between the ROI time series and the time series of all other brain voxels. All connectivity maps (from 98 controls, separate for right–left and left–right phase encoding) were averaged to obtain a single functional lesion network map for every lesion. These individual lesion network maps represent regions potentially affected by functional diaschisis. LNSM was then carried out as described before with non-parametric permutation testing (26, 34). Continuous scores from the HADS-D were entered into a regression analysis using a mass-univariate general linear model. The statistical inference was based on the null-distribution of cluster sizes (using a voxelwise threshold of $p < 0.001$) obtained with 5,000 random permutations. The result was thresholded at p(FWE) < 0.05. All analyses were restricted to voxels with at least 10% gray matter tissue probability. In analogy to Padmanabhan et al. (4), the analyses were repeated in a mask for the middle frontal gyrus (MFG) derived from the Harvard-Oxford atlases (35) without gray matter masking, with a correction p(FWE) < 0.05 on cluster- and voxel-level, without correction for multiple comparisons and with a cut-off value of HADS-D > 10 for PSD. For the calculation of a network damage score which might be predictive for PSDS, we also followed the procedure described by Padmanabhan et al. (4). Since all analyses using a MFG mask were negative, we chose a spherical ROI with a 9 mm diameter around the peak coordinates (MNI: x = −32, y = 12, z = 36) reported by Padmanabhan and colleagues (4). The network damage score was calculated as follows: a network map for this ROI, representing the 'depression circuit', was computed using the normative functional connectome data as described above. Then for each of our patients a network damage score was computed as the sum of the intensity (*t*-values) of all voxels in the depression circuit that overlap with the patient's lesion. Lesion size was controlled with a residualized network damage score after regression against lesion size. Then these network damage scores were compared between patients with depression (HADS-D > 10) and those without (HADS-D < 11). Statistical significance was calculated using a permutation equivalent of a t-test with one million permutations (4). The analyses were repeated with a HADS-D of > 7 as a cut-off and continuous HADS-D values.

3. Results

Mean HADS-D 6 months post stroke was 4.4 ± 3.7. Lesions were rather small (18.3 ± 38.4 ml) with a predominantly subcortical distribution (see Figure 1A). In patients with HADS-D > 7, lesions were larger (34.0 vs. 14.5 ml, $p < 0.01$). Median time post-stroke for the imaging used to delineate lesions was 5 days (interquartile range 4 days). Further clinical and demographic characteristics are provided in Supplementary Table S1.

3.1. SVR-LSM

We tested for associations of lesion location with depressive symptoms post-stroke using lesion locations and the HADS-D 6 months post-stroke in a multivariate lesion symptom mapping approach (SVR-LSM). Lesion overlap with a minimum of 5 lesions covered 20.0% of the brain mask, thus most frontal, parietal, temporal, occipital, cerebellar and brain stem regions were not included in the analysis (see lesion overlap in Figure 1A). With SVR-LSM, one cluster of 12.49 ml [p(FWE) = 0.004] in the right hemisphere survived permutation-based FWE-correction on cluster-level. This cluster localized mainly to the subcortical white matter and the putaminal, insular and inferior frontal gray matter (see Figure 1C; Supplementary Table S2). The white matter tracts with most overlap where the right corticospinal tract and the superior thalamic radiation and to a lesser extent the right inferior fronto-occipital fasciculus [labels based on the XTRACT atlas (36)]. The subcortical gray matter with most overlap was the right putamen and to a lesser extent the caudate nucleus. The main cortical gray matter

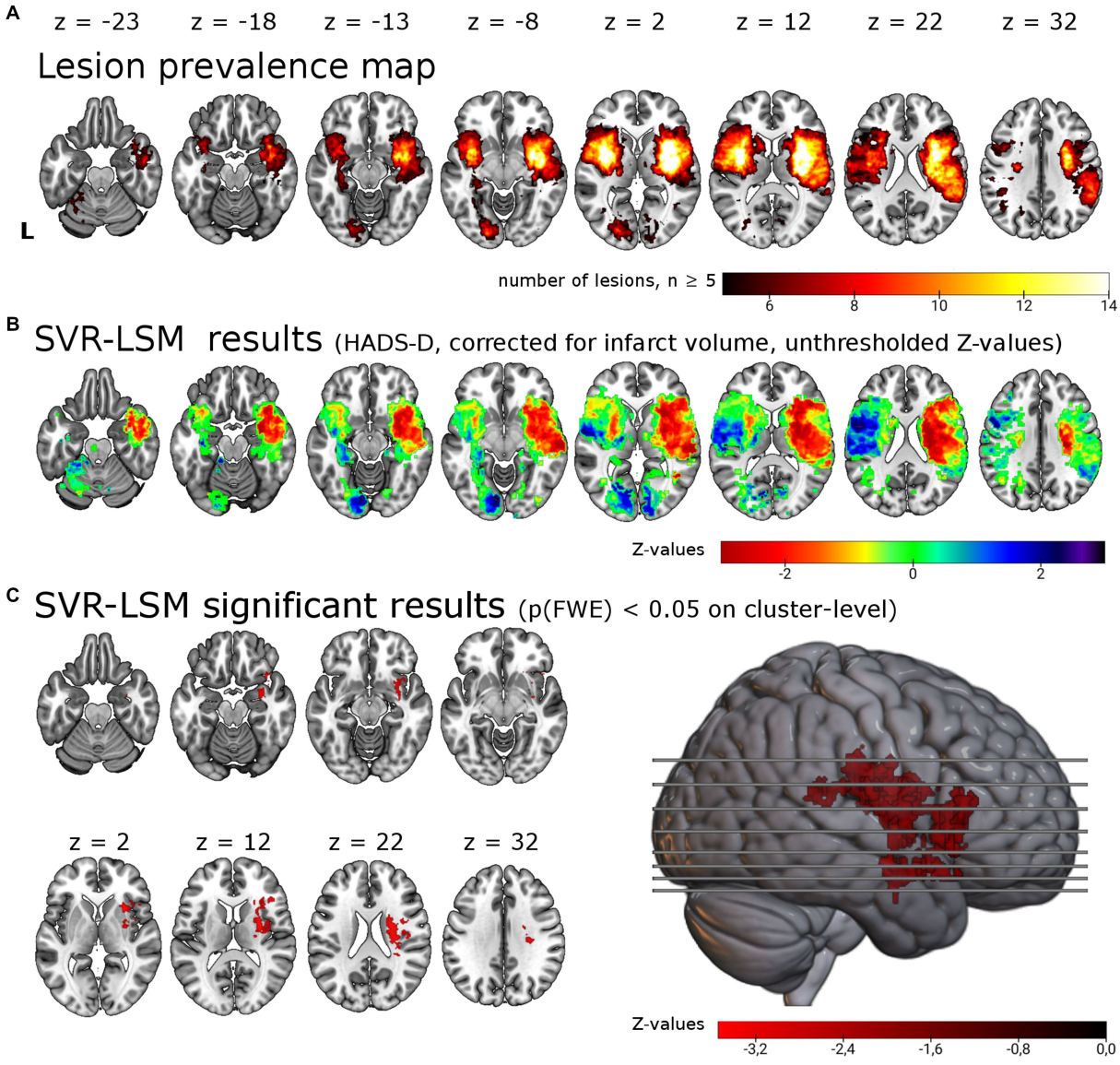

FIGURE 1
Support vector regression lesion-symptom mapping for depressive symptoms 6 months post-stroke. **(A)** Lesion overlap of all 257 patients included in the analysis masked with a minimum lesion overlap of ≥5. **(B)** Unthresholded results for the SVR-LSM with the continuous HADS-D scale. Note that values (*z*-scores)<0 in warm colors correspond to an association between lesions and higher symptom scores. **(C)** Results thresholded with $p<0.005$ on voxel-level and p(FWE)<0.05 on cluster-level resulted in a single cluster of 12.49ml in the right hemisphere, shown here in the lateral view and axial slices. The cluster encompasses in particular the right insula (22.0% of the cluster), the right putamen (18.1%) and the right inferior frontal gyrus (14.2%). L=left.

structures with most overlap were the right insular cortex and the right inferior frontal gyrus and to a lesser extent the right superior, middle and inferior temporal gyrus, the right orbitofrontal cortex, the right hippocampus [based on the LONI atlas (37)] and the right amygdala [based on the Harvard-Oxford brain atlas (35)]. When the analyses were repeated with age, sex, stroke severity (NIHSS) and functional impairment (Barthel-Index) as covariate in analogy with the analyses by Weaver and colleagues, the identified cluster was smaller but with a similar anatomical distribution [one cluster in the right hemisphere with 6.4 ml, p(FWE) = 0.023, see Supplementary Table S2].

3.2. SVR-SDSM

We tested for associations of structural disconnection with depressive symptoms post-stroke using lesion derived structural connectivity and the HADS-D 6 months post-stroke in a multivariate lesion symptom mapping approach (SVR-SDSM). As opposed to the analyses of lesion locations (SVR-LSM), structural disconnection maps seeded from the individual lesion masks were the basis for this set of analyses. Overlap of the binarized structural disconnection maps with a minimum of five resulted in the inclusion of most supratentorial white matter tracts and the corticospinal tract (see Figures 2A,B). With SVR-SDSM one cluster of 5.86 ml in the right hemisphere survived permutation-based FWE-correction on cluster-level with p(FWE) = 0.024. This cluster was localized in the white matter of the right temporal lobe (see Figure 2C; Supplementary Table S2) beneath the inferior, middle and superior temporal gyrus [based on the LONI atlas (37)]. The white matter tracts overlapping with this cluster were the right inferior longitudinal fasciculus, the right middle longitudinal fasciculus and the uncinate fasciculus [with labels based on the XTRACT atlas (36)]. The second

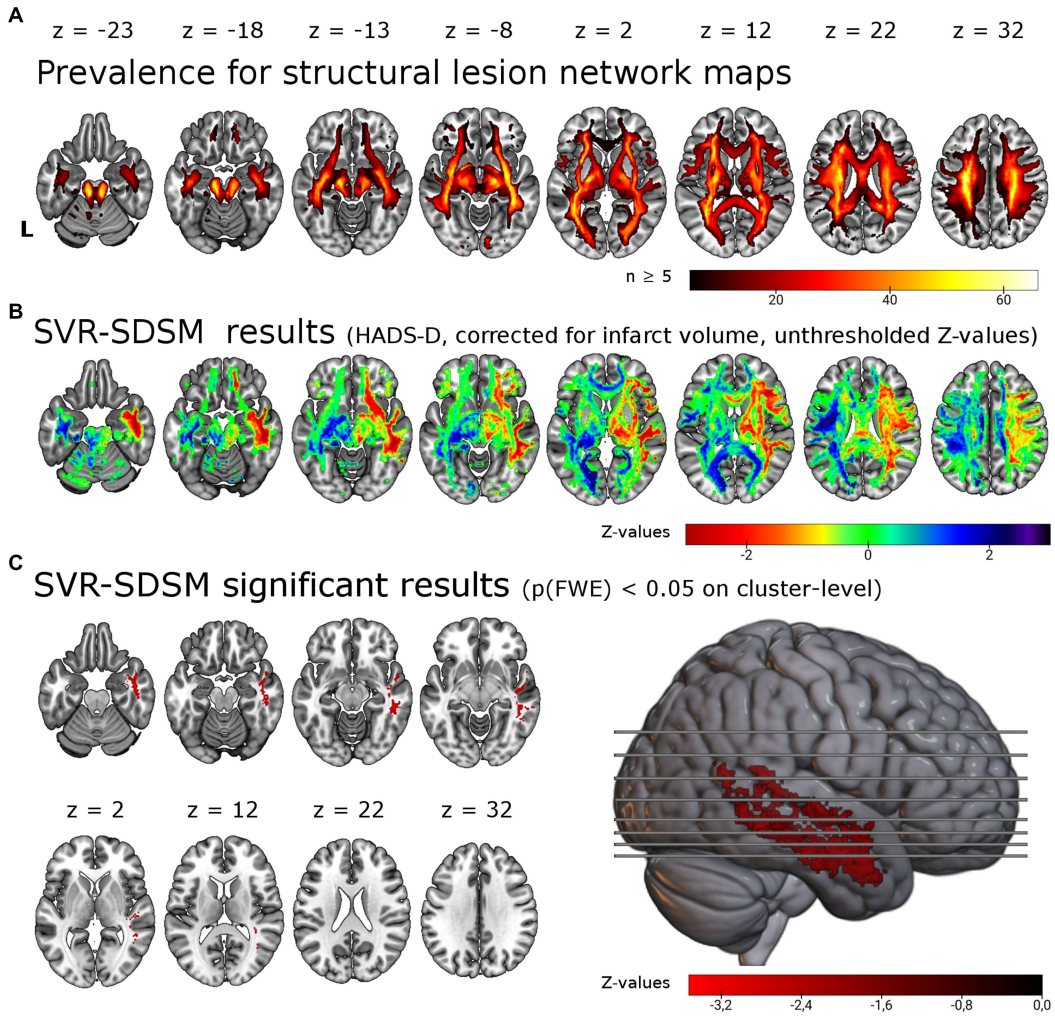

FIGURE 2
Support vector regression structural-disconnection mapping for depressive symptoms 6months post-stroke. **(A)** Overlap of all binarized (threshold of ≥60%) disconnection maps shows good coverage of cerebral white matter. The map is restricted to a minimum overlap of ≥5 disconnection maps. **(B)** Unthresholded results for the SVR-SDSM with the continuous HADS-D score. Note that values (*z*-scores)<0 in warm colors correspond to an association of disconnection with higher symptom scores. **(C)** Results thresholded with $p<0.005$ on voxel-level and p(FWE)<0.05 on cluster-level resulted in a single cluster in the right temporal lobe, shown here in the lateral view and axial slices. This significant cluster ($p=0.024$) of 5.86ml size encompasses in particular the right inferior longitudinal fasciculus (37.7% of the cluster), the right middle longitudinal fasciculus (20.6%) and right the uncinate fasciculus (8.6%). L=left.

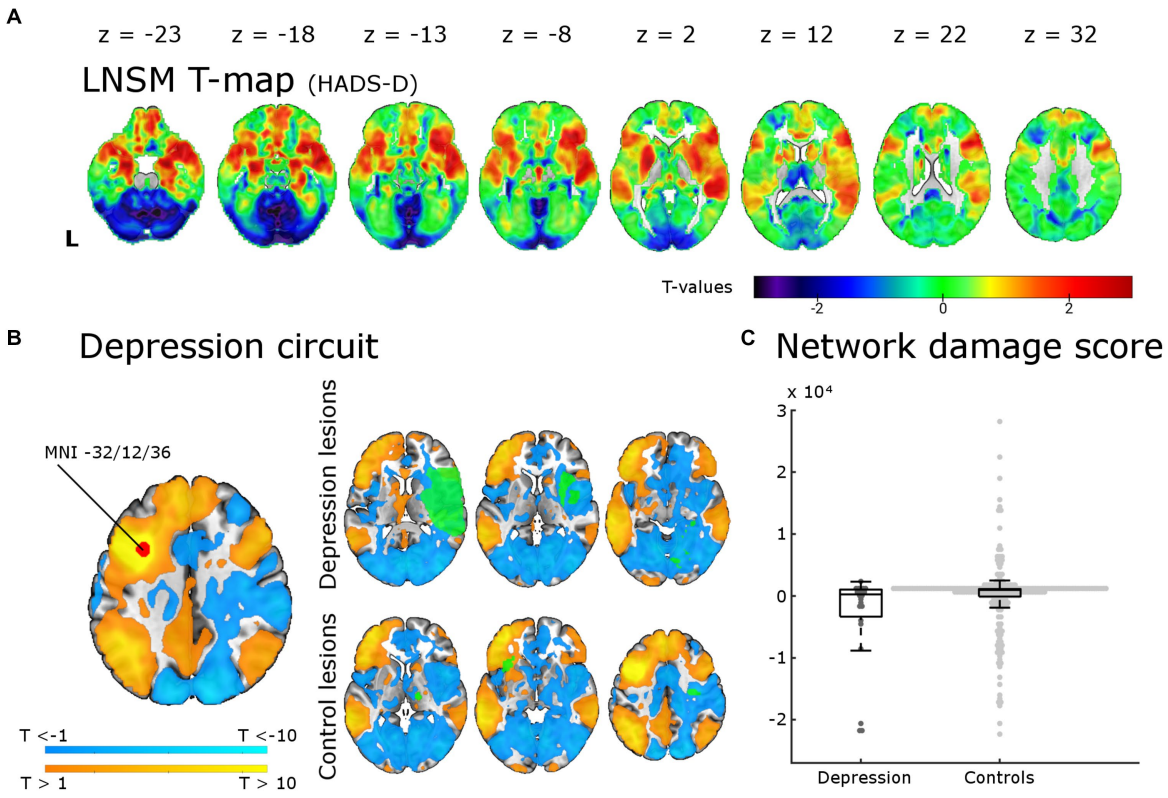

FIGURE 3
Lesion network-symptom mapping for depressive symptoms 6months post-stroke and network damage scores. Results from the LNSM with the continuous HADS-D scale at 6 months post-stroke. **(A)** The unthresholded map of T-values shows a bilateral frontal, temporal and basal ganglia maximum, but there was no significant association between functional lesion network map strength and depressive symptoms [p(FWE)<0.05 at cluster-level]. The analysis remained negative also when applying a mask for the bilateral middle frontal gyrus, when using a binary cut-off at HADS-D>10 and when uncorrected for multiple comparisons (not shown here). **(B)** The depression circuit was derived from a region-of-interest (ROI) with a 9 mm diameter sphere (shown in red) around the peak coordinates (x=−32, y=12, z=36) reported by Padmanabhan and colleagues. The ROIs whole brain functional connectivity was calculated with the normative connectome of 100 healthy subjects. Warmer colors indicating positive connectivity to the ROI and cool colors negative connectivity. This constitutes the 'depression circuit' as described by Padmanabhan and colleagues. In green six random lesions of patients with and without depressive symptoms (binary cut-off >10 on the HADS-D) are shown for illustration as an overlay on the 'depression circuit' – the intersection of the lesions with the depression circuit then results in the network damage score. **(C)** The network damage scores of patients with and without severe depressive symptoms did not differ significantly (p=0.93). All data points are shown in the box plot with the exception of one outlier (NDS 6.3×10^4, depression group).

largest cluster, which was not significant [p(FWE) = 0.108, 1.67 ml], was located in the right frontal lobe mostly within the uncinate fasciculus. Disconnection in these regions was associated with more severe depressive symptoms but there were no voxels where disconnection was associated with a lower depressive symptom score.

3.3. LNSM

We tested for associations of regions potentially affected by functional diaschisis with depressive symptoms post-stroke using lesion derived functional connectivity and the HADS-D 6 months post-stroke in a mass-univariate approach. Figure 3A displays unthresholded LNSM results. We found no statistically significant association between functional lesion network strength and depressive symptoms post-stroke. Following the results of Padmanabhan et al. in a second step, we restricted the analysis to the left and right MFG. This also resulted in no significant association: regardless of the use or omission of gray matter masking, of cluster-or voxel-level inference and even the very liberal significance threshold p(uncorrected) < 0.05 of Padmanabhan et al. (4). Finally, we calculated the 'depression circuit' (see Figure 3B) in analogy to Padmanabhan et al. (4). Patients with more severe depressive symptoms (HADS-D > 10) did not differ from those with less depressive symptoms (p = 0.93) in their network damage scores (see Figure 3C). This also remained unchanged with different cut-offs (HADS-D > 7: p = 0.57; continuous HADS-D: p = 0.48).

4. Discussion

We combined three recent approaches to infer structure–function relationships in this lesion-symptom mapping study for post-stroke depressive symptoms in a large patient cohort. We analyzed relationships between PSDS 6 months after stroke and lesion location (SVR-LSM), structural disconnection (SVR-SDSM) and localized

functional diaschisis (LNSM). We identified an association of higher depression scores with (1) lesions in the right insular cortex, putamen and inferior frontal gyrus and (2) structural disconnection in the white matter of the right temporal lobe, but (3) no association with localized functional diaschisis.

The direct effects of lesion locations on depressive symptoms have been extensively studied in PSD over the past 40 years, yet results on specific brain regions, anterior–posterior gradients or even lesion laterality are too heterogeneous to draw consistent conclusions (6, 9). This has been ascribed, in part, to the rather imprecise methods used for structure–function inference, but may be overcome with voxel-based methods (38). With SVR-LSM, we identified an association of PSDS with lesions in several cortical and subcortical gray matter regions and the subcortical white matter. The structures affected to the largest extend were the right insula, the right putamen and the right inferior frontal gyrus along with the right corticospinal tract and the right superior thalamic radiation. This replicates and extends our previous finding using univariate VLSM, were we identified a significant association of PSDS with lesions of the right dorsal putamen (10). However, all eight present VLSM studies together are not conclusive (6): three studies were based on small samples in specific brain regions (39–41) and two larger studies were negative (4, 13). But there are now three lesion-symptom-mapping studies – with a total of nearly 2,000 patients – that identify an association of post-stroke depressive symptoms with specific lesion locations: the study by Weaver and colleagues (11), the recent study by Pan and colleagues (6) and the current analysis. The results are at least partly overlapping: the associated lesion locations are mainly (11) or exclusively [(12), this study] located in the right hemisphere, affect both white matter tracts and gray matter regions [(11, 12), this study] and encompass both basal ganglia [(11), this study] and cortical gray matter [(11, 12), this study]. The study by Weaver and colleagues represented a significant advance because of the multivariate LSM approach (11, 23, 24). By analyzing our independent data in a very similar way, we are able to confirm several of their findings. Namely the involvement of the right basal ganglia, the right hippocampus and right amygdala. Since our prior mass-univariate analysis only identified the right putamen (10), this reanalysis likely demonstrates a higher sensitivity of multivariate approaches to unveil the neurobiological basis of more complex brain functions represented in distributed brain networks and therefore hidden to classic VLSM analyses (6, 23, 24, 38). Notably, the results of Weaver and colleagues and our cohort converge in the right basal ganglia and amygdala despite differences in the time point (3 vs. 6 months), behavioral assessment (GDS vs. HADS) and patient cohort (Korean vs. German) (11). A meta-analysis of previous studies also identified an association of right hemispheric lesions with depressive symptoms 1–6 months post stroke (42). Weaver and colleagues and Pan and colleagues were reluctant to draw the conclusion that the right hemisphere is specifically associated with PSDS (6, 43). It is certainly true that these results implicate several regions in the right hemisphere with PSDS rather than the right hemisphere itself (11). Moreover, since absence of evidence is not evidence of absence, we cannot dismiss a possible contribution of regions within the left hemisphere based on our results. It is, for instance, possible that the left basal ganglia may also be involved (see Figure 1A), but were not significant due to insufficient statistical power. Still, one may conclude that it is at least unlikely that damage in almost all left cortical regions covered by our analyses contributes to PSDS (see direction of effect in the left cortical regions in Figure 1A). But the area with sufficient lesion overlap for the analyses was small, so only about 20% the brain was included in these analyses (see Figure 1B). The underrepresentation of patients with moderate to severe aphasia and thus large cortical lesions in the left frontal and temporal lobe certainly contributed to the limited lesion coverage and precludes the inference of a right-lateralized depression network. Since we used the HADS, patients with moderate to severe language comprehension deficits could not be included. With the Aphasic Depression Rating Scale, a possible alternative is available (44). A large patient cohort assessed with this scale and/or a psychiatric examination could provide a spatially less biased analysis.

We believe that the diverse regions identified must be understood in a connectome based account of depression as a network disorder (8, 45). Several of the identified regions are plausible major components of such a depression network. The subcortical gray matter regions identified were the right striatum [(10, 11), this analysis] and the right pallidum (11). The striatum has been consistently implied in MDD and PSD due to its prominent role in reward mechanisms, anhedonia, apathy and motivation (46, 47). Both accelerated striatal gray matter volume loss in MDD (48) and prediction of MDD based on lower striatal volume have been reported (49). Moreover, depression is highly prevalent in Parkinson's disease, which is in turn characterized by striatal dysfunction (50, 51). Also, deep brain stimulation of the striatum (ventral putamen) and nucleus accumbens is effective for the treatment of MDD (52, 53). The cortical regions involved are more diverse. The prefrontal cortex is the cortical region most consistently associated with MDD (54) and the left dorsolateral prefrontal cortex has been established as the most reliable site for the transcranial magnetic stimulation treatment of MDD (55). None of the three large lesion-symptom mapping studies identified the dorsolateral prefrontal cortex, but several other areas of gray matter: inferior frontal gyrus [(12), this analysis], insula [(12), this analysis], superior and middle temporal gyrus [(12), this analysis], inferior temporal gyrus (11), inferior parietal cortex (12), and the amygdala and hippocampus [(11), this analysis]. The anterior insula is one of the functionally most diverse structures in the brain, but it has been consistently associated with emotion regulation (56) and has even been discussed as the location where subjective feelings of emotion are generated (57, 58). Reduced gray matter volume in the right insula, among many other regions, has been conclusively demonstrated in MDD (59). The amygdala is a central part of the emotion circuits of the brain (60) and reduced gray matter volume in the amygdala has been described in late life depression (61) and MDD (62, 63). The right inferior frontal gyrus has also been implied in MDD in the sense that larger gray matter volume in the IFG predicted better clinical outcome in MDD after 5 years (54), both striatum and IFG are relevant for reward mechanisms (64) and reduced IFG activation leads to negative processing bias (65). Several white matter regions were also consistently associated with PSDS in lesion-symptom mapping analyses: the corona radiata [(11, 12), this analysis], the superior longitudinal fasciculus (11, 12) and the posterior thalamic radiation (11, 12). Increased fractional anisotropy has been described in the superior longitudinal fasciculus and the internal capsule in MDD compared to healthy controls (66).

Together, the identification of the right frontal operculum and the right putamen support a frontostriatal model of PSD (6). Frontostriatal dysfunction has been identified both in MDD and late life depression (67). Clinically, patients with late life depression, but also MDD, are characterized by prominent dysexecutive symptoms together with depressed mood. In these patients the disproportionate affection of frontostriatal connections has been proposed to be the neurobiological correlate of depressed mood and executive dysfunction (67). Cognitive deficits are also predictive of PSD (1). Further evidence for a frontostriatal theory of depression comes from neuromodulatory therapeutic interventions in MDD: both deep brain stimulation in the ventral capsule/ventral striatum and transcranial magnetic stimulation in the dorsolateral prefrontal cortex are effective (53).

In addition to the direct lesion effects discussed up to this point, the depression network may also become dysfunctional when its nodes are structurally disconnected or affected by functional diaschisis. Because both, white and gray matter seem to be involved in PSDS, we complemented our analyses of direct lesion effects (SVR-LSM) with indirect methods in search of both structural disconnection (SVR-SDSM) and functional diaschisis (LNSM, network damage score). We identified an association of PSDS with structural disconnection in the white matter of the right temporal lobe in our cohort, but could not find an association with localized functional diaschisis.

Affection of the uncinate fasciculus has been implied in MDD (68) and dysfunction of the superior longitudinal fasciculus in rumination (69) and suicidal ideation (70). An association between white matter damage and depressive symptoms has long been assumed based on the studies of white matter hyperintensities in late life 'vascular depression' (71). The disproportionate decline of white matter compared to gray matter due to cerebral small vessel disease led to the disconnection hypothesis of vascular depression (67). The best evidence for a contribution of structural disconnection in white matter tracts that pass through the temporal lobes comes from studies on white matter hyperintensities and late-life depression (72). Structural disconnection in the right temporal lobe in patients with PSDS was also identified by two other studies that used indirect measures of structural disconnection (11, 12). Apart from the right parahippocampal white matter, they identified the right anterior thalamic radiation (11) and bilateral temporal white matter, bilateral prefrontal and posterior parietal white matter and the posterior corpus callosum (12). Taken together, the three studies that used indirect measures of structural disconnection demonstrate partially overlapping results with the best evidence for an involvement of the right temporal white matter. In our cohort, we found no association of PSDS with structural disconnection in the left hemisphere (see Figure 2A). In contrast the study by Pan and colleagues provides strong evidence for a bilateral pattern of structural disconnection (12). Based on their large and well-characterized cohort they were able to go further and calculate a structural damage score. The score was derived from the degree of overlap of individual disconnection maps with the white matter regions where an association of structural diaschisis with PSD had been identified. This structural disconnection score was the strongest predictor in a multifactorial prediction model that included known risk factors of PSD such as cognitive deficits, stroke severity, functional status, sex, lesion size, and age (12). Taken together, the three studies based on indirect measures for structural diaschisis support a brain network theory of depression and point to a prominent role of frontal and temporal structural disconnection underlying PSDS. The study by Pan and colleagues furthermore provides evidence for the behavioral relevance of structural disconnection in PSD and its possible application in multifactorial prediction models for PSD (6).

We were unable to reproduce the results reported by Padmanabhan et al. who had identified functional diaschisis in the DPLFC in PSD patients and described a 'depression circuit' that had the potential to predict PSD based on lesion location. The strongest support for an involvement of the DLPFC in patients with MDD comes from studies converging on the left DLPFC as a suitable target for a network-guided transcranial magnetic stimulation treatment of depressive symptoms (73, 74). This has even been demonstrated in patients with PSD (75, 76). The lack of consistency of our result with these findings might be explained by differences in lesion aetiology (only stroke vs. stroke, intracerebral haemorrhage and traumatic brain lesion), behavioral scales (HADS scale vs. several other scales) or the time of assessment (6 months vs. 3 months – 30 years post-stroke). Alternatively it could be related to the method itself: while LNSM has certainly contributed to the understanding of the network damage in several neurological and psychiatric symptoms and syndromes [e.g., (19, 25, 26, 77–81)], it has also been demonstrated that indirect measures of functional diaschisis – such as LNSM – explain less variance in stroke symptoms than indirect measures of structural connectivity, direct measures of functional connectivity and lesion location (82, 83). Moreover, functional lesion network-mapping tends to generate anatomically plausible patterns, which is also the case here (see Figure 1A where many of the regions identified with the other two methods seem to fall onto the functional disconnection map), but accounts for very little behavioral variance (82). The direct measurement of functional diaschisis, although laborious in acute stroke patients, has been proposed to better understand the networks involved and discover compensatory mechanism that may be exploited therapeutically (6, 82). Methodological improvements of LNM may also prove fruitful. A recent work by Trapp and colleagues, which was conceptually similar to the LNM analysis presented here but used a different analytic approach, did indeed show that diaschisis to specific brain regions has an association with higher or lower risk for developing depressive symptoms. To uncover this association they had to rely on a very large cohort of >500 patients with different lesion aetiologies because of the at best modest strength of the uncovered correlation. They demonstrate that the 'risk' and 'resilience' regions "are not randomly distributed but fall primarily within two functional networks with lesions of the salience network associated with increased depressive symptoms ('risk' nodes) and lesions of default mode network associated with reduced depressive symptoms ('resilience' nodes)" (84). Thus, indirect measures of diaschisis might indeed be useful for the prediction of PSDS, but only as one additional factor in a multifactorial biopsychosocial disease model for PSDS. Their work and a study by Pini et al. show that further methodological adaptations of LNM can improve structure–function inference (85). But even if LNM may not be useful for prediction, the accurate anatomical distribution of functional connectivity maps may still be used to determine the regions involved (53). With this approach, Siddiqi and colleagues have described the convergence of stroke lesions that cause depression (also evaluated in a large cohort of 461 patients) and stimulation sites used to treat depression (with deep brain or transcranial magnetic stimulation) on a common brain circuit. This circuit is characterized by positive functional

connectivity bilaterally to the dorsolateral prefrontal cortex, frontal eye fields, inferior frontal gyrus, intraparietal sulcus and extrastriate visual cortex and negative connectivity to the subgenual cingulate cortex and ventromedial prefrontal cortex, thus implying even more regions bilaterally in a distributed depression network (53). In addition and in an unexpected twist, they have recently demonstrated that LNM of white matter lesions in multiple sclerosis patients with depressive symptoms maps onto the same depression network (86).

We believe that our analyses are not conclusive because of several further limitations. An important limitation is the small area with sufficient lesion coverage for SVR-VLSM (see Figure 1B). Our study shares this limitation with many previous VLSM studies (38, 87). It has recently been estimated that sample sizes of up to 3,000 patients are needed to achieve a sufficient lesion coverage for true whole brain analyses (87), although it must be added that very rarely affected brain regions can contribute little variance to frequent symptom such as PSD. Data sharing can overcome insufficient lesion coverage. While our data may not be made publicly available due to data protection regulations, we have and will share them upon request. Second, HADS is an established tool to screen for depression but not suited to establish the diagnosis and is probably not the most sensitive and specific screening instrument (88). Since depression is not a uniform phenomenon, a more detailed behavioral characterization might prove fruitful to differentiate lesion effects on depressive subsymptoms (i.e., anhedonia or cognitive control) which are likely to arise from dysfunction in different neuronal circuits. Even more so since depression may itself be understood, in the psychopathological network theory, as a complex network of symptoms where symptom-symptom interactions drive and sustain the depressive symptoms (6, 89, 90). If so, structure–function inference could be improved with the identification of driving symptoms which should then be related to lesion locations, disconnection or diaschisis (6). Third, we have no measures on cognitive impairments or functional impairment after 6 months and thus cannot account for their potential confounding effect. Fourth, in our cohort lesion size correlated with depressive symptoms (see Supplementary Table S1). While we controlled for lesion size in SVR-LSM and SVR-SDSM as recommended, we cannot completely rule out an effect of lesion size on our results since the effect of lesion size is not spatially homogenous (23, 91). Fifth, because of the cluster based inference it cannot be concluded that every identified region is indeed associated with the symptom but rather that there is a region within the cluster that shows the association (92). Finally, we would like to point out that the results reported here are of exploratory nature because this data set has been analyzed before with a mass univariate VLSM as initially intended (10).

To summarize, based on multivariate analyses of lesion location and indirect measures of disconnection, our results extend a previous study with this data set and partly confirm similar recent studies on the role of lesion locations in PSDS. Specifically, we identified an association of lesions in the right insular cortex, right putamen and inferior frontal gyrus with PSDS. Furthermore, structural disconnection in the white matter of the right temporal lobe was associated with PSDS, but there was no evidence for a contribution of functional diaschisis to PSDS. These analyses show the potential of indirect measures of disconnection and diaschisis for structure–function inference. Still, even larger cohorts, which include patients with aphasia and a more detailed behavioral characterization, are needed to leverage the full potential of LNSM and SDSM for our understanding of PSDS.

5. Resource identification initiative

SPM: RRID:SCR_007037; MATLAB: RRID:SCR_001622; SPSS: RRID:SCR_019096.

Data availability statement

The raw data supporting the conclusions of this article will be made available by the authors, without undue reservation.

Ethics statement

The studies involving human participants were reviewed and approved by the ethics committee of the Medical Faculty of Leipzig University. The patients provided their written informed consent to participate in this study.

Author contributions

JK, DS, and MW conceptualized the study. PB and M-LB had major role in patient acquisition. K-TH had major role in acquisition of neuroimaging data. JK and MW had major role in preprocessing of neuroimaging data, analyzed the data, and performed all statistical analyses. JK drafted the manuscript. All authors contributed to the article and approved the submitted version.

Funding

The work on this study was funded by the German Research Foundation (DFG Grant SA 1723/5-1 to DS and JK) and the Medical Faculty of the University of Leipzig (Grant 990101-113 to M-LB, Clinician Scientist Program to MW). Part of the study cohort was recruited with financial support by Merz Pharma GmbH & Co. KGaA (Frankfurt, Germany; Grant BGAAF-0136 to PB) and IPSEN Pharma GmbH (Munich, Germany; Grant BGAAF-0135 to PB). The funders were not involved in the study design, collection, analysis, interpretation of data, the writing of this article, or the decision to submit it for publication. The open access publication in Frontiers in Neurology was funded in part by the Open Access Publishing Fund of Leipzig University supported by the German Research Foundation within the program Open Access Publication Funding.

Acknowledgments

We want to thank all patients who participated in the study. We thank Hans-Ralf Schneider for contributions to data preprocessing. Finally, we thank Andrew DeMarco for his valuable advice during the review process.

Conflict of interest

The authors declare that the research was conducted in the absence of any commercial or financial relationships that could be construed as a potential conflict of interest.

Publisher's note

All claims expressed in this article are solely those of the authors and do not necessarily represent those of their affiliated organizations, or those of the publisher, the editors and the reviewers. Any product that may be evaluated in this article, or claim that may be made by its manufacturer, is not guaranteed or endorsed by the publisher.

Supplementary material

The Supplementary material for this article can be found online at: https://www.frontiersin.org/articles/10.3389/fneur.2023.1144228/full#supplementary-material

References

1. Ayerbe L, Ayis S, Wolfe CD, Rudd AG. Natural history, predictors and outcomes of depression after stroke: systematic review and meta-analysis. *Br J Psychiatry*. (2013) 202:14–21. doi: 10.1192/bjp.bp.111.107664

2. Ayerbe L, Ayis S, Crichton SL, Rudd AG, Wolfe CD. Explanatory factors for the increased mortality of stroke patients with depression. *Neurology*. (2014) 83:2007–12. doi: 10.1212/WNL.0000000000001029

3. Ginkel D M-v, Janneke M, Hafsteinsdóttir TB, Lindeman E, Ettema RG, Grobbee DE, et al. In-hospital risk prediction for post-stroke depression. *Stroke*. (2013) 44:2441–5. doi: 10.1161/strokeaha.111.000304

4. Padmanabhan JL, Cooke D, Joutsa J, Siddiqi SH, Ferguson M, Darby RR, et al. A human depression circuit derived from focal brain lesions. *Biol Psychiatry*. (2019) 86:749–58. doi: 10.1016/j.biopsych.2019.07.023

5. Akiskal HS, McKinney WT. Overview of recent research in depression. Integration of ten conceptual models into a comprehensive clinical frame. *Arch Gen Psychiatry*. (1975) 32:285–305. doi: 10.1001/archpsyc.1975.01760210019001

6. Pan C, Li G, Sun W, Miao J, Qiu X, Lan Y, et al. Neural substrates of poststroke depression: current opinions and methodology trends. *Front Neurosci*. (2022) 16:812410. doi: 10.3389/fnins.2022.812410

7. Mayman N, Stein LK, Erdman J, Kornspun A, Tuhrim S, Jette N, et al. Risk and predictors of depression following acute ischemic stroke in the elderly. *Neurology*. (2021) 96:e2184–91. doi: 10.1212/wnl.0000000000011828

8. Fox MD. Mapping symptoms to brain networks with the human connectome. *N Engl J Med*. (2018) 379:2237–45. doi: 10.1056/NEJMra1706158

9. Nickel A, Thomalla G. Post-stroke depression: impact of lesion location and methodological limitations-a topical review. *Front Neurol*. (2017) 8:498. doi: 10.3389/fneur.2017.00498

10. Klingbeil J, Brandt M-L, Wawrzyniak M, Stockert A, Schneider HR, Baum P, et al. Association of lesion location and depressive symptoms poststroke. *Stroke*. (2022) 53:e467–71. doi: 10.1161/STROKEAHA.122.039068

11. Weaver NA, Lim J-S, Schilderinck J, Biessels GJ, Kang Y, Kim BJ, et al. Strategic infarct locations for poststroke depressive symptoms: a lesion-and disconnection-symptom mapping study. *Biol Psychiatry Cogn Neurosci Neuroimaging*. (2021) 8:387–96. doi: 10.1016/j.bpsc.2021.09.002

12. Pan C, Li G, Jing P, Chen G, Sun W, Miao J, et al. Structural disconnection-based prediction of poststroke depression. *Transl Psychiatry*. (2022) 12:461. doi: 10.1038/s41398-022-02223-2

13. Sagnier S, Munsch F, Bigourdan A, Debruxelles S, Poli M, Renou P, et al. The influence of stroke location on cognitive and mood impairment. A voxel-based lesion-symptom mapping study. *J Stroke Cerebrovasc Dis*. (2019) 28:1236–42. doi: 10.1016/j.jstrokecerebrovasdis.2019.01.010

14. Catani M, Dell'Acqua F, Bizzi A, Forkel SJ, Williams SC, Simmons A, et al. Beyond cortical localization in clinico-anatomical correlation. *Cortex*. (2012) 48:1262–87. doi: 10.1016/j.cortex.2012.07.001

15. Von MC. *Die Lokalisation im Grosshirn und der Abbau der Funktion durch kortikale Herde*. Wiesbaden: Bergmann (1914).

16. Foulon C, Cerliani L, Kinkingnéhun S, Levy R, Rosso C, Urbanski M, et al. Advanced lesion symptom mapping analyses and implementation as BCBtoolkit. *Gigascience*. (2018) 7:1–17. doi: 10.1093/gigascience/giy004

17. Thiebaut de Schotten M, Forkel SJ. The emergent properties of the connected brain. *Science*. (2022) 378:505–10. doi: 10.1126/science.abq2591

18. Geschwind N. Disconnexion syndromes in animals and man. I. *Brain*. (1965) 88:237–94. doi: 10.1093/brain/88.2.237

19. Boes AD, Prasad S, Liu H, Liu Q, Pascual-Leone A, Caviness VS, et al. Network localization of neurological symptoms from focal brain lesions. *Brain*. (2015) 138:3061–75. doi: 10.1093/brain/awv228

20. Haan B de, Clas P, Juenger H, Wilke M, Karnath H-O. Fast semi-automated lesion demarcation in stroke. *Neuroimage Clin* (2015) 9:69–74. doi:10.1016/j.nicl.2015.06.013

21. Rorden C, Brett M. Stereotaxic display of brain lesions. *Behav Neurol*. (2000) 12:191–200. doi: 10.1155/2000/421719

22. Rorden C, Bonilha L, Fridriksson J, Bender B, Karnath H-O. Age-specific CT and MRI templates for spatial normalization. *NeuroImage*. (2012) 61:957–65. doi: 10.1016/j.neuroimage.2012.03.020

23. DeMarco AT, Turkeltaub PE. A multivariate lesion symptom mapping toolbox and examination of lesion-volume biases and correction methods in lesion-symptom mapping. *Hum Brain Mapp*. (2018) 39:4169–82. doi: 10.1002/hbm.24289

24. Zhang Y, Kimberg DY, Coslett HB, Schwartz MF, Wang Z. Multivariate lesion-symptom mapping using support vector regression. *Hum Brain Mapp*. (2014) 35:5861–76. doi: 10.1002/hbm.22590

25. Wawrzyniak M, Stockert A, Klingbeil J, Saur D. Voxelwise structural disconnection mapping: methodological validation and recommendations. *Neuroimage Clin*. (2022) 35:103132. doi: 10.1016/j.nicl.2022.103132

26. Wawrzyniak M, Klingbeil J, Zeller D, Saur D, Classen J. The neuronal network involved in self-attribution of an artificial hand: a lesion network-symptom-mapping study. *NeuroImage*. (2018) 166:317–24. doi: 10.1016/j.neuroimage.2017.11.011

27. Klingbeil J, Wawrzyniak M, Stockert A, Brandt M-L, Schneider H-R, Metelmann M, et al. Pathological laughter and crying: insights from lesion network-symptom-mapping. *Brain*. (2021) 144:3264–76. doi: 10.1093/brain/awab224

28. Sperber C, Dadashi A. The influence of sample size and arbitrary statistical thresholds in lesion-network mapping. *Brain*. (2020) 143:e40. doi: 10.1093/brain/awaa094

29. Yeo BT, Krienen FM, Sepulcre J, Sabuncu MR, Lashkari D, Hollinshead M, et al. The organization of the human cerebral cortex estimated by intrinsic functional connectivity. *J Neurophysiol*. (2011) 106:1125–65. doi: 10.1152/jn.00338.2011

30. Glasser MF, Sotiropoulos SN, Wilson JA, Coalson TS, Fischl B, Andersson JL, et al. The minimal preprocessing pipelines for the human connectome project. *NeuroImage*. (2013) 80:105–24. doi: 10.1016/j.neuroimage.2013.04.127

31. Power JD, Barnes KA, Snyder AZ, Schlaggar BL, Petersen SE. Spurious but systematic correlations in functional connectivity MRI networks arise from subject motion. *NeuroImage*. (2012) 59:2142–54. doi: 10.1016/j.neuroimage.2011.10.018

32. Buxton RB. The physics of functional magnetic resonance imaging (fMRI). *Rep Prog Phys*. (2013) 76:096601. doi: 10.1088/0034-4885/76/9/096601

33. Logothetis NK, Pauls J, Augath M, Trinath T, Oeltermann A. Neurophysiological investigation of the basis of the fMRI signal. *Nature*. (2001) 412:150–7. doi: 10.1038/35084005

34. Nichols TE, Holmes AP. Nonparametric permutation tests for functional neuroimaging: a primer with examples. *Hum Brain Mapp*. (2002) 15:1–25. doi: 10.1002/hbm.1058

35. Makris N, Goldstein JM, Kennedy D, Hodge SM, Caviness VS, Faraone SV, et al. Decreased volume of left and total anterior insular lobule in schizophrenia. *Schizophr Res*. (2006) 83:155–71. doi: 10.1016/j.schres.2005.11.020

36. Warrington S, Bryant KL, Khrapitchev AA, Sallet J, Charquero-Ballester M, Douaud G, et al. XTRACT - standardised protocols for automated tractography in the human and macaque brain. *NeuroImage*. (2020) 217:116923. doi: 10.1016/j.neuroimage.2020.116923

37. Shattuck DW, Mirza M, Adisetiyo V, Hojatkashani C, Salamon G, Narr KL, et al. Construction of a 3D probabilistic atlas of human cortical structures. *NeuroImage*. (2008) 39:1064–80. doi: 10.1016/j.neuroimage.2007.09.031

38. Karnath H-O, Sperber C, Rorden C. Mapping human brain lesions and their functional consequences. *NeuroImage*. (2018) 165:180–9. doi: 10.1016/j.neuroimage.2017.10.028

39. Gozzi SA, Wood AG, Chen J, Vaddadi K, Phan TG. Imaging predictors of poststroke depression: methodological factors in voxel-based analysis. *BMJ Open*. (2014) 4:e004948. doi: 10.1136/bmjopen-2014-004948

40. Grajny K, Pyata H, Spiegel K, Lacey EH, Xing S, Brophy C, et al. Depression symptoms in chronic left hemisphere stroke are related to dorsolateral prefrontal cortex damage. *J Neuropsychiatr Clin Neurosci*. (2016) 28:292–8. doi: 10.1176/appi.neuropsych.16010004

41. Kim NY, Lee SC, Shin J-C, Park JE, Kim YW. Voxel-based lesion symptom mapping analysis of depressive mood in patients with isolated cerebellar stroke: a pilot study. *Neuroimage Clin*. (2017) 13:39–45. doi: 10.1016/j.nicl.2016.11.011

42. Wei N, Yong W, Li X, Zhou Y, Deng M, Zhu H, et al. Post-stroke depression and lesion location: a systematic review. *J Neurol*. (2015) 262:81–90. doi: 10.1007/s00415-014-7534-1

43. Bruder GE, Stewart JW, McGrath PJ. Right brain, left brain in depressive disorders: clinical and theoretical implications of behavioral, electrophysiological and neuroimaging findings. *Neurosci Biobehav Rev*. (2017) 78:178–91. doi: 10.1016/j.neubiorev.2017.04.021

44. Benaim C, Cailly B, Perennou D, Pelissier J. Validation of the aphasic depression rating scale. *Stroke*. (2004) 35:1692–6. doi: 10.1161/01.STR.0000130591.95710.20

45. Fornito A, Zalesky A, Breakspear M. The connectomics of brain disorders. *Nat Rev Neurosci*. (2015) 16:159–72. doi: 10.1038/nrn3901

46. Der-Avakian A, Markou A. The neurobiology of anhedonia and other reward-related deficits. *Trends Neurosci*. (2012) 35:68–77. doi: 10.1016/j.tins.2011.11.005

47. Schmahmann JD, Pandya DN. Disconnection syndromes of basal ganglia, thalamus, and cerebrocerebellar systems. *Cortex*. (2008) 44:1037–66. doi: 10.1016/j.cortex.2008.04.004

48. Sacchet MD, Camacho MC, Livermore EE, Thomas EA, Gotlib IH. Accelerated aging of the putamen in patients with major depressive disorder. *J Psychiatry Neurosci*. (2017) 42:164–71. doi: 10.1503/jpn.160010

49. Talati A, van Dijk MT, Pan L, Hao X, Wang Z, Gameroff M, et al. Putamen structure and function in familial risk for depression: a multimodal imaging study. *Biol Psychiatry*. (2022) 92:932–41. doi: 10.1016/j.biopsych.2022.06.035

50. Prange S, Klinger H, Laurencin C, Danaila T, Thobois S. Depression in patients with Parkinson's disease: current understanding of its neurobiology and implications for treatment. *Drugs Aging*. (2022) 39:417–39. doi: 10.1007/s40266-022-00942-1

51. Kulisevsky J, Pagonabarraga J, Pascual-Sedano B, García-Sánchez C, Gironell A. Prevalence and correlates of neuropsychiatric symptoms in Parkinson's disease without dementia. *Mov Disord*. (2008) 23:1889–96. doi: 10.1002/mds.22246

52. Drobisz D, Damborská A. Deep brain stimulation targets for treating depression. *Behav Brain Res*. (2019) 359:266–73. doi: 10.1016/j.bbr.2018.11.004

53. Siddiqi SH, Taylor SF, Cooke D, Pascual-Leone A, George MS, Fox MD. Distinct symptom-specific treatment targets for circuit-based neuromodulation. *Am J Psychiatr*. (2020) 177:435–46. doi: 10.1176/appi.ajp.2019.19090915

54. Pizzagalli DA, Roberts AC. Prefrontal cortex and depression. *Neuropsychopharmacology*. (2022) 47:225–46. doi: 10.1038/s41386-021-01101-7

55. Cash RF, Weigand A, Zalesky A, Siddiqi SH, Downar J, Fitzgerald PB, et al. Using brain imaging to improve spatial targeting of transcranial magnetic stimulation for depression. *Biol Psychiatry*. (2021) 90:689–700. doi: 10.1016/j.biopsych.2020.05.033

56. Uddin LQ, Nomi JS, Hébert-Seropian B, Ghaziri J, Boucher O. Structure and function of the human insula. *J Clin Neurophysiol*. (2017) 34:300–6. doi: 10.1097/WNP.0000000000000377

57. Damasio A. Feelings of emotion and the self. *Ann N Y Acad Sci*. (2003) 1001:253–61. doi: 10.1196/annals.1279.014

58. Gasquoine PG. Contributions of the insula to cognition and emotion. *Neuropsychol Rev*. (2014) 24:77–87. doi: 10.1007/s11065-014-9246-9

59. Schmaal L, Hibar DP, Sämann PG, Hall GB, Baune BT, Jahanshad N, et al. Cortical abnormalities in adults and adolescents with major depression based on brain scans from 20 cohorts worldwide in the ENIGMA major depressive disorder working group. *Mol Psychiatry*. (2017) 22:900–9. doi: 10.1038/mp.2016.60

60. LeDoux JE. Emotion circuits in the brain. *Annu Rev Neurosci*. (2000) 23:155–84. doi: 10.1146/annurev.neuro.23.1.155

61. Schweitzer I, Tuckwell V, Ames D, O'Brien J. Structural neuroimaging studies in late-life depression: a review. *World J Biol Psychiatry*. (2001) 2:83–8. doi: 10.3109/15622970109027497

62. Lorenzetti V, Allen NB, Fornito A, Yücel M. Structural brain abnormalities in major depressive disorder: a selective review of recent MRI studies. *J Affect Disord*. (2009) 117:1–17. doi: 10.1016/j.jad.2008.11.021

63. Sheline YI, Gado MH, Price JL. Amygdala core nuclei volumes are decreased in recurrent major depression. *Neuroreport*. (1998) 9:2023–8. doi: 10.1097/00001756-199806220-00021

64. Wang KS, Delgado MR. Corticostriatal circuits encode the subjective value of perceived control. *Cereb Cortex*. (2019) 29:5049–60. doi: 10.1093/cercor/bhz045

65. Li H, Wei D, Sun J, Zhang Q, Qiu J. Fronto-limbic alterations in negatively biased attention in young adults with subthreshold depression. *Front Psychol*. (2017) 8:1354. doi: 10.3389/fpsyg.2017.01354

66. Abraham M, Mundorf A, Brodmann K, Freund N. Unraveling the mystery of white matter in depression: a translational perspective on recent advances. *Brain Behav*. (2022) 12:e2629. doi: 10.1002/brb3.2629

67. Alexopoulos GS. Frontostriatal and limbic dysfunction in late-life depression. *Am J Geriatr Psychiatry*. (2002) 10:687–95. doi: 10.1097/00019442-200211000-00007

68. Bracht T, Linden D, Keedwell P. A review of white matter microstructure alterations of pathways of the reward circuit in depression. *J Affect Disord*. (2015) 187:45–53. doi: 10.1016/j.jad.2015.06.041

69. Pisner DA, Shumake J, Beevers CG, Schnyer DM. The superior longitudinal fasciculus and its functional triple-network mechanisms in brooding. *Neuroimage Clin*. (2019) 24:101935. doi: 10.1016/j.nicl.2019.101935

70. Davey DK, Jurick SM, Crocker LD, Hoffman SN, Sanderson-Cimino M, Tate DF, et al. White matter integrity, suicidal ideation, and cognitive dysfunction in combat-exposed Iraq and Afghanistan veterans. *Psychiatry Res Neuroimaging*. (2021) 317:111389. doi: 10.1016/j.pscychresns.2021.111389

71. Taylor WD, Aizenstein HJ, Alexopoulos GS. The vascular depression hypothesis: mechanisms linking vascular disease with depression. *Mol Psychiatry*. (2013) 18:963–74. doi: 10.1038/mp.2013.20

72. Sheline YI, Price JL, Vaishnavi SN, Mintun MA, Barch DM, Epstein AA, et al. Regional white matter hyperintensity burden in automated segmentation distinguishes late-life depressed subjects from comparison subjects matched for vascular risk factors. *Am J Psychiatry*. (2008) 165:524–32. doi: 10.1176/appi.ajp.2007.07010175

73. Sackeim HA, Aaronson ST, Carpenter LL, Hutton TM, Mina M, Pages K, et al. Clinical outcomes in a large registry of patients with major depressive disorder treated with transcranial magnetic stimulation. *J Affect Disord*. (2020) 277:65–74. doi: 10.1016/j.jad.2020.08.005

74. Berlim MT, van den Eynde F, Daskalakis ZJ. High-frequency repetitive transcranial magnetic stimulation accelerates and enhances the clinical response to antidepressants in major depression: a meta-analysis of randomized, double-blind, and sham-controlled trials. *J Clin Psychiatry*. (2013) 74:e122–9. doi: 10.4088/JCP.12r07996

75. Jorge RE, Robinson RG, Tateno A, Narushima K, Acion L, Moser D, et al. Repetitive transcranial magnetic stimulation as treatment of poststroke depression: a preliminary study. *Biol Psychiatry*. (2004) 55:398–405. doi: 10.1016/j.biopsych.2003.08.017

76. Frey J, Najib U, Lilly C, Adcock A. Novel TMS for stroke and depression (NoTSAD): accelerated repetitive transcranial magnetic stimulation as a safe and effective treatment for post-stroke depression. *Front Neurol*. (2020):11. doi: 10.3389/fneur.2020.00788

77. Darby RR, Horn A, Cushman F, Fox MD. Lesion network localization of criminal behavior. *Proc Natl Acad Sci U S A*. (2018) 115:601–6. doi: 10.1073/pnas.1706587115

78. Darby RR, Joutsa J, Burke MJ, Fox MD. Lesion network localization of free will. *Proc Natl Acad Sci U S A*. (2018) 115:10792–7. doi: 10.1073/pnas.1814117115

79. Darby RR, Laganiere S, Pascual-Leone A, Prasad S, Fox MD. Finding the imposter: brain connectivity of lesions causing delusional misidentifications. *Brain*. (2017) 140:497–507. doi: 10.1093/brain/aww288

80. Klingbeil J, Wawrzyniak M, Stockert A, Karnath H-O, Saur D. Hippocampal diaschisis contributes to anosognosia for hemiplegia: evidence from lesion network-symptom-mapping. *NeuroImage*. (2020) 208:116485. doi: 10.1016/j.neuroimage.2019.116485

81. Joutsa J, Corp DT, Fox MD. Lesion network mapping for symptom localization: recent developments and future directions. *Curr Opin Neurol*. (2022) 35:453–9. doi: 10.1097/WCO.0000000000001085

82. Salvalaggio A, De Grazia DF, Michele ZM, Thiebaut de Schotten M, Corbetta M. Post-stroke deficit prediction from lesion and indirect structural and functional disconnection. *Brain*. (2020) 143:2173–88. doi: 10.1093/brain/awaa156

83. Souter NE, Wang X, Thompson H, Krieger-Redwood K, Halai AD, Lambon Ralph MA, et al. Mapping lesion, structural disconnection, and functional disconnection to symptoms in semantic aphasia. *Brain Struct Funct*. (2022) 227:3043–61. doi: 10.1007/s00429-022-02526-6

84. Trapp NT, Bruss JE, Manzel K, Grafman J, Tranel D, Boes AD. Large-scale lesion symptom mapping of depression identifies brain regions for risk and resilience. *Brain*. (2022) 146:1672–85. doi: 10.1093/brain/awac361

85. Pini L, Salvalaggio A, Filippo Grazia M de, Zorzi M, Thiebaut de Schotten M, Corbetta M. A novel stroke lesion network mapping approach: improved accuracy yet still low deficit prediction. *Brain Commun* (2021) 3:fcab259. doi:10.1093/braincomms/fcab259

86. Siddiqi SH, Kletenik I, Anderson MC, Cavallari M, Chitnis T, Glanz BI, et al. Lesion network localization of depression in multiple sclerosis. *Nat Mental Health*. (2023) 1:36–44. doi: 10.1038/s44220-022-00002-y

87. Weaver NA, Kuijf HJ, Aben HP, Abrigo J, Bae H-J, Barbay M, et al. Strategic infarct locations for post-stroke cognitive impairment: a pooled analysis of individual patient data from 12 acute ischaemic stroke cohorts. *Lancet Neurol*. (2021) 20:448–59. doi: 10.1016/s1474-4422(21)00060-0

88. Meader N, Moe-Byrne T, Llewellyn A, Mitchell AJ. Screening for poststroke major depression: a meta-analysis of diagnostic validity studies. *J Neurol Neurosurg Psychiatry*. (2013) 85:198–206. doi: 10.1136/jnnp-2012-304194

89. Borsboom D. Psychometric perspectives on diagnostic systems. *J Clin Psychol*. (2008) 64:1089–108. doi: 10.1002/jclp.20503

90. Fried EI, Cramer AO. Moving forward: challenges and directions for psychopathological network theory and methodology. *Perspect Psychol Sci*. (2017) 12:999–1020. doi: 10.1177/1745691617705892

91. Mah Y-H, Husain M, Rees G, Nachev P. Human brain lesion-deficit inference remapped. *Brain*. (2014) 137:2522–31. doi: 10.1093/brain/awu164

92. Friston KJ, Holmes A, Poline JB, Price CJ, Frith CD. Detecting activations in PET and fMRI: levels of inference and power. *NeuroImage*. (1996) 4:223–35. doi: 10.1006/nimg.1996.0074

frontiers | Frontiers in Neurology

TYPE Original Research
PUBLISHED 20 June 2023
DOI 10.3389/fneur.2023.1175576

OPEN ACCESS

EDITED BY
Wei Zhang,
Peking University, China

REVIEWED BY
Chuh-Hyoun Na,
University Hospital RWTH Aachen, Germany
Lei Gao,
Wuhan University, China
Max Ostrinsky Krucoff,
Medical College of Wisconsin and Marquette University, United States

*CORRESPONDENCE
Alessandro Salvalaggio
✉ alessandro.salvalaggio@unipd.it
Maurizio Corbetta
✉ maurizio.corbetta@unipd.it

RECEIVED 27 February 2023
ACCEPTED 22 May 2023
PUBLISHED 20 June 2023

CITATION
Sansone G, Pini L, Salvalaggio A, Gaiola M, Volpin F, Baro V, Padovan M, Anglani M, Facchini S, Chioffi F, Zagonel V, D'Avella D, Denaro L, Lombardi G and Corbetta M (2023) Patterns of gray and white matter functional networks involvement in glioblastoma patients: indirect mapping from clinical MRI scans. *Front. Neurol.* 14:1175576. doi: 10.3389/fneur.2023.1175576

Patterns of gray and white matter functional networks involvement in glioblastoma patients: indirect mapping from clinical MRI scans

Giulio Sansone[1], Lorenzo Pini[2], Alessandro Salvalaggio[1,2]*, Matteo Gaiola[1], Francesco Volpin[3], Valentina Baro[4], Marta Padovan[5], Mariagiulia Anglani[6], Silvia Facchini[1], Franco Chioffi[3], Vittorina Zagonel[5], Domenico D'Avella[4], Luca Denaro[4], Giuseppe Lombardi[5] and Maurizio Corbetta[1,2,7]*

[1]Department of Neuroscience, University of Padova, Padova, Italy, [2]Padova Neuroscience Center (PNC), University of Padova, Padova, Italy, [3]Division of Neurosurgery, Azienda Ospedaliera Università di Padova, Padova, Italy, [4]Academic Neurosurgery, Department of Neurosciences, University of Padova, Padova, Italy, [5]Department of Oncology, Oncology 1, Veneto Institute of Oncology IOV-IRCCS, Padova, Italy, [6]Neuroradiology Unit, University Hospital of Padova, Padova, Italy, [7]Venetian Institute of Molecular Medicine (VIMM), Fondazione Biomedica, Padova, Italy

Background: Resting-state functional-MRI studies identified several cortical gray matter functional networks (GMNs) and white matter functional networks (WMNs) with precise anatomical localization. Here, we aimed at describing the relationships between brain's functional topological organization and glioblastoma (GBM) location. Furthermore, we assessed whether GBM distribution across these networks was associated with overall survival (OS).

Materials and methods: We included patients with histopathological diagnosis of IDH-wildtype GBM, presurgical MRI and survival data. For each patient, we recorded clinical-prognostic variables. GBM core and edema were segmented and normalized to a standard space. Pre-existing functional connectivity-based atlases were used to define network parcellations: 17 GMNs and 12 WMNs were considered in particular. We computed the percentage of lesion overlap with GMNs and WMNs, both for core and edema. Differences between overlap percentages were assessed through descriptive statistics, ANOVA, post-hoc tests, Pearson's correlation tests and canonical correlations. Multiple linear and non-linear regression tests were employed to explore relationships with OS.

Results: 99 patients were included (70 males, mean age 62 years). The most involved GMNs included ventral somatomotor, salient ventral attention and default-mode networks; the most involved WMNs were ventral frontoparietal tracts, deep frontal white matter, and superior longitudinal fasciculus system. Superior longitudinal fasciculus system and dorsal frontoparietal tracts were significantly more included in the edema ($p<0.001$). 5 main patterns of GBM core distribution across functional networks were found, while edema localization was less classifiable. ANOVA showed significant differences between mean overlap percentages, separately for GMNs and WMNs (p-values<0.0001). Core-N12 overlap predicts higher OS, although its inclusion does not increase the explained OS variance.

Discussion and conclusion: Both GBM core and edema preferentially overlap with specific GMNs and WMNs, especially associative networks, and GBM core

follows five main distribution patterns. Some inter-related GMNs and WMNs were co-lesioned by GBM, suggesting that GBM distribution is not independent of the brain's structural and functional organization. Although the involvement of ventral frontoparietal tracts (N12) seems to have some role in predicting survival, network-topology information is overall scarcely informative about OS. fMRI-based approaches may more effectively demonstrate the effects of GBM on brain networks and survival.

KEYWORDS

glioblastoma, functional gray matter networks, functional white matter networks, MRI, overall survival, patterns

1. Background

Glioblastoma (GBM) is the most common primary malignant tumor of the central nervous system in the adult population. The incidence rate for GBM is 3–5 people per 100.000 per year (1–4). Despite advances in neurosurgery, neuro-oncology and radiotherapy, overall survival (OS) at 5 years is currently about 6.8%, with a median OS around 15 months (3, 4). The main prognostic factors are: age at diagnosis, performance status before surgery, extent of resection, eligibility to radio- or chemotherapies, O-6-methylguanine-DNA methyltransferase promoter (MGMT) methylation and gender (5, 6). Interestingly, pre-surgical GBM size does not predict patient survival (7).

Concerning their anatomical distribution, GBMs are thought to originate from neural stem cells within the so-called "subventricular zones" (8–10), from which they putatively grow and spread through the white matter (WM) of frontal, temporal and parietal lobes, disrupting the overlaying gray matter (GM) (11–13). On the other hand, occipital and infratentorial localizations are much less frequent. Tumor location might be associated with a relatively worse or better prognosis, depending on the extent of tumor resection allowed by the "neurological eloquence" of that region (7).

Previous neuroradiological studies have shown that brain tumors cause not only structural but also functional alterations in brain networks (14–18), in both ipsilesional and contralesional hemispheres (19, 20). Resting-state functional MRI (rs-fMRI) studies have identified a small number of GM functional networks (GMNs) based upon the temporal correlation of the blood oxygenation level dependent (BOLD) signal between distinct cortical regions. Yeo et al. (21) proposed a hierarchical parcellation of the brain cortex into 7 main cortical GMNs: visual (VIS), somatomotor (SMN), dorsal attention (DAN), ventral-attention (VAN), limbic (LMB), frontoparietal (FPN) and default-mode (DMN) networks. These could be furtherly fractionated into 17 sub-networks, of which somatomotor A, somatomotor B, peripheral vision and central vision are predominantly local networks confined to sensory and motor cortices. The other networks are more distributed across multiple lobes, are related to cognitive functions and are known as associative networks. Interestingly, rs-fMRI studies showed that WM and GM exhibit similar low-frequency signal powers, moreover in task-related fMRI studies it was found that external stimuli could reliably induce a hemodynamic response within the WM, with a profile similar to that observed in GM, though with a smaller peak amplitude (22). The study of WM fMRI signals in neuro-oncology is still widely unexplored and its relevance is potentially very high since GBM is predominantly a WM disease. As an example, some authors have found decreased functional connectivity with DMN in the corpus callosum of glioma patients, potentially explained by tumor-dependent Wallerian degeneration (18). Notably, functional atlases of WM have been defined: in particular, Peer et al. (23) showed the existence of 12 WM functional networks (WMNs). Half of these showed good anatomical correspondence with structural WM tracts, whereas the remaining half simultaneously corresponded to multiple tracts, presumably allowing coordinated activity across multiple GMNs. Furthermore, these were subdivided into superficial WMNs, correlated with established GMNs, and deep WMNs, which do not show such strong correlations and have been postulated to represent the putative means of communication between different GMNs (23). Atlases of resting state fMRI-derived GMNs and WMNs can be currently used for mapping purposes (21, 23).

GBMs are not uniformly distributed across brain functional networks and larger tumors usually encompass both WM and GM. Mandal et al. (13) have recently discovered that gliomas are prevalent within the aforementioned Yeo's associative networks and areas harboring stem-like brain cells. They also found that functional connectivity measures [based on Miller's connectome (24)], such as nodal strength, as well as cellular and genetic data explained about 58% of the variance in glioma distribution frequency. In another study, the same authors used independent component analysis to decompose low- and high-grade glioma lesions into 3 principal areas of co-lesioned brain regions ("lesion covariance networks" or "LCNs"), which showed anatomical correspondence to different structural WM tracts and functional connectivity networks [obtained from Miller et al. (24)]. The differences in OS that they found between LCNs, however, were mainly driven by molecular determinants, rather than glioma distribution (25). Recently, a network-based anatomical approach has been proposed for the classification of brain tumors in relation to the cognitive outcome (26).

As for fMRI studies, Liu et al. (27) for the first time implemented fMRI data into the prediction of glioma patient survival, discovering that functional connectivity-derived features increased the accuracy of patient survival prediction. Other rs-fMRI studies showed that OS correlated with specific patterns of BOLD synchronization between tumor core and distant brain regions (28, 29). fMRI studies have the

advantage of directly measuring the impact of GBMs on brain functional organization. Moreover, BOLD-signal may also be related to the tumoral neoangiogenesis (30).

Despite recent advances, much remains to be learned about the impact of brain tumors on the brain's functional networks and their relationship to survival. Advanced MRI studies are costly, time-consuming and not always feasible, especially for large-scale studies or in clinical practice. Hence, the aim of the present study was to use conventional clinical MRI scans to quantify the spatial relationships between GBM lesions and brain's functional organization, in terms of relative overlap of the neoplastic core and perilesional edema region with both Yeo's 17 GMNs and Peer's 12 WMNs, without using fMRI-derived functional connectivity data. Moreover, we aimed at exploring differences between distinct tumor-network overlap percentages, as well as identifying potential patterns of GBM distribution across functional networks. Lastly, we investigated whether the extent of the overlap between core or edema regions and specific GMNs or WMNs improves the prediction of patient survival, in addition to the known clinical-prognostic factors. Since we used anatomical MRI images, our approach may be reproducible in a clinical setting. As compared to Mandal et al.'s (13) study, we used a 17-network parcellation to increase the specificity of GBM to GMNs relationships. Furthermore, to our knowledge, this is the first study to quantify the spatial relationship between GBM lesions and WMNs. Finally, this study is the first to investigate potential links among GBM perilesional edema, functional connectivity networks and patient survival, as edema has been shown to harbor valuable information in previous studies (31). Overall, the present study investigates the spatial relationships between GBM and functional networks, in the wake of an emerging field called "cancer neuroscience."

2. Materials and methods

2.1. Patients

This retrospective study was conducted on a cohort of patients with a histologically confirmed, newly diagnosed GBM, IDH wild-type, according to the WHO 2021 classification (32). The inclusion criteria were: (1) a histologically confirmed, newly diagnosed GBM, IDH wild-type; (2) the availability of presurgical MRI acquisition, which had to include T2w, FLAIR, pre- and post-contrast T1w sequences; (3) availability of OS data. The exclusion criteria were: GBM recurrence, MRI acquisition with a low magnetic field scanner (magnetic lower than 1.5 T), lack of axial plane acquisition in at least one among FLAIR, pre- and post-contrast T1w sequences, the presence of macroscopic artifacts in MR structural images, and radiologic evidence of previous brain diagnostic or therapeutic invasive procedures (e.g., stereotactic biopsy). For each patient, the following additional clinical, surgical and prognostic variables were recorded: age, gender, Stupp protocol, radicality of surgical resection (biopsy, partial resection and gross total resection), ECOG performance status and MGMT promoter methylation status.

The study was approved by the ethical committee of the Province of Padua (Comitato Etico per la Sperimentazione Clinica della Provincia di Padova n. 70n/AO/20). The study was performed in accordance with the Declaration of Helsinki and its latest amendments.

2.2. Preprocessing of MR images

Structural images were pre-processed before manually delineating the tumor volume. Preprocessing included image bias field correction (33) and skull stripping (34). Structural images were then coregistered to the pre-contrast T1w of the patient to improve the segmentation of the tumor. Manual segmentation was performed in the native space using the ITK-Snap toolbox version 3.8.0[1] (35) slice-by-slice by a neurology resident and a neurology intern (GS and MG) and checked by an experienced neurologist (AS) and neuroradiologist (MA). The following areas were segmented into two regions of interest (ROI) for each tumor: tumor core (including areas of necrosis, contrast-enhancing tumor or CET and non-contrast-enhancing tumor or nCET) and edema. The segmentations were performed in a step-wise manner, starting from CET, then the necrosis, the edema and, eventually, nCET. The criteria used to differentiate the last two regions were the following (36, 37): edema typically has a "finger-like appearance," extends concentrically around CET, is characterized by predominant WM involvement, relative "sparing" of subcortical GM nuclei, possible extension along the internal or external capsule and diffuse/generalized mass-effect. Moreover, edema tends to show a marked T2/FLAIR hyperintensity, often fading towards the periphery. Conversely, nCET is characterized by extension beyond CET margin with an eccentric appearance, involves GM and WM more equally (including subcortical GM nuclei) and determines a more localized mass effect, with associated anatomical distortion. Furthermore, T2/FLAIR hyperintensity is relatively milder, as compared with edema. CET, necrosis and nCET (if applicable) were labeled as "core." Lesions were subsequently normalized through the "virtual brain grafting" approach (38). This approach was chosen based on the size of brain tumors. Usually, brain lesions are normalized through a cost functional masking approach, but this might result in lower quality for large lesions (39) as in our case. The adopted approach generates a donor brain template using the native non-lesioned hemisphere and one hemisphere from a synthetic template brain image (38). For each subject, the donor brain was registered to the MNI space using the Advanced Normalization Tools (40). The transformation matrix was finally applied to the lesion masks using a *nearest neighbor* interpolation approach and resampled to a 1x1x1 mm space.

2.3. Tumor-networks overlap computation

For GMNs, Yeo's parcellation (21) was employed, including the following 17 subnetworks: central vision, peripheral vision, somatomotor A, somatomotor B, dorsal attention A, dorsal attention B, salient ventral attention A, salient ventral attention B, limbic A, limbic B, control network A, control network B, control network C, default mode network A, default mode network B, default mode network C and temporo-parietal networks. We also included deep GM nuclei (basal ganglia and thalami) and hippocampi from Harvard-Oxford subcortical atlas (41) as 18th and 19th parcels for subsequent analyses (i.e., the computation of GM overlap percentages). For WMNs, Peer's parcellation (23) was used, including the following 12

1 www.itksnap.org

networks: cingulum and associated tracts (N1), uncinate and middle temporal lobe tracts (N2), sensorimotor superficial WM system (N3), forceps minor system (N4), superior longitudinal fasciculus system (N5), visual superficial WM system (N6), inferior longitudinal fasciculus system (N7), inferior corticospinal tract (N8), posterior cerebellar tracts (N9), dorsal frontoparietal tracts (N10), deep frontal WM (N11), ventral frontoparietal tracts (N12). For each normalized lesion we computed the percentage of overlap with each network, independently for the WMNs and GMNs, as an expression of the ratio between the number of lesion voxels encompassing a specific network and the number of lesion voxels within a specific tissue, that is GM for GMNs and WM for WMNs. Hence, each overlap percentage represents the mask voxels overlapping a specific network, normalized for the mask voxels overlapping all networks of the same tissue (WM or GM). Such computation was performed both with the GBM core and the edema separately. Other overlap percentages were also computed: "not normalized" overlap percentages were calculated as the ratio between the number of lesion voxels encompassing a specific network and the total number of lesion voxels, for core and edema separately; "alternative" overlap percentages were calculated as the ratio between the number of lesion voxels encompassing a specific network and the total number of that network's voxels; these additional types of overlap percentages were also included in multiple linear regression models (see Supplementary Tables S3, S4).

For each tumor and tissue mask (core and edema) an in-house Python script was written for the following steps: (i) uploading nifti files conveying mask information as vector array; (ii) uploading Peer's WM and Yeo's GM nifti atlases in the same vector space (atlas vectors express specific values for each network); (iii) computing the sum of tumor-mask voxels encompassing each vector-network value; (iv) computing the overlap percentages defined above. All the procedure was run through an ASUS TUF Dash F15 machine (12th Gen Intel(R) Core (TM) i7-12650H 2.30 GHz) running on a Ubuntu 20.04.6 LTS (Focal Fossa) environment.

2.4. Statistical analyses

Three levels of analyses were performed: (i) descriptive statistics of network involvement through analysis of variance (ANOVA, not including subcortical GM nuclei) to assess differences between networks, independently for WMNs/GMNs and core/edema, as well as with post-hoc comparisons, (ii) assessment of the mutual relationships between the computed overlap percentages through Pearson's correlations and canonical correlation analysis, a machine learning approach used to measure the association between two sets of variables (performed according to our previous paper (42)); (iii) assessment of the relationships between OS and GBM distribution across functional networks, through linear and non-linear regression tests. For multiple linear regression, independent quantitative and ordinal variables were z-scored preliminarily. These analyses were performed between OS (dependent variable) and each of the following groups of overlap percentages (independent variables), separately: (1) overlap between the GBM core and GMNs, (2) between GBM edema and GMNs, (3) between the GBM core and WMNs and (4) between GBM edema and WMNs. Multiple linear regression analyses were also performed including the following regressors, either with and without the network overlap percentages: age, ECOG performance status, Stupp protocol, radicality of surgical resection (total, subtotal, biopsy), MGMT promoter methylation status, presurgical lesion (core or edema) volume. In addition to the aforementioned analyses, we also investigated relationships between network overlap percentages and the radicality of surgery, through Pearson's correlation tests. The significance level (alpha) was set to 0.05 and Bonferroni corrections were applied to multiple comparisons and correlations.

Moreover, we performed a non-linear regression analysis by means of the Boruta algorithm, designed to find a subset of features that are relevant to a given classification/regression task (43). The core algorithm behind it is random forests, a methodology able to find non-linear relationships between the dependent and independent variables.

3. Results

A total of 99 patients were enrolled, 70 were males, the median age was 62 years (interquartile range = 17 years); the median OS was 12.7 months (interquartile range = 15.4 months). No statistically significant differences were found between overlap percentages among age groups (Bonferroni-corrected p-values >0.05). Out of 99 patients, 85 had a pre-surgical 3 T MRI study, while 14 had a 1.5 T MRI scan. 86 patients had 3D pre-, post-contrast T1 and FLAIR sequences, while the remaining 13 had at least one non-3D among these sequences. 92 out of 99 patients had detectable edema. Mean GBM core volume was 42.8 cm^3 (standard deviation = 29.2 cm^3), while mean GBM edema volume was 52.6 cm^3 (standard deviation 43.4 cm^3). Table 1 summarizes clinical, surgical and prognostic variables for all patients included. 6 patients had missing data concerning the type of surgical operation that lead to GBM diagnosis and, among these, 5 had missing data regarding MGMT promoter methylation status, thus were not considered for survival analyses that included clinical-prognostic factors as regressors. The frequency maps of the distribution of the core and the edema are shown in Figure 1.

3.1. Overlap percentages: descriptive statistics and frequencies

The GBM core mostly overlapped with the following GMNs: somatomotor B (mean overlap percentage = 11.3%), salient ventral attention A (10.6%), default mode network B (8.6%), salient ventral attention B (7.4%), control network A (7.1%), limbic A (5.1%). Regarding WMNs, the most involved ones were: N12 (ventral frontoparietal tracts, 16.9%), N5 (superior longitudinal fasciculus system, 13.4%), N11 (deep frontal WM, 12.1%), N7 (inferior longitudinal fasciculus system, 11.4%). Concerning edema, the most overlapped GMNs were: somatomotor B (14.2%), salient ventral attention A (9.8%), control network A (9.6%), default mode network B (7.6%), default mode network A (6.7%). As for WMNs: N5 (superior longitudinal fasciculus system, 24%), N12 (ventral frontoparietal tracts, 14.8%), N11 (deep frontal WM 12%). Overlaps with the aforementioned networks altogether accounted for 50% of overlap within each of the four overlap categories. Descriptive statistics for computed overlap percentages are shown in Tables 2, 3, while mean overlap percentages are represented graphically in Figures 2, 3.

10.3389/fneur.2023.1175576

TABLE 1 Summary of patient characteristics and clinical/surgical variables.

Patient number	Age	Gender	Overall survival (months)	Radicality of resection	Stupp protocol	MGMT promoter methylation	ECOG performance status	Core volume (cm^3)	Edema volume (cm^3)
1	67	Male	29.74	PR	Yes	Yes	1	38.52	14.94
2	59	Male	12.37	PR	Yes	No	0	64.04	54.12
3	50	Male	10.03	PR	Yes	Yes	1	123.05	12.63
4	62	Male	10.95	PR	Yes	Yes	1	69.99	41.14
5	74	Male	3.65	PR	Yes	Yes	0	22.46	72.79
6	67	Male	4.21	PR	Yes	No	1	30.61	16.83
7	41	Male	8.98	GTR	Yes	No	0	22.07	45.92
8	77	Male	16.35	PR	Yes	Yes	2	74.36	74.75
9	47	Male	18.42	GTR	Yes	No	1	66.28	40.46
10	62	Male	10.16	GTR	Yes	No	1	11.69	0.00
11	61	Male	54.47	GTR	Yes	Yes	0	17.25	1.77
12	54	Male	19.18	GTR	Yes	No	1	57.16	0.00
13	69	Male	9.97	PR	Yes	No	1	54.36	4.88
14	61	Male	19.51	GTR	Yes	No	1	53.36	17.18
15	71	Male	26.71	PR	Yes	Yes	1	60.96	18.92
16	68	Female	1.81	PR	Yes	No	3	62.69	24.04
17	45	Male	4.8	PR	Yes	No	1	12.95	63.74
18	75	Male	2.63	B	No	No	3	34.12	80.16
19	64	Male	21.48	PR	Yes	Yes	1	35.04	10.97
20	65	Male	10.95	PR	Yes	No	2	45.30	90.41
21	71	Male	7.37	GTR	Yes	Yes	1	23.61	109.65
22	37	Male	16.97	PR	Yes	No	0	32.65	147.66
23	44	Female	3.55	PR	Yes	No	2	140.88	26.57
24	50	Male	30.1	PR	Yes	No	1	115.76	30.71
25	67	Male	2.2	PR	Yes	No	2	24.80	0.00
26	45	Male	47.63	GTR	Yes	Yes	0	9.75	0.00
27	54	Male	2.27	PR	No	No	3	40.24	83.20
28	41	Male	14.74	PR	Yes	Yes	0	49.89	40.21
29	76	Male	8.88	PR	Yes	Yes	2	27.50	92.32
30	60	Female	2.34	PR	Yes	Yes	2	68.30	92.09
31	75	Female	2.96	PR	Yes	No	2	82.85	139.36
32	67	Female	29.64	PR	Yes	No	0	33.12	62.50
33	65	Male	7.89	PR	Yes	Yes	2	82.75	74.66
34	69	Male	32.7	PR	Yes	Yes	2	53.33	5.99
35	65	Male	21.78	PR	Yes	No	0	50.12	96.74
36	54	Male	26.38	PR	No	Yes	0	11.08	67.66
37	76	Female	2.24	PR	Yes	Yes	3	62.96	89.49
38	53	Female	12.14	PR	Yes	Yes	0	17.48	57.65
39	72	Female	4.61	PR	Yes	Yes	3	101.71	35.15
40	75	Male	20.69	PR	Yes	Yes	1	34.14	24.00
41	73	Male	3.98	PR	Yes	No	3	7.66	74.58
42	71	Female	18.55	PR	Yes	Yes	1	38.93	35.35
43	68	Male	2.73	PR	No	No	1	53.32	9.71

(Continued)

10.3389/fneur.2023.1175576

TABLE 1 (Continued)

Patient number	Age	Gender	Overall survival (months)	Radicality of resection	Stupp protocol	MGMT promoter methylation	ECOG performance status	Core volume (cm^3)	Edema volume (cm^3)
44	64	Female	2.73	PR	No	Yes	3	10.32	7.67
45	79	Female	6.97	PR	Yes	No	2	26.50	46.87
46	70	Female	6.35	PR	Yes	No	2	16.23	89.81
47	63	Male	7.5	PR	Yes	No	1	21.86	62.65
48	61	Male	10.59	PR	Yes	No	0	88.58	60.82
49	57	Male	13.88	PR	Yes	No	0	31.00	19.34
50	67	Female	14.41	PR	Yes	No	0	22.91	132.54
51	67	Male	0.99	PR	Yes	Yes	2	92.60	112.73
52	67	Female	25.36	GTR	Yes	Yes	0	73.79	121.33
53	76	Male	3.72	B	No	Yes	2	46.32	19.87
54	45	Male	26.45	PR	Yes	No	0	5.54	17.79
55	70	Male	16.18	PR	Yes	No	1	59.95	99.98
56	56	Male	23.88	PR	Yes	Yes	0	22.27	10.18
57	73	Female	5.76	PR	No	Yes	2	76.76	7.81
58	56	Male	15.1	PR	Yes	No	1	44.63	115.24
59	73	Female	20.76	PR	Yes	Yes	2	84.88	15.82
60	68	Female	10.53	PR	Yes	No	0	11.89	14.22
61	54	Male	13.59	GTR	Yes	No	0	42.37	211.67
62	69	Female	37.24	GTR	Yes	Yes	1	15.29	37.05
63	68	Female	17.93	PR	Yes	No	1	25.22	107.82
64	70	Male	12	PR	Yes	Yes	1	29.16	25.96
65	64	Female	4.08	GTR	Yes	No	3	29.36	17.02
66	59	Male	15.66	PR	Yes	Yes	1	57.72	135.79
67	46	Male	31.61	PR	Yes	No	1	28.84	107.97
68	47	Male	2.99					13.94	2.13
69	67	Male	10.13	GTR	Yes	No	2	17.77	86.51
70	77	Female	2.99					16.66	0.00
71	81	Female	9.97	GTR	Yes	Yes	3	9.02	34.64
72	48	Male	14.97	PR	Yes	No	0	32.05	144.50
73	73	Female	1.68				4	85.39	50.88
74	45	Male	20.1	PR	Yes	No	2	18.44	35.37
75	70	Male	5.99	PR	Yes	Yes	1	16.33	47.73
76	53	Male	23.29	PR	Yes	Yes	1	15.00	52.24
77	58	Male	23.62	GTR	Yes	Yes	0	40.79	1.29
78	72	Male	21.19		Yes	No	2	41.74	38.76
79	71	Male	10.56	GTR	Yes	Yes	1	97.37	36.70
80	44	Male	3.72					60.30	0.00
81	65	Male	14.14	PR	Yes	No	1	23.56	11.66
82	78	Male	10.36	PR	Yes	No	1	31.48	59.71
83	71	Male	5.82				1	25.50	6.55
84	54	Male	13.06	PR	Yes	No	1	15.74	3.18
85	70	Male	6.35	PR	Yes	Yes	0	18.04	71.39

(Continued)

TABLE 1 (Continued)

Patient number	Age	Gender	Overall survival (months)	Radicality of resection	Stupp protocol	MGMT promoter methylation	ECOG performance status	Core volume (cm^3)	Edema volume (cm^3)
86	39	Male	22.4	GTR	Yes	No	1	103.34	39.18
87	71	Male	9.51	PR	Yes	No	0	48.60	67.92
88	74	Female	16.25	PR	Yes	Yes	1	100.66	94.33
89	65	Male	21.88	GTR	Yes	No	0	14.60	0.00
90	60	Female	23.45	GTR	Yes	No	0	22.01	50.52
91	64	Male	4.21	PR	Yes	No	2	49.57	50.95
92	68	Male	4.14	PR	Yes	Yes	1	0.68	44.18
93	20	Female	14.67	PR	No	No	0	27.00	47.81
94	57	Male	18.82	GTR	Yes	No	0	24.24	110.77
95	68	Male	24.31	PR	Yes	Yes	1	32.27	82.37
96	44	Male	13.59	PR	Yes	No	0	17.12	47.98
97	64	Female	21.71	PR	Yes	Yes	1	31.39	108.83
98	47	Female	25.26	GTR	Yes	Yes	1	30.28	100.25
99	66	Female	40.49	GTR	Yes	Yes	0	70.30	2.08

GTR, gross total resection; PR, partial resection; B, biopsy; blank cells represent missing data.

3.2. Correlation analyses between overlap percentages

We found several significant positive correlations between overlap percentages, some of which regarded functionally inter-related GMNs and WMNs (23): for both core and edema, overlap with N2 (uncinate and middle-temporal lobe tracts) positively correlated with default mode network B overlap (core: $R=0.62$, $p<0.0001$; edema; $R=0.58$, $p<0.0001$), the same was found between N6 (visual superficial WM system), central (core: $R=0.9$, $p<0.0001$; edema: $R=0.95$, $p<0.0001$) and peripheral vision networks (core: $R=0.55$, $p<0.0001$; edema: $R=0.6$, $p<0.0001$), as well as between N3 (sensorimotor superficial WM system) and somatomotor A network (core: $R=0.71$, $p<0.0001$; edema: $R=0.8$, $p<0.0001$). Only for core, overlap with N1 positively correlated with control network C ($R=0.49$, $p<0.0001$) and default mode network A ($R=0.37$, $p=0.0001$). Only for edema, overlap with N12 positively correlated with somatomotor B ($R=0.71$, $p<0.0001$). The complete results of correlation analyses are shown in Supplementary Figures S1, S2 (only results that survived Bonferroni correction are shown), Concerning correlations with the radicality of surgery, we found that overlaps between the GBM core and somatomotor-B ($R=0.23$, $p=0.03$), between the GBM core and DMN-B ($R=0.24$, $p=0.02$) and between the edema and somatomotor-B ($R=0.24$, $p=0.02$) were associated to a wider resection, however, these correlations did not survive Bonferroni correction for multiple comparisons (the complete set of results are shown in Supplementary Table S4).

3.3. Canonical correlation analysis

Concerning the GBM core, 5 modes were identified as statistically significant compared to a random distribution ($n=1000$; $p<0.05$; Figure 4). The first mode highlighted a relationship mainly involving visual superficial WM system (N6) and inferior longitudinal fasciculus system (N7) from the WM side, and the central vision network from the GM matrix; the second mode was mainly related to sensorimotor superficial WM system (N3), as well as the somatomotor A and B GMNs; mode 3 was related to uncinate and middle temporal lobe tracts (N2), inferior longitudinal fasciculus system (N7) and limbic A network; mode 4 to N2 and default-mode network B; mode 5 to N3, inferior corticospinal tract (N8), somatomotor A and subcortical GM nuclei. Regarding negative loadings: deep frontal WM (N11) was negatively related to modes 1, 3 and 4, while ventral frontoparietal tracts (N12) was to mode 4 and 5. Moreover, mode 4 was negatively related to control network A and subcortical GM nuclei, whereas mode 5 was to somatomotor B, default-mode network B and temporo-parietal network.

Lastly, 5 modes were identified for network overlaps with the GBM edema, in which the number of positive and negative relationships decrease from mode 1 to 5 (Figure 5).

3.4. ANOVA

Four ANOVA tests showed significant differences in the degree of overlap between GBM lesions and different brain networks. In particular, this was true for overlaps between the GBM core and GMNs ($F=7.8$, $p<0.001$), the GBM edema and GMNs ($F=17.5$, $p<0.001$), the GBM core and WMNs ($F=10.9$, $p<0.001$), as well as between the GBM edema and WMNs ($F=39.3$, $p<0.001$). Significant Bonferroni-corrected post-hoc comparisons are shown in Supplementary Tables S1, S2.

10.3389/fneur.2023.1175576

TABLE 2 Descriptive statistics of overlap percentages between the GBM core and functional brain networks.

Functional networks		CORE		
		Involvement frequency (threshold 0.5%)*	Mean	Standard deviation
Gray matter networks	Central Vision	16.16%	2.9%	10.5%
	Peripheral Vision	18.18%	2.8%	8.9%
	Somatomotor A	22.22%	4.3%	15.0%
	Somatomotor B	54.55%	11.3%	20.3%
	Dorsal Attention A	26.26%	4.0%	9.5%
	Dorsal Attention B	32.32%	3.3%	7.4%
	Salient Ventral Attention A	78.79%	10.6%	11.4%
	Salient Ventral Attention B	57.58%	7.5%	10.5%
	Limbic A	30.30%	5.1%	10.9%
	Limbic B	15.15%	1.5%	6.1%
	Control network A	54.55%	7.2%	11.2%
	Control network B	46.46%	4.2%	6.8%
	Control network C	11.11%	0.9%	3.2%
	Default Mode Network A	47.47%	5.4%	11.2%
	Default Mode Network B	68.69%	8.7%	13.9%
	Default Mode Network C	29.29%	2.2%	5.5%
	Temporo-Parietal	49.49%	4.5%	9.4%
	Subcortical gray matter (basal ganglia and thalami)	55.56%	11.2%	18.6%
	Hippocampus	35.35%	2.5%	5.3%
White matter networks	N1 (Cingulum and associated tracts)	44.44%	4.7%	8.9%
	N2 (Uncinate and middle temporal lobe tracts)	52.53%	8.0%	13.3%
	N3 (Sensorimotor superficial white-matter system)	40.40%	8.9%	19.2%
	N4 (Forceps minor system)	32.32%	5.0%	10.7%
	N5 (Superior longitudinal fasciculus system)	83.84%	13.4%	16.0%
	N6 (Visual superficial white-matter system)	40.40%	5.3%	13.2%
	N7 (Inferior longitudinal fasciculus system)	59.60%	11.4%	12.9%
	N8 (Inferior corticospinal Tract)	43.43%	8.0%	14.6%
	N9 (Posterior cerebellar tracts)	18.18%	0.2%	0.6%
	N10 (Dorsal frontoparietal tracts)	46.46%	5.8%	9.6%
	N11 (Deep frontal white matter)	46.46%	12.2%	18.8%
	N12 (Ventral frontoparietal tracts)	82.83%	16.9%	16.6%

*overlap percentages < 0.5% were not counted.

3.5. Comparison between the GBM core and edema overlap percentages

The mean percentage overlap with the hippocampi was significantly lower for the edema region (0.4%) as compared with the lesion core (2.5%) ($p < 0.001$). Concerning WMNs, N5 (superior longitudinal fasciculus system) and N10 (dorsal fronto-parietal tracts) overlapped significantly more with the edema region (24 and 10.7%, respectively) than the core region (13.4 and 5.8%, respectively) (both p-values<0.001). In contrast, N8 and N9 overlapped more with the core (8 and 0.2%, respectively) than with the edema region (2.5 and 0.03%, respectively) (p-values = 0.004 and 0.001, respectively). Other comparisons did not reach significance after Bonferroni correction for multiple comparisons.

3.6. Association between OS and GBM distribution across functional networks

Multiple linear regression models are summarized in Table 4. The models only including clinical-prognostic variables and core size were statistically significant with an explained variance (adjusted R^2) of 0.34 ($F = 8.7$, $p < 0.001$); significant regressors were ECOG with $\beta = -4$ and $p < 0.001$, radicality of surgery with $\beta = 2.5$ and $p = 0.01$, MGMT status

TABLE 3 Descriptive statistics of overlap percentages between the GBM edema and functional brain networks.

Functional networks		EDEMA		
		Involvement frequency (threshold 0.5%)	Mean	Standard deviation %
Gray matter networks	Central Vision	22.83%	2.92%	8.46%
	Peripheral Vision	25.00%	2.16%	7.66%
	Somatomotor A	50.00%	5.33%	10.12%
	Somatomotor B	80.43%	14.21%	14.53%
	Dorsal Attention A	54.35%	4.66%	7.57%
	Dorsal Attention B	68.48%	6.30%	7.94%
	Salient Ventral Attention A	89.13%	9.83%	8.59%
	Salient Ventral Attention B	58.70%	6.41%	8.54%
	Limbic A	27.17%	2.19%	5.54%
	Limbic B	17.39%	1.06%	3.13%
	Control network A	83.70%	9.59%	9.08%
	Control network B	71.74%	6.48%	8.90%
	Control network C	19.57%	0.86%	2.44%
	Default Mode Network A	70.65%	6.73%	8.34%
	Default Mode Network B	76.09%	7.62%	10.07%
	Default Mode Network C	35.87%	1.02%	1.88%
	Temporo-Parietal	52.17%	5.47%	9.20%
	Subcortical gray matter (basal ganglia and thalami)	65.22%	6.72%	12.93%
	Hippocampus	18.48%	0.43%	1.14%
White matter networks	N1 (Cingulum and associated tracts)	73.91%	3.92%	3.84%
	N2 (Uncinate and middle temporal lobe tracts)	53.26%	4.90%	8.82%
	N3 (Sensorimotor superficial white-matter system)	77.17%	7.96%	9.56%
	N4 (Forceps minor system)	39.13%	4.88%	8.47%
	N5 (Superior longitudinal fasciculus system)	94.57%	23.96%	13.24%
	N6 (Visual superficial white-matter system)	43.48%	4.09%	10.07%
	N7 (Inferior longitudinal fasciculus system)	65.22%	10.34%	11.71%
	N8 (Inferior corticospinal Tract)	38.04%	2.47%	6.63%
	N9 (Posterior cerebellar tracts)	0%	0.03%	0.07%
	N10 (Dorsal frontoparietal tracts)	81.52%	10.67%	8.61%
	N11 (Deep frontal white matter)	67.39%	11.98%	14.78%
	N12 (Ventral frontoparietal tracts)	93.48%	14.80%	14.28%

Only the 92 patients with edema were included in these calculations.
*overlap percentages < 0.5% were not counted.

with $\beta = 5.8$ and $p = 0.003$. Similar results were found for the model including edema size with an explained variance (adjusted R^2) of 0.31 ($F = 7.5$, $p < 0.001$), significant regressors were ECOG with $\beta = -4$ and $p < 0.001$, radicality of surgery with $\beta = 2.2$ and $p = 0.02$, MGMT status with $\beta = 4.2$ and $p = 0.029$.

After adding network overlap percentages to the clinical variables as regressors, we did not obtain an increase in explained OS variance. In particular, when we included the core-GMNs overlap percentages, adjusted R^2 decreased to 0.20 ($F = 2$, $p = 0.01$), significant regressors were ECOG with $\beta = -3.9$ and $p = 0.006$, radicality of surgery with $\beta = 2.5$ and $p = 0.04$, MGMT status with $\beta = 7.2$ and $p = 0.005$. Similarly, when we included edema-GMNs overlap percentages as regressors, the explained variance (adjusted R^2) further decreased to 0.19 ($F = 1.8$, $p = 0.025$), significant regressors were ECOG with $\beta = -4.2$ and $p = 0.002$, while radicality of surgery and MGMT status' value of ps were 0.069 and 0.064, respectively. When core-WMN overlap percentages were added as regressors, the explained variance (adjusted R^2) was 0.32 ($F = 3.6$, $p < 0.001$), significant regressors were ECOG with $\beta = -3.7$ and $p = 0.004$, MGMT status with $\beta = 6.3$ and $p = 0.003$, N12 with $\beta = 3.6$ and $p = 0.03$, while the value of p for radicality of surgery was 0.063. Finally, when we included edema-WMN overlap percentages as regressors, the adjusted R^2 was 0.33 ($F = 3.5$, $p < 0.001$), significant regressors were ECOG with $\beta = -3.4$ and $p = 0.004$, radicality of surgery with $\beta = 2.2$ and $p = 0.03$, while the value of p for MGMT status was 0.056.

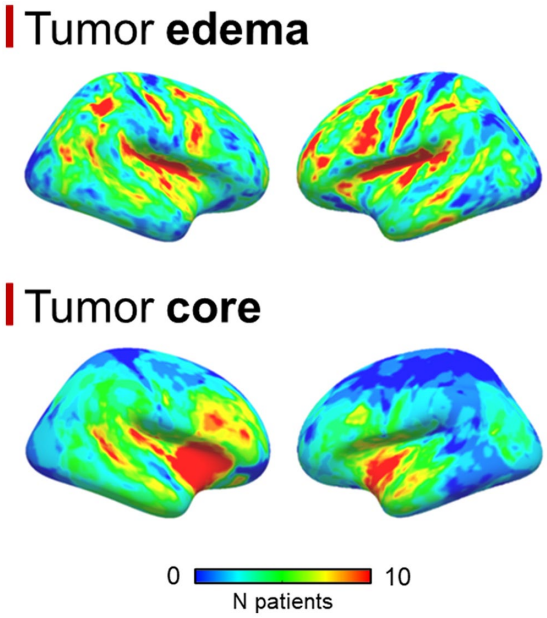

FIGURE 1
Surface space-projected distribution frequency maps for the GBM core and the edema.

Models only including network overlap percentages as regressors, as well as regression models including "not normalized" and "alternative" overlap percentages (see "Tumor-networks overlap computation" paragraph in the *Methods* section), are shown in Supplementary Table S3.

According to the non-linear approach (i.e., Boruta analysis), the most important features for OS were ECOG and overlap between tumor core with N12. When overlaps with edema were considered, ECOG was the only relevant feature for OS (Figure 6).

4. Discussion

4.1. Main results

Our data shows that GBMs are distributed differently across GMNs and WMNs: the GBM preferentially locates in associative networks, confirming the results that Mandal et al. obtained in a different GM networks parcellation (13). In particular, we found five main patterns of GBM core distribution across functional networks. Furthermore, although we found similar values of mean edema-network overlap percentages, edema does not seem to have a well-defined network-based anatomical distribution. The second main result is that OS was not clearly associated with the distribution of

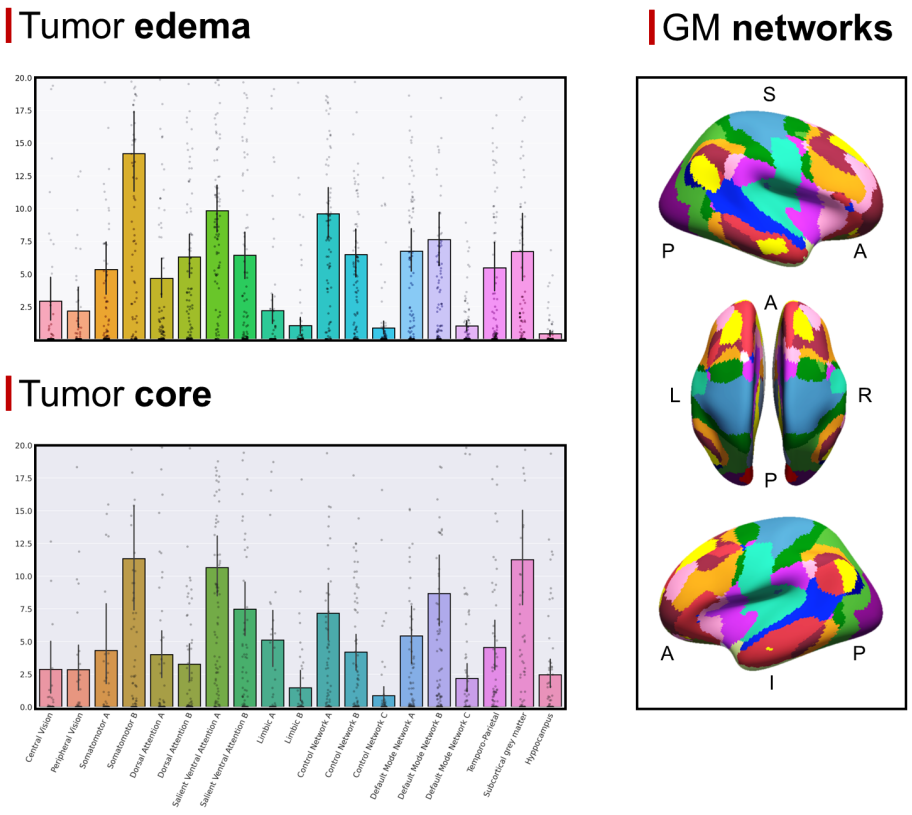

FIGURE 2
(Top left section) Mean overlap percentages between the GBM edema and Yeo's GMNs, plus subcortical GM nuclei and hippocampi. **(Bottom left section)** Mean overlap percentages between the GBM core and Yeo's GMNs, plus subcortical GM nuclei and hippocampi. **(Right section)** Yeo's GMN atlas is depicted with colors representing different networks (subcortical gray matter nuclei and hippocampi are not shown).

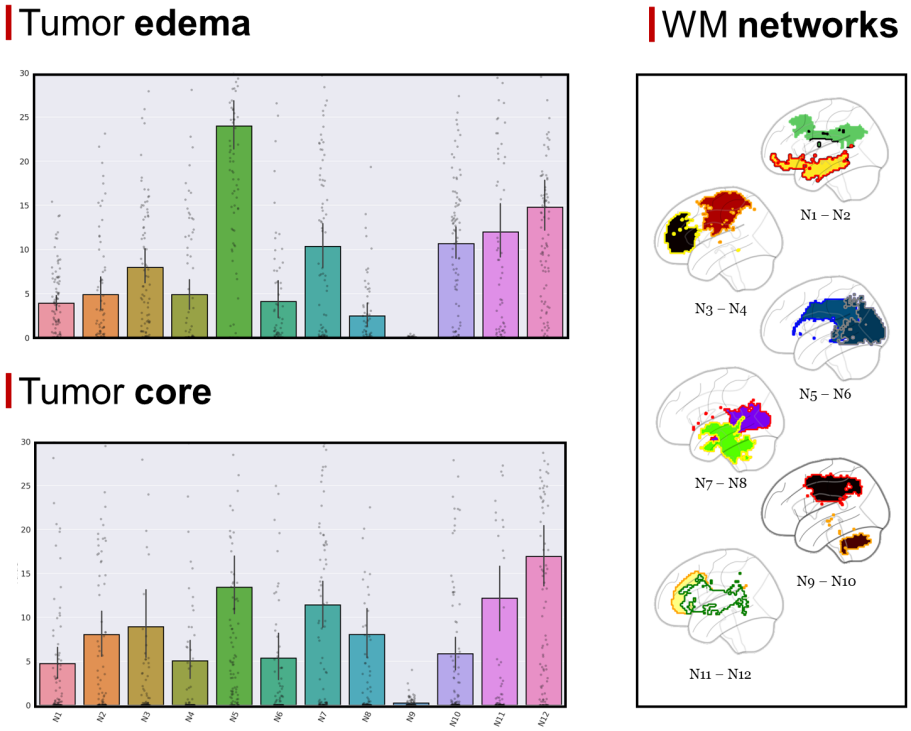

FIGURE 3
(Top left section) Mean overlap percentages between the GBM edema and Peer's 12 WMNs. **(Bottom left section)** Mean overlap percentages between GBM core and Peer's 12 WMNs. **(Right section)** Peer's 12 WMNs are shown in sagittal view, with colors representing different networks: green for N1 (Cingulum and associated tracts), yellow with red border for N2 (Uncinate and middle temporal lobe tracts), red with orange border for N3 (Sensorimotor superficial white-matter system), black with yellow border for N4 (Forceps minor system), blue with dark blue border for N5 (superior longitudinal fasciculus system), blue with gray border for N6 (Visual superficial white-matter system), violet with red border for N7 (Inferior longitudinal fasciculus system), green with yellow border for N8 (Inferior corticospinal Tract), brown with orange border for N9 (Posterior cerebellar tracts), black with red border for N10 (Dorsal frontoparietal tracts), yellow with orange border for N11 (Deep frontal white matter), white with green border for N12 (Ventral frontoparietal tracts).

GBM across functional brain networks. In contrast to previous similar studies, we also considered the functional network anatomy of WM, hence highlighting its potential importance, as GBM is predominantly a WM disease.

4.2. GBM distribution across functional brain networks

Concerning GM and core lesions, about 14% of the overlap is with subcortical nuclei (thalami and basal ganglia); about 50% of the overlap is with a small number of GMNs – six networks – of which five are associative networks. The only sensory-motor network is the somatomotor B network, which spans the ventral part of the posterior frontal and anterior parietal lobes. The other five include fronto-parietal networks both on the lateral and medial surfaces of the brain. Naturally, the edema region involves more overlap (~93%) with GMNs compared to subcortical GM nuclei, but also in this case around 50% of the overlap occurs with only five networks, of which four are associative in nature.

Regarding WMNs, about half of the region of the GBM core or edema overlaps with association WMNs connecting long-range fronto-temporo-parietal regions either ventrally (ventral frontoparietal tracts, deep frontal WM) or dorsally (superior longitudinal fasciculus system). More focal short-range tracts like the sensory-motor, dorsal or uncinate tracts overlapped less with core or edema regions. Another interesting finding was the lower involvement of the hippocampi by the edema region, compared with the core. This is explained since edema typically distributes within WM, with relative sparing of GM (36).

Remarkably, canonical correlation analysis allowed us to identify five main patterns in which GBM core distributes across WMNs and GMNs. As far as the GBM core is concerned, the first pattern mainly implies visual GMNs and WMNs, the second somatomotor GMNs and WMNs, while the third one mainly regarded temporal networks (uncinate and middle temporal lobe tracts/N2, inferior longitudinal fasciculus system/N7 and limbic network). The fourth mode concerns uncinate and middle temporal lobe tracts (N2) and default-mode network B; the fifth pattern, instead, reflects the course of the whole corticospinal tract, from the cortex, passing through the internal capsule and adjacent basal ganglia, to the inferior portion of the pathway. Interestingly, such pattern only regards the dorsal part of the somatomotor network, while it is negatively correlated with the ventral portion. These findings might indicate that the potential migration of GBM cells along the corticospinal tract preferentially occurs from/towards dorsal regions, for reasons yet to be clarified. Frontoparietal or deep frontal WM networks were negatively associated with these patterns, except for the second one. In particular, our data suggest that when GBMs have certain distribution modes, they tend not to affect specific networks: deep frontal WM (patterns

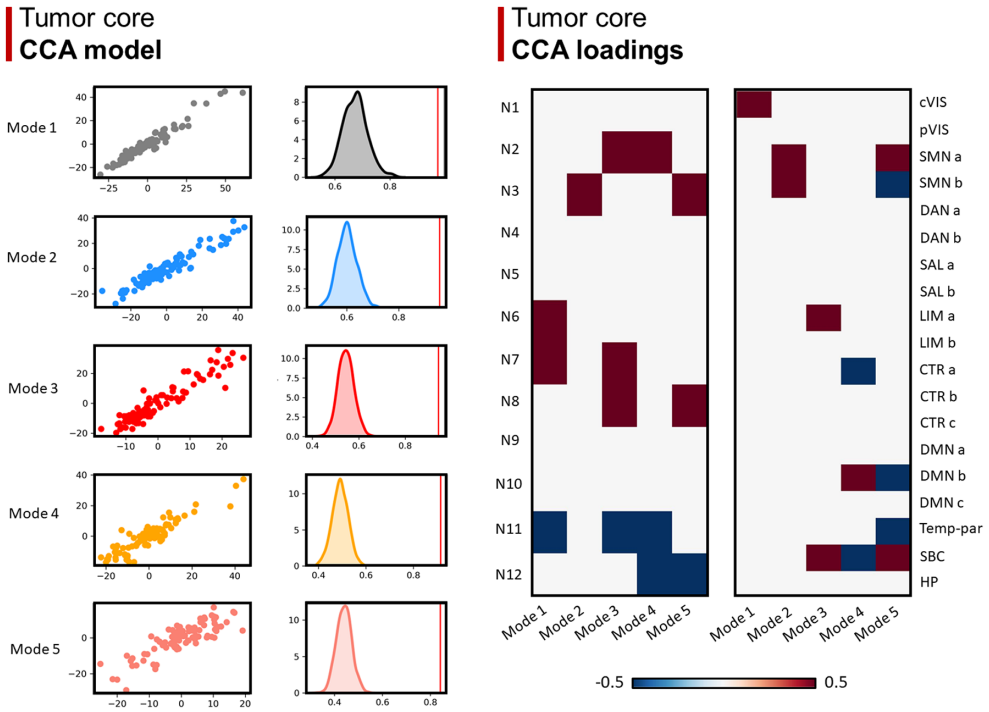

FIGURE 4
Canonical correlation analysis (CCA) between WMN and GMN overlap percentages with GBM core. **Left panel (CCA model)**: 5 modes were identified (r>0.8; p<0.001), surviving statistical significance after a permutation (n=1,000) comparison approach (p<0.0001). **Right panel (CCA loadings)**: patterns (or modes) of WMN and GMN overlap with the GBM core are shown for each mode. N1 to N12 represent the white matter functional networks (WMNs); cVIS: central vision; pVIS: peripheral vision; SMN a: somatomotor A; SMN b: somatomotor B; DAN a: dorsal attention A; DAN b: dorsal attention B; SAL a: salient ventral attention A; SAL b: salient ventral attention B; LIM a: limbic A; LIM b: limbic B; CTR a: control A; CTR b: control B; CTR C: control C; DMN a: default-mode A; DMN b: default-mode B; DMN c: default-mode C; Temp-par: temporo-parietal; SBC: subcortical gray matter nuclei; HP: hippocampus.

1, 3, 4), ventral frontoparietal tracts (patterns 4, 5), control network A (pattern 4), subcortical GM nuclei (pattern 4), somatomotor B (pattern 4), default-mode network B (pattern 5) or temporo-parietal network (pattern 5).

Concerning edema, the five identified modes were less classifiable, indicating a more diffuse involvement of networks, often extending far beyond the anatomical location of the GBM core. The great contrast in the number of loadings between different modes perhaps indicates the higher interindividual variability of edema extension, compared to the core: while GBM distribution seems to follow an anatomical (network-based) pattern, the edema follows an anatomical (not network-based) path involving the WM structure across many networks. Overall, the differences between the results found for the GBM edema and core, discussed above, suggest that the anatomical location of the latter one can be more effectively subdivided into a discrete number of categories or "patterns," based on both GMNs and WMNs. On the contrary, the distribution of edema is characterized by a higher extent of variability and unpredictability.

4.3. Interrelated GMNs and WMNs are co-lesioned by GBM

It is well-known that glioma cells form synapses with neurons, in which a signaling based upon glutamate and other molecules generates self-amplifying auto/paracrine loops that are thought to contribute to several neoplastic processes including tumor growth and migration (44–48). Such molecules are neuron activity-dependent, thus recent studies have postulated a possible link between the aforementioned phenomena and neuronal activation itself (49–53). Moreover, Mandal et al. (25) used independent component analysis to decompose low- and high-grade glioma lesions into 3 principal areas of co-lesioned brain regions ("lesion covariance networks" or "LCNs"), which showed anatomical correspondence to different structural WM tracts and functional connectivity networks (obtained from Miller et al. (24)), interpreted as the tendency of glioma cells to migrate along neuronal networks that support glioma cell proliferation. In our study, we too obtained some evidence furtherly indicating a possible link between GBM localization or spreading and brain functional connectivity: correlation analyses showed that some functionally and anatomically inter-related GMNs and WMNs tended to be co-lesioned by GBM. In particular, Peer et al. (23) showed that N2 (uncinate and middle-temporal lobe tracts) has a high degree of functional correlation with the default mode network and, in our work, their involvements by GBM positively correlate one with another. Similarly, overlap with peripheral and central vision networks positively correlates with the associated WMN N6 (visual superficial WM system), as did somatomotor network A with N3 (sensorimotor superficial WM system). Such results practically mirror the "modes" of the GBM core distributions, identified through canonical correlation analysis. Additional remarkable results, coherent with Peer's aforementioned inter-network correlations, were found between control network and N1 (cingulum and associated

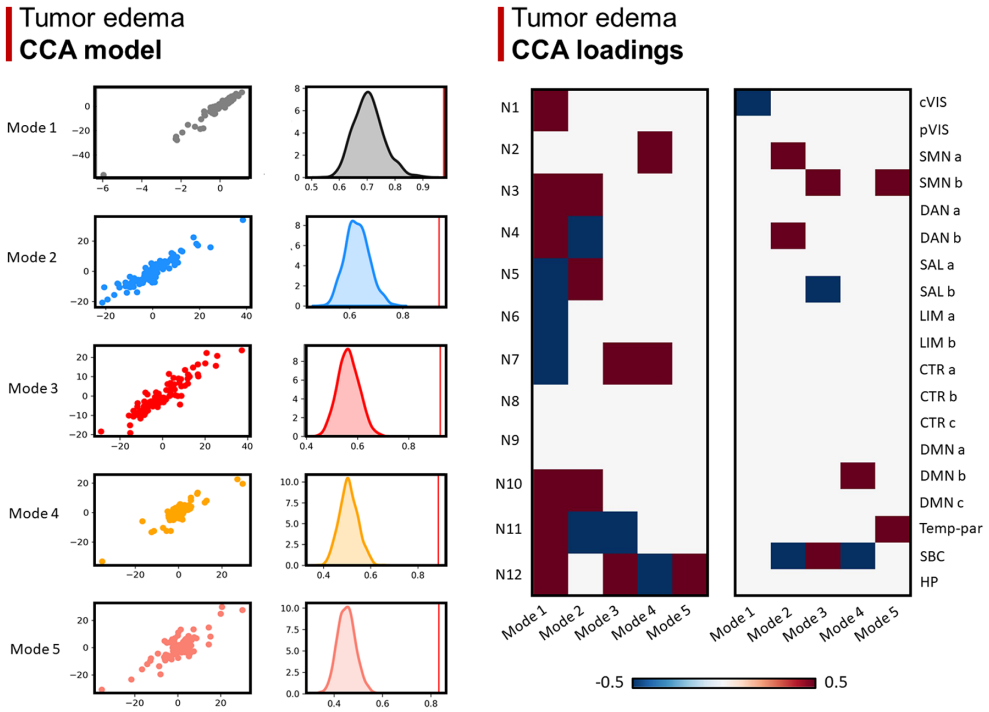

FIGURE 5
Canonical correlation analysis (CCA) between WMN and GMN overlap percentages with GBM edema. **Left panel (CCA model)**: 5 modes were identified (r>0.8; p<0.001), surviving statistical significance after a permutation (n=1,000) comparison approach (p<0.0001). **Right panel (CCA loadings)**: patterns (or modes) of WMN and GMN overlap with the GBM edema are shown for each mode. N1 to N12 represent the white matter functional networks (WMNs); cVIS: central vision; pVIS: peripheral vision; SMN a: somatomotor A; SMN b: somatomotor B; DAN a: dorsal attention A; DAN b: dorsal attention B; SAL a: salient ventral attention A; SAL b: salient ventral attention B; LIM a: limbic A; LIM b: limbic B; CTR a: control A; CTR b: control B; CTR C: control C; DMN a: default-mode A; DMN b: default-mode B; DMN c: default-mode C; Temp-par: temporo-parietal; SBC: subcortical gray matter nuclei; HP: hippocampus.

tracts), default mode network and N1, as well as between somatomotor B and N12 (ventral frontoparietal tracts), although the latter association was only found within perilesional edema. In Peer's original article, among the superficial WMNs, N1, N2 and N12 strongly correlated with widely distributed GMNs (DMN, dorsal attention, ventral attention and frontoparietal control networks), suggesting a role for these networks in allowing communication between distant regions of GMNs. Conversely, other superficial networks mostly showed a high correlation with the overlying GMNs, possibly indicating the presence of short-range connections between them. Therefore, while the co-localisation of GBMs in N3 and somatomotor or N6 and visual networks might be predominantly explained by the shared topology of the networks, the joint involvement of N1 or N2 and the aforementioned associative GMNs might imply a contribution of their intrinsic activity. Hence, in line with the aforementioned studies and our results, we too hypothesize that the preferential distribution of GBM across certain functional networks might not merely reflect their most frequent anatomical locations, but may be, at least in part, influenced by the activity of brain functional networks themselves.

4.4. OS and GBM distribution across functional brain networks

According to a large amount of previous literature, we found that OS was predicted by MGMT methylation status, Surgery extension and ECOG performance status. The level of explained variance ranged from 31 to 34%. When we added GMN overlap percentages the variance explained (adjusted R^2) was lower (around 20%), suggesting that this anatomical information does not help in predicting OS, while it was similar to the models only including clinical-prognostic variables when we added WMN overlap percentages. In line with linear regression results, Boruta regression showed that none of the GMN overlap percentages are important features for OS regression, while the extent to which the GBM core overlaps ventral frontoparietal tracts (N12) seems to have some role in predicting a longer survival. Around half of this network's volume is constituted by components of well-defined anatomical tracts, in particular the anterior thalamic radiation, the superior longitudinal fasciculus and, to a lesser extent, the corticospinal tract. From a functional point of view, N12 is highly correlated to somatomotor, ventral and dorsal attention networks.

Overall, however, we did not find any robust association between OS and GBM distribution across functional brain networks. Also Mandal et al.'s (25) work was coherent with our findings, as the differences in OS that they found between LCNs were mainly driven by molecular determinants, rather than glioma distribution, and lost significance when distinguishing GBM from low-grade gliomas. In contrast, previously mentioned studies found that fMRI-derived data, in particular functional connectivity between intra-tumoral and extra-tumoral regions,

TABLE 4 Multiple linear regression models (dependent variable is overall survival/OS for all models).

CORE					EDEMA				
Model: Independent variables or regressors: GBM core volume; age; ECOG performance status; radicality of surgical resection (biopsy, partial resection, gross total resection); MGMT promoter methylation status; Stupp protocol.					Model: Independent variables or regressors: GBM edema volume; age; ECOG PS; radicality of surgical resection (biopsy, partial resection, gross total resection); MGMT promoter methylation status; Stupp protocol.				
Model parameters	adjusted R^2	0.34			Model parameters	adjusted R^2	0.31		
	F	8.7				F	7.5		
	p	**<0.001**				p	**<0.001**		
Significant regressors	Variable	MGMT	ECOG	Radicality of surgery	Significant regressors	Variable	MGMT	ECOG	Radicality of surgery
	β	5.8	−4	2.5		β	4.2	-4	2.2
	p	0.003	<0.001	0.01		p	0.029	<0.001	0.02
Model: Independent variables or regressors: percentages of overlap between GBM core and GMNs; GBM core volume; age; ECOG performance status; radicality of surgical resection (biopsy, partial resection, gross total resection); MGMT promoter methylation status; Stupp protocol.					Model: Independent variables or regressors: percentages of overlap between GBM edema and GMNs; GBM edema volume; age; ECOG performance status; radicality of surgical resection (biopsy, partial resection, gross total resection); MGMT promoter methylation status; Stupp protocol.				
Model parameters	adjusted R^2	0.2			Model parameters	adjusted R^2	0.19		
	F	2				F	1.8		
	p	**0.01**				p	**0.025**		
Significant regressors	Variable	MGMT	ECOG	Radicality of surgery	Significant regressors	Variable	ECOG		
	β	7.2	−3.9	2.5		β	−4.2		
	p	0.005	0.006	0.04		p	0.002		
Model: Independent variables or regressors: percentages of overlap between GBM core and WMNs; GBM core volume; age; ECOG PS; radicality of surgical resection (biopsy, partial resection, gross total resection); MGMT promoter methylation status; Stupp protocol.					Model: Independent variables or regressors: percentages of overlap between GBM edema and WMNs; GBM edema volume; age; ECOG performance status; radicality of surgical resection (biopsy, partial resection, gross total resection); MGMT promoter methylation status; Stupp protocol.				
Model parameters	adjusted R^2	0.32			Model parameters	adjusted R^2	0.33		
	F	3.6				F	3.5		
	p	**<0.001**				p	**<0.001**		
Significant regressors	Variable	MGMT	ECOG	N12	Significant regressors	Variable	ECOG	Radicality of surgery	
	β	6.3	−3.7	3.6		β	−3.4	2.2	
	p	0.003	0.004	0.03		p	0.004	0.03	

were significantly associated with patient survival (27–29). Our interpretation of such discrepancy is that the mere overlap between GBM and brain networks is not informative enough of the actual functional impairment caused. Thus, we believe that *in-vivo* functional connectivity techniques (including either fMRI and/or neurophysiology) are needed to measure the real impact that the GBM-driven network dysfunction has on patient survival. Nonetheless, our work showed that the WM and its functional activity might harbor valuable information for a better understanding of GBM pathophysiology and its prognostication. In fact, other approaches to investigate the relationships between GBM and WM organization have already been tested: in their recently submitted work, Salvalaggio et al. discovered a novel negative prognostic factor, the density index (i.e., the density of WM fibers overlapped by GBMs), showing the promising potential of structural connectivity-based studies in neuro-oncology (54).

4.5. Limitations

This study has some limitations. (1) Yeo's atlas is the most widely used for GMNs, although we cannot exclude that using different atlas would influence the results; (2) the lower age of the healthy subjects' cohorts used for Yeo's and Peer's atlases compared to our patient sample; (3) the exact nature of the fMRI signal within WM, from which WMNs were identified, is still partially uncertain. While there is evidence that both task-evoked and resting state BOLD signals in WM seem to be, at least in part, caused by hemodynamic changes associated with neural WM activity, the existence of other sources of fMRI signals have been postulated, such as spiking-related metabolic demands and activity of astrocytes and NO-producing neurons (52). To date, the entire biophysical basis of fMRI signals within WM is not utterly understood (22). (4) Another limitation of the present study is the absence of a comparison of the topological network overlap data to functional connectivity modifications induced by GBM, investigable with fMRI. (5) Lastly, our work lacks neuropsychological data, which could be integrated in future studies.

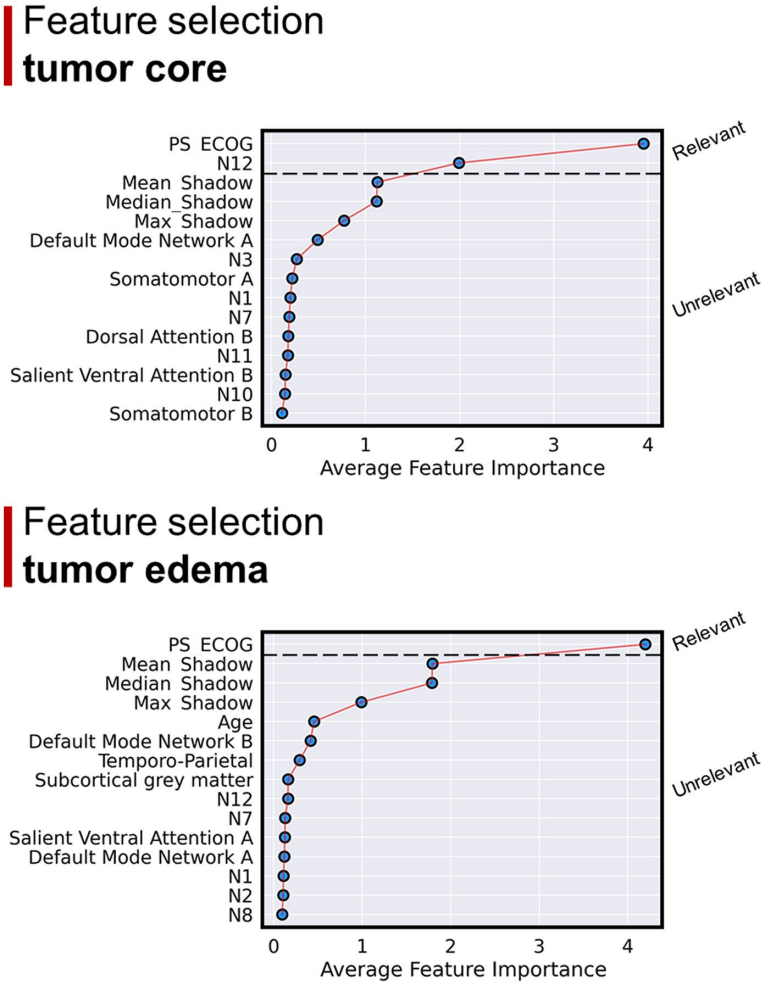

FIGURE 6
Results of the Boruta regression analysis. Considering GBM core overlap percentages: the main regressors explaining OS were ECOG and overlap with N12. Considering GBM edema overlap percentages: ECOG was the only relevant feature for OS regression.

4.6. Conclusion

In conclusion, the GBM core and edema preferentially overlap certain GMNs, specifically associative networks, and related WMNs, involved in cognitive functions. Five main patterns of GBM core distribution across functional networks were found. GBM lesions tended to impact jointly some interrelated white and gray matter functional systems, suggesting that tumor growth and spreading might not be independent of brain activity. Although the involvement of ventral frontoparietal tracts (N12) seems to have some role in predicting a longer survival, network-topology information is overall scarcely informative about OS.

Data availability statement

The raw imaging data supporting the conclusions of this article will be made available by the authors, upon reasonable request.

Ethics statement

The study was approved by the Ethical Committee of the Province of Padua (Comitato Etico per la Sperimentazione Clinica della Provincia di Padova n. 70n/AO/20). Written informed consent for participation was not required for this study in accordance with the national legislation and the institutional requirements.

Author contributions

GS, LP, AS, and MC designed the study. VB, FV, FC, DD'A, MP, LD, VZ, and GL were in charge of the patients and provided clinical and survival data. GS, MG, MA, and AS generated the lesion masks. LP, GS, and AS analyzed the imaging data. GS, LP, AS, and MC participated in the interpretation of data. GS, AS, LP, and MC wrote the manuscript. All authors contributed to the article and approved the submitted version.

Funding

MC was supported by Fondazione Cassa di Risparmio di Padova e Rovigo (CARIPARO)—Ricerca Scientifica di Eccellenza 2018 (Grant Agreement number 55403); Italian Ministero della Salute, Brain connectivity measured with high-density electroencephalography: a novel neurodiagnostic tool for stroke (NEUROCONN; RF-2018-1236689); Celeghin Foundation Padova (CUP C94I20000420007); BIAL foundation grant (No. 361/18); Horizon 2020 European School of Network Neuroscience—European School of Network Neuroscience (euSNN), H2020-SC5-2019-2 (Grant Agreement number 860563); Horizon 2020 research and innovation program; Visionary Nature Based Actions For Heath, Wellbeing & Resilience in Cities (VARCITIES), Horizon 2020-SC5-2019-2 (Grant Agreement number 869505); Italian Ministero della Salute: Eye-movement dynamics during free viewing as biomarker for assessment of visuospatial functions and for closed-loop rehabilitation in stroke (EYEMOVINSTROKE; RF-2019-12369300).

Conflict of interest

The authors declare that the research was conducted in the absence of any commercial or financial relationships that could be construed as a potential conflict of interest

Publisher's note

All claims expressed in this article are solely those of the authors and do not necessarily represent those of their affiliated organizations, or those of the publisher, the editors and the reviewers. Any product that may be evaluated in this article, or claim that may be made by its manufacturer, is not guaranteed or endorsed by the publisher.

Supplementary material

The Supplementary material for this article can be found online at: https://www.frontiersin.org/articles/10.3389/fneur.2023.1175576/full#supplementary-material

References

1. Ostrom QT, Gittleman H, Liao P, Vecchione-Koval T, Wolinsky Y, Kruchko C, et al. CBTRUS statistical report: primary brain and other central nervous system tumors diagnosed in the United States in 2010-2014. *Neuro-Oncology*. (2017) 19:v1–v88. doi: 10.1093/neuonc/nox158

2. Davis FG, Smith TR, Gittleman HR, Ostrom QT, Kruchko C, Barnholtz-Sloan JS. Glioblastoma incidence rate trends in Canada and the United States compared with England, 1995-2015. *Neuro-Oncology*. (2020) 22:301–2. doi: 10.1093/neuonc/noz203

3. Lin D, Wang M, Chen Y, Gong J, Chen L, Shi X, et al. Trends in intracranial glioma incidence and mortality in the United States, 1975-2018. *Front Oncol*. (2021) 11:748061. doi: 10.3389/fonc.2021.748061

4. Wen PY, Weller M, Lee EQ, Alexander BM, Barnholtz-Sloan JS, Barthel FP, et al. Glioblastoma in adults: a Society for Neuro-Oncology (SNO) and European Society of Neuro-Oncology (EANO) consensus review on current management and future directions. *Neuro-Oncology*. (2020) 22:1073–113. doi: 10.1093/neuonc/noaa106

5. Gittleman H, Ostrom QT, Stetson LC, Waite K, Hodges TR, Wright CH, et al. Sex is an important prognostic factor for glioblastoma but not for nonglioblastoma. *Neuro-Oncol Pract*. (2019) 6:451–62. doi: 10.1093/nop/npz019

6. Gorlia T, van den Bent MJ, Hegi ME, Mirimanoff RO, Weller M, Cairncross JG, et al. Nomograms for predicting survival of patients with newly diagnosed glioblastoma: prognostic factor analysis of EORTC and NCIC trial 26981-22981/CE.3. *Lancet Oncol*. (2008) 9:29–38. doi: 10.1016/S1470-2045(07)70384-4

7. Stummer W, Reulen H-J, Meinel T, Pichlmeier U, Schumacher W, Tonn J-C, et al. Extent of resection and survival in glioblastoma MULTIFORME. *Neurosurgery*. (2008) 62:564–76. doi: 10.1227/01.neu.0000317304.31579.17

8. Lee JH, Lee JE, Kahng JY, Kim SH, Park JS, Yoon SJ, et al. Human glioblastoma arises from subventricular zone cells with low-level driver mutations. *Nature*. (2018) 560:243–7. doi: 10.1038/s41586-018-0389-3

9. Jung E, Alfonso J, Osswald M, Monyer H, Wick W, Winkler F. Emerging intersections between neuroscience and glioma biology. *Nat Neurosci*. (2019) 22:1951–60. doi: 10.1038/s41593-019-0540-y

10. Singh SK, Clarke ID, Terasaki M, Bonn VE, Hawkins C, Squire J, et al. Identification of a cancer stem cell in human brain tumors. *Cancer Res*. (2003) 63:5821–8.

11. Meier R, Pahud de Mortanges A, Wiest R, Knecht U. Exploratory analysis of qualitative MR imaging features for the differentiation of glioblastoma and brain metastases. *Front Oncol*. (2020) 10:1–13. doi: 10.3389/fonc.2020.581037

12. Bilello M, Akbari H, Da X, Pisapia JM, Mohan S, Wolf RL, et al. Population-based MRI atlases of spatial distribution are specific to patient and tumor characteristics in glioblastoma. *NeuroImage Clin*. (2016) 12:34–40. doi: 10.1016/j.nicl.2016.03.007

13. Mandal AS, Romero-Garcia R, Hart MG, Suckling J. Genetic, cellular, and connectomic characterization of the brain regions commonly plagued by glioma. *Brain*. (2021) 143:3294–307. doi: 10.1093/BRAIN/AWAA277

14. Derks J, Reijneveld JC, Douw L. Neural network alterations underlie cognitive deficits in brain tumor patients. *Curr Opin Oncol*. (2014) 26:627–33. doi: 10.1097/CCO.0000000000000126

15. Wang C, Van Dyk K, Cho N, Raymond C, Choi J, Salamon N, et al. Characterization of cognitive function in survivors of diffuse gliomas using resting-state functional MRI (rs-fMRI). *Brain Imaging Behav*. (2022) 16:239–51. doi: 10.1007/s11682-021-00497-6

16. Leuthardt EC, Guzman G, Bandt SK, Hacker C, Vellimana AK, Limbrick D, et al. Integration of resting state functional MRI into clinical practice - a large single institution experience. *PLoS One*. (2018) 13:e0198349–16. doi: 10.1371/journal.pone.0198349

17. Kocher M, Jockwitz C, Caspers S, Schreiber J, Farrher E, Stoffels G, et al. Role of the default mode resting-state network for cognitive functioning in malignant glioma patients following multimodal treatment. *NeuroImage Clin*. (2020) 27:102287. doi: 10.1016/j.nicl.2020.102287

18. Tordjman M, Madelin G, Gupta PK, Cordova C, Kurz SC, Orringer D, et al. Functional connectivity of the default mode, dorsal attention and fronto-parietal executive control networks in glial tumor patients. *J Neuro-Oncol*. (2021) 152:347–55. doi: 10.1007/s11060-021-03706-w

19. Maesawa S, Bagarinao E, Fujii M, Futamura M, Motomura K, Watanabe H, et al. Evaluation of resting state networks in patients with gliomas: connectivity changes in the unaffected side and its relation to cognitive function. *PLoS One*. (2015) 10:1–13. doi: 10.1371/journal.pone.0118072

20. Fekonja LS, Wang Z, Cacciola A, Roine T, Aydogan DB, Mewes D, et al. Network analysis shows decreased ipsilesional structural connectivity in glioma patients. *Commun Biol*. (2022) 5:258. doi: 10.1038/s42003-022-03190-6

21. Yeo BTT, Krienen FM, Sepulcre J, Sabuncu MR, Lashkari D, Hollinshead M, et al. The organization of the human cerebral cortex estimated by intrinsic functional connectivity. *J Neurophysiol*. (2011) 106:1125–65. doi: 10.1152/jn.00338.2011

22. Li J, Biswal BB, Wang P, Duan X, Cui Q, Chen H, et al. Exploring the functional connectome in white matter. *Hum Brain Mapp*. (2019) 40:4331–44. doi: 10.1002/hbm.24705

23. Peer M, Nitzan M, Bick AS, Levin N, Arzy S. Evidence for functional networks within the human brain's white matter. *J Neurosci*. (2017) 37:6394–407. doi: 10.1523/JNEUROSCI.3872-16.2017

24. Miller KL, Alfaro-Almagro F, Bangerter NK, Thomas DL, Yacoub E, Xu J, et al. Multimodal population brain imaging in the UK biobank prospective epidemiological study. *Nat Neurosci*. (2016) 19:1523–36. doi: 10.1038/nn.4393

25. Mandal AS, Romero-Garcia R, Seidlitz J, Hart MG, Alexander-Bloch AF, Suckling J. Lesion covariance networks reveal proposed origins and pathways of diffuse gliomas. *Brain Commun*. (2021) 3:1–13. doi: 10.1093/braincomms/fcab289

26. Dadario NB, Ivan M, Sughrue ME. Standardizing connectome-based brain tumor surgery through a network-based surgical nomenclature. *J Neuro-Oncol*. (2023) 161:657–9. doi: 10.1007/s11060-023-04249-y

27. Liu L, Zhang H, Wu J, Yu Z, Chen X, Rekik I, et al. Overall survival time prediction for high-grade glioma patients based on large-scale brain functional networks. *Brain Imaging Behav*. (2019) 13:1333–51. doi: 10.1007/s11682-018-9949-2

28. Sprugnoli G, Rigolo L, Faria M, Juvekar P, Tie Y, Rossi S, et al. Glioma BOLD connectivity profile and its relationship to patients' survival. *Neuro-Oncology Adv*. (2022) 4:1–22. doi: 10.1093/noajnl/vdac153

29. Daniel AGS, Park KY, Roland JL, Dierker D, Gross J, Humphries JB, et al. Functional connectivity within glioblastoma impacts overall survival. *Neuro-Oncology*. (2021) 23:412–21. doi: 10.1093/neuonc/noaa189

30. Ben Bashat D, Artzi M, Ben Ami H, Aizenstein O, Blumenthal DT, Bokstein F, et al. Hemodynamic response imaging: a potential tool for the assessment of angiogenesis in brain tumors. *PLoS One*. (2012) 7:e49416–8. doi: 10.1371/journal.pone.0049416

31. Salvalaggio A, Silvestri E, Sansone G, Pinton L, Magri S, Briani C, et al. Magnetic resonance imaging correlates of immune microenvironment in glioblastoma. *Front Oncol*. (2022) 12:1–11. doi: 10.3389/fonc.2022.823812

32. Louis DN, Perry A, Wesseling P, Brat DJ, Cree IA, Figarella-Branger D, et al. The 2021 WHO classification of tumors of the central nervous system: a summary. *Neuro-Oncology*. (2021) 23:1231–51. doi: 10.1093/neuonc/noab106

33. Tustison NJ, Avants BB, Cook PA, Zheng Y, Egan A, Yushkevich PA, et al. N4ITK: improved N3 Bias correction. *IEEE Trans Med Imaging*. (2010) 29:1310–20. doi: 10.1109/TMI.2010.2046908

34. Doshi J, Erus G, Ou Y, Gaonkar B, Davatzikos C. Multi-Atlas Skull-Stripping. *Acad Radiol*. (2013) 20:1566–76. doi: 10.1016/j.acra.2013.09.010

35. Yushkevich PA, Gao Y, Gerig G. ITK-SNAP: an interactive tool for semi-automatic segmentation of multi-modality biomedical images. *Annu Int Conf IEEE Eng Med Biol Soc*. (2016):3342–5. doi: 10.1109/EMBC.2016.7591443

36. Lasocki A, Gaillard F. Non-contrast-enhancing tumor: a new frontier in glioblastoma research. *Am J Neuroradiol*. (2019) 40:758–65. doi: 10.3174/ajnr.A6025

37. Lasocki A, Gaillard F, Tacey M, Drummond K, Stuckey S. Morphologic patterns of noncontrast-enhancing tumor in glioblastoma correlate with IDH1 mutation status and patient survival. *J Clin Neurosci*. (2018) 47:168–73. doi: 10.1016/j.jocn.2017.09.007

38. Radwan AM, Emsell L, Blommaert J, Zhylka A, Kovacs S, Theys T, et al. Virtual brain grafting: enabling whole brain parcellation in the presence of large lesions. *NeuroImage*. (2021) 229:117731. doi: 10.1016/J.NEUROIMAGE.2021.117731

39. Nachev P, Coulthard E, Jäger HR, Kennard C, Husain M. Enantiomorphic normalization of focally lesioned brains. *NeuroImage*. (2008) 39:1215–26. doi: 10.1016/J.NEUROIMAGE.2007.10.002

40. ANTs by stnava. Available at: http://stnava.github.io/ANTs/ (Accessed June 2, 2020)

41. Atlases - FslWiki. Available at: https://fsl.fmrib.ox.ac.uk/fsl/fslwiki/Atlases (Accessed February 3, 2023)

42. Pini L, de Lange SC, Pizzini FB, Boscolo Galazzo I, Manenti R, Cotelli M, Galluzzi S, Cotelli MS, Manenti R, Cotelli M, van den Heuvel MP, et al. A low-dimensional cognitive-network space in Alzheimer's disease and frontotemporal dementia. *Alzheimer's Res Ther*. (2022) 14:1–14. doi: 10.1186/s13195-022-01145-x

43. Kursa MB, Rudnicki WR. Feature selection with the boruta package. *J Stat Softw*. (2010) 36:1–13. doi: 10.18637/jss.v036.i11

44. Wang J, Yi L, Kang Q, Mei ZJ, Qing CT, Philippe HJ, et al. Glioma invasion along white matter tracts: a dilemma for neurosurgeons. *Cancer Lett*. (2022) 526:103–11. doi: 10.1016/j.canlet.2021.11.020

45. Monje M. Synaptic communication in brain cancer. *Cancer Res*. (2020) 80:2979–82. doi: 10.1158/0008-5472.CAN-20-0646

46. Huberfeld G, Vecht CJ. Seizures and gliomas - towards a single therapeutic approach. *Nat Rev Neurol*. (2016) 12:204–16. doi: 10.1038/nrneurol.2016.26

47. Zhang J, Wu G, Miller CP, Tatevossian RG, Dalton JD, Tang B, et al. Whole-genome sequencing identifies genetic alterations in pediatric low-grade gliomas. *Nat Genet*. (2013) 45:602–12. doi: 10.1038/ng.2611

48. Chen H, Judkins J, Thomas C, Wu M, Khoury L, Benjamin CG, et al. Mutant IDH1 and seizures in patients with glioma. *Neurology*. (2017) 88:1805–13. doi: 10.1212/WNL.0000000000003911

49. Ishiuchi S, Yoshida Y, Sugawara K, Aihara M, Ohtani T, Watanabe T, et al. Ca2+−permeable AMPA receptors regulate growth of human glioblastoma via Akt activation. *J Neurosci*. (2007) 27:7987–8001. doi: 10.1523/JNEUROSCI.2180-07.2007

50. Ishiuchi S, Tsuzuki K, Yoshida Y, Yamada N, Hagimura N, Okado H, et al. Blockage of Ca2+−permeable AMPA receptors suppresses migration and induces apoptosis in human glioblastoma cells. *Nat Med*. (2002) 8:971–8. doi: 10.1038/nm746

51. Venkatesh HS, Johung TB, Caretti V, Noll A, Tang Y, Nagaraja S, et al. Neuronal activity promotes glioma growth through neuroligin-3 secretion. *Cells*. (2015) 161:803–16. doi: 10.1016/j.cell.2015.04.012

52. Venkatesh HS, Morishita W, Geraghty AC, Silverbush D, Gillespie SM, Arzt M, et al. Electrical and synaptic integration of glioma into neural circuits. *Nature*. (2019) 573:539–45. doi: 10.1038/s41586-019-1563-y

53. Venkatesh H, Monje M. Neuronal activity in ontogeny and oncology. *Trends in Cancer*. (2017) 3:89–112. doi: 10.1016/j.trecan.2016.12.008

54. Salvalaggio A, Pini L, Gaiola M, Velco A, Sansone G, Anglani M, Fekonja L, Chioffi F, Picht T, Thiebaut De Schotten M, Zagonel V, Lombardi G, D'Avella DCM, et al. White Matter Density Predicts Overall Survival in Glioblastoma: A New Connectivity Framework for Brain Tumors. *Ann Neurol*. (2022) 92:S211–S211

frontiers | Frontiers in Neurology

TYPE Systematic Review
PUBLISHED 30 June 2023
DOI 10.3389/fneur.2023.1100067

OPEN ACCESS

EDITED BY
Alessandra Griffa,
Université de Genève, Switzerland

REVIEWED BY
Joshua C. Cheng,
Beth Israel Deaconess Medical Center and Harvard Medical School, United States
Alexandre Boutet,
University of Toronto, Canada

*CORRESPONDENCE
Mohammad Hadi Aarabi
✉ mohammadhadiarabi@gmail.com

RECEIVED 16 November 2022
ACCEPTED 21 June 2023
PUBLISHED 30 June 2023

CITATION
Nabizadeh F and Aarabi MH (2023) Functional and structural lesion network mapping in neurological and psychiatric disorders: a systematic review.
Front. Neurol. 14:1100067.
doi: 10.3389/fneur.2023.1100067

Functional and structural lesion network mapping in neurological and psychiatric disorders: a systematic review

Fardin Nabizadeh[1,2] and Mohammad Hadi Aarabi[3]*

[1]Neuroscience Research Group (NRG), Universal Scientific Education and Research Network (USERN), Tehran, Iran, [2]School of Medicine, Iran University of Medical Sciences, Tehran, Iran, [3]Department of Neuroscience and Padova Neuroscience Center (PNC), University of Padova, Padua, Italy

Background: The traditional approach to studying the neurobiological mechanisms of brain disorders and localizing brain function involves identifying brain abnormalities and comparing them to matched controls. This method has been instrumental in clinical neurology, providing insight into the functional roles of different brain regions. However, it becomes challenging when lesions in diverse regions produce similar symptoms. To address this, researchers have begun mapping brain lesions to functional or structural networks, a process known as lesion network mapping (LNM). This approach seeks to identify common brain circuits associated with lesions in various areas. In this review, we focus on recent studies that have utilized LNM to map neurological and psychiatric symptoms, shedding light on how this method enhances our understanding of brain network functions.

Methods: We conducted a systematic search of four databases: PubMed, Scopus, and Web of Science, using the term "Lesion network mapping." Our focus was on observational studies that applied lesion network mapping in the context of neurological and psychiatric disorders.

Results: Following our screening process, we included 52 studies, comprising a total of 6,814 subjects, in our systematic review. These studies, which utilized functional connectivity, revealed several regions and network overlaps across various movement and psychiatric disorders. For instance, the cerebellum was found to be part of a common network for conditions such as essential tremor relief, parkinsonism, Holmes tremor, freezing of gait, cervical dystonia, infantile spasms, and tics. Additionally, the thalamus was identified as part of a common network for essential tremor relief, Holmes tremor, and executive function deficits. The dorsal attention network was significantly associated with fall risk in elderly individuals and parkinsonism.

Conclusion: LNM has proven to be a powerful tool in localizing a broad range of neuropsychiatric, behavioral, and movement disorders. It holds promise in identifying new treatment targets through symptom mapping. Nonetheless, the validity of these approaches should be confirmed by more comprehensive prospective studies.

KEYWORDS

lesion network mapping, connectivity, lesions, stroke, network, localization

Introduction

For many years, the method of understanding the function of a specific brain region was through the study of focal brain lesions that occurred as a result of strokes, tumors, and hemorrhages. If patients with similar symptoms had overlapping lesions in a specific brain region, we could pinpoint those neurological symptoms or behavioral deficits to that region (1, 2). Traditional lesion mapping has been the cornerstone of clinical neurology, providing valuable insights into the functional roles of different brain regions. However, most neurological and psychiatric symptoms cannot be traced back to a single region; instead, they involve a network of interconnected regions (3). Additionally, patients exhibiting similar symptoms may have lesions located in diverse areas, which poses a challenge to traditional lesion mapping in pinpointing those symptoms (4). Such symptom overlap could potentially be due to the disruption of an underlying, cohesive brain network (5, 6).

One strategy to address this challenge is through the implementation of lesion network mapping (LNM), a methodology that connects brain lesions to either functional or structural networks to identify common brain circuits tied to diverse lesion locations (4, 7).

This technique operates on the hypothesis that a lesion present at any location within a network mapped for a specific symptom has the potential to trigger that symptom (4, 8). The process of performing LNM overlap studies comprises four stages: Firstly, lesions are traced into a standardized brain atlas, establishing a foundation for connectivity analyses (9) (Figure 1). Secondly, an assessment is undertaken to determine the connectivity of each lesion location with other brain regions, using either structural or functional normative human connectome data. Thirdly, correlations between lesion locations and all other brain voxels are thresholded to delineate a map of interconnected regions. Finally, these maps from each patient are superimposed to pinpoint brain regions that are most frequently connected to lesion locations associated with the symptom in question (10). In addition, certain studies incorporate voxelwise statistical analyses, either by leveraging continuous outcomes or by contrasting patients with controls, with the aim of elucidating common networks associated with symptomatic lesions (11, 12). The availability of large-scale functional and anatomical normative maps, like those offered by the Human Connectome Project data, provide a robust foundation for correlating lesion locations with a shared network, thereby facilitating the study of neurological and psychiatric symptoms (13).

This methodology has been broadly utilized since its introduction in 2015 for the localization of an array of neuropsychiatric, behavioral, and movement disorders (8, 10, 14–18). Previous investigations have substantiated the validity of LNM; while several outcomes confirmed primary hypotheses concerning the neuroanatomical underpinnings of specific symptoms (19), some unexpected findings also emerged from LNM studies. For instance, a notable association between the putamen and hemichorea-hemiballism was identified, despite earlier evidence suggesting the involvement of the subthalamic nucleus in the genesis of hemichorea-hemiballism (20). As such, LNM may offer an innovative avenue to further investigate the functionality of brain networks.

The intent of this systematic review is to spotlight recent studies that have utilized LNM to map neurological and psychiatric

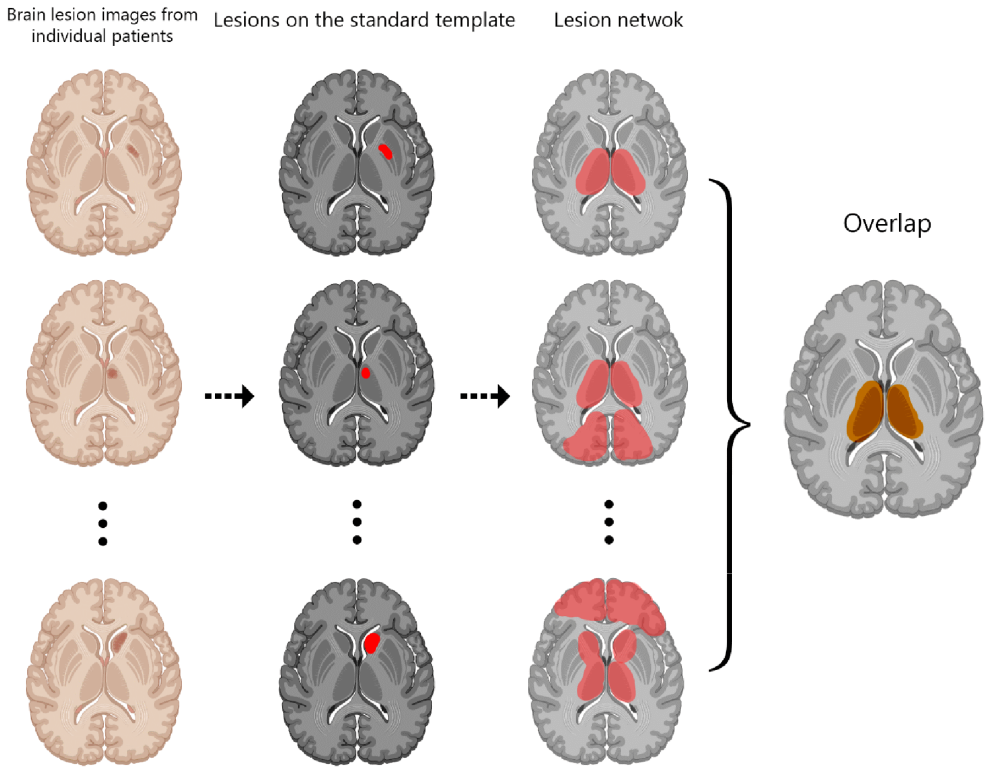

FIGURE 1
Lesion network mapping procedure.

symptoms, thereby providing insight into how this methodology enhances our comprehension of the function of distinct brain regions.

Methods and materials

This systematic review was conducted in adherence to the Preferred Reporting Items for Systematic Reviews and Meta-Analyses (PRISMA) guidelines (21).

Literature search and eligibility criteria

A literature search was performed on PubMed, Scopus, Embase, and Web of Science in June 2022 using the term "Lesion network mapping." In addition, we manually reviewed the reference lists of pertinent review studies to identify relevant research. Inclusion criteria encompassed observational studies on LNM in neurological and psychiatric disorders. Exclusions were made for case reports, review articles, and non-English language studies.

Study selection

Two researchers (F.N, M.A) independently examined the titles and abstracts and eliminated irrelevant studies. Subsequently, the remaining articles' full texts were scrutinized, and studies were selected based on our eligibility criteria.

Data extraction

Data was collated from the selected studies using a pre-designed data sheet. The collected information included: author, publication year, study design, data source, sample size, age, gender distribution, study duration, underlying disease, lesion cause, lesion location, lesion type, investigated symptom or disorders, number of subjects with investigated symptoms or disorders, analytical software used, normative data, and LNM findings.

Quality assessments

The quality of the included studies was evaluated using the Newcastle-Ottawa scale (NOS) for observational studies, which operates on a scoring range from 0 to 8 (22).

Results

Search results

Our literature search and additional records resulted in 69 studies after eliminating duplicates (Figure 2). Post title and abstract screening, 10 studies were excluded. Ultimately, a total of 52 studies involving 6,814 subjects were included in our systematic review following a full-text review (4–8, 10–12, 14–20, 23–57).

Among the incorporated studies, 39 were cross-sectional, ten were case–control, two were cohort studies, and the remaining one was a longitudinal study. In terms of data sources, 30 studies utilized private data, 20 used published case reports, and two studies employed both private data and published case reports. Notably, 41 studies utilized FSL as their analytical software. A detailed overview of the characteristics of the included studies can be found in Table 1. Among the analyzed studies, functional LNM was performed in 38, structural LNM was conducted in 7, and both forms of LNM were employed in 7 studies. The quality assessment indicated that the mean NOS score of the included studies was 7.48.

Functional lesion network mapping

Non-motor symptoms were found to be associated with fronto-parieto-temporal networks (24), sensorimotor and ventral attention networks (29), and the thalamic mediodorsal nucleus (14). Executive function deficits demonstrated connectivity with the anterior cingulate cortex, dorsomedial prefrontal cortex, and frontoparietal network (16). Symptoms such as prosopagnosia, anosognosia for hemiplegia, and diminished mind-wandering revealed connections to the left frontal cortex, anterior cingulate cortex, right fusiform face area (10), right posterior hippocampus (33), and left inferior parietal lobule (35) respectively.

Symptoms such as loss of consciousness, mania, and delusional misidentifications were associated with connectivity to the dorsal brainstem (37), right orbitofrontal cortex, right inferior temporal gyrus, right frontal pole (27), and left retro splenial and right frontal cortex (7). Additionally, hallucinations were linked to the extrastriate visual cortex (4) and to the cerebellar vermis, inferior cerebellum, and right superior temporal sulcus (5). Lesions causing autoscopic phenomena showed functional connections to the bilateral temporoparietal junction (23).

Cortical vertigo showed associations with connectivity to the posterior insula (52). Lesions causing obsessive–compulsive disorder (OCD) and depression were linked to the dorsal anterior cingulate cortex and left dorsolateral prefrontal cortex (11, 30).

Findings indicate that behavioral deficits were better predicted by direct measures of functional MRI connectivity than indirect functional disconnection (38). Moreover, Darby et al. (15) identified that criminal behavior was associated with a shared network encompassing the inferior orbitofrontal cortex, anterior temporal lobes, and intraparietal sulcus (Table 2).

Movement disorders, such as essential tremor, Parkinsonism, freezing of gait, and Holmes tremor, were linked to networks involving the cerebellum and thalamus (32), midbrain, basal ganglia, cingulate cortex, and cerebellum (19), and red nucleus, thalamus, globus pallidus, and cerebellum (17), respectively.

Hemichorea hemiballism, cervical dystonia, and increased fall risk were associated with the posterolateral putamen (20), cerebellum and somatosensory cortex (26), and the dorsal attention network (28), respectively. Additionally, asymmetric step length after a unilateral stroke demonstrated functional connectivity to the dorsolateral prefrontal cortex (18).

Speech disorders such as semantic aphasia, foreign accent syndrome, and apraxia of speech were associated with distinctive patterns of structural and functional disconnection (58), and networks

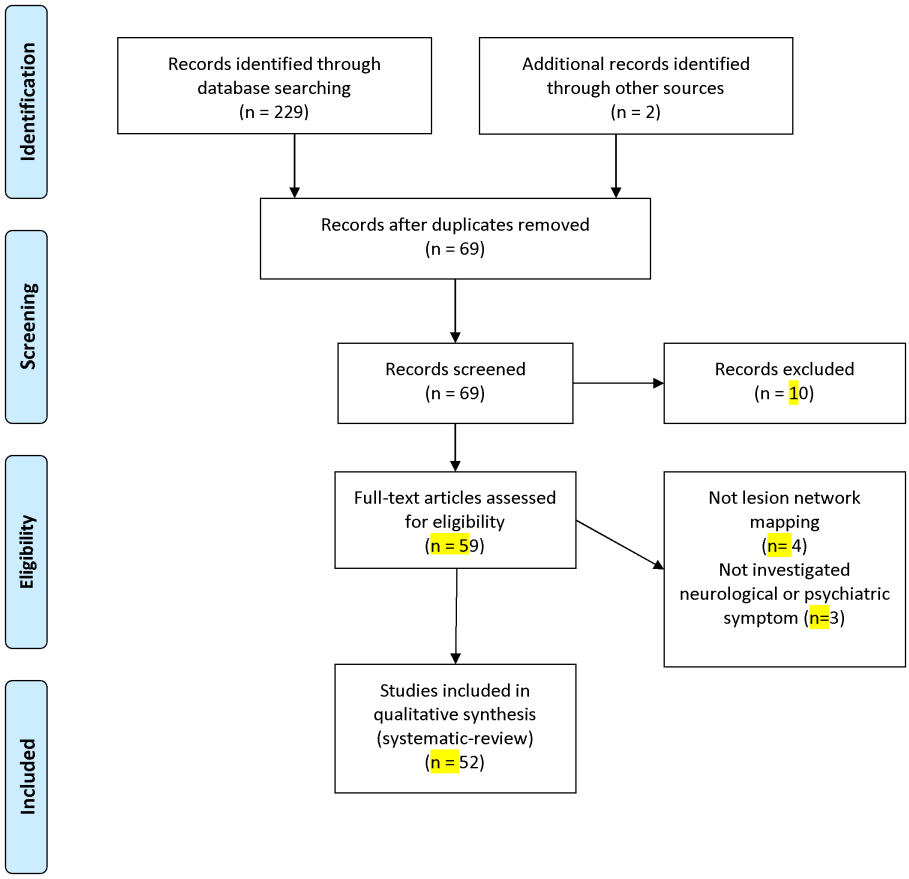

FIGURE 2
PRISMA flow diagram depicting the flow of information through the different phases of a systematic review.

involving the bilateral lower and middle portions of the precentral gyrus and medial frontal cortex (31).

Studies using functional connectivity revealed several region and network overlaps across different movement or psychiatric disorders (Figure 3 and Table 3). The cerebellum appeared in a common network for conditions such as essential tremor relief (32), parkinsonism (19), Holmes tremor (17), freezing of gait (8), cervical dystonia (26), and tics (6). It also showed functional connections to tuberous sclerosis lesions in children with infantile spasms (59). The thalamus demonstrated involvement in a common network for essential tremor relief (32) and Holmes tremor (17), and showed significant functional connectivity with lesions associated with executive function deficits (16). The midbrain, basal ganglia, and cingulate cortex were connected to lesions causing parkinsonism (19) and were part of the common network implicated in tics (6).

The dorsal attention network was significantly correlated with the Physiological Profile Assessment (PPA) score, which measures fall risk in elderly individuals (28), and demonstrated functional connectivity related to focal brain lesions causing parkinsonism (19). It was also part of the frontoparietal network, which showed functional connectivity overlap in regions connected to epileptogenic mass lesions (34). Moreover, the sensorimotor network showed significant overlap in lesions causing cognitive impairment assessed by the MoCA score (29), and was connected to resection cavity maps in patients with body awareness disorders (42).

Structural lesion network mapping

The emerging evidence underscores the reciprocal nature of structural and functional Lesion Network Mapping (LNM) in elucidating the nexus between cerebral lesions and cognitive functionality (24, 29, 51). Structural mapping has pinpointed specific regions, such as the right insular and frontal operculum, superior temporal gyrus, and putamen, whose impairment tends to precipitate cognitive deficits (51). Concurrently, functional mapping has demystified the distinctive brain networks correlated with various cognitive faculties, exemplified by the fronto-parieto-temporal network (24).

The intricate neural networks engaged in spatial perception have been brought to light, with aberrations in the right ventrolateral prefrontal and right temporal clusters linked to spatial delusions (47). Importantly, the integral role of the left retro splenial and right frontal cortex in spatial information processing has been underscored, underlining their pivotal contribution to spatial cognition and awareness (48).

Furthermore, the studies spotlight the necessity of incorporating structural connectivity into the neurological evaluation of stroke sequelae for optimal therapeutic results (38). Structural LNM exhibited superior reliability in forecasting post-stroke behavioral repercussions compared to its functional counterpart. However, there were instances where direct measures of functional connectivity

outperformed, underscoring the indispensable role of a holistic evaluation of both structural and functional connectivity to tailor personalized therapeutic interventions for stroke survivors.

The critical role of the frontal lobe in gait regulation was reaffirmed in the context of motor and speech disorders (18). The choice of LNM methodology appears to be contingent upon the specific functional impairment in question, with functional mapping outperforming in the domain of language deficits, while structural mapping took the lead for motor deficits (24). Both techniques unveiled significant pathways, indicating that diverse lesion types might disrupt distinct neural circuits, thus informing rehabilitative strategies post-stroke (45). For example, the left anterior thalamic radiation and bilateral superior longitudinal fasciculus were highlighted as significant pathways by both methodologies (45).

Lastly, the studies emphasized the significance of comprehending the intricate structural praxis network in limb apraxia patients (53). The indirect structural disconnection method discerned significant pathological alterations in the white matter within an extensively interconnected fronto-temporo-parietal network, incorporating both short and long-distance association fibers (53). This revelation suggests that the disparate topographical outcomes reported in earlier lesion mapping studies might not exclusively arise from methodological variations but could also be attributed to the inherent limitations of univariate topographical mapping techniques.

Discussion

This review consolidates and critically assesses existing knowledge on the application of Lesion Network Mapping (LNM) methods in the diagnosis and treatment of neurological and psychiatric disorders. Our findings underscore the complementary role of functional and structural LNM, emphasizing their potential utility in improving therapeutic outcomes in neurological afflictions. Our analysis draws attention to certain brain regions and networks integral to specific neurological domains. For instance, the fronto-parieto-temporal network emerged as pivotal to cognitive functioning, while the dorsal anterior cingulate cortex and the left dorsolateral prefrontal cortex demonstrated considerable relevance for obsessive–compulsive disorder. These insights indicate that LNM may aid in pinpointing viable targets for neuromodulation interventions across various neurological disorders. The examined studies also underlined the indispensable role of LNM in deciphering the intricacies of motor and speech disorders. These studies highlighted the use of LNM in identifying brain regions and neural pathways implicated in diverse movement disorders, such as Parkinsonism, Essential Tremor, and Holmes Tremor. Consequently, we can anticipate LNM's instrumental role in informing neuromodulation strategies tailored to specific motor and speech disorders, such as cervical dystonia and hemichorea hemiballismus. Our results suggest that the choice of LNM method should align with the specific type of functional deficit under consideration. Since the advent of LNM studies in 2015, numerous investigations have successfully employed this technique to elucidate how alterations in functional and structural networks can account for symptoms post focal brain lesions.

Moreover, our analysis identified several overlaps between different regions and networks implicated in diverse psychiatric and neurological disorders. Both structural (51) and functional LNM (24, 29) pinpointed the fronto-parieto-temporal network as integral to cognitive function, thereby asserting a potent correlation between this network and cognitive impairment. Furthermore, studies revealed that damage to the right ventrolateral prefrontal and right temporal cluster (47), coupled with alterations in the left retro splenial and right frontal cortex (7), could precipitate spatial perception deficits and engender delusions of space. Intriguingly, both functional LNM (54) and structural disconnectome-based analyses (57) associated the left dorsolateral prefrontal cortex with depression. This concurrence insinuates a common neural foundation for depressive symptoms, stressing the necessity of considering both structural and functional connectivity when attempting to comprehend the neurological underpinnings of varying disorders and enhancing treatment outcomes. The complex neural networks implicated in these disorders can guide the formulation of tailored treatment strategies and facilitate a deeper understanding of their neurobiological origins. By delineating these overlaps and parallels, we underscore the interwoven nature of the brain and its instrumental role across an array of disorders.

Our study unearthed a significant overlap within the thalamus for essential tremor relief, Holmes tremor, and executive function deficits. This intriguing finding challenges the conventional practice of symptom localization that ascribes particular symptoms to specific, isolated brain regions. Instead, it accentuates the importance of investigating the complex interactions among various brain regions and acknowledges the distributed nature of neural processing (4, 24). This shared neural substrate within the thalamus proposes potential unified therapeutic targets for these conditions, underscoring the imperative for a more holistic approach when studying neurological and psychiatric disorders. By harmonizing the strengths of both conventional localization and network-based perspectives, researchers can attain a comprehensive understanding of the brain's structure and function, ultimately leading to more effective treatment strategies for a multitude of disorders.

The neurobiological mechanisms underlying brain disorders and the localization of brain function are traditionally explored by identifying abnormalities within the brain and contrasting them with matched controls, as exemplified by the study of hemiparesis following stroke lesions. However, this process becomes complex when the lesion is located in an unanticipated region or when numerous heterogeneous lesions are observed in disparate locations. For instance, hemiparkinsonism patients with varied causal lesions outside the nigrostriatal tract were found to map onto a common network (19). Moreover, most neurological and psychiatric symptoms cannot be ascribed to a single region; instead, they involve a network of interconnected areas. As such, LNM has proven to be a significant advance over traditional lesion analysis, enabling the localization of symptoms across different lesion locations, a task that was previously unachievable (60).

Focal brain lesions have been observed to modify resting functional connectivity and reduce the variability of neural states, thereby limiting the brain's ability to process information (59, 61, 62). Empirical evidence from previous studies has indicated that alterations in functional connectivity following focal brain lesions are not restricted to a singular network but engage numerous regions (63). Strokes tend to affect white matter and subcortical regions more often than the cortex. Given that white matter contains numerous fiber pathways, strokes within these regions can result in widespread alterations (59, 64).

TABLE 1 Charcteristics and imaging findings of the included studies.

Author	Year	Study design	Source of data	Sample size	Age	Females	Period of study	Underlying disease	Cause of lesion	Location of the lesions	Type of lesion	Studied symptom or disorder	Number of subjects with symptom	Software	Lesion network mapping	Normative data	NOS
Souter	2022	Cross-sectional	Private	23	62.2 ± 11.9	NR	NR	Stroke	Stroke	Heterogenous	Infarction	Semantic Aphasia	23	MATLAB	Functional and structural	Brain Genomics Superstruct Project (GSP) with 191 healthy participants	7
Bowren	2022	Cross-sectional	Private	593	53–61	324	NR	Stroke	Stroke	NR	Ischemic	Cognitive and motor outcomes	593	FSL	Functional and structural	Human Connectome Project (HCP) with 303 healthy participants	8
Crockett	2022	Cross-sectional	Private	160	74.62	99	NR	Cerebral small vessel disease	Cerebral small vessel disease		Ischemic	Fall risk	160	FSL	Functional	Brain Genomics Superstruct Project (GSP) with 1000 healthy participants	7
Ganos	2022	Cross-sectional	Case reports	22	25.3 ± 20.7	NR	Until 2020	Heterogenous	Heterogenous	Basal ganglia, temporal and parietal lobes, the insula, corpus callosum, thalamus, internal capsule, midbrain, pons and medulla oblongata.	Heterogenous	Tics	22	FSL	Functional	Brain Genomics Superstruct Project (GSP) with 1000 healthy participants	8
Joutsa	2022	Case-control	Private	129	33.7	58	NR	Brain injury	NR	Heterogenous	NR	Addiction	129	FSL	Functional and structural	Brain Genomics Superstruct Project (GSP) with 1000 healthy participants	8

(Continued)

10.3389/fneur.2023.1100067

TABLE 1 (Continued)

Author	Year	Study design	Source of data	Sample size	Age	Females	Period of study	Underlying disease	Cause of lesion	Location of the lesions	Type of lesion	Studied symptom or disorder	Number of subjects with symptom	Software	Lesion network mapping	Normative data	NOS
Blondiaux	2021	Cross-sectional	Private	26	NR	NR	NR	Focal epilepsy	Focal epilepsy	NR	NR	Autoscopic phenomena	26	FSL	Functional	Brain Genomics Superstruct Project (GSP) with 98 healthy participants	6
Cohen	2021	Cohort	Private	123	2.66	60	NR	Tuberous sclerosis	Tuberous sclerosis		Tumoral	Infantile Spasms	74	FSL	Functional	Brain Genomics Superstruct Project (GSP) with 1000 healthy participants	8
Crockett	2021	Cross-sectional	Private	160	74.62	99	NR	Cerebral small vessel disease	Cerebral small vessel disease		Ischemic	Global cognition	160	FSL	Functional	Brain Genomics Superstruct Project (GSP) with 1000 healthy participants	7
Germann	2021	Cohort	Private	11	23–44	6	NR	Obsessive compulsive disorder patients underwent focused ultrasound capsulotomy	NR	NR	NR	Obsessive compulsive disorder	11	MATLAB	Functional	Brain Genomics Superstruct Project (GSP) with 1000 healthy participants	7
Higashiyama	2021	Cross-sectional	Case reports	25	37–72	16	Until 2017	Ischemic stroke and brain tumor	Infarction and tumor		Infarct, tumoral	Foreign accent syndrome	25	FSL	Functional	Brain Genomics Superstruct Project (GSP) with 1000 healthy participants	8

(Continued)

10.3389/fneur.2023.1100067

TABLE 1 (Continued)

Author	Year	Study design	Source of data	Sample size	Age	Females	Period of study	Underlying disease	Cause of lesion	Location of the lesions	Type of lesion	Studied symptom or disorder	Number of subjects with symptom	Software	Lesion network mapping	Normative data	NOS
Pini	2021	Cross-sectional	Private	123	53	63	NR	Stroke	Stroke	NR	NR	Behavioral deficits	123	FSL	Functional	Brain Genomics Superstruct Project (GSP) with 176 healthy participants	7
Cotovio	2020	Cross-sectional	Case reports	505	54.9 ± 17.7	NR	Until 2017	Heterogenous	NR	Wide range of cortical and subcortical areas	Infarct	Mania	15	FSL	Functional	Brain Genomics Superstruct Project (GSP) with 1000 healthy participants	8
Hwang	2020	Case-control	Private	49	54.8	24	NR	Patients with neurological disorders	Ischemic or hemorrhagic stroke	Thalamus	Ischemic and infarct	Executive Function	15	FSL	Functional	Brain Genomics Superstruct Project (GSP) with 303 healthy participants	8
Klingbeil	2020	Case-control	Private	49	NR	NR	NR	Stroke	Stroke	Heterogenous	Ischemic	Anosognosia for hemiplegia	25	SPM	Functional	NR	6
Kyeong	2020	Cross-sectional	Private	39	67.3 ± 2.6	NR	NR	Stroke	Stroke	Heterogenous	Ischemic	Asymmetric step length	39	FSL	Functional and structural	Brain Genomics Superstruct Project (GSP) with 1000 healthy participants and Cambridge Centre for Ageing and Neuroscience (Cam-CAN)	7

(Continued)

10.3389/fneur.2023.1100067

TABLE 1 (Continued)

Author	Year	Study design	Source of data	Sample size	Age	Females	Period of study	Underlying disease	Cause of lesion	Location of the lesions	Type of lesion	Studied symptom or disorder	Number of subjects with symptom	Software	Lesion network mapping	Normative data	NOS
Mansouri	2020	Case-control	Private and case reports	51	NR	23	NR	Tumor	Tumor	Frontal, temporal, and parietal	Tumoral	Epilepsy	51	MATLAB	Functional	Brain Genomics Superstruct Project (GSP) with 1000 healthy participants	7
Philippi	2020	Case-control	Private	48	60	25	NR	Brain injury	Brain injury	Heterogenous	NR	Mind-wandering	29	FSL	Functional	Brain Genomics Superstruct Project (GSP) with 98 healthy participants	8
Salvalaggio	2020	Cross-sectional	Private	132	49.8 ± 9.0 years (visual left) and 54.9 ± 11.9 years (motor right limbs)	NR	NR	Stroke	Stroke	NR	NR	Behavioral deficits	132	FSL	Functional and structural	Human Connectome Project (HCP) with 176 healthy participants	8
Snider	2020	Case-control	Private	171	58	NR	NR	NR	NR	NR	NR	Loss of consciousness	171	FSL	Functional	Brain Genomics Superstruct Project (GSP) with 1000 healthy participants	8
Albazron	2019	Case-control	Private	195	6.8 ± 4.2	84	1988–2017	Pediatric patients who underwent cerebellar tumor resection	Tumor	Medulloblastoma, ependymoma, and astrocytoma/glioma	Tumoral	Cerebellar cognitive affective syndrome	48	FSL	Functional	Brain Genomics Superstruct Project (GSP) with 98 healthy participants	7

(Continued)

10.3389/fneur.2023.1100067

TABLE 1 (Continued)

Author	Year	Study design	Source of data	Sample size	Age	Females	Period of study	Underlying disease	Cause of lesion	Location of the lesions	Type of lesion	Studied symptom or disorder	Number of subjects with symptom	Software	Lesion network mapping	Normative data	NOS
Cohen	2019	Cross-sectional	Case reports	44	39	12	2000–2019	Stroke	Stroke	Right fusiform face area		Prosopagnosia	44	FSL	Functional	Brain Genomics Superstruct Project (GSP) with 1000 healthy participants	8
Corp	2019	Cross-sectional	Case reports	25	23–84	11	Until 2017	Heterogenous	Heterogenous	Cerebellum, pons, midbrain, thalamus, globus pallidus interna, basal ganglia, putamen	Haemorrhage (*n*=7), Infarct (*n*=10), Cyst (*n*=3), Tumour (*n*=2), MS plaques (*n*=1), Glioma (*n*=1), and Angioma (*n*=1)	Idiopathic cervical dystonia	25	FSL	Functional	Brain Genomics Superstruct Project (GSP) with 1000 healthy participants	8
Joutsa	2019	Cross-sectional	Case reports	36	NR	NR	Until 2016	NR	Ischemi or hemorrhagi	Midbrain, cerebellum, basal ganglia, pons, medulla, cere bellum, and occipital lobe	Ischemic or hemorrhagic	Holmes tremor	36	LEAD-DBS	Functional	Brain Genomics Superstruct Project (GSP) with 1000 healthy participants	7
Kim	2019	Cross-sectional	Case reports	89	NR	NR	NR	NR	NR	NR	NR	Hallucinations	89	SPM	Functional	Brain Genomics Superstruct Project (GSP) with 1000 healthy participants	6
Darby	2018	Cross-sectional	Case reports	40	9–62	NR	NR	Heterogenous	Heterogenous	NR	Heterogenous	Criminal behaviour	17	FSL and LEAD-DBS	Functional	Brain Genomics Superstruct Project (GSP) with 1000 healthy participants	7

(Continued)

10.3389/fneur.2023.1100067

TABLE 1 (Continued)

Author	Year	Study design	Source of data	Sample size	Age	Females	Period of study	Underlying disease	Cause of lesion	Location of the lesions	Type of lesion	Studied symptom or disorder	Number of subjects with symptom	Software	Lesion network mapping	Normative data	NOS
Joutsa	2018	Cross-sectional	Case reports	11	59–90	4	Until 2016	Stroke	Stroke	Heterogenous	Ischemic	Essential tremor	11	FSL	Functional	Brain Genomics Superstruct Project (GSP) with 1000 healthy participants	8
Joutsa	2018	Cross-sectional	Case reports	29	16–83	13	Until 2017	Heterogenous	Stroke, Haemorrhage, tumor, Hypoxia	Heterogenous	Ischemic, Haemorrhagic, tumoral	Parkinsonism	29	FSL and LEAD-DBS	Functional	Brain Genomics Superstruct Project (GSP) with 1000 healthy participants	8
Darby	2017	Cross-sectional	Case reports	17	9–62	NR	NR	Heterogenous	Heterogenous	NR	Heterogenous	Delusional misidentifications	17	FSL	Functional	Brain Genomics Superstruct Project (GSP) with 1000 healthy participants	7
Fasano	2016	Cross-sectional	Case reports	14	35–80	3	1993–2013	Heterogenous	Stroke, Haemorrhage, tumor	Heterogenous	Ischemic, Haemorrhagic, tumoral	Freezing of gait	14	FSL	Functional	Brain Genomics Superstruct Project (GSP) with 98 healthy participants	8
Laganiere	2016	Cross-sectional	Case reports	29	60.2	NR	Until 2014	Stroke	Stroke	Cortex (*n*=8), STN (*n*=8), putamen (*n*=6), caudate (*n*=5), midbrain (*n*=1), and subcortical white matter (*n*=1)	Ischemic	Hemichorea-hemiballismus	29	FSL	Functional	Brain Genomics Superstruct Project (GSP) with 98 healthy participants	8

(Continued)

10.3389/fneur.2023.1100067

TABLE 1 (Continued)

Author	Year	Study design	Source of data	Sample size	Age	Females	Period of study	Underlying disease	Cause of lesion	Location of the lesions	Type of lesion	Studied symptom or disorder	Number of subjects with symptom	Software	Lesion network mapping	Normative data	NOS
Boes	2015	Cross-sectional	Private and case reports	23	61 ± 19	NR	NR	Heterogenous	Heterogenous	Heterogenous	Heterogenous	Peduncular hallucinosis	23	FSL	Functional	Brain Genomics Superstruct Project (GSP) with 98 healthy participants	8
Darby	2018	Cross-sectional	Case reports	28	67.3	NR	NR	Stroke and Hemorrhage	Stroke and Hemorrhage	Anterior cingulate cortex (ACC) (21% of cases), globus pallidus (29%), thalamus (25%), caudate (18%), and brainstem (11%)	Ischemic, Haemorrhagic	Akinetic mutism	28	FSL and LEAD-DBS	Functional	Brain Genomics Superstruct Project (GSP) with 1000 healthy participants	8
Ferguson	2019	Cross-sectional	Case reports	53	57.5 ± 13	34	NR	Heterogenous	Heterogenous	Heterogenous	Heterogenous	Amnesia	53	FSL	Functional	Brain Genomics Superstruct Project (GSP) with 1000 healthy participants	8
Ferguson	2021	Cross-sectional	Private	193	NR	NR	NR	Brain tumor resection and brain injury	Tumor and head truama	Heterogenous	Heterogenous	Spirituality and religiosity	193	FSL and 3D slicer	Functional	Brain Genomics Superstruct Project (GSP) with 1000 healthy participants	7
Fischer	2016	Case-control	Private	36	57.3 6 16.5	NR	NR	Heterogenous	Heterogenous	Pons, midbrain, and Medulla	Heterogenous	Coma	12	FSL	Functional	Brain Genomics Superstruct Project (GSP) with 98 healthy participants	8

(Continued)

10.3389/fneur.2023.1100067

TABLE 1 (Continued)

Author	Year	Study design	Source of data	Sample size	Age	Females	Period of study	Underlying disease	Cause of lesion	Location of the lesions	Type of lesion	Studied symptom or disorder	Number of subjects with symptom	Software	Lesion network mapping	Normative data	NOS
Herbert	2019	Cross-sectional	Private	14	40.07 ± 11.08	6	2011–2018	Brain tumor resection	Glioma	Pons, midbrain, and Medulla	Tumoral and resection	Bodily awareness	14	MATLAB and SPM	Functional	Local data of 18 healthy participants	8
Jimenez-Marin	2022	Cross-sectional	Private	54	68.7	29	NR	Stroke	Stroke	Heterogenous	Ischemic, Haemorrhagic	Poststroke sensorimotor outcomes	54	MATLAB and SPM	Functional and structural	Brain Genomics Superstruct Project (GSP) with 1000 healthy participants	8
Padmanabhan	2019	Case-control	Private	358	59.3	86	NR	Ischemic stroke, intracerebral hemorrhage, and penetrating traumatic brain injury	Ischemic stroke, intracerebral hemorrhage, and penetrating traumatic brain injury	Heterogenous	Heterogenous	Depression	58	FSL	Functional	Brain Genomics Superstruct Project (GSP) with 1000 healthy participants	7
Kletenik	2022	Case-control	Case reports	69	NR	NR	NR	Tumor, Stroke and Hemorrhage	Heterogenous	Heterogenous	Heterogenous	Blindsight	34	FSL and 3D slicer	Functional	Brain Genomics Superstruct Project (GSP) with 1000 healthy participants	8
Siddiqi	2021	Cross-sectional	Private	713	NR	NR	NR	Stroke, Parkinson's disease, Epilepsy, Penetrating traumatic brain injury, and Major depressive disorder	Stroke, DBS, TMS	Heterogenous	Heterogenous	Neuropsychiatric disease	713	FSL and MATLAB	Functional	Brain Genomics Superstruct Project (GSP) with 1000 healthy participants	8

(Continued)

10.3389/fneur.2023.1100067

TABLE 1 (Continued)

Author	Year	Study design	Source of data	Sample size	Age	Females	Period of study	Underlying disease	Cause of lesion	Location of the lesions	Type of lesion	Studied symptom or disorder	Number of subjects with symptom	Software	Lesion network mapping	Normative data	NOS
Alves	2022	Cross-sectional	Case reports	67	NR	NR	NR	Stroke	Stroke	Heterogenous	Heterogenous	Delusions of space	67	FSL	Structural	Human Connectome Project with 178 healthy participants	7
Conrad	2022	Cross-sectional	Case reports	10	NR	NR	NR	Stroke	Stroke	Anterior long insular gyrus (IV) and posterior long insular gyrus (V), and extended to the anterior insula.	Ischemic	Cortical vertigo	10	FSL	Functional and structural	Human Connectome Project with 178 healthy participants for structural and 100 healthy participants for functional	8
Cotovio	2022	Cross-sectional	Case reports	687	NR	NR	NR	Heterogenous	NR	Wide range of cortical and subcortical areas	Heterogenous	Mania	56	FSL	Functional	Human Connectome Project with 937 healthy participants and Max Planck Institute (MPI)-Leipzig Mind Brain Body with 189 healthy participants	6

(Continued)

10.3389/fneur.2023.1100067

TABLE 1 (Continued)

Author	Year	Study design	Source of data	Sample size	Age	Females	Period of study	Underlying disease	Cause of lesion	Location of the lesions	Type of lesion	Studied symptom or disorder	Number of subjects with symptom	Software	Lesion network mapping	Normative data	NOS
Dulyan	2022	Longitudinal	Private	62	53.7	28	NR	Stroke	Stroke	Thalamus, putamen, caudate, pallidum, hippocampus, amygdala, nucleus accumbens, insula, subcallosal cingulate, paracingulate, and parahippocampal areas	Ischemic and Hemorrhagic	Motor dysfunction	62	MATLAB	Structural	Human Connectome Project with 163 healthy participants	7
Jiang	2023	Cross-sectional	Private	167	58.1	0	2003–2006	Brain injury	Brain injury	Heterogenous	NR	Emotion Regulation	167	FSL	Functional	Brain Genomics Superstruct Project (GSP) with 1000 healthy participants	7
Kolskar	2022	Cross-sectional	Private	102	66.3	26	NR	Stroke	Stroke	Heterogenous	Ischemic and Hemorrhagic	Cognitive impairment	102	MATLAB	Structural	Human Connectome Project with 170 healthy participants	8
Li	2023	Cross-sectional	Case reports	23	NR	13	NR	Stroke	Stroke	Heterogenous	Ischemic and Hemorrhagic	Vertigo	23	FSL and LEAD-DBS	Functional	Brain Genomics Superstruct Project (GSP) with 1000 healthy participants	8

(Continued)

10.3389/fneur.2023.1100067

TABLE 1 (Continued)

Author	Year	Study design	Source of data	Sample size	Age	Females	Period of study	Underlying disease	Cause of lesion	Location of the lesions	Type of lesion	Studied symptom or disorder	Number of subjects with symptom	Software	Lesion network mapping	Normative data	NOS
Ulrichsen	2021	Cross-sectional	Private	239	65.8	68	NR	Stroke	Stroke	Heterogenous	Ischemic and Hemorrhagic	Fatigue	84	FSL	Structural	Human Connectome Project with 170 healthy participants	8
Rosenzopf	2022	Cross-sectional	Private	101	57.7	37	NR	Stroke	Stroke	Left hemisphere	Ischemic and Hemorrhagic	Limb apraxia	31	FSL	Structural	IIT Human Brain Atlas	7
Siddiqi	2023	Cross-sectional	Private	281	48.7	205	2015–2017	Multiple sclerosis	Multiple sclerosis	Heterogenous	MS lesions	Depression	281	FSL and MATLAB	Functional	Brain Genomics Superstruct Project (GSP) with 1000 healthy participants	8
Sotelo	2019	Cross-sectional	Private	13	63.4	7	NR	Stroke	Stroke	Heterogenous	Ischemic and Hemorrhagic	Motor impairment	13	FSL and MATLAB	Structural	Private	7
Weaver	2023	Cross-sectional	Private	553	69	233	NR	Stroke	Stroke	Heterogenous	Ischemic and Hemorrhagic	poststroke depressive symptoms	553	BCBtoolkit	Structural	Private	7

NR, Not Reported; NOS, Newcastle-Ottawa Scale; SPM, Statistical Parametric Mapping; FSL, FMRIB Software Library.

10.3389/fneur.2023.1100067

TABLE 2 LNM findings of the included studies.

Studied symptom or disorder	Number of subjects with symptom	Lesion network mapping findings	Author	Year
Addiction	129	1- Lesions disrupting smoking addiction occurred in many different brain locations but were characterized by a specific pattern of brain connectivity. This pattern involved positive connectivity to the dorsal cingulate, lateral prefrontal cortex, and insula and negative connectivity to the medial prefrontal and temporal cortex, 2- This circuit was reproducible across independent lesion cohorts, associated with reduced alcohol addiction risk, and specific to addiction metrics. Hubs that best matched the connectivity profile for addiction remission were the paracingulate gyrus, left frontal operculum, and medial fronto-polar cortex	Joutsa	2022
Akinetic mutism	28	Brain network defined by functional connectivity to the anterior cingulate cortex	Darby	2018
Amnesia	53	Over 95% of amnesia-causing lesion locations were functionally connected to a single location in the hippocampus	Ferguson	2019
Anosognosia for hemiplegia	25	Right posterior hippocampus showed significantly greater normative lesion connectivity for anosognosia for hemiplegia	Klingbeil	2020
Asymmetric step length	39	Functional: At least 85% of lesions showed functional network overlap in the bilateral frontal lobe. Structural: The overlap of lesion-derived structural networks was high (85%) and occurred specifically within the corona radiata of the lesional hemisphere	Kyeong	2020
Autoscopic phenomena	26	1- Autoscopic phenomena localize to bilateral temporo-parietal junction, 2- Out-of-body-experience resulted from a brain network connected to bilateral angular gyrus, right precuneus, and right inferior frontal gyrus, differing from autoscopic hallucination with a brain network connected to bilateral precuneus, inferior temporal gyrus, and cerebellum, 3- Heautoscopy resulted from a brain network connected to left inferior frontal gyrus, left insula and left parahippocampus	Blondiaux	2021
Behavioral deficits	123	This principal component functional disconnection approach localized mainly cortical voxels of high signal-to-noise; and it yielded networks with high anatomical specificity, and strong behavioural correlation	Pini	2021
Behavioral deficits	132	Functional: Prediction from indirect functional disconnection was scarce or negligible except for the right visual field deficits. Prediction from direct measures of functional MRI functional connectivity in a subset of patients was clearly superior to indirect functional disconnection. Structural: The indirect estimation of structural connectivity damage successfully predicted behavioural deficits post-stroke to a level comparable to lesion information. However, indirect estimation of functional disconnection did not predict behavioural deficits	Salvalaggio	2020
Blindsight	34	The functional connectivity observed between the lesion locations and the ipsilesional medial pulvinar was found to be significantly associated with blindsight. However, no significant differences in connectivity were identified with respect to other brain regions, which have been previously implicated in blindsight	Kletenik	2022
Bodily awareness	14	The resection cavity maps in patients with body awareness disorders exhibited robust connectivity to a sensorimotor network consisting of the antero-dorsal precuneus, paracentral lobule, supplementary motor area, superior parietal lobule, supramarginal gyrus, insula, and premotor cortex	Herbert	2019
Cerebellar cognitive affective syndrome	48	1- Cerebellar region most associated with cerebellar cognitive affective syndrome was functionally connected to the thalamic mediodorsal nucleus, 2- higher connectivity between lesion location and the mediodorsal nucleus predicts cerebellar cognitive affective syndrome occurrence	Albazron	2019

(Continued)

TABLE 2 (Continued)

Studied symptom or disorder	Number of subjects with symptom	Lesion network mapping findings	Author	Year
Cognitive and motor outcomes	593	The Boston Naming Test linked with most results converging on a fronto-parieto-temporal network. Two principal components were linked to the Token Test, and these seeds also converged primarily on a fronto-parieto-temporal network. Results based on the delayed recall trial from the Rey Auditory Verbal Learning Test identified only two networks: a lateral occipital-precuneate network, and a network spanning primary and secondary visual cortices. Functional lesion network mapping performed best for the prediction of language deficits, and structural lesion network mapping performed best for the prediction of motor deficit	Bowren	2022
Cognitive impairment	102	An analysis of the disconnectome illustrated that increased disconnection in the right insular and frontal operculum, superior temporal gyrus, and putamen was related to a decline in MoCA performance, suggesting that lesions in regions linked to these brain regions are more likely to result in cognitive impairment	Kolskar	2022
Coma	12	A small region in the rostral dorsolateral pontine tegmentum is significantly associated with coma-causing lesions and is functionally connected to the ventral anterior insula and pregenual anterior cingulate cortex	Fischer	2016
Cortical vertigo	10	Structural disconnection: The fronto-insular tracts, specifically fronto-insular tracts 4 and 5, facilitate connections between the parietal operculum and the posterior regions of the insula as well as the inferior fronto-occipital fascicle (IFOF). Additionally, the third division of the superior longitudinal fascicle (SLF III) was affected to a greater extent. It is important to note that in cases with vertigo, two white matter tracts were disconnected, namely the fibers of the splenium of the corpus callosum in all 10 cases and posterior segments of the arcuate fascicle in 9 out of 10 cases. These white matter tracts were not affected in lesions without vertigo. Functional: The functional connectivity networks (FCNs) share common subcortical components, which include the vestibular nuclei (VN) and the cerebellar vestibular and ocular motor representations located in lobules IX (nodulus, uvula) and X (flocculus/paraflocculus). In addition, cortical network hubs comprise the PIVC, the posterior insular cortex (PIC) and the adjacent superior temporal gyrus, as well as vestibular multisensory areas located further away, such as the ventral intraparietal area (VIP), motion-sensitive areas MT+ in the temporal lobe, and cingulate visual sulcus (CSv), along with the ocular motor areas of the parietal (lateral parietal area—LIP) and frontal lobes (frontal eye fields, FEF, and dorsolateral prefrontal cortex, DLPFC)	Conrad	2022
Criminal behaviour	17	1- All 17 lesions temporally associated with criminal behavior were functionally connected (i.e., positively correlated) to the inferior orbitofrontal cortex and anterior temporal lobes, and most (16 of 17) were connected to the vmPFC and nucleus accumbens. 2- All 17 lesions were functionally connected (i.e., negatively correlated) with the intra parietal sulcus, and 15 of 17 were functionally connected with the dorsolateral prefrontal cortex	Darby	2018
Delusional misidentifications	17	1- All 17 lesion locations were functionally connected to the left retrosplenial cortex, 2- Similarly, 16 of 17 lesion locations were functionally connected to the right frontal cortex	Darby	2017
Delusions of space	67	Lesions caused delusion of space were assocaited with disconnection right ventrolateral prefrontal and right temporal cluster	Alves	2022
Depression	58	There was a notable increase in connectivity between the lesions of depressed individuals and a specific area of the left dorsal lateral prefrontal cortex when compared to the lesions of non-depressed individuals	Padmanabhan	2019

(Continued)

TABLE 2 (Continued)

Studied symptom or disorder	Number of subjects with symptom	Lesion network mapping findings	Author	Year
Depression	281	The present study demonstrated that the functional connectivity of multiple sclerosis (MS) lesion locations with our pre-determined depression circuit (involving the dorsolateral prefrontal cortex, subgenual cingulate, and ventromedial prefrontal cortex) was significantly linked with the severity of depression in MS patients. Furthermore, this association was observed specifically in relation to depression and not with other symptoms associated with MS	Siddiqi	2023
Emotion Regulation	167	The construction of the brain network for regulating emotions utilizing lesion-related information was characterized by the functional association with the left ventrolateral prefrontal cortex	Jiang	2023
Epilepsy	51	Greatest functional connectivity overlap was in Frontoparietal Network, Ventral Attention Network, and the Limbic Network—with percentage volume overlap of 19.5%, 19.1%, 19.1%, and 12.5%, respectively	Mansouri	2020
Essential tremor	11	All 11 lesion locations were connected to the bilateral thalamus, bilateral cerebellum, left globus pallidus, and left putamen	Joutsa	2018
Executive Function	15	Thalamic lesion sites associated with more severe deficits in executive function showed stronger functional connectivity with anterior cingulate cortex, dorsomedial prefrontal cortex, and frontoparietal network, compared to thalamic lesions not associated with executive dysfunction	Hwang	2020
Fall risk	160	There was significant correlations between the percentage of lesion related disruption of the dorsal attention network and Physiological Profile Assessment (PPA) score; and between disruption of both the sensorimotor and ventral attention networks with foam sway. There were no significant associations with floor sway or gait speed	Crockett	2022
Fatigue	84	There was no significant associations between the disconnectome maps and the clinical measures	Ulrichsen	2021
Foreign accent syndrome	25	At least 80% of lesions showed network overlap in the bilateral lower and middle por tions of the precentral gyrus and in the medial frontal cortex	Higashiyama	2021
Freezing of gait	14	(13/14) of lesions were functionally connected to a focal area in the dorsal medial cerebellum	Fasano	2016
Global cognition	160	The visual, ventral attention, and frontoparietal networks had significant overlap with the lesion network. After controlling for multiple comparisons, level of lesion network overlap with both the sensorimotor network and ventral attention network was significantly correlated with MoCA score. Thus, the disruption to the sensorimotor and ventral attention networks, associated with the poorer global cognition	Crockett	2021
Hallucinations	89	Hallucinations was defined by connectivity to the cerebellar vermis, inferior cerebellum, and the right superior temporal sulcus	Kim	2019
Hemichorea-hemiballismus	29	At least 90% of lesions showed network overlap in the posterolateral putamen	Laganiere	2016
Holmes tremor	36	All lesion locations were connected to a common brain circuit with nodes in the red nucleus, thalamus, globus pallidus, and cerebellum	Joutsa	2019
Idiopathic cervical dystonia	25	Positive connectivity to the cerebellum and negative connectivity to the somatosensory cortex were specific markers for cervical dystonia	Corp	2019
Infantile Spasms	74	Infantile spasms connected to the globi pallidi and cerebellar vermis	Cohen	2021
Limb apraxia	31	The present study identified significant pathological changes in the white matter of a densely interconnected fronto-temporo-parietal network consisting of both short and long distance association fibers. Accordingly, the results imply that the divergent topographical outcomes reported in prior lesion mapping investigations may not solely stem from variations in research methodology but also from the limitations inherent in univariate topographical mapping techniques to reveal the complex structural praxis network	Rosenzopf	2022

(Continued)

TABLE 2 (Continued)

Studied symptom or disorder	Number of subjects with symptom	Lesion network mapping findings	Author	Year
Loss of consciousness	171	The map of regions anticorrelated to the dorsal brainstem thus defines a distributed brain circuit that, when damaged, is most likely to cause loss of consciousness. This circuit showed a slight posterior predominance and had peaks in the bilateral claustrum	Snider	2020
Mania	15	Lesion locations showed a unique pattern of functional connectivity to the right orbitofrontal cortex, right inferior temporal gyrus, and right frontal pole	Cotovio	2020
Mania	56	The researchers evaluated the effect of utilizing distinct connectomes on the outcomes of lesion network mapping for mania. Their findings indicated that the conclusions were dependable and uniform, regardless of the specific connectome employed for the analysis	Cotovio	2022
Mind-wandering	29	Lesion network mapping analyses showed the strongest association of reduced mind-wandering with the left inferior parietal lobule	Philippi	2020
Motor dysfunction	62	The isolated lesions reflect a symmetrical but predominantly right-sided lack of connection, with a greater degree of overlap noted in the ventral visual pathways, internal capsule, and perisylvian white matter	Dulyan	2022
Motor impairment	13	They found significantly reduced indirect connectivity in the frontal and parietal lobes, ipsilesional subcortical regions and bilateral cerebellum after stroke	Sotelo	2019
Neuropsychiatric disease	713	The severity of depression was found to be associated with specific lesion and stimulation sites, which were connected to a consistent brain circuit across multiple datasets. The circuits derived from lesions, deep brain stimulation, and transcranial magnetic stimulation were comparable, and the circuits derived from patients with major depression and those with other diagnoses were similar as well. The connectivity of these circuits was predictive of the out-of-sample antidepressant efficacy of deep brain stimulation and transcranial magnetic stimulation sites. Furthermore, a separate analysis involving 29 lesions and 95 stimulation sites identified a unique circuit for the motor symptoms of Parkinson's disease	Siddiqi	2021
Obsessive compulsive disorder	11	Lesion functional connectivity with two distinct frontal regions, the dorsal anterior cingulate cortex and the left dorsolateral pre frontal cortex was highly correlated with individual symptom improvement	Germann	2021
Parkinsonism	29	Lesion locations causing parkinsonism were functionally connected to a common network of regions including the midbrain, basal ganglia, cingulate cortex, and cerebellum	Joutsa	2018
Peduncular hallucinosis	23	22 of 23 lesions were negatively correlated with extrastriate visual cortex	Boes	2015
poststroke depressive symptoms	553	Utilizing disconnectome-based analyses, the results of this study demonstrated that disruptions in the white matter of the right parahippocampal region, as well as the right thalamus and pallidum, and the right anterior thalamic radiation were significantly linked to the manifestation of depressive symptoms following a stroke	Weaver	2023
Poststroke sensorimotor outcomes	54	Functional: The functional lesion-disconnectivity technique produced the highest behavioral association local network maps, which indicated that the brainstem (specifically the pons), left supramarginal gyrus (in the portion overlapping with the secondary somatosensory cortex), left thalamus, bilateral superior frontal cortex (in the portion overlapping with the premotor cortex and supplementary motor area), left inferior parietal cortex, and right precentral cortex (in the portion overlapping with the primary motor cortex and primary sensory cortex) were involved in both unimodal and multimodal associations. Structural: The top behavioral association maps generated by lesion network mapping techniques using structural lesion-disconnectivity analysis showed that several major tracts, including the forceps major, left frontal aslant tract, left anterior thalamic radiation, bilateral superior longitudinal fasciculus, and bilateral optic radiation, were heavily involved in both unimodal and multimodal analyses	Jimenez-Marin	2022

(Continued)

TABLE 2 (Continued)

Studied symptom or disorder	Number of subjects with symptom	Lesion network mapping findings	Author	Year
Prosopagnosia	44	All 44 lesion locations were functionally connected, through negative correlation, with regions in the left frontal cortex, and anterior cingulate cortex, and also, positevly correlated with right fusiform face area	Cohen	2019
Semantic Aphasia	23	There was significant overlap in the distinct patterns of structural and functional disconnection	Souter	2022
Spirituality and religiosity	193	The peak association with changes in spiritual acceptance was connectivity between lesion locations and the periaqueductal grey	Ferguson	2021
Tics	22	Tic-inducing lesions mapped to a common network map, which comprised the insular cortices, cingulate gyrus, striatum, globus pallidus internus, thalami, and the cerebellum	Ganos	2022
Vertigo	23	Analysis demonstrated that the functional connectivity established between the locations of the lesions and the bilateral ventral posterior insula was highly sensitive (observed in 22 out of a total of 23 lesions) and precise in diagnosing vertigo resulting specifically from lesions	Li	2023

LNM, Lesion Network Mapping.

The pioneering study employing LNM was conducted by Boes et al. (4), investigating peduncular hallucinosis subsequent to subcortical lesions. These lesions were hypothesized to disrupt the extrastriate visual cortex, despite their heterogeneous locations. The researchers found that 22 out of 23 lesions demonstrated a negative correlation with the extrastriate visual cortex. Moreover, a study by Kim et al. discovered that lesions causing hallucinations localized to a shared brain network, encompassing the cerebellar vermis, inferior cerebellum, and the right superior temporal sulcus (5). Following the promising results of this inaugural LNM study, the method was applied to elucidate long-standing neurological enigmas characterized by heterogeneous lesions dispersed across different regions (6, 18, 31).

Considering the comparable effects of deep brain stimulation (DBS) and therapeutic lesions, a promising avenue for LNM involves leveraging the identified regions associated with disorders or common networks linked to beneficial brain lesions as therapeutic targets for DBS (65, 66). A pertinent example is the observed clinical improvement in patients where DBS electrode connectivity was in the claustrum, which was also identified as a shared network for lesions causing parkinsonism *via* LNM (19). Further, the exploration of beneficial brain lesions that alleviate symptoms to pinpoint optimal DBS targets should extend to various neurological or psychiatric disorders. However, it's important to note that beneficial brain lesions are exceedingly rare. A study by Joutsa et al. demonstrated that varied lesion locations resulting in essential tremor relief overlapped in a common network within the cerebellum and thalamus, known targets for deep brain stimulation in the management of tremors (32).

Furthermore, a recent study by the same group delved into brain lesions associated with addiction improvement, identifying the paracingulate gyrus and the left frontal operculum. The medial frontopolar cortex emerged as the best-matching connectivity profile for addiction remission (39). These discoveries could pave the way to optimal treatment targets for addiction disorders, lending support to ongoing neuromodulation trials (67). However, it is clear that additional research is required to understand how to extrapolate and interpret LNM findings to identify the most suitable therapeutic targets.

When lesion connections coincide within a single brain network, it's reasonable to infer that the network has a causative role in symptom production. Nevertheless, the regions at the network's core may not be crucial in symptom development (68). The correlation between symptoms and the central region of the network is gleaned from brain connectivity patterns. Consequently, regional associations gleaned from LNM must be appraised in comparison with functional neuroimaging results.

A prominent question within LNM pertains to the neurobiological mechanism at play when a network is disrupted by lesions. Although lesions induce dysfunction at their locations, the remote impact of lesions on functional loss in interconnected regions—dependent on the type of connection—remains a topic of debate (69). Dysfunctions in excitatory connections could lead to decreased activity, while disruption in inhibitory connections could result in increased activity (26). Furthermore, it remains uncertain whether the labeling of functional connectivity as positive or negative can indicate decreases or increases in activity, respectively.

LNM's focus has largely been on the spatial aspect of symptoms induced by lesions, often neglecting the temporal component. Investigating the temporal aspect of symptoms is just as important, given that symptoms evolve over time due to recovery processes and dynamic changes post-injury (3).

Limitation and future direction

While the development of LNM has yielded intriguing results, complete elucidation of neurological enigmas via this method alone remains a considerable distance away. More robust studies are necessary, particularly those utilizing prospective data that assess pre-and post-lesion symptoms. Salvalaggio et al. (38) have previously suggested that direct and indirect measures of functional networks may not be as sensitive to behavioral deficits compared to using

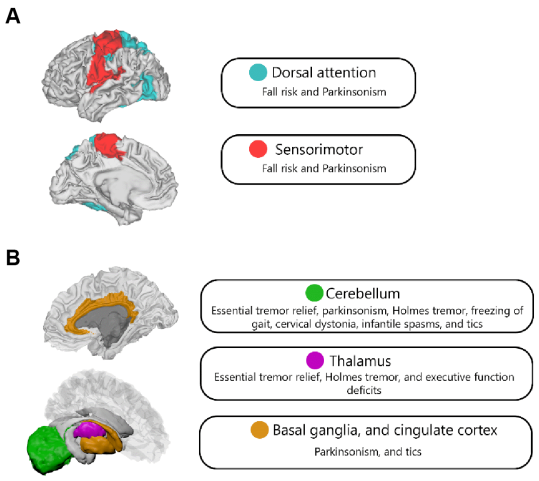

FIGURE 3
Network **(A)** and region **(B)** overlap across different psychiatric and neurological disorders in functional LNM studies.

TABLE 3 Common brain regions and networks across neurological and psychiatric disorders.

Common brain regions	
Anterior Cingulate Cortex	Involved in executive function deficits, prosopagnosia, and anosognosia for hemiplegia
Left Frontal Cortex	Connected to prosopagnosia, anosognosia for hemiplegia, and reduced mind-wandering
Cerebellum	Common in networks involving essential tremor, Parkinsonism, Holmes tremor, freezing of gait, cervical dystonia, tics, hallucinations, and infantile spasms in children with tuberous sclerosis
Thalamus	Involved in essential tremor, Holmes tremor, and executive function deficits

Common networks	
Frontoparieto-temporal Network	Linked to non-motor symptoms
Sensorimotor Network	Connected to non-motor symptoms and cognitive impairment
Frontoparietal Network	Associated with executive function deficits and epileptogenic mass lesions
Dorsal Attention Network	Linked to Parkinsonism and fall risk

structural disconnections, possibly due to the coincidence of structural disconnections with structural damage following lesions. However, Cohen et al. contended that the poor outcome of LNM in predicting behavioral deficits in Salvalaggio et al.'s study could be attributed to methodological considerations (25). Ferguson et al. (40) presented contrasting results, affirming the value of LNM in localizing behavioral deficits. These discrepancies underscore the need for future studies to compare and enhance LNM methods. Furthermore, the efficacy of LNM in identifying therapeutic targets should be examined by strategically placing DBS electrodes in the proposed hub of a network (69).

Cotovio et al. (27) probed the effects of utilizing distinct connectomes on LNM outcomes for mania, concluding that the findings remained consistent and reliable, regardless of the specific connectome used for analysis. Future directions could involve refining normative connectome atlases using higher resolution imaging, integrating results from various connectomes obtained during different tasks, and employing age-and sex-matched datasets for each patient. As functional and structural normative data often involve young, healthy individuals, employing normative lifespan data could yield deeper insights into brain function and enable more accurate symptom mapping. While most studies use normative connectomes, the exploration of disease-specific connectomes may provide more precise results.

Moreover, Bonkhoff et al. (70) discovered that women tend to experience more severe strokes than men, and a recent large-scale study highlighted the effect of sex on neuroimaging metrics over time (71). Thus, incorporating sex-specific normative data in LNM could enhance the precision of this approach.

While we have primarily considered functional and structural networks as relatively stable entities in this review, research increasingly shows that these networks are dynamically changing over time. These temporal fluctuations in connectivity patterns are believed to be crucial for flexible cognitive function, and disturbances in these dynamics have been linked to various neurological and psychiatric conditions. Incorporating these dynamic changes into LNM analyses could therefore potentially increase the sensitivity of the method to detect functional abnormalities linked to behavioral deficits. This integration of dynamics would be a novel addition to the methodology and potentially offers a new avenue for understanding brain function and dysfunction.

Another important discussion point to add is the development and application of machine learning techniques in the context of LNM. Recent advancements in machine learning and artificial intelligence (AI) present exciting opportunities for further refining and enhancing the predictive power of LNM. Machine learning models could be trained to predict the likelihood of specific deficits or symptom severity based on the observed lesion distribution and connectivity disruptions. Such models could provide clinicians with additional tools for prognosis and treatment planning, complementing the traditional, more qualitative approaches.

Lastly, the inter-individual variability in brain connectivity and anatomy should not be overlooked. Even among healthy individuals, there can be substantial differences in the structure and functional connectivity of the brain. This variability might influence the impact of a lesion on cognitive and behavioral function and might partly explain the heterogeneity observed in clinical outcomes following brain damage. Future studies could consider incorporating measures of inter-individual variability into the LNM framework to provide more personalized predictions about treatment outcomes. This could be especially relevant when considering DBS targets, as the optimal target might differ slightly between individuals due to this variability.

These proposed additions aim to enrich the current findings and provide a more comprehensive view of the applications and potential advancements in lesion network mapping.

Methodological consideration

There are several important methodological considerations that should be addressed in LNM.

Normalization and standardization

While LNM has proven to be a powerful tool in understanding brain disorders, it's important to note that the results are highly dependent on the normalization and standardization of brain images. Subtle variations in these processes can lead to significant differences in results. Moreover, the choice of template used for spatial normalization can significantly impact the localization of brain regions and networks. Future studies should aim to implement standardized preprocessing pipelines to ensure the reliability and reproducibility of results.

Limitations of normative connectomes

Most studies used normative connectomes in their LNM analyses. Although this approach provides a general framework for analyzing brain networks, it overlooks inter-individual variability. Individualized connectomes that account for each patient's unique brain architecture may provide more precise mapping results and should be the focus of future research.

Thresholding and statistical analysis

The manner in which network connections are thresholded and analyzed can greatly influence the results of LNM. The application of overly stringent thresholds may fail to capture weaker, yet potentially significant, network connections, whereas lenient thresholds may lead to false positive findings. The choice of statistical tests and corrections for multiple comparisons also plays a crucial role in the interpretation of results.

Choice of parcellation scheme

The way in which the brain is divided into distinct regions, or parcels, can significantly impact the results of network analyses. Different parcellation schemes can yield differing, and sometimes conflicting, results. Hence, the choice of parcellation scheme should be carefully considered and justified in future LNM studies.

Multimodal integration

The integration of multiple imaging modalities (e.g., structural MRI, functional MRI, diffusion tensor imaging) can provide complementary insights into the brain's structure–function relationships. Despite this, many studies still focus on a single imaging modality, potentially missing important aspects of network functionality and connectivity.

While LNM presents an exciting tool in neurology and neuroimaging, attention to these methodological considerations is critical for the advancement of the field and to ensure the reliability and validity of findings.

Conclusion

LNM offers solid findings in localizing a wide range of neuropsychiatric, behavioral, and movement disorders. Furthermore, LNM is anticipated to identify new treatment targets through symptom mapping. However, the veracity of these methodologies must be validated through more comprehensive prospective studies.

Data availability statement

The original contributions presented in the study are included in the article/supplementary material, further inquiries can be directed to the corresponding author.

Author contributions

FN and MA contributed to searching and writing and revising the manuscript. All authors contributed to the article and approved the submitted version.

Funding

MA is funded by the EU-project euSNN European School of Network Neuroscience (MSCA-ITN-ETN H2020-860563).

Conflict of interest

The authors declare that the research was conducted in the absence of any commercial or financial relationships that could be construed as a potential conflict of interest.

Publisher's note

References

1. Raymont V, Salazar AM, Krueger F, Grafman J. "studying injured minds" - the Vietnam head injury study and 40 years of brain injury research. *Front Neurol.* (2011) 2:15. doi: 10.3389/fneur.2011.00015

2. Rorden C, Karnath HO. Using human brain lesions to infer function: a relic from a past era in the fMRI age? *Nat Rev Neurosci.* (2004) 5:813–9. doi: 10.1038/nrn1521

3. Fornito A, Zalesky A, Breakspear M. The connectomics of brain disorders. *Nat Rev Neurosci*. (2015) 16:159–72. doi: 10.1038/nrn3901

4. Boes AD, Prasad S, Liu H, Liu Q, Pascual-Leone A, Caviness VS, et al. Network localization of neurological symptoms from focal brain lesions. *Brain*. (2015) 138:3061–75. doi: 10.1093/brain/awv228

5. Kim NY, Hsu J, Talmasov D, Joutsa J, Soussand L, Wu O, et al. Lesions causing hallucinations localize to one common brain network. *Mol Psychiatry*. (2021) 26:1299–309. doi: 10.1038/s41380-019-0565-3

6. Ganos C, Al-Fatly B, Fischer JF, Baldermann JC, Hennen C, Visser-Vandewalle V, et al. A neural network for tics: insights from causal brain lesions and deep brain stimulation. *Brain*. (2022) 145:4385–97. doi: 10.1093/brain/awac009

7. Darby RR, Laganiere S, Pascual-Leone A, Prasad S, Fox MD. Finding the imposter: brain connectivity of lesions causing delusional misidentifications. *Brain*. (2017) 140:497–507. doi: 10.1093/brain/aww288

8. Fasano A, Laganiere SE, Lam S, Fox MD. Lesions causing freezing of gait localize to a cerebellar functional network. *Ann Neurol*. (2017) 81:129–41. doi: 10.1002/ana.24845

9. Joutsa J, Fox MD. Chapter 15 - using brain lesions to inform connectomic DBS In: A Horn, editor. *Connectomic Deep Brain Stimulation*. Cambridge: Academic Press (2022). 325–37.

10. Cohen AL, Soussand L, Corrow SL, Martinaud O, Barton JJS, Fox MD. Looking beyond the face area: lesion network mapping of prosopagnosia. *Brain*. (2019) 142:3975–90. doi: 10.1093/brain/awz332

11. Padmanabhan JL, Cooke D, Joutsa J, Siddiqi SH, Ferguson M, Darby RR, et al. A human depression circuit derived from focal brain lesions. *Biol Psychiatry*. (2019) 86:749–58. doi: 10.1016/j.biopsych.2019.07.023

12. Siddiqi SH, Schaper FLWVJ, Horn A, Hsu J, Padmanabhan JL, Brodtmann A, et al. Brain stimulation and brain lesions converge on common causal circuits in neuropsychiatric disease. Nature human. *Behaviour*. (2021) 5:1707–16. doi: 10.1038/s41562-021-01161-1

13. Glasser MF, Smith SM, Marcus DS, Andersson JLR, Auerbach EJ, Behrens TEJ, et al. The human connectome Project's neuroimaging approach. *Nat Neurosci*. (2016) 19:1175–87. doi: 10.1038/nn.4361

14. Albazron FM, Bruss J, Jones RM, Yock TI, Pulsifer MB, Cohen AL, et al. Pediatric postoperative cerebellar cognitive affective syndrome follows outflow pathway lesions. *Neurology*. (2019) 93:e1561–71. doi: 10.1212/WNL.0000000000008326

15. Darby RR, Horn A, Cushman F, Fox MD. Lesion network localization of criminal behavior. *Proc Natl Acad Sci U S A*. (2018) 115:601–6. doi: 10.1073/pnas.1706587115

16. Hwang K, Bruss J, Tranel D, Boes AD. Network localization of executive function deficits in patients with focal thalamic lesions. *J Cogn Neurosci*. (2020) 32:2303–19. doi: 10.1162/jocn_a_01628

17. Joutsa J, Shih LC, Fox MD. Mapping holmes tremor circuit using the human brain connectome. *Ann Neurol*. (2019) 86:812–20. doi: 10.1002/ana.25618

18. Kyeong S, Kim DH. Lesion-based structural and functional networks in patients with step length asymmetry after stroke. *NeuroRehabilitation*. (2021) 48:133–8. doi: 10.3233/NRE-201555

19. Joutsa J, Horn A, Hsu J, Fox MD. Localizing parkinsonism based on focal brain lesions. *Brain*. (2018) 141:2445–56. doi: 10.1093/brain/awy161

20. Laganiere S, Boes AD, Fox MD. Network localization of hemichorea-hemiballismus. *Neurology*. (2016) 86:2187–95. doi: 10.1212/WNL.0000000000002741

21. Moher D, Liberati A, Tetzlaff J, Altman DG. Preferred reporting items for systematic reviews and meta-analyses: the PRISMA statement. *BMJ*. (2009) 339:b2535. doi: 10.1136/bmj.b2535

22. Lo CK-L, Mertz D, Loeb M. Newcastle-Ottawa scale: comparing reviewers' to authors' assessments. *BMC Med Res Methodol*. (2014) 14:45. doi: 10.1186/1471-2288-14-45

23. Blondiaux E, Heydrich L, Blanke O. Common and distinct brain networks of autoscopic phenomena. *Neuroimage Clin*. (2021) 30:102612. doi: 10.1016/j.nicl.2021.102612

24. Bowren M, Bruss J, Manzel K, Edwards D, Liu C, Corbetta M, et al. Post-stroke outcomes predicted from multivariate lesion-behaviour and lesion network mapping. *Brain*. (2022) 145:1338–53. doi: 10.1093/brain/awac010

25. Cohen AL, Ferguson MA, Fox MD. Lesion network mapping predicts post-stroke behavioural deficits and improves localization. *Brain*. (2021) 144:E35. doi: 10.1093/brain/awab002

26. Corp DT, Joutsa J, Darby RR, Delnooz CCS, Van De Warrenburg BPC, Cooke D, et al. Network localization of cervical dystonia based on causal brain lesions. *Brain*. (2019) 142:1660–74. doi: 10.1093/brain/awz112

27. Cotovio G, Faro Viana F, Fox MD, Oliveira-Maia AJ. Lesion network mapping of mania using different normative connectomes. *Brain Struct Funct*. (2022) 227:3121–7. doi: 10.1007/s00429-022-02508-8

28. Crockett RA, Hsu CL, Dao E, Tam R, Alkeridy W, Eng JJ, et al. Mind the gaps: functional networks disrupted by white matter hyperintensities are associated with greater falls risk. *Neurobiol Aging*. (2022) 109:166–75. doi: 10.1016/j.neurobiolaging.2021.09.023

29. Crockett RA, Hsu CL, Dao E, Tam R, Eng JJ, Handy TC, et al. Painting by lesions: White matter hyperintensities disrupt functional networks and global cognition. *NeuroImage*. (2021) 236:118089. doi: 10.1016/j.neuroimage.2021.118089

30. Germann J, Elias GJB, Neudorfer C, Boutet A, Chow CT, Wong EHY, et al. Potential optimization of focused ultrasound capsulotomy for obsessive compulsive disorder. *Brain*. (2021) 144:3529–40. doi: 10.1093/brain/awab232

31. Higashiyama Y, Hamada T, Saito A, Morihara K, Okamoto M, Kimura K, et al. Neural mechanisms of foreign accent syndrome: lesion and network analysis. *Neuroimage Clin*. (2021) 31:102760. doi: 10.1016/j.nicl.2021.102760

32. Joutsa J, Shih LC, Horn A, Reich MM, Wu O, Rost NS, et al. Identifying therapeutic targets from spontaneous beneficial brain lesions. *Ann Neurol*. (2018) 84:153–7. doi: 10.1002/ana.25285

33. Klingbeil J, Wawrzyniak M, Stockert A, Karnath HO, Saur D. Hippocampal diaschisis contributes to anosognosia for hemiplegia: evidence from lesion network-symptom-mapping. *NeuroImage*. (2020) 208:116485. doi: 10.1016/j.neuroimage.2019.116485

34. Mansouri AM, Germann J, Boutet A, Elias GJB, Mithani K, Chow CT, et al. Identification of neural networks preferentially engaged by epileptogenic mass lesions through lesion network mapping analysis. *Sci Rep*. (2020) 10:10989. doi: 10.1038/s41598-020-67626-x

35. Philippi CL, Bruss J, Boes AD, Albazron FM, Deifelt Streese C, Ciaramelli E, et al. Lesion network mapping demonstrates that mind-wandering is associated with the default mode network. *J Neurosci Res*. (2021) 99:361–73. doi: 10.1002/jnr.24648

36. Pini L, Salvalaggio A, De Filippo De Grazia M, Zorzi M, Thiebaut de Schotten M, Corbetta M. A novel stroke lesion network mapping approach: improved accuracy yet still low deficit prediction. *Brain Commun*. (2021) 3:fcab259. doi: 10.1093/braincomms/fcab259

37. Snider SB, Hsu J, Darby RR, Cooke D, Fischer D, Cohen AL, et al. Cortical lesions causing loss of consciousness are anticorrelated with the dorsal brainstem. *Hum Brain Mapp*. (2020) 41:1520–31. doi: 10.1002/hbm.24892

38. Salvalaggio A, De Filippo De Grazia M, Zorzi M, Thiebaut de Schotten M, Corbetta M. Post-stroke deficit prediction from lesion and indirect structural and functional disconnection. *Brain*. (2020) 143:2173–88. doi: 10.1093/brain/awaa156

39. Joutsa J, Moussawi K, Siddiqi SH, Abdolahi A, Drew W, Cohen AL, et al. Brain lesions disrupting addiction map to a common human brain circuit. *Nat Med*. (2022) 28:1249–55. doi: 10.1038/s41591-022-01834-y

40. Ferguson MA, Lim C, Cooke D, Darby RR, Wu O, Rost NS, et al. A human memory circuit derived from brain lesions causing amnesia. *Nat Commun*. (2019) 10:3497. doi: 10.1038/s41467-019-11353-z

41. Fischer DB, Boes AD, Demertzi A, Evrard HC, Laureys S, Edlow BL, et al. A human brain network derived from coma-causing brainstem lesions. *Neurology*. (2016) 87:2427–34. doi: 10.1212/WNL.0000000000003404

42. Herbet G, Lemaitre AL, Moritz-Gasser S, Cochereau J, Duffau H. The antero-dorsal precuneal cortex supports specific aspects of bodily awareness. *Brain*. (2019) 142:2207–14. doi: 10.1093/brain/awz179

43. Darby RR, Joutsa J, Burke MJ, Fox MD. Lesion network localization of free will. *Proc Natl Acad Sci*. (2018) 115:10792–7. doi: 10.1073/pnas.1814117115

44. Ferguson MA, Schaper F, Cohen A, Siddiqi S, Merrill SM, Nielsen JA, et al. A neural circuit for spirituality and religiosity derived from patients with brain lesions. *Biol Psychiatry*. (2022) 91:380–8. doi: 10.1016/j.biopsych.2021.06.016

45. Jimenez-Marin A, De Bruyn N, Gooijers J, Llera A, Meyer S, Alaerts K, et al. Multimodal and multidomain lesion network mapping enhances prediction of sensorimotor behavior in stroke patients. *Sci Rep*. (2022) 12:22400. doi: 10.1038/s41598-022-26945-x

46. Kletenik I, Ferguson MA, Bateman JR, Cohen AL, Lin C, Tetreault A, et al. Network localization of unconscious visual perception in Blindsight. *Ann Neurol*. (2022) 91:217–24. doi: 10.1002/ana.26292

47. Alves PN, Silva DP, Fonseca AC, Martins IP. Mapping delusions of space onto a structural disconnectome that decouples familiarity and place networks. *Cortex*. (2022) 146:250–60. doi: 10.1016/j.cortex.2021.11.008

48. Conrad J, Boegle R, Ruehl RM, Dieterich M. Evaluating the rare cases of cortical vertigo using disconnectome mapping. *Brain Struct Funct*. (2022) 227:3063–73. doi: 10.1007/s00429-022-02530-w

49. Dulyan L, Talozzi L, Pacella V, Corbetta M, Forkel SJ, Thiebaut de Schotten M. Longitudinal prediction of motor dysfunction after stroke: a disconnectome study. *Brain Struct Funct*. (2022) 227:3085–98. doi: 10.1007/s00429-022-02589-5

50. Jiang J, Ferguson MA, Grafman J, Cohen AL, Fox MD. A lesion-derived brain network for emotion regulation. *Biol Psychiatry*. (2023) S0006-3223:00081-1. doi: 10.1016/j.biopsych.2023.02.007

51. Kolskår KK, Ulrichsen KM, Richard G, Dørum ES, de Schotten MT, Rokicki J, et al. Structural disconnectome mapping of cognitive function in poststroke patients. *Brain Behav*. (2022) 12:e2707. doi: 10.1002/brb3.2707

52. Li Y, Qi L, Schaper FLWVJ, Wu D, Friedrich M, Du J, et al. A vertigo network derived from human brain lesions and brain stimulation. *Brain Communications*. (2023) 5:fcad071. doi: 10.1093/braincomms/fcad071

53. Rosenzopf H, Wiesen D, Basilakos A, Yourganov G, Bonilha L, Rorden C, et al. Mapping the human praxis network: an investigation of white matter disconnection in limb apraxia of gesture production. *Brain Commun*. (2022) 4:fcac004. doi: 10.1093/braincomms/fcac004

54. Siddiqi SH, Kletenik I, Anderson MC, Cavallari M, Chitnis T, Glanz BI, et al. Lesion network localization of depression in multiple sclerosis. *J Neurol*. (2023) 1:36–44. doi: 10.1038/s44220-022-00002-y

55. Sotelo MR, Kalinosky BT, Goodfriend K, Hyngstrom AS, Schmit BD. Indirect structural connectivity identifies changes in brain networks after stroke. *Brain Connect*. (2020) 10:399–410. doi: 10.1089/brain.2019.0725

56. Ulrichsen KM, Kolskår KK, Richard G, Alnæs D, Dørum ES, Sanders A-M, et al. Structural brain disconnectivity mapping of post-stroke fatigue. *Neuroimage Clin*. (2021) 30:102635. doi: 10.1016/j.nicl.2021.102635

57. Weaver NA, Lim JS, Schilderinck J, Biessels GJ, Kang Y, Kim BJ, et al. Strategic infarct locations for Poststroke depressive symptoms: a lesion-and disconnection-symptom mapping study. *Biol Psychiatry Cogn Neurosci Neuroimaging*. (2023) 8:387–96. doi: 10.1016/j.bpsc.2021.09.002

58. Souter NE, Wang X, Thompson H, Krieger-Redwood K, Halai AD, Lambon Ralph MA, et al. Mapping lesion, structural disconnection, and functional disconnection to symptoms in semantic aphasia. *Brain Struct Funct*. (2022) 227:3043–61. doi: 10.1007/s00429-022-02526-6

59. Corbetta M, Siegel JS, Shulman GL. On the low dimensionality of behavioral deficits and alterations of brain network connectivity after focal injury. *Cortex*. (2018) 107:229–37. doi: 10.1016/j.cortex.2017.12.017

60. Carrera E, Tononi G. Diaschisis: past, present, future. *Brain*. (2014) 137:2408–22. doi: 10.1093/brain/awu101

61. Seyedmirzaei H, Shafie M, Kargar A, Golbahari A, Bijarchian M, Ahmadi S, et al. White matter tracts associated with alexithymia and emotion regulation: a diffusion MRI study. *J Affect Disord*. (2022) 314:271–80. doi: 10.1016/j.jad.2022.07.039

62. Seyedmirzaei H, Nabizadeh F, Aarabi MH, Pini L. Neurite orientation dispersion and density imaging in multiple sclerosis: a systematic review. *J Magn Reson Imaging*. (2023). doi: 10.1002/jmri.28727

63. Baldassarre A, Ramsey L, Hacker CL, Callejas A, Astafiev SV, Metcalf NV, et al. Large-scale changes in network interactions as a physiological signature of spatial neglect. *Brain*. (2014) 137:3267–83. doi: 10.1093/brain/awu297

64. Corbetta M, Ramsey L, Callejas A, Baldassarre A, Hacker Carl D, Siegel Joshua S, et al. Common behavioral clusters and subcortical anatomy in stroke. *Neuron*. (2015) 85:927–41. doi: 10.1016/j.neuron.2015.02.027

65. Dougherty DD. Deep brain stimulation: clinical applications. *Psychiatr Clin North Am*. (2018) 41:385–94. doi: 10.1016/j.psc.2018.04.004

66. Kapur N. Paradoxical functional facilitation in brain-behaviour research: a critical review. *Brain*. (1996) 119:1775–90. doi: 10.1093/brain/119.5.1775

67. Hanlon CA, Dowdle LT, Henderson JS. Modulating neural circuits with transcranial magnetic stimulation: implications for addiction treatment development. *Pharmacol Rev*. (2018) 70:661–83. doi: 10.1124/pr.116.013649

68. Fox MD. Mapping symptoms to brain networks with the human connectome. *N Engl J Med*. (2018) 379:2237–45. doi: 10.1056/NEJMra1706158

69. Joutsa J, Corp DT, Fox MD. Lesion network mapping for symptom localization: recent developments and future directions. *Curr Opin Neurol*. (2022) 35:453–9. doi: 10.1097/WCO.0000000000001085

70. Bonkhoff AK, Schirmer MD, Bretzner M, Hong S, Regenhardt RW, Brudfors M, et al. Outcome after acute ischemic stroke is linked to sex-specific lesion patterns. *Nat Commun*. (2021) 12:3289. doi: 10.1038/s41467-021-23492-3

71. Bethlehem RAI, Seidlitz J, White SR, Vogel JW, Anderson KM, Adamson C, et al. Brain charts for the human lifespan. *Nature*. (2022) 604:525–33. doi: 10.1038/s41586-022-04554-y

Frontiers in Neurology

Explores neurological illness to improve patient care

The third most-cited clinical neurology journal explores the diagnosis, causes, treatment, and public health aspects of neurological illnesses. Its ultimate aim is to inform improvements in patient care.

Discover the latest Research Topics

See more →

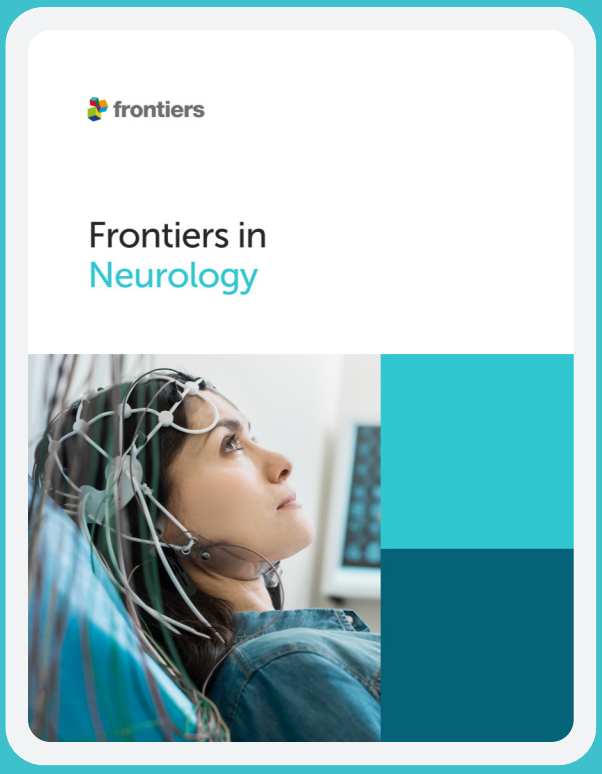

Frontiers

Avenue du Tribunal-Fédéral 34
1005 Lausanne, Switzerland
frontiersin.org

Contact us

+41 (0)21 510 17 00
frontiersin.org/about/contact